CRANFIELD UNIVERSITY

MUHAMMAD ADEEL AWAN

Compensation of Low Performance Steering System Using Torque Vectoring

DEPARTMENT OF ENGINEERING & APPLIED SCIENCES
Weapon And Vehicle Systems Group

PhD THESIS
Academic Year: 2012-13

Supervisors:
Dr. David Purdy
Dr. Amer Hameed

JULY 2012

CRANFIELD UNIVERSITY

DEPARTMENT OF ENGINEERING & APPLIED SCIENCES
Weapon And Vehicle Systems Group

PhD THESIS
Academic Year: 2012-13

Muhammad Adeel Awan

Compensation of Low Performance Steering System Using Torque Vectoring

Supervisors:
Dr. David Purdy
Dr. Amer Hameed
JULY 2012

This thesis is submitted in partial fulfilment of the requirements for the degree of Doctor of Philosophy

Acknowledgements

Writing the acknowledgement section brings a big sigh of relief for a PhD candidate. For me this moment would not have been possible without the help of the Almighty, without whose blessing I am nothing.

After this my special gratitude goes to Dr. David Purdy, my supervisor and mentor, who was always there with patience and persistence, whether it was early morning discussions or emails from abroad. Many of the ideas in this thesis were developed with his suggestions and guidance.

I was lucky enough to have two supervisors instead of one. I am very grateful to Dr. Amer Hameed for initiating this project and for providing me with valuable guidance, advice and support. Without his forthcoming support the idea of steer-by-wire test vehicle would not have materialised.

I would also like to thank my advisory committee, Dr. Hugh Goyder and Mr. Dave Simner, for taking the time to read and critique my work. A special thanks go to Mr. John Crocker and Mr. James Harber for their unconditional support in vehicle testing and laboratory work. Their role as the test drivers is commendable, because without them the experimentation phase would not have been completed. I am also thankful to NP Aerospace for partially sponsoring my work.

Lastly I would like to thank all of my family members for their supportive role. My mother's prayers were always there with me. A special thanks go to my wife and children who allowed me to pursue my goal at the cost of their time. Without their support I would have struggled all along.

Abstract

In this work torque vectoring methods are used to compensate for a low performance steer-by-wire system. Currently a number of vehicle manufacturers are considering introducing steer-by-wire into their range of vehicles. Some of the key concerns for the manufacturers are safety and cost. The safety can be subdivided in the integrity of the steering system and the effect on handling. The focus of this study is the use of low cost steering actuators on a vehicle and identify its effects on the vehicle's handling response. The test vehicle is dune buggy modified to accommodate the low performance steer-by-wire system without a direct mechanical link between the steering wheel and the wheels and equipped with various sensors to data recording.

In order to investigate the influence of torque vectoring system on the steer-by-wire, an eight degrees of freedom vehicle model in Matlab/Simulink has been developed. The eight degrees of freedom are longitudinal and lateral translations, yaw and roll motion and rotation of each wheel. The Matlab/Simulink model also includes the dynamics of the actuators, which is validated against the experimental data. The actuator was shown to have a bandwidth of less than 0.3 Hz. The eight degrees of freedom model's response was validated against experimental data for both steady state and transient response up to 0.5 g. The tyre forces and moments are implemented by using the Dugoff tyre model, which has been validated against experimentally measured data.

The torque vectoring system uses the cascade approach based on a reference model, which uses a two degrees of freedom (bicycle model) to generate the reference signal for control purposes. The upper level yaw controller is based on the optimal control theory and uses the LQR (Linear-quadratic regulator) approach. The lower level wheel slip controller is based on a sliding-mode structure and prevents tyre force saturation. The simulation results show that the vehicle augmented with the torque vectoring system outperforms the low performance steer-by-wire vehicle and also the vehicle with conventional steering arrangement.

Contents

List of Figures

List of Tables

Chapter 1

Introduction

Contents

1.1 Introduction

The recent advancements in the embedded electronics, software, sensors and actuators have paved the way for X-by-wire systems into the military and commercial vehicles. Throttle-by-wire, brake-by-wire, and steer-by-wire are few among the systems that electrification of vehicles has brought into the limelight. This thesis explores the idea of steer-by-wire system in which the vehicle is steered without any mechanical connection between the steering handle and wheels. This modern X-by-wire system has its own merits and limitations and is a popular subject of investigations. The steering system plays a critical role in vehicle's safety by influencing its handling response. Therefore, the main focus of this thesis is to investigate the handling performance of the vehicle fitted with a low performance steer-by-wire system. Another part of the task is to improve the handling response of the steer-by-wire vehicle using the torque vectoring technique.

The ideal strategy to investigate the research questions would have been to take a test vehicle and fit it with a steer-by-wire system comprising of low performance actuators. Then perform experiments on this test vehicle to identify its handling response. In order to evaluate the effect of torque vectoring system, the test vehicle would have been fitted with four in-wheel motors and integrated with the controller. Then this upgraded test vehicle would have been subjected to the same experiments and improvement in its

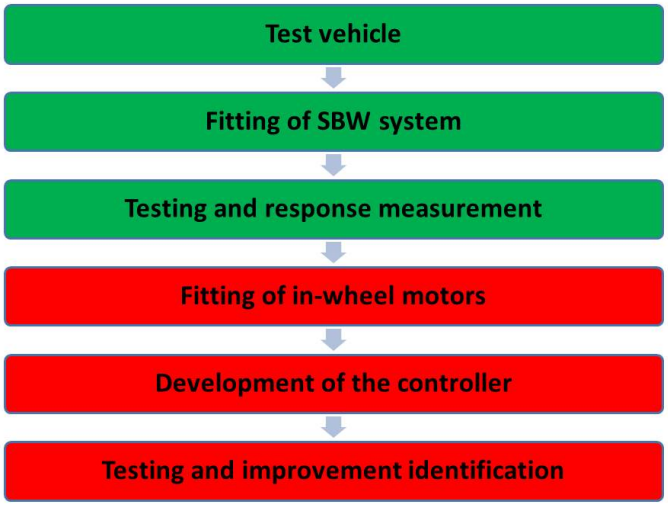

Figure 1.1: Proposed ideal strategy

handling response would have been noted. This ideal strategy has been laid-out in Fig. 1.1.

However, the financial constraints did not allow to follow the ideal strategy in toto. Figure 1.2 shows the steps that have been taken to accomplish the research. The first three steps in Fig. 1.1 and Fig. 1.2 are same. For

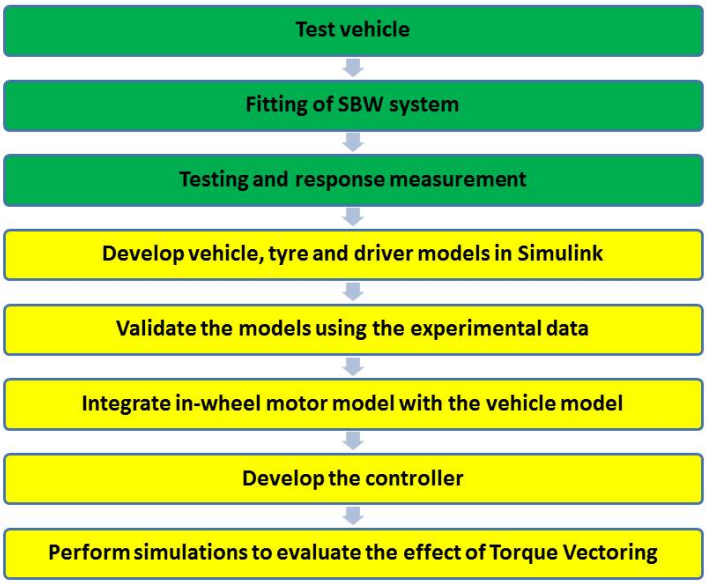

Figure 1.2: The adopted strategy

this purpose a test vehicle, fitted with low cost actuators, has been used. The experiments revealed that the delayed response of the steering system adversely affects the vehicle's handling response and makes it unsafe for high speed manoeuvres. For further investigation the vehicle, tyre and driver models have been developed using Simulink. These models have been validated using the data collected during the experiments. The vehicle model is further integrated with the in-wheel motor models in Simulink to study the effect of torque vectoring on the whole system. This work also includes the design of a cascade controller, which monitors the vehicle yaw-rate and compensate the poor performance through torque vectoring.

1.2 Motivation

The motivation for this work is to envisage a future vehicle with a low cost steer-by-wire system. This idea raises the need to explore the possibilities that allow the replacement of a conventional steering system with a steer-by-wire system. Due to its critical nature generally a steer-by-wire system contains high performance actuators. These high performance actuators/motors are costly and therefore do not provide a feasible solution for production vehicles. This work investigates the possibility of using the low cost actuators as a part of the steer-by-wire system.

In order to overcome the limited performance of these low cost actuators this thesis explores the compensation by torque vectoring techniques. This provides control over the torque distribution to all wheels of a vehicle. Generally this technique is implemented by a mechanical differential; however, this work uses in-wheel electric motors to implement the torque vectoring mechanism as these are being considered for both civilian and military vehicles.

1.3 Aim and Objectives

The aim of this work is to make the handling response of the steer-by-wire vehicle, comprising of low performance actuators, to be as good as or better than a conventional vehicle. To achieve this goal the torque vectoring technique has to be employed, which uses in-wheel motors to compensate for the low performance steering system.

To achieve the above mentioned goal an in depth understanding of the system is required. This understanding is built up by theoretical and experimental analysis, which give insight to the vehicle's handling behaviour with and without the steer-by-wire system. Following is the list of objectives, which leads to achieve the desired aim:

- Review the peer work published by researchers relevant to this field.
- Designing of suitable models that can represent the vehicle and tyres in the theoretical investigation.
- Setting-up a test vehicle with a steer-by-wire system, comprising of low performance actuators.
- Validating the vehicle and tyre models using the handling data collected through the test vehicle.
- Investigation of the actuator's response and development of its mathematical model.
- Investigation and designing of a controller that can control the torque distribution between the left-right side of the vehicle.

1.4 Outline

The thesis is arranged in six chapters. At the outset of this thesis, Chapter 1 briefly describes the aim and objectives set to achieve the desired goal. Chapter 2 covers a review of the literature relating to this work. This work covers five different but interlinked areas, which are mandatory to investigate to design a controller for a steer-by-wire vehicle. Therefore this chapter is divided into five sections to review the literature related to each domain separately.

In Chapter 3, mathematical models for vehicle, tyre and driver preview controller are discussed and developed. The section related to vehicle modelling covers both linear and non-linear vehicle models. The section on tyres, gives overview of forces and moments generated by the tyres. The next section describes the technique, which is used in this thesis to model the driver behaviour in conjunction with the vehicle model. All of these models are used later to design and validate the controller.

The vehicle, tyre and driver models developed in Chapter 3 are validated experimentally in Chapter 4. This chapter also gives overview of the equipment, their arrangement and the experiments carried out to fulfil the purpose. The chapter begins with tyre testing carried out to identify lateral characteristics of the tyres and concludes with the full vehicle testing as per recommendations given in the relevant standards.

Chapter 5 is about the techniques that are used in this work to develop and tune the controller for the system. The chapter begins with a section, which builds the case for why a controller is required to assist the steer-by-wire vehicle. The following section describes the objectives to be achieved through

the controller and the strategy to achieve these objectives. The chapter ends with a discussion on the simulation results, which are carried out to evaluate the performance of the proposed controller.

The thesis finishes with Chapter 6, which gives an overview of the work and presents the conclusions drawn in reference to the aim and objectives set in Chapter 1. This chapter also highlights the future areas of research based on the outcomes of this work.

1.5 Contribution

The contribution made in this work is as follows:

- A model of the low performance steer-by-wire system has been developed and validated experimentally.
- A vehicle model, having eight degrees of freedom, integrated with the low performance steer-by-wire model has been developed and validated with a limited set of experiments. This model is available for further parametric investigations.
- A cascade controller for torque vectoring has been developed. This thesis has successfully shown that a low performance steer-by-wire system can perform like a conventional steering system once integrated with the proposed controller.

Chapter 2

Literature Review

Contents

2.1 Introduction

This chapter discusses the published work pertaining to the field of steer-by-wire (SBW), lateral and yaw handling of a vehicle, theoretical modelling techniques for tyre force formulation, and vehicle lateral control systems. A section is also included which covers the research relevant to modelling techniques that have been used to simulate a driver-in-loop scenario. The following sections are arranged in a manner that each one begins with a brief historical overview and ends with a current state of research trend. Each section is followed by a summary which encompasses the discussion about the approach followed in this thesis and reasoning for the selection.

2.2 Steer-by-Wire System

Since the inception of high speed automobiles, the automotive engineers are in a constant pursuit to enhance their manoeuvrability and stability. The earlier versions of automobiles were steered by a tiller. In order to improve the directional control, the tiller was replaced by a steering wheel. The steering wheel is connected to the wheels by means of mechanical linkages and transfers the driver's commands to the wheels through the linkages. This effort to

enhance the steering system of a vehicle by introducing the steering wheel dates back to 1893 when a Frenchman, name Alfred Vacheron, introduced the steering wheel to his race case [Dick 2005]. These efforts to improve the vehicle stability and steerability continued on and resulted in the form of anti-lock brake system (ABS), differential braking, yaw control, traction control, and active steering system, which made their way to the production models. Among these performance enhancement systems active steering phenomenon, being the least matured, still lures the researchers.

An active steering system is one which uses an auxiliary arrangement to assist the driver in controlling the vehicle. The active steering system can have various forms; it can be a conventional steering arrangement assisted by an electric motor/hydraulic pump or an arrangement in which the steering wheel is not directly connected to the wheels and the wheels are steered by actuators that receive commands through a microprocessor. The latter steering arrangement is termed as steer-by-wire system and is one of the advanced forms of the active steering systems.

Active steering goes back to at least the sixties [Ackermann 1999] when Kasselmann and Keranen [Kasselmann 1969] studied an active steering system in which a proportional feedback controller augmented the front steering angle by monitoring the vehicle yaw-rate with a gyro. However, the technological limitations of that era prevented the practical implementation of the idea. In late eighties and nineties when the advancements in the field of embedded electronics brought sensors and more computational power to the engineers' disposal, they picked up the idea again. In this era the idea of active steering was mostly considered to investigate the four wheel steer (4WS) concept for stability and manoeuvrability enhancement of a vehicle.

Ackermann in one of his early nineties publication [Ackermann 1990] cites previous work of various researchers who investigated control laws for rear wheel active steering to augment the front conventional steering. The paper proposed a robust compensator/actuator design that required no tuning because of its decoupling properties. The author described the aim as to show that feedback control can improve the robustness of the driver-car system with respect to the uncertain operating conditions. However, to make his case the author used a two degrees of freedom bicycle model with linear tyres, which limits the applicability of the proposed strategy to a low acceleration scenario. Moreover, the discussion is not supported by any simulated or experimental result so it can be concluded that this paper was an effort by the author to initiate a debate about influencing the vehicle lateral stability by steering the rear wheels.

Yu and Moskwa [Yu 1994] in mid nineties presented an approach that combined active steering and independently controlled wheel torques. The

authors developed a control algorithm utilising the input-output linearization technique and sliding mode control law. In this work the proposed controller block performs two functions; first interprets the steering and braking actions commanded by a driver and secondly generate control signals for steering and braking system. The steering commands are implemented by actuator motors independently for front and rear wheels. The simulated results shown by the authors suggest improved behaviour of a controlled 4WS vehicle over an uncontrolled one. For these simulations the authors assumed that the road coefficients of friction are available to the proposed controller; however, the road friction estimation in real time is still a research area under active investigation [Ahn 2012]. Moreover, the authors during their investigation ignored the dynamics of the actuators used for four wheel steering, which can greatly influence the performance of the controller.

Kleine and J. L. Van Niekerk [Kleine 1998] in their work highlighted the efforts made by researchers in the field of 4WS. The categorised the previous work in three (3) groups; open loop, closed loop and decoupling mode. The authors based the classification on the methods that were employed to control the rear wheels steer input. The open loop term refers to the systems in which the rear wheels steering was controlled on the basis of vehicle speed and any instability in the vehicle motion does not influence the amount of this steering angle. The closed loop term referred to a system which used feedback of system states to correct the rear wheel steer angle. The authors used the term decoupling for those systems which employed techniques to decouple certain vehicle lateral modes from one another by steering the rear wheels. The authors in their article combined the concept of decoupling and steer-by-wire to improve the dynamics of a vehicle. For this purpose the authors developed a full state feedback controller to make use of front and rear steer independently and decoupled the vehicle side slip and yaw rate for a two degrees of freedom model. The authors used the active rear steer to keep the vehicle side slip at zero but it increases the understeer behaviour of a vehicle and therefore a driver has to steer more. The paper proposes an active front wheel steer to add an additional amount of steer to that of supplied by the driver to over come this deficiency. The authors have included results to support their suggestion that the interference of active front steer improves the vehicle's handling response; however, this proposed solution has one drawback. In comparison to a conventional understeer vehicle the front wheels of the proposed vehicle would reach to the lateral force saturation point earlier thus making the vehicle to be unstable for a sharp turn manoeuvre. Moreover, the decoupling of yaw rate and vehicle side slip was not complete once the authors introduced a three degrees of freedom model because of the side slip term in the yaw equation. The authors ignored the disturbance by

citing it to be very small, which may not be the case for a more complex model. This fact makes the task for controller more difficult to control the yaw rate while keeping the vehicle side slip at zero.

Ackermann et al. [Ackermann 1999] in their article compared the active braking and active steering approaches in order to control the yaw and roll dynamics of a vehicle. The reason behind this effort was to evaluate the effectiveness of an active steering system as an alternative or in combination with an active braking system for yaw disturbance attenuation. Assuming the centre of gravity of a vehicle lies in the middle of its wheelbase and taking the total tyre force to be independent of the direction in which it acts they suggested that the steering requires only a quarter of the front wheel tyre force compared to asymmetric braking of the front wheels to generate similar amount of torque about z-axis. In another example the authors combined both of the active systems to improve the vehicle's lateral response during μ-split braking situation by generating a counter torque through active steering to balance the yaw motion developed by sudden braking on a partially wet road surface. In order to support their statements the authors presented two robust control concepts for yaw disturbance rejection and rollover avoidance respectively. In order to make their case the authors referred a steering control method discussed in an earlier article [Ackermann 1997], which was aimed to achieve decoupling of the vehicle's yaw and lateral motions. The limitation of the proposed controller is that its effectiveness has been evaluated for a single track vehicle model using disturbances of low frequencies, which limits its applicability in high acceleration manoeuvres. For the rollover controller the single track model is extended to include the influence of the vehicle's centre of gravity and assumed that this height remains same during motion. Using this simple non-linear vehicle model the authors simulated a highway exit scenario and suggested that intervention of active steering along with the braking avoided the vehicle rollover. Thus from this published work it can be established that the combination of active steering and active braking has potential to improve the vehicle handling and stability but require further investigation with a complex vehicle model.

Hayama et al. [Hayama 2000] published an article in which they investigated the improvement of vehicle stability through introduction of active steering control. The aim of their research was to develop a steer-by-wire system that obtains a better effect, on a vehicle's lateral stability, than that of a direct yaw control (DYC). For this purpose the authors presented results collected through an experimental vehicle, which performed full braking manoeuvre on a μ-split surface. This experiment was performed three times, once without the intervention of a control system, then with a DYC system and lastly with an active SBW system. The results presented by the authors suggest that the

vehicle assisted by an active SBW system deviated less from the target course during the manoeuvre. The authors presented the strategy which was used to control the active steering system but did not discuss the DYC system in detail. Moreover, in discussion the authors linked the lateral deviation to a fact that most of the stability controllers actuate when they detect a deviation of the vehicle yaw-rate from the reference during braking. They termed this lag time to have detrimental effect on the stability of a vehicle during extreme braking cases; however, the authors have not mention about the time delay induced by the steer-by-wire actuators. In addition to this the paper neither explains the method adopted to calculate the control gains nor discusses the target yaw value estimation strategy. The authors ended the paper with an improved active SBW control system which minimises the detection time lag by monitoring the brake light signal. The results presented by the authors show further decrease in lateral deviation from the desired path but even the new proposed controller does not take the actuator dynamics into account.

The article published by Segawa et al. [Segawa 2001] is an extension of the above discussed idea, presented by Hayama et al [Hayama 2000]. In this article the authors compared the performance of a 4WS control strategy presented by Ito et al. (in Japanese) [Ito 1986] with the active front steer control strategy presented by Hayama et al. The 4WS control strategy is termed as D^* controller in the article referring to the feedback value that takes both yaw-rate and lateral acceleration into account. The comparison includes testing using a driving simulator and a test vehicle equipped with a steer-by-wire system. On the driving simulator a vehicle motion travelling in a straight line across a crosswind was simulated. The results published in the paper suggest that a vehicle not taking its states feedback into account drifted away from the straight ahead path and the driver had to intervene to stabilise the vehicle. On the other hand the active front steering controllers taking yaw rate and D^* value (yaw rate and lateral acceleration) as a feedback respectively assisted the vehicle to follow the desired path without the driver's intervention. The reaction time of the D^* controller was slightly quicker as compared to the yaw rate controller. The lane change tests performed using the test vehicle on a packed snow ground also suggest that the controlled vehicle outperforms the uncontrolled one. The yaw rate and D^* controller helps the driver to complete the manoeuvre without slipping off the track. The results again show that the D^* controller utilising the 4WS system performs better in terms of the desired path following. This suggests that a front SBW system augmented by an additional active system improves a vehicle's lateral stability performance.

Yih et al. [Yih 2005] published an article in which they developed a full state feedback control law to augment a driver's steering command through an active steering system. This feedback controller is based on vehicle's yaw

rate and side slip information. The article can be divided into three parts; one which emphasises on the techniques to estimate the vehicle states, other which employs the controller to influence the vehicle's handling characteristics and the last contains experimental results. The state estimation part is unique in terms that the authors used a combination of global positioning system (GPS) and inertial navigation system (INS) to estimate the vehicle's side slip angle. The vehicle's side slip angle not being directly measurable is generally estimated by integrating inertial sensors or using a physical vehicle model. Both of these methods have constraints like direct integration methods can accumulate sensors errors and the physical model dependent methods can be sensitive to changes in the vehicle parameters [Ryu 2002]. The estimation method employed in this paper uses GPS signal to correct the inertial sensor's output thus minimising the chances of error accumulation during integration. The controller section includes a two degrees of freedom bicycle model for reference signal generation. The controller concept was validated by experimenting on a SBW vehicle which was a modified version of a production vehicle. They replaced the steering column by a brushless DC servomotor and the steering wheel was fitted with a feedback motor to simulate the steering resistance from the road. They retained the hydraulic assist unit to augment the DC motor force during driving, thus allowing a smaller actuator to serve the purpose. Furthermore, to keep the modification simple they kept the conventional rack and pinion arrangement intact; however, this arrangement does not allow to exploit full advantage of SBW system. In experimental part the authors presented results to demonstrate the influence of their proposed control algorithm on the vehicle's performance. In one test the weight distribution of the vehicle was altered by adding extra weight at rear, which made the vehicle slightly oversteer. By changing the active steer control gains, the oversteer effect was cancelled out thus facilitating the driver to keep the vehicle under control. The experiments were conducted by driving the vehicle at the speed of 13.4 m/s (48 km/h) and the information about the controller performance at higher speeds has not been provided. Moreover, the high performance GPS and INS integration system used to assist the controller is a costly product and is not readily available on a production vehicle. The results suggest the proposed technique to be useful but has not been compared with any other control system commercially available like DYC.

Wilwert et al. [Wilwert 2005] published a chapter on the automotive X-by-Wire systems in *The Industrial Communication Technology Handbook*. The chapter discusses the problems and constraints linked to the design of X-by-Wire systems in general and SBW is particular. According to the authors one of the main hurdles in general acceptance of these X-by-Wire systems is the safety. They categorised the other constraints under the headings of cost,

size, power requirements and dependability. However, the authors foresee that the technological advancements in the embedded electronics and software will also pave the way for the SBW systems as other X-by-Wire systems have been integrated in to production vehicles. The reasoning behind this statement is that the SBW system has certain advantages over a conventional system that authors have highlighted as follows:

- Removal of steering column eliminates the chance of injury due to it thus adds to the driver safety and reduces the vehicle's weight.
- Variable steering adjustment according to the vehicle speed enhances the driver comfort and vehicle controllability.

Another important point that the authors have highlighted in this text is the end-to-end response time i.e. the time between the driver's request and the response of a physical system, and considered it as a major performance factor. In order to enhance the safety the authors recommended the steer-by-wire system be able to tolerate a single failure as per the recommendation of Safety Integrity Level 4 (SIL 4) defined in the European Functional Safety standard [sta 2010]. This chapter is a good read to gain information about the design related problems of automotive X-by-Wire systems especially the steer-by-wire system. However, the focus was more emphasised on the communication protocols that are used for automotive X-by-Wire systems.

Most of the above papers mainly focus on using the SBW system as an aid to influence the vehicle's handling characteristics. The removal of mechanical linkage between the steering wheel and the road wheels gives rise to another challenge and that is to make the new steering system behave like a conventional one. Yao [Yao 2006] in his article highlighted the basic functional requirements that a SBW system must fulfil. The requirements identified by Yao can be summarised as follows:

- The steering system should be able to transfer the driver's commands to the road wheels in real time without bias, offset or time delay.
- The steering system should be able to provide the driver a steering feel depending on the road forces acting on the wheels.
- The steering wheel should be able to return to its middle position due to aligning moment force.

The aim of the article was to discuss the steering control system that makes a SBW system to perform the above mentioned tasks. In order to make the wheels track the steering motion with a minimal lag the author used

a position servo feedback control structure. The author has analysed the steering requirements in terms of control design problems and implemented the control system in an experimental vehicle. The article is concluded with experimental results, which show output of various tests performed relevant to above mentioned requirements. The steering wheel command tracking test was performed by measuring the driver input and wheels movement. The result presented in the article shows that the wheels are able to follow the sine wave input of 0.5 Hz frequency with varying amplitude of 0.5 to 3 degrees. However, the author does not include any information about the system's performance for an input of higher frequency or a greater amplitude. The test conducted to check the proposed system's ability to automatically return the steering wheel to its middle position, shows that the steering system was able to accomplish the job. The author during the discussion mentioned that the vehicle speed has been taken into account to adjust the steering wheel return rate to its middle position, but the results shown do not contain the vehicle speed information. In essence this paper is a good effort by the author to highlight the practical aspects, which a designer must consider while designing a SBW system. These requirements directly effect the overall performance of a SBW system because they influence the way the road tyre interaction information is transferred to a driver and the driver being an integral part of the steering system makes critical decisions on the basis of this information.

Du et al. [Du 2006] published an article in which they presented an electromechanical steering system for vehicles. In the proposed system the hydraulic assist system has been replaced by an asynchronous servo motor. The authors presented a concept of in which the steering system is equipped with two pinions, meant to transfer the steering torque from the steering handle to the wheels. The additional torque generated by the servo motor was introduced to the system through an additional servo pinion. Although this arrangement does not provide the advantage of independent wheel steer as offered by a SBW system but it can be considered as a fail-safe approach to keep the vehicle steerable in a case of the servo motor failure. From the vehicle manufacturer's prospective occupant safety is utmost important and this is evident from the design selection, by the Volkswagen researchers, for the steering system. This approach can be considered as an initial step towards the advanced form of active steering systems. The authors formulated the electromechanical system model in detail using Langrangean formalism and implemented it as the steering system of a multibody full vehicle model. The modelling section covers the servo motor design and its control aspects in detail but does not provide in-depth information about the vehicle model. The authors used *alaska* (a simulation tool for electromechanical systems by Chemnitz University) to simulate the performance of the proposed steering

system. They simulated ISO lane change manoeuvre and sinusoidal steering for a stationary vehicle to show that the designed servo motor is able to generate the additional torque required by the steering control system. However, simulated results to show the effect of the proposed system on the performance of the vehicle have not been included in the discussion.

In order to exploit the full potential of an active steering system the heavy and costly mechanical components must be replaced by electrical components. However, electronic and electrical components have quite different failure behaviour and in general lower reliability than mechanical components [Isermann 2001]. Rolf Isermann in this article highlighted the need of inducing fault tolerant properties within such systems. This can be achieved by enabling the system to detect an abnormal behaviour of components and processes based on measured signals. Isermann has classified the fault detection methods based on measured signals into three types. The first two methods are based on limit value checking and signal model analysis respectively; but the article mainly discusses the fault detection method based on a reference process model. The author discussed this technique for various automotive X-by-Wire systems and to detect fault for sensors measuring the vehicle's lateral behaviour, the single track vehicle model has been suggested. Discussing the steer-by-wire systems the author stressed on the system's importance and consequences in terms of its failure. The author has classified it as a high-integrity system which requires the faults to be compensated in such a way that they do not lead to system failure. This level of tolerance can be achieved by using high quality and redundancy of components. Moreover, such high demanding systems not only depend on hardware redundancy but also require fault tolerant control algorithms. The discussion at the end suggests that the author favours for the model based approach for fault detection in an electrical system; however, the approach is based on an assumption that the process model used for the detection purpose agrees well with the real one. Moreover, the simplified models are based on linear behaviour of a system and therefore do not serve the purpose in a non-linear scenario like the single track model suggested by the author for lateral fault detection is unable to handle a scenario beyond 0.3 g.

Pimentel's article [Pimentel 2004] is another effort in this direction and aimed to design a fault tolerant architecture for a steer-by-wire system. The author identified the following three modes of failure in a steer-by-wire system.

- The road-wheels do not respond to a command from the hand-wheel.
- The road-wheels turn by themselves without any command from the driver.

- There is no road feedback to the driver.

To accomplish the task the author developed a hardware based and a corresponding software based architecture. Both of these architectures were implemented in a simulated environment using CANoe (CAN Open Environment), a simulation and testing tool for electronic control units. In concluding discussion the author suggests that the proposed system architecture showed encouraging performance during simulation of different failure scenarios in CANoe, but simulation results have not been included in the paper. The actual hardware implementation of the proposed system was also not completed by the time the paper was published. But the effort suggests that the researchers are aware of the problems that can be faced by a steer-by-wire system and they are exploring the possible solutions to keep the vehicle under control in the case of system's malfunction due to the failure of a component like resistor or capacitor.

Frömmig et al. [Frömmig 2010] published a paper which was aimed to objectify the subjective characteristics of the steering system to reduce the development period and subsequently the development cost. The authors selected the electromechanical steering type because it allows to develop the steering assistance torque of any magnitude and direction independent from the steering wheel torque applied by the driver. The active steering system calculates both the magnitude and direction using an embedded software in the electronic control unit (ECU), thus allowing an addition of a supporting torque to the driver's command. While conducting the study to develop and calibrate an electromechanical steering system with respect to an optimal and brand specific steering feel, the authors conducted experiments using 8 female and 13 male drivers. In these subjective tests the steering system was subjected to different types of disturbances of duration $200 \sim 500\ ms$ and amplitude of $0.25 \sim 0.4\ Nm$, when the vehicle was travelling in a straight line with the speed of 80 and 100 km/h. Among other things, the authors also analysed the driver's behaviour and his/her subjective impressions of the vehicle's response. They found that the driver reacts in a sensitive manner if a proper torque is not applied by the steering system as per his/her anticipation. The authors supported their argument by presenting results which showed that the steering input supplemented by an additional torque, generated by an active steering system, helped the drivers to reject the external disturbances effectively and enhanced the controllability. From this discussion one thing is evident that the authors used servo motor to support the torque requirement; however, they did not consider a scenario in which the servo motor's response was non-instantaneous.

Eckert et al. [Eckert 2010] in the recent past presented their work in a con-

ference organised by FISITA. The objective of their article was to highlight the progress made by "Continental-Chassis & Safety Division" in the advanced driver assistance systems. These active assistance systems are meant to enhance the vehicle controllability and safety by integration of vehicle surrounding sensors, active braking, active steering and torque vectoring. The authors made comparison of safety provided by brake-by-wire (BBW) and steer-by-wire systems in an emergency situation. For this purpose they selected an obstacle avoidance scenario and studied the vehicle safety at different speeds and road conditions. The BBW system assists the driver by stopping the vehicle before collision whereas the SBW system, using the sensors input, avoids the obstacle by changing the lane. The results presented in the article suggest that during an obstacle avoidance situation in an urban area, where the vehicle speed is low, an active braking system requires less distance to avoid the collision. Again at low speed if the driving conditions are wet then both systems, BBW and SBW, require the same amount of distance to avoid the collision. However, in a non-urban scenario, where a vehicle is usually moving at a higher speed, the SBW system dominates the BBW system in terms of distance requirement. For the dry conditions the BBW system needs 39% more distance to avoid the collision and for a wet surface it requires almost double the distance as compared to that of a SBW vehicle. These results help to infer that a combination of BBW and SBW can assist the driver to avoid a dangerous situation. With a proper network of auxiliary sensors the collaboration BBW and SBW can even autonomously control the vehicle to avoid a collision. For this work the authors used the information of the available tyre/road friction value in their control algorithm. Such information is obtainable in a test vehicle with the help of costly equipment but in production vehicles the accurate information of such parameters is generally not available.

Niederkofler et al. [Niederkofler 2011] in their publication extended the concept discussed by Ralf Orend in IFAC World Congress 2005. Ralf in his paper [Orend 2005] presented the possibility of achieving the desired vehicle motion by independently controlling the tyre forces at each wheel. However adhering to the theme of the conference his emphasis was more focused on the control strategy. Niederkofler et al. in their paper discussed the development aspect in more detail. They used this novel idea to optimise the mechanical design of the steering system in terms of energy requirement, power output and size, which are important aspects for mass production of vehicles. Furthermore, they exploited the idea of possible vehicle control in the case of a steer actuator failure. Using simulations they have shown a 4WS vehicle having independent steerable wheels can perform better in an actuator malfunction scenario as compared to a front wheel steering vehicle. For this purpose they simulated a lane change manoeuvre using a front wheel steering and a 4WS

vehicle. Both of the vehicles were travelling with a constant velocity of 25 m/s and had to follow a reference path. The results presented by the authors show that the 4WS vehicle is able to follow the desired trajectory even when one of its front wheel actuators failed during the manoeuvre. On the contrary the front wheel steering vehicle became unstable for a similar failure scenario. Based on these finding the authors recommended the rear wheel steering system along with a torque vectoring system to enhance the vehicle's controllability in hazardous driving situations. However, most of the vehicles are designed only with front steering system therefore it will also be useful to identify the ways to bring a vehicle of such configuration under control during an actuator failure scenario.

As the above paper [Niederkofler 2011] suggests that inclusion of a rear wheel steering system benefits in terms of better vehicle handling, Burgio et al. [Burgio 2010] has also used an active rear steering (ARS) system in their work to enhance the vehicle driving and handling behaviour. In the introductory section they have highlighted the fact that the revival of interest into the rear wheel steering technology owes to the recent advancements in the electric drives and control techniques. The authors have put their weight in the favour of an independent wheel steer arrangement over a rack solution in which a single actuator is responsible for the required motion. In their opinion the independent steer solution provides a better dynamic response and helps to reduce the overall size of the steering system. Furthermore they added that an active steering system helps the braking system by operating the wheel in high μ region during the μ split manoeuvres. In this paper they have also designed a controller for an active rear system and evaluated its performance by simulations. For simulation purposes they modified an existing vehicle model available in MSC Adams with an ARS system and compared its performance with that of a passive one. The authors simulated a double lane change manoeuvre and found that the active vehicle is able to complete the manoeuvre, without hitting the pylons, with a speed 8.2 % higher than that of the passive vehicle. Moreover, when a simulation for both of the configurations moving with a same speed was performed, the measured states like yaw rate and front steer angle showed that the vehicle equipped with an active rear wheel steering experienced lower yaw rate values. These results presented by the authors show the effectiveness of ARS technology over a passive vehicle but they did not inlcude a comparison with any other vehicle stability system to discuss ARS effectiveness against it.

Weiskircher et al. [Weiskircher 2011] have evolved the concept a step further and included in-wheel motors instead of a combustion engine as the prime movers. The possibility of independent control on the steering and motion actuators allows a vehicle to be optimised for agility and safety. To study the

concept the authors have used a scaled version of an experimental vehicle equipped with electric drive that provide independent torque for each wheel and a steer-by-wire system that allows the steering control of the front wheels to be decoupled from the steering wheel. In this paper the authors developed a non-linear motion controller and studied the vehicle behaviour. The authors observed that the steering controller response is slower than the electric torque control loop. The authors main emphasis was to apply various control methods and evaluate the control performance and its effect on the energy consumption of the car.

Wang and Wang [Wang 2011b] published an article in which they presented an approach to detect a faulty motor using vehicle dynamics and motion signals. The authors presented this idea to overcome the limitations that other fault diagnosis and fault tolerant control methods, for electric motors, inherit by only monitoring the current and voltages. The authors based their approach on an assumption that the motor control gain reduces when a fault occurs on the motor or motor driver. The controller designed by the authors is meant to maintain vehicle stability and track the desired vehicle motions when an in-wheel motor fails. Once the fault is detected and isolated, the proposed controller readjusts the other motors' motion to relieve the torque demand on the faulty motor. To support their idea the authors built a high-fidelity full vehicle model in CarSim and simulated different manoeuvres. The outcome of J-turn manoeuvre was recorded by measuring vehicle longitudinal velocity, in-wheel motor torques, vehicle yaw rate and trajectory. The result showing the vehicle trajectory suggests that the controller helped the vehicle to follow the reference trajectory when one of its motor went out of order. The velocity and yaw rate of the controlled vehicle also followed the desired values whereas the uncontrolled vehicle was unable to do so. Similar sort of results were obtained when the vehicle was subjected to a single lane change manoeuvre. Although this article is mainly focussed on the in-wheel motor failure and diagnosis but this approach can be used for other electrical systems comprising of electric motors like a steer-by-wire system. This paper is another example of the attention that the fault tolerant approach is getting to make such systems suitable for production vehicles. In this paper the authors assumed that only a single motor is failing at a time and the vehicle speed during the simulations was also kept low especially during the J-turn manoeuvre where the vehicle was moving at the speed of 10 km/h. Therefore, further investigations are required to explore complex scenarios, like failing of two or more motors simultaneously, to verify the effectiveness of the presented approach.

Summary

The above discussion highlights the fact that the active steering system has been popular among researchers for the last few decades. In late eighties and early nineties it saw an initial boom when rear steering capability was introduced on a few production vehicles like Honda Prelude and Mitsubishi Galant. However, the limitation in the available technology at the current time slowed down its momentum. The new generation of electronics and sensing devices helped to revive the concept in the new millennium and few high end production vehicles have been offered with a front wheel steer assist technology (BMW 5-series) and four-wheel-active-steering (Infiniti G37), which help a driver to keep the vehicle on a desired path with minimal effort. Because of the high price tags, such features are currently offered as an optional system. But many of the authors cited above believe that an active steering capability contributes towards the safety and stability of a vehicle and therefore its availability on production models in future is imminent.

Steer-by-Wire systems are an advanced form of active steering systems. This concept enables the researchers to exploit those domains that the conventional or electromechanical steering system cannot offer. Independent wheel steer, compact size, simple structure and less dependency on the fossil fuels are a few of the advantages that make the steer-by-wire system a potential consideration for the future vehicles. Like all evolving technologies steer-by-wire systems have a number of concerns that are highlighted by various researchers. The first argument is *safety* and the consequences in the case of system failure. This concern has given birth to fail-safe and fault-tolerant approaches as discussed by Isermann et al. [Isermann 2002]. The fail-safe approach offers a mechanical backup whereas fault-tolerant approach lacks such an auxiliary arrangement. The first approach although addressing the safety concern in a direct manner but is costly, heavy and does not allow the advantages offered by the electrical systems to be fully exploited. Whereas the second approach, fault tolerant, is gaining more attention because of its applicability to other electrical systems too. Both hybrid and electric vehicles are heavily dependant on the performance of electric motors, just like as steer-by-wire system is. A paper published by Wang and Wang [Wang 2011b] is an example of the attention the fault-tolerant approach is getting. In addition, the manufacturers of the electrical components are trying to improve reliability and integrity to gain the potential market share.

This new type of steering system although fulfils a large number of requirements for steering systems of the future [Du 2006] but there are legal requirements to be fulfilled before bringing such systems on road. Efforts have been made in this direction to cover the legal aspects of this evolving technology.

Steer-by-Wire Working Group is a consortium of more than 20 off-highway vehicle manufacturers, suppliers, and organisations, which is working to define a certifiable reference architecture for a complete steer-by-wire application without mechanical backup for on-road use [web c]. This group's mission also includes the criteria that must be adhered to ensure the safety and functional requirement. They are working hand-in-hand with the TÜV NORD Group, which is a German organisation responsible to validate the safety of products, to secure the future of steer-by-wire systems. In addition to this the revision 2 of UNECE regulation R79 document [web e], which is a regulatory document regarding the steering equipment agreed by several member countries of United Nations, states the provision of steer-by-wire systems on the vehicles.

From the above it can be conceived that once the safety and legal aspects will be covered in a proper manner, the steer-by-wire systems will become an essential part of the future vehicles. This conclusion can be further strengthened by the fact that most of the research work published in the recent past has directly or in-directly had involvement from the major automobile players. However, there are still some grey areas which need to be addressed. The literature mentioned above cover various aspects of the steer-by-wire system but fails to address the physical limitations of the steering actuators. Few authors like [Yu 1994, Wilwert 2003, Weiskircher 2011] have mentioned that delays in response, which can effect the system performance but none has included the actuator dynamics in their work to investigate the consequence. Moreover, as the efforts are diverted to bring these systems to production vehicles; cost is one of the major factors that decide the fate of any new technology. In order to generate the demand from the consumer market it is critical to keep the cost of these systems at par with the conventional steering systems. The majority of the work referred to is either using a high performance actuator or facilitating a lower power motor with the hydro-assist system to get the desired steering action at wheels. So there is a need to evaluate the performance of a steer-by-wire system comprising the low cost actuators without any auxiliary support. In this thesis, such system will be investigated and the effect of its performance on the vehicle handling behaviour will be discussed.

As the steering commands directly effect the lateral handling response of a vehicle therefore in the next section literature related to vehicle lateral handling and modelling will be reviewed.

2.3 Vehicle Modelling

Since the inception of the automobile, the improvement in its performance is a prime area of interest for the researchers. The early vehicles were modi-

fied versions of horsedrawn buggies fitted with single cylinder engines. Noise, vibration, discomfort and unsafe handling were a few of the the common problems among these vehicles [Platt 1968]. The examination of the earlier research work reveals that the power-plant efficiency, chassis design and suspension improvement for better ride were popular domains among engineers at that time. This statement holds strong if one reads Platt's paper [Platt 1968] that encompasses Lanchester's research work in great detail. Dr. F. W. Lanchester was among the leading engineers who contributed a lot towards the automobile research in terms of published papers in journals. However, these publications or his contemporaries work cover little about the lateral dynamics and handling aspect of the vehicle. The reason for this deficiency is linked to the lack of experimental data, explaining the tyre characteristics during lateral motion, at that time [Olley 1946].

The research in the handling domain gained momentum in 1930s when information about the tyre characteristics and their dependence upon the slip angles was first published by a French engineer, *Broulheit* [Broulheit 1925]. Later on a book was published by Becker, Fromm and Maruhn [Becker 1931] on shimmy in automobiles, which included some results of dynamic testing of tyres on rotating drums. Bradley and Allen [Bradley 1930] during their experimental work to assist the investigative research about skidding of vehicles published some results that show increase in the *"Sideway force coefficient"* with increase in the *"wheel misalignment angle"*. The authors used these terminologies to represent the lateral force and the wheel slip angle respectively. These resources are considered as the foremost publications that provided some insight to the researchers about the forces that are generated when tyre moves with a slip-angle. These findings helped engineers like Olley to explore new branches of vehicle dynamics especially its handling characteristics. Olley's comments during the discussion session on Lanchester's paper [Lanchester 1936] explain the vehicle understeering and oversteering phenomenon in a same manner as presented in current text books like Gillespie [Gillespie 1992]. Later on he published articles of his own [Olley 1938, Olley 1946] in which he discussed the useful concepts related to the tyre forces and vehicle response in terms of handling characteristics in a greater detail.

The World War-II diverted all civilian research efforts to meet the wartime goals, which also hampered the progress in the automotive sector. In 1956, a group of researchers from Cornell Aeronautical Laboratory (C.A.L) presented a series of papers [Milliken 1956] in which they used their knowledge of aircraft dynamics and control to investigate the directional characteristics of vehicles when subjected to fixed controlled inputs. This research programme also aimed to investigate the tyre characteristics that are useful in the ve-

hicle stability and control analysis. This research effort was to fill the gap that emerged due to the lack of research efforts in exploring the complex science of vehicle handling. Milliken and Whitcomb in their introductory paper [Milliken 1956] highlighted the concerns with these words *".....In some quarters, apathy prevails toward the complexity of analytical procedures that might be utilised for the study of handling, whereas in others the belief exists that knowledge currently available in practical design is adequate for the foreseeable future"*. Prominent researchers in the automobile domain were aware of such issues and therefore did not find the vehicle research domain at par with that of aircraft one. Olley raised this issue in his paper [Olley 1938] using these words *".....It seems strange that the automobile industry went on for 35 years, building cars piecemeal this way with no real conception of the complete vehicle. Aircraft engineers, on the other hand, got busy from the very start, with wind tunnels and flight tests to find out how their vehicles actually operated"*.

Later Leonard Segel, who was also a member of this C.A.L research team, presented two papers [Segel 1956, Segel 1957] in which he developed and substantiated a linear vehicle model having three degrees of freedom i.e. roll, yaw, and lateral motion. This can be counted as one of the earliest efforts made to investigate the influence of vehicle parameters on its steady-state and transient behaviour. The highlight of these publications is that an extensive experimental work had been undertaken to support the investigation. These experimental results have been utilised to validate the equations of motion that describe the directional behaviour of a vehicle. Segel has termed such vehicle behaviour generated either due to the steering inputs or by external disturbances, as *handling*. The author also discussed the subjective aspects of this term and linked it to following two properties of a vehicle evaluated by a driver:

- *The ease and precision with which it is possible to steer the vehicle or achieve a desired path.*

- *The ease with which this path or handling is maintained.*

Whitcomb [Whitcomb 1956] published a simplified version of Segel's model in his article with the assumption the vehicle roll can be ignored. He presented a two degree of freedom model and suggested that this simplified modelling approach would suffice the approximation requirements for a vehicle restrained from rolling. By using this assumption the authors were able to ignore the vehicle width and combined the wheels in the centre of the vehicle (the classical bicycle model). In this paper the vehicle motion had been investigated

in terms of yawing and lateral degree of freedom. The authors used two different vehicles parameters to study their response characteristics by using the proposed theory. However, like Segel [Segel 1956] the authors had also used a linear tyre model to evaluate the vehicles behaviour even for the high lateral acceleration zone, which raise doubts to the results discussed in the paper. But still this model is a useful tool for linear range investigation and therefore is widely used for vehicle control purposes.

The work published by Hales [Hales 1969] is an extension to the linear case presented above. In his article Hales investigated the lateral behaviour of a vehicle in the steady-state conditions. The quantities of a vehicle which he has analysed in detail are understeer, static-margin and slip/steer gradient. The author analysed these quantities theoretically and experimentally when a vehicle following a steady-state path, circular motion in this case, is perturbed. His findings included that the understeer is the most important measure of vehicle behaviour among the three mentioned earlier. For experimental verification he used a constant radius test procedure and the tethering testing method developed by MIRA [Barter 1969]. In this procedure a test vehicle is fastened with a boom to the heavier tethering vehicle, which is moved in a steady-state manner and measurements of forces and angles are made. The position selected to attach the tether restrained the motion of the test vehicle in the horizontal plane but did not interfere with its roll, pitch, and yaw motions.

The advancements in the computer technology helped the researchers to increase the complexity of vehicle models and analyse more demanding scenarios. Okada et al. [Okada 1973] used computer simulations to study the vehicle behaviour during high lateral acceleration manoeuvres. They used a non-linear vehicle model with seven degrees of freedom, which included yaw, roll, pitch, lift and lateral position of the vehicle along with two degrees of freedom for the steering system, to evaluate the vehicle response in three fundamental motions i.e. circular motion, slalom motion and straight running motion against the disturbances. Garrott et al. [Garrott 1981] simulated a vehicle model having 17 degrees of freedom to analyse its handling capability using severe manoeuvres involving acceleration/braking and cornering. The modelling process extended to development of vehicle models of increased complexity including suspension and other non-linearities. These initial efforts involved deriving the equations of motion manually and then using a suitable computer code to find their solutions. The same has been expressed by Sayers [Sayers 1996]; while shedding light on the history of vehicle modelling in his introductory paragraphs Sayer has highlighted the work that has taken the vehicle modelling from paper and pencil to a computer. He also mentioned the advantages and disadvantages of using multibody programmes

for the same purpose. Although these software tools provide a great amount of information about the vehicle behaviour and does not ask the operators to solve the equations of motion themselves but require an in-depth information about the vehicle and takes longer time to provide the results. Thus the accuracy of results provided by such software tools are highly dependent on the quality of the data available with the user. Sayers presented a simplified multibody model having 18 degrees of freedom, which produced comparable results to that of a full multibody programme.

Blundell [Blundell 1999a, Blundell 1999b, Blundell 2000a, Blundell 2000b] published a series of four papers that explored the contributions of these advanced multibody software in vehicle modelling and handling simulations. He argued that although the vehicle handling performance evaluation is predominantly dependant on the human judgement but the automotive manufacturers still rely on the performance indicators like lateral acceleration, roll angle, and yaw-rate to verify the design success. These indicators help a designer to judge how good a vehicle design is performing with the required handling qualities. Therefore these specialist multibody dynamics programmes have been made available on a commercial basis, which can help a designer to tune the model down to the component level. However, the complexity of vehicle modelling is an ongoing debate between two school of thoughts; industry oriented researchers generally produce complex vehicle models with all the suspension linkages and bushes along with their non-linear properties, whereas the academic researchers put their weight behind simple and efficient modelling techniques. Sharp has expressed similar sort of thoughts in [Sharp 1991]: "*Models do not possess intrinsic value. They are for solving problems. They should be thought of in relation to the problem or range of problems which they are intended to solve. The ideal model is that with minimum complexity which is capable of solving the problems of concern with an acceptable risk of the solution being 'wrong'. This acceptable risk is not quantifiable and it must remain a matter of judgement. However, it is clear that diminishing returns are obtained for model elaboration.*" Blundell in his series of papers developed four vehicle models comprising of varied complexity level of suspension modelling using a commercial multibody software "ADAMS". The handling behaviour of three simpler models was compared with the output of the complex one and evaluated with the experimental results. The simple models showed a good level of accuracy with minimal parameters requirements, which supports the statement by Sharp quoted above.

The two degrees of freedom model has already been mentioned above and Sharp declares it the simplest useful model of the vehicle lateral dynamics [Sharp 2002]. This model is widely mentioned and discussed in the text related to vehicle modelling and handling [Dixon 1988, Ellis 1994,

Gillespie 1992]. Researchers working in the field of vehicle stability and control have extensively used such simple modelling techniques to conduct their work like Ackermann [Ackermann 1990] used the same modelling concept to study the effect of a robust steering on the vehicle handling qualities. Harada [Harada 1995] analysed the the active rear wheel steering strategy using the vehicle bicycle model having two degrees of freedom. Abe [Abe 1999] used an extended version of this modelling approach, known as the planar vehicle model, with the linear tyres. Drakunov et al. [Drakunov 2000] also included the rotational degree of freedom for each wheel while deriving an algorithm for the vehicle yaw control. Ryu [Ryu 2004] utilised both the two degrees of freedom bicycle and planar models in his work to develop vehicle parameters estimators. Similarly Yih et al. [Yih 2005] used a two degrees of freedom bicycle model to support their case that an active steering case can alter the handling characteristics of a vehicle. Bajçinca et al. [Bajçinca 2005] also employed the classical linearised single track model for their investigation related to a robust controller for a steer-by-wire vehicle. Goodarzi et al. [Goodarzi 2008] made use of a two degrees of freedom planar vehicle model to derive a new automatic path control strategy that integrated the steering control and direct yaw control. Kreutz et al. [Kreutz 2009] discussed model based control strategies for an active rear wheel steering system in which they used a linear single track model.

The three degrees of freedom model having vehicle body roll as an additional degree of freedom to the lateral and yaw movement has also been extensively used for vehicle handling studies. This model is also mentioned as the four degrees of freedom model if the vehicle longitudinal speed is not held constant during the analysis. If the distance between the vehicle roll centre and centre of mass of the body is not negligible then at high speed manoeuvres the vehicle roll effects its handling behaviour by influencing the vertical load on each individual wheel. This model has been discussed in detail in the vehicle dynamics text books [Dixon 1996, Abe 2009]. Ro and Kim [Ro 1996] used a linear three degrees of vehicle model with suspension compliance effect to develop a 4 wheel steer system based on a sliding mode controller. Chen and Peng [Chen 2001] developed a three degrees of freedom vehicle model and validated it against the experimental response of a 1997 Jeep Cherokee published by Salaani et al. [Salaani 1999]. They used this model to present an anti-rollover control algorithm for sport utility vehicles. Zheng et al. [Zheng 2006] used an eight degrees of freedom non-linear model to simulate the vehicle behaviour and a two degrees of freedom linear model as the reference model to design a controller for vehicle stability enhancement. Whereas Osborn and Shim [Osborn 2006] used a seven degrees of freedom non-linear model to develop a control algorithm for an independent torque distribution

to each wheel. They validated this model against a *carSIM* vehicle model. Mashadi et al. [Mashadi 2010] in their work used two, four, and eight degrees of freedom vehicle models to present their idea that a controller based on a four degrees of freedom model outperforms the two degrees of freedom controller to a certain extent in severe conditions. The simulation results suggest that both the controllers based on two and four degrees of freedom models perform at par up to an extent where the electric motors, meant for providing counter yaw moment, do not reach to their operational saturation point. Ding and Taheri [Ding 2010b] in their work presented a control algorithm that makes use of active front steering and direct yaw moment control based on the classical two degrees of freedom linear model for the controller design and an eight degrees freedom non-linear model for the vehicle simulation.

Summary

The previous section is an effort to review the modelling techniques that are used to model a vehicle and evaluate its handling performance. The current trend in academia suggests that simple models are preferred in comparison to more complex techniques due to the limitation of vehicle data availability. The researchers have successfully shown that seven and eight degrees of freedom models are able to simulate the vehicle handling behaviour with good correlation to experiments. Moreover, for a controller design, a two degrees of freedom vehicle model is an acceptable approach with the majority of researchers. This approach is simple and requires less computational resource.

Following this approach this thesis will also use a linear vehicle model having two degrees of freedom for the control design purpose and seven and eight degrees of freedom non-linear model for vehicle simulation. The seven degrees of freedom are longitudinal, lateral, yaw motions and angular motion of each wheel. The eighth degrees of freedom is the roll motion of vehicle. The main constituents of non-linearities in such models are tyres therefore the next section will cover the literature related to the tyre dynamics.

2.4 Tyre Modelling

The tyres play a pivotal role in vehicle handling. They are responsible for generating the forces and moments that overcome the aerodynamic resistance and ground disturbances and help to keep the vehicle on the desired path. These forces generated by tyres are of fundamental importance because they are the only directional forces the driver has control over. Moreover, they are one of the major sources that introduce non-linearities to the handling

behaviour. Hence, the representation of tyre characteristics in an analytical study of vehicle dynamics has been an area of interest for a long time. Several simple and complex models have been suggested by various researchers to facilitate this requirement. Tyre models can be classified into two main categories; ***physical*** and ***empirical***. Physical models are an attempt to theoretically describe the tyre forces as function of carcass deformation, tread displacement and friction between the tyre and ground, whereas an empirical formulation uses combination of different mathematical functions to fit the experimental results.

Physical modelling approach

As mentioned in the previous section, while covering the vehicle handling and modelling aspects, the earlier work that sheds light on the tyre characteristics and its ability to generate side forces dates back to mid 1920s and early 1930s when Broulheit [Broulheit 1925], Bradley [Bradley 1930] and Becker et al. [Becker 1931] published their findings gathered during the experimental work. Peng et al. [Peng 1994] termed that era as the time when the study of lateral behaviour of tyres originated and attempts were made to mathematically model the pneumatic tyre. These early attempts were more inclined to represent the tyre characteristics using models that can explain the theory based on some physical phenomenon. The model proposed by Fiala [Fiala 1954] is one such effort and he presented the tyre as a spring-beam structure, as shown in Fig. 2.1. Fiala's work described the tyre behaviour

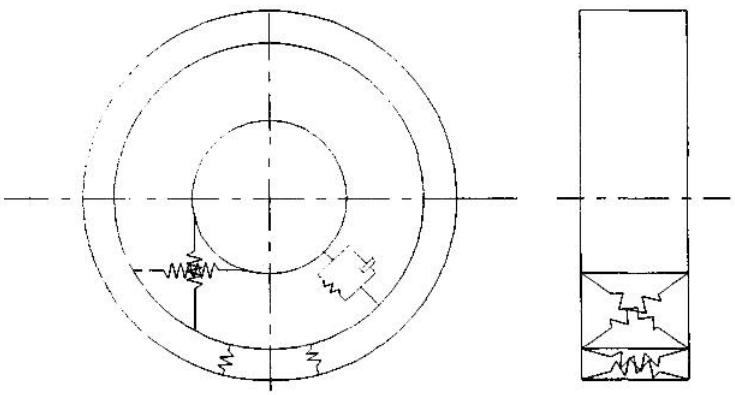

Figure 2.1: Beam model by Fiala [Peng 1994]

using a set of limited parameters that were based on the physical properties of tyres. His work did not take the influence of camber angle on the lateral force generated by tyres. This work gained a lot of popularity among the

researchers as they were able to include a better description of tyre characteristics in their work but this simple model has some limitations. Blundell and Harty [Blundell 2004] have summarised these limitations as follows:

1. *The model cannot represent combined cornering and braking or cornering and driving.*

2. *Lateral force and aligning moment resulting from camber angle are not modelled.*

3. *The variation in cornering stiffness at zero slip angle with tyre load is not considered.*

4. *The offsets in lateral force or aligning moment at zero slip angle due to conicity and ply steer are not represented.*

These limitations restrict their use for pure-slip and zero-camber scenario and therefore can be used in limited conditions.

The brush model proposed by Fromm is another attempt to physically model the tyre from the same era, 1950s, in which the tyre has been modelled as a combination of an elastic tread band and rigid carcass [Peng 1994]. A simple layout of the brush model is shown in Fig. 2.2. The horizontal displace-

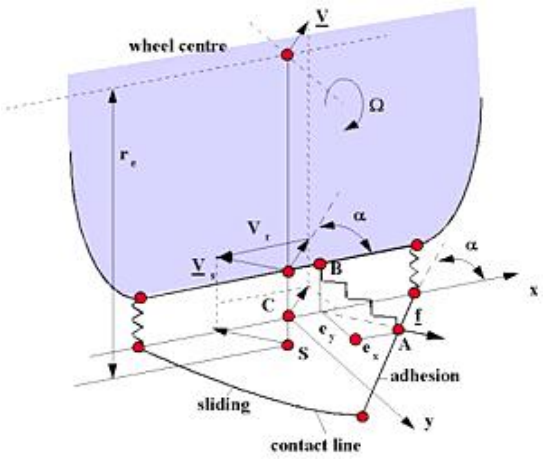

Figure 2.2: Brush model proposed by Fromm [web a]

ment of springs in this figure represents the tread deformation process in the lateral direction. The region marked as *adhesion* shows the tread behaviour when the force of friction is enough to maintain the direction of tread along the wheel heading. The region marked as *sliding* indicates the area where the adhesive forces are not sufficient to prevent the tread from slidding.

Wong [Wong 2001] has compared the basic beam model with the stretched string model proposed by Temple and von Shlippe, which is also a physical model. The major difference between the two is that the stretched string model allows the discontinuities of the slope to be modelled whereas the beam model does not [Wong 2001]. Both of these models include a few parameters that are not easy to obtain and therefore Segel proposed a simpler model that assumes no-sliding criteria thus eliminating such difficult to find parameters [Wong 2001]. All these models are valid for small slip angles. Peng [Peng 1994] also mentioned attempts from Lines and Crolla to use spring and damper combination to represent tyre behaviours.

An advanced form of physical tyre models involves complex structural modelling using finite element method. Such tyre models are generally employed to study the tyre-terrain interaction. Shoop [Shoop 2001] developed a 3-dimensional tyre-terrain finite element model to simulate the impact of deformable terrain on the tyre performance. Such research has a significant importance for the tyres used in the military, agriculture, mining, and construction industry. Oertel [Oertel 1999] developed a tyre model, named as RMOD-K, using the same approach to study the effect of road disturbances on the ride comfort. Such models provide useful information that helps to improve the tyre design, which results in terms of better vehicle mobility and ride comfort.

The above mentioned physical models are good in terms of explaining the theory of what's happening in the contact patch but require number of parameters to do so. For this reason they are computationally expensive and therefore for simulations purpose they are resource hungry [Ding 2010a]. Remarks given by Pacejka in his book [Pacejka 2006] also suggest the same: "*Obviously, the complex physically based models are better suited to examine the effects of the change of a physical parameter such as material stiffness and cross section contour. The more empirically oriented models are better equipped to investigate the effect of changing performance parameters such as cornering and vertical stiffness without effecting remaining properties*". So attempts had been made to use the tabulated test data and their interpolated results to represent the tyre forces during the vehicle simulations. However, Harty and Blundell [Blundell 2007] do not find these models suitable for studies involving variation in tyre design parameters. Moreover, these efforts did not benefit in terms of computational requirements also.

Empirical modelling approach

On the other hand the empirical models are based on curve fitting techniques to reproduce tyre characteristics that have been measured experimentally.

These methods include set of coefficients and parameters, which may not have physical meaning but provide promising results when combined in the form of series, parabolic or trigonometric formulations. These models are comparatively less demanding for computational resources and therefore suitable for problems involving computer simulations of whole vehicle. The empirical formulation in its simplest form has been used by Segel [Segel 1956, Segel 1957], where the steady-state lateral properties of the tyre, collected by the rolling drum equipment experiment, were expressed as a function of wheel's slip angle. For this simple linear relationship to be valid the slip angle must be small.

In 1960s researchers extended their efforts to include combined braking into the models. One of these is a working report published by National Highway Safety Bureau [Dugoff 1969] in the late sixties that provided a base to the authors for publishing a paper [Dugoff 1970] covering the technique to describe lateral and longitudinal tyre forces as analytical function of the normal load, sideslip, and longitudinal slip. This work is an extension of Fiala's work because it does not only give estimation of lateral and longitudinal forces in pure slip conditions but also extend this estimation to the combined slip scenario. This formulation does not cover the dedicated estimation of aligning moment but uses the product of side force and pneumatic trail. This is a crude assumption with a considerable error but the authors neglected it to overcome the limitation in terms of available computational resources at that time. The results obtained in this work were very promising and had qualitative agreement with the limited experimental data available at that time.

In 1975, Krauter [Krauter 1975] published a paper in which he attempted to determine the truck tyre-road characteristics from the truck behaviour measurements. In this work the author used a simplified version of the tyre model, presented by Dugoff et al. [Dugoff 1970], to reduce the simulation resources requirement. The suggested procedure required to compare the behaviour of a full-size truck with that of a simulated one, but due to non-availability of the vehicle a computer model was used instead of a real vehicle. This raise doubts about the procedure applicability in general although the simulated results presented in this paper show the tyre characteristics matching up to an acceptable extent. The suggested procedure in the paper demands repetition of the test manoeuvres in an accurate manner. Moreover, the input to the simulation model should be a true and accurate representation of the input to the real truck. These limitations make difficult to establish the feasibility and practicality of the proposed method.

Bernard et al. [Bernanrd 1977] presented a semi-emprical tyre model, which was aimed to represent the tyre characteristics for a combined brak-

ing and steering manoeuvre. The article included a comprehensive historical overview of efforts made to model tyre forces for the combined slip scenario. The authors especially highlighted the efforts made by Krempl [Krempl 1967] for publishing the data that provided a clearer picture of the interaction between the lateral and longitudinal tyre forces. The authors found these results helpful in establishing a semi-empirical formulation to predict the shear-forces at the tyre-road interface during the combined cornering manoeuvres. Another review paper related to the shear-force development has been published by Pacejka and Sharp [Pacejka 1991], which covers both the physical and empirical formulation in detail. They have included extended discussion on the Brush model giving due consideration to various parameters influencing the model output. The work also covered the empirical formulation for pure and combined slip scenarios. In 1980, Guntur and Sankar [Guntur 1980] presented a simulation friendly version of the Dugoff tyre model [Dugoff 1970] by utilising the assumptions used by Krauter [Krauter 1975] in his work. The method suggested by the authors made use of the friction circle concept to simulate the tyre forces in both slip scenarios, pure and combined.

Another well established empirical tyre model was presented by Bakker et al. [Bakker 1987] in late eighties. They published a new mathematical expression to represent the experimental tyre data obtained from steady-state pure cornering or pure braking experiments. This empirical formula is known as ***magic formula*** in the literature [Wong 2001, Genta 2006, Blundell 2007]. In this work trigonometric functions have been used instead of series function because of its capability to express the measured data with great accuracy. This work gained success to describe the following for pure slip conditions:

- the side force as a function of slip angle
- the brake force as a function of longitudinal slip
- the self aligning torque as a function of slip angle

Bakker et al. [Bakker 1987] showed good correlation between the test data and the tyre curves obtained by the magic formula. This effort proved itself to be the basis for further development. The authors published an improved version of the tyre model in 1989 [Bakker 1989] and 1992 [Pacejka 1992]. The aim of these publications was to describe mathematically the tyre characteristics obtained during pure cornering and braking and then use in a model to simulate the behaviour in a combined slip situation [Bakker 1989].

As mentioned earlier Bakker et al. [Bakker 1987] described their new formulation using trigonometric functions because of the opinion that it is a

reliable technique of representing the tyre data for complex theoretical analysis. Series and polynomial formulation were avoided because of the following reasons cited in Bakker et al. [Bakker 1987]:

- *relatively many coefficients are needed to get a close curve fit,*
- *the resulting curves have a wavy look, which implies that the variation of the slope along the curve differs considerably from that of the measured data,*
- *extrapolation beyond the fitted range often yields large deviations,*
- *in general, the coefficients do not describe the typifying quantities in a recognisable way, which makes it impossible to change these quantities in a controlled, simple way.*

Their new formulation depicts the tyre behaviour over a wider range of operating conditions. For simplicity the formulae are derived for pure traction or acceleration and cornering. For this purpose Bakker et al. [Bakker 1987] conducted experiments under steady-state conditions and measured following quantities:

- side force (lateral) vs wheel slip angle
- brake force (longitudinal) vs longitudinal slip
- self-aligning torque vs wheel slip angle

The speed of the vehicle during the cornering manoeuvre and braking was kept at $70km/h$ and $60km/h$ respectively. In this study the number of coefficients were reduced by linking them with vertical load (F_z) and camber angle (γ). Including the influence of F_z and γ not only helped to reduce the number of coefficients but also provided the option to calculate the forces and torques at vertical loads that were not included in the experiments [Bakker 1987]. In the original work [Bakker 1987, Bakker 1989, Pacejka 1992] the combined slip situation was modelled from a physical point of view [Pacejka 2006]. Later on a purely empirical method based function has been introduced to find the desired characteristics. This empirical weighing function multiplied by the original function to give the interactive effects of slip ratio on the cornering force [Wong 2001].

In addition to the above mentioned models there are several other ideas floated by the researchers working in this field. Peng et al. [Peng 1994] introduced a new lateral tyre model comprising of a parallel spring and hysteric damping unit. Using a spring and damper combination to represent

the tyre carcass and viscous damper to simulate the tyre-road interaction brings it in the category of physical models, which find little attention for handling analysis nowadays. Allen et al. [Allen 1997] proposed a tyre model for both on- and off-road surface conditions. The authors extended the work of Szostak [Szostak 1988] to include the off-road surface conditions. Sharp and Bettella [Sharp 2003] presented tyre forces and moments using the normalization technique. They used the similarity method in association with the Magic formula to reduce its dependency on large number of parameters.These parameters require extensive testing, which is very much demanding in terms of time and associated costs. Brach and Brach [Brach 2009] in their paper compared five different tyre models from three different simulation programmes to evaluate their applicability for accident reconstruction simulations. To conduct their study the authors simulated two hypothetical scenarios using the accident reconstruction software PC-Crash, HVE and VCRware. The aim was to introduce the tyre models that were used to simulate for accidental reconstruction purpose by different simulation programmes.

Summary

The discussion from previous sections suggests that the empirical models are an appropriate choice to simulate tyre behaviour in the analytical studies. Both of the empirical tyre models discussed above are widely used by the researchers for the same purpose. Casanova [Casanova 2000], Blake [Siegler 2002] and Leung [Leung 2010] used magic tyre model by Pacejka in their doctoral work whereas Kleine [Kleine 1998], Buckholtz [Buckholtz 2002], Rossetter [Rossetter 2003], Mirzaei et al.[Mirzaei 2008] and Hsu [Hsu 2009] made use of Dugoff model to simulate tyre forces in their research. Both of the models have their own limitations; magic formula tyre model simulates the tyre forces in an excellent manner but involves number of unknown parameters that require extensive testing to be determined [Rossetter 2003]. Moreover, the magic formula is comparatively heavy than the Dugoff's tyre model in terms of computational resource requirement [Guntur 1980].

On the other hand Dugoff model is prone to show error at higher slip values when compared with the experimental results [Ding 2010a]. But with a limited tyre testing facilities on hand, it is the most appropriate selection by virtue of the reduced number of parameters that are required to be determined by experiments.

2.5 Driver Modelling

The driver modelling as a subject encompasses a very wide spectrum of mathematical techniques that have been used to study the driver behaviour and its effect on vehicle behaviour. Plöchl and Edelmann [Plöchl 2007] give the early driver modelling efforts to mid 1950s and early 1960s when the area was explored to understand the human behaviour as a driver. During that era although the main efforts were diverted towards the mathematical modelling of vehicle dynamics, but the researchers started to investigate the vehicle driver interaction during that time.

Macadam in his work [Macadam 2003] gave a detailed review of the research that has been carried out during the last few decades. Keeping the broadness of the subject in view he focused his effort to cover the control aspect of a driver model that includes steering, braking/acceleration, lateral and longitudinal control of the vehicle. Macadam links this investigation approach to the early work that was carried out to understand the characteristics of the human as a machine controller. A human behaviour during driving can be attributed to several aspects like physical, psychological and emotional. A human collects information through its sensory organs, processes it and then reacts accordingly. These steps are counted as physical limitations and bring a time delay when a human driver model is integrated with a vehicle system.

Limiting a driver model to the task of following a desired path the modelling can be reduced to a control theory problem as discussed by Jürgensohn [Jürgensohn 2007]. Keeping the physical aspects in view a driver model can be presented in the form of a transfer function. For a path following driver model look-ahead or preview utilisation is an important aspect. It is a key property that allows human drivers to adjust their actions in order to keep the vehicle on the desired track.

Sheridan [Sheridan 1966] proposed three preview control models to analyse the human response in a constrained preview environment. One of these models computes its trajectory on the basis of the vehicle's current position and future deviation from the ideal path. The future error estimate is dependant on the look-ahead distance, which is the distance the driver can preview.

A similar approach has been discussed by Guo and Fancher [Guo 1983] where they presented a preview-follower concept to model the closed loop system consisting of a driver and vehicle. The focus of the work was to explore the preview capability of the driver by treating path inputs rather than the external disturbances. The paper explored in detail the effect of driver delay and look-ahead time on the system response. The authors concluded that the 2^{nd} and 3^{rd} order follower outperform the higher order driver models in terms of both damping and response error. The publication also included validation

of simulation results by means of experimental data.

Guo and Guan [Guo 1993] further explored the idea of driver models especially meant for lateral tracking and categorised them as *compensation tracking* and *preview tracking* models. The main differentiation between the two types is that the former does not use the future path information whereas the later one does. In this paper the authors discussed closed loop control models for both scenarios; one in which the vehicle's heading varies very little and other in which this change cannot be ignored like U-turn manoeuvre or figure of 8. For the second scenario the authors proposed transformation of path coordinates of the look-ahead point in to the driver's local coordinate system. This arrangement allows the assumption of small heading angle change to remain valid.

Mokhiamar and Abe [Mokhiamar 2002] used a closed loop driver vehicle system having a first order preview model to analyse their control approach effectiveness for vehicle stability. However, as they were considering the lane change manoeuvre as the bench mark therefore the coordinates transformation was not required. Sharp et al. [Sharp 2000] further enhanced this preview controller concept and strengthened the driver input by adding vehicle lateral offset from the current intended position, difference between the vehicle attitude angle and the tangent angle of the intended path at the current position to the preview path information. These preview inputs and state feedback inputs multiplied by respective gains and summed up to calculate the steer angle required to keep the vehicle on the desired path. However, the authors did not explain in detail how the set of these control gains has to be calculated.

Chatzikomis and Spentzas [Chatzikomis 2009] in their article did not find the heading error feedback at the current location of the vehicle to be an efficient approach. They suggested that the future information for the desired heading angle should be compared with the current heading information to calculate the steer input to strengthening the approach. Both of the previous mentioned articles used the distance covered by the vehicle to calculate its current location and deviation from the ideal path to follow. Moreover, both of the articles suggested dividing the look-ahead distance in to smaller sections for the purpose of error calculation. The results presented in both papers suggest that the driver model is able to follow the ideal path in an efficient manner. However, the initial work required to generate the heading and path curvature data for the ideal path is tedious and becomes further difficult if the desired path involves sharp corners and U-turns. In addition to this both papers do not include the vehicle heading information to conclude whether the vehicle followed the ideal path with the correct orientation or not.

A multi-input driver model presented by Horiuchi and Yuhara [Horiuchi 2000] takes into account the time lag due to informa-

tion processing in the central nervous system and a delay arising due to the dynamics of the muscular system. The inputs to the driver model are the lateral position error and the current yaw angle. Odhams and Cole [Odhams 2009] also considered the neuromuscular delays in their proposed linear preview driver model. These advanced versions are good to improve the theoretical understanding of human steering control but require extensive data because the driver's age and health have significant effect on such properties. Ishio et al. [Ishio 2008] have published experimental results to show that how age affects the parameters, which identify the responsiveness and preview behaviour of a driver. Although this paper was more focused on the vehicle handling quality evaluation but these experiments highlight the efforts involved to tune the proposed driver model.

Summary

The above discussion briefly describes the history and trends followed in modelling the human driver while analysing the vehicle stability. It is quite difficult to cater for all human properties in a single model and therefore different approaches are adopted to study various aspects. In this thesis the purpose of the driver model is to keep the vehicle on the desired track and therefore a preview control technique, discussed in [Abe 2009, Ishio 2008], has been chosen to model the driver behaviour. In order to enable the driver model to follow extreme manoeuvres, like U-turn, the future path information has been transformed into the driver local coordinate system, as discussed by Guo [Guo 1993]. To identify the current location of the vehicle and compare it with the desired position, the travelled distance has been calculated as proposed by Sharp et al. [Sharp 2000].

2.6 Vehicle Control Systems for Handling

In mid nineties Shladover [Shladover 1995] published a review paper that broadly discussed the advancement in vehicle control systems within the past three decades. This paper not only covers the historical development of vehicle control systems but also discusses various methods of their classification. According to the author the term "Advanced Vehicle Control Systems" has been adopted for intelligent systems that provide the driver with safety warnings or assistance in controlling his vehicle, including the extension to full control of vehicle motions. The conceptual development of such ideas dates back to the early forties and fifties but the implementation of advanced control algorithms for automotive applications started in mid seventies and early

eighties when the power of microprocessors was unleashed [Tomizuka 1995]. Nowadays control algorithms are employed for a variety of objectives like enhancing the fuel efficiency, boosting the vehicle performance or increasing the passengers' safety and there is vast research material available covering such aspects. However, this thesis is oriented towards directional stability and handling phenomenon of a vehicle and therefore this section will mainly deal with those publications, which focus more on issues of vehicle dynamics and control. The vehicle handling aspect is of such importance that Shladover's paper predominantly covers the publications related to lateral, longitudinal and integrated lateral/longitudinal control. In general, the control of vehicle motions to improve handling, ride and traction/braking performance is termed as vehicle chassis control.

Among others the two main sources that influence the vehicle handling performance and stability are:

- Steering input
- Tyre characteristics

The automotive researchers explored both of these avenues to improve the vehicle steerability and stability. Four wheel steering (4WS) was one of the hot topic within research circles in eighties and nineties. Ackermann [Ackermann 1990] exploited this idea to control the vehicle yaw rate by employing active front and rear wheel steering. Yu and Moskwa [Yu 1994] also used 4WS to enhance vehicle cornering ability. For this purpose they developed a control algorithm, using the sliding model theory, that coordinates steering and braking commands. This approach employs steering of rear wheels in addition to the front steering angle in order to improve the vehicle's manoeuvrability. This idea of controlling the vehicle handling performance made its way onto few production vehicles such as the Honda Prelude. The rear wheel steering has been implemented either by mechanical linkages or by electromechanical actuators. The mechanical linkage arrangement provides a fixed ratio wheel steering whereas the active steering arrangement allows a greater flexibility. Harada's publication [Harada 1995] is another example of researchers interest in this domain. He used a linear preview driver model in conjunction with a two degrees of freedom vehicle model. He considered the effect of time delay of the actuators and the computation time on the active rear wheel system's performance. The investigation was meant to identify the reasons for quantitative differences between the theoretical control strategies and their practical implementation. He further explored the influence of such delays on the driver's work load and his ability to follow the desired course. The author proposed a control algorithm based on optimal regulator theory

which defines the necessary gains for an effective rear active steering system. Ro and Kim [Ro 1996] again used the idea of 4WS to demonstrate the vehicle's performance enhancement in terms of handling. In their work they have also used a sliding mode controller to autonomously steer the rear wheels. By simulations they have shown that the algorithm is capable of making the vehicle model follow a reference model having shorter rise and settling time for a step steer input. The simulations involved a preview tracking driver model and results have been shown for J-turn, lane change and side wind disturbance scenarios.

In mid nineties, four wheel steering was considered as the most common chassis control for the improvement of handling performance [Furukawa 1997]. The four wheel steering control uses front wheel steer angle, which varies the lateral force, as the control signal. In the low lateral acceleration range the tyre lateral force is proportional to the steering input but once a vehicle enters into the high lateral acceleration range the relationship between the force and steer angle becomes non-linear. Moreover, in high lateral acceleration manoeuvres the vertical loading on the tyres is also effected due to body's roll and it also increases the non-linearities within the system, most significantly the tyres. These variables make it difficult to design the control algorithm for a four wheel steering controller that can perform effectively in both situations [Furukawa 1997]. Keeping these limitations in view the authors, Furukawa and Abe, in this paper investigated the effectiveness of direct yaw control techniques using the tyres' traction forces. According to them "*if the traction force and braking force are properly distributed to the right and left wheels, yaw moment in accordance with the forces distributed will be obtained and thus the vehicle lateral motion can be accurately controlled*". This approach is generally termed as Direct Yaw Moment Control (DYC) and is quite robust while the tyres are functioning within their limits. Tomizuka and Hedrick [Tomizuka 1995] have also identified traction as a key component for robust longitudinal and lateral control. This is one of the reason that the majority of the latest automobiles are equipped with anti-lock braking system (ABS) and anti-slip control systems, which form a part of chassis control systems.

Abe [Abe 1999] further published results of his investigation related to vehicle dynamics and control. In this paper he developed a side slip controller using the sliding surface approach. The results shown in this paper suggest that the direct yaw control approach adopted by the author significantly improves the vehicle performance. However, monitoring the vehicle side slip is a complicated job that requires sophisticated equipment or estimation techniques. Abe has used an adaptive estimator for the purpose, which uses an on-board tyre model to calculate the lateral forces. This method theoretically

helps to get rid of error induced by pseudo-integration of measured lateral acceleration but at the same time raise the question of the complexity of the tyre model to be employed. Vehicle chassis control requires feedback with minimum time delay to keep the vehicle stable, but using a complex tyre model may increase the on-board computational requirements. Keeping this discussion aside, the author showed that adopting DYC instead of 4WS for the purpose of chassis control is more advantageous in terms of performance for the higher acceleration range.

In mid nineties the active suspension systems, 4WS and 4WD systems were investigated and developed extensively but the traction control systems were still unexplored in full [Doniselli 1994]. Mainly it was because of the difficulties arising in splitting the torque between the left and right hand side of the vehicle and implementation of a control scheme using mechanical devices. Doniselli et al. [Doniselli 1994] identified the promising potential of controlling the traction force distribution between the left and right wheels by *torque splitting* and theoretically investigated the overall efficiency of such systems using non-conventional differentials. They considered ten different differentials for splitting the torque between the left and right driving wheels of the same axle and examined the power dissipation (efficiency). They further proposed a torque split control algorithm that enhances the maximum attainable steady-state centripetal acceleration and vehicle responsiveness. The controller processes the yaw rate error and multiply it with a gain factor in a linear manner to calculate the torque split. The numerical simulation results include frequency response, step-steer, lane change, and wind-gust manoeuvres. The results, presented in this paper, show that a vehicle with the proposed control system performs better than a conventional vehicle for all such manoeuvres.

Both 4WS and traction control system have their merits and demerits. Keeping this aspect in view Ackermann et al. [Ackermann 1999] published an article, which discussed the advantages of using an active steering system to complement an individual wheel braking system, a type of traction control system. They made comparison of a stand alone braking system's performance with that of one complemented by an active steering system. The results shown in the paper suggest that a vehicle prone to rollover, because of its high centre of gravity location, can avoid a rollover scenario once fitted with the proposed control system. Horiuchi et al. [Horiuchi 1999], citing the limitations of 4WS system control beyond the linear range, proposed a nonlinear predictive control (NLPC) which integrates active four wheel steering and four wheel torque control. This controller takes longitudinal velocity, lateral velocity and yaw rate as the reference states into account for tracking purpose. The simulation results included in the paper show comparison between 4WS system and an integrated control system. The results presented

suggest a performance improvement and robustness when the integrated controller assists the vehicle, when it is subjected to varying road conditions and braking under μ-split conditions. The integrated control also helped to lower the tyres workload compared to the case of a 4WS vehicle. The tyre workload is a performance measure defined by the authors by taking the ratio between the resultant tyre force and the maximum available tyre force. The authors also included a simple preview predictor driver model to investigate the effects of integrated control on a closed loop driver-vehicle system. The simulation results show that the integrated control assisted the driver to achieve the severe lane change task whereas the 4WS vehicle could not accomplish the manoeuvre.

Doniselli et al. [Doniselli 1994] suggested in their publication that the torque-splitting problems could be avoided if each driven wheel is fitted with an independently controlled engine. Fitting a separate engine for each driven wheel of a production vehicle is not technically and financially feasible. However, the idea of controlling each wheel independently has so much potential attached to it that the researchers kept on exploring it. With recent improvements in electric motor technology and batteries endurance, the researchers found an alternative for the internal combustion engine. The electric motors, other than being environment friendly, have an added advantage of being possible to be controlled more precisely and with a faster response than internal combustion engines [ichiro Sakai 1999]. Moreover, in the form of in-wheel motors they provide an opportunity to control the torque of each drive wheel independently. Thus, the idea of DYC, suggested by Furukawa and Abe [Furukawa 1997], can be employed more conveniently with in-wheel electric motors. Sakai et al. [ichiro Sakai 1999] in their article have explored the idea of using in-wheel electric motors for DYC by torque-splitting/vectoring method. They have presented a robust model matching controller (R-MMC) as a novel method of DYC. The proposed controller has shown good external disturbance rejection properties when the vehicle is following a straight line path; however, the controller has performance limitations when the vehicle is moving on a low frictional surface. All the results, presented in this article, related to R-MMC investigation are based on simulations and do not have any experimental validation.

Sakai et al [ichiro Sakai 2001] published another paper which again explored the advantages offered by an electric motor in the field of vehicle dynamics. This time their investigation is supported by the experiments performed on a vehicle equipped with four in-wheel motors. Sakai et al in their work utilised the motor speed and motor torque instead of the vehicle chassis velocity to detect the wheel's skid. This approach was adopted to eliminate the error associated with estimating the absolute wheel velocity by measur-

ing the acceleration of the chassis or approximating from the velocity of the nondriven wheels during braking or cornering scenarios. The wheel slip controller developed in this work can independently control the wheels rotation. They simulated a rapid braking scenario of a vehicle on a low frictional surface with and without control. Without the controller the vehicle becomes unstable whereas in the controlled vehicle the rapid locking of each wheel is avoided by monitoring the states of the in-wheel motor, thus allowing the vehicle to complete the manoeuvre in a stable condition. Controlling the wheel rotational velocity independently is an example of torque vectoring and the experimental results show that the electric motors have a sufficient potential to replace mechanical clutches and differentials, which are generally employed for torque vectoring purpose.

Esmailzadeh et al. [Esmailzadeh 2001] in 2001 while discussing the potential role of electric motors in the future generation of vehicles predicted that the future electric vehicles would have in-wheel motor configuration instead of a single motor concept introduced by major commercial ventures like General Motors (GM EV1), Toyota (RAV4-EV) and Peugeot (106E). Recent display of SIM-LEI (Leading Efficiency In-Wheel Motor) at Tokyo Motor Show 2011 suggests that the time is not far-off when such vehicles will be available for mass production. Figure 2.3 shows the vehicle designed and produced by SIM-Drive and it has four in-wheel motors, each delivering 65 kW of power, and can travel 333 kilometres on a single charge [web b]. Keeping the future

Figure 2.3: SIM-LEI: An electric vehicle with 4 in-wheel motors

prospects in view Esmailzadeh et al. in their article discussed various control strategies to utilise the independent in-wheel motor for DYC. For this purpose they developed a dynamic vehicle model, with in-wheel motors, having

8 degrees of freedom. The authors have also included a comprehensive tyre model which is able to generate forces in combined slip scenarios. For control purposes a two-layer closed loop control system has been used. The first layer consists of a linear preview driver model and the second layer has 4 independent PI controllers. The simulations were performed using a Simulink model and various open and closed loop manoeuvres were simulated. The results presented in the paper suggest that a vehicle with left and right controlled torque vectoring shows dynamic performance very much similar to those of a complex mechanical differential. An example of such a complex mechanical differential has been discussed by Sawase et al. [Sawase 2006] which has been installed in production vehicles by Mitsubushi Motors Corporation (MMC). This paper discusses in detail how the engineers at MMC have made use of torque vectoring technology to develop an Active Yaw Control (AYC) system, which enhanced the vehicle's performance during a combined slip scenario.

A great number of publications in the recent past suggest that the researchers are gaining momentum in exploring the advantages offered by small size, high torque electric motors. Kaiser et al. [Kaiser 2011] presented a control strategy for torque vectoring a hybrid vehicle using two independent electric motors installed within the rear wheels. These two electrically driven wheels in addition to the front engine powered wheels are used by the authors to generate a desire yaw rate by taking inputs from the steering wheel and acceleration pedal. In this paper a Linear Quadratic Gaussian (LQG) controller is used to calculate the desired yaw rate and a PID controller to cancel the longitudinal disturbances. Simulations performed using a 14 degrees of freedom vehicle model with a modified Dugoff tyre model show that using the torque vectoring method has extended the region of linear vehicle behaviour. Tuncay et al. [Tuncay 2011] presented their efforts to design and manufacture a brushless DC in-wheel motor capable of generating 15 kW of power to drive a hybrid vehicle. The main focus of their paper was the DC motor design but during the experimentation phase they installed the said motors in a Fiat Linea and concluded that the hub type electric drives have a promising future in vehicle technology. A paper by Wang et al. [Wang 2011a] discusses the integration of a power assisted steering and torque distribution control system. In this work the authors explored the independent driving characteristics of four wheel independent drive electric vehicle. The paper includes design of a yaw moment controller and a traction controller based on an optimal longitudinal slip control method. The simulations are performed for both open and closed loop scenarios. The closed loop manoeuvres include a preview follower driver model with a single point preview strategy. The results show that the torque vectoring system integrated within the vehicle helps to reduce the driver's steering effort and increase driving safety.

	SMC	PI/PID	OCT	Fuzzy Logic
Wheel slip/ Traction Control	[Buckholtz 2002] [Zheng 2006] [Goodarzi 2007] [Chu 2010] [Xu 2011] [Kang 2005]	[Osborn 2006] [Ding 2010b] [Esmailzadeh 2001]	[Ghike 2009]	[Tekin 2010]
Yaw Control	[Yoshioka 1999] [Mokhiamar 2003] [Mokhiamar 2006] [Rieveley 2007] [Zhou 2010]	[Bang 2001]	[Shino 2001] [Zheng 2006] [Goodarzi 2008] [Xiong 2009] [Mashadi 2011] [Esmailzadeh 2002] [Park 2001]	[Boada 2005] [Kim 2008] [Tekin 2010]

Table 2.1: Recent control techniques generally used in vehicle dynamics

Table 2.1 shows the control strategies that are commonly used to control the vehicle lateral and longitudinal motions. The terms SMC, PID, OCT stand for sliding mode control, proportional-integral-derivative control and optimal control theory respectively. The table shows that optimal control strategies like Linear Quadratic Regulator (LQR) and Linear Quadratic Gaussian (LQG) are popular among researchers to control the yaw rate of vehicles. SMC because of its robustness properties is also a popular tool for monitoring and regulating the vehicle yaw rate and traction forces. Other control strategies include Fuzzy-logic and PID control.

Summary

The previous section identified the current trends in vehicle dynamics and control. It has been shown that the researchers are mostly use steering, tyre forces and their combination to influence the vehicle motions in lateral and longitudinal directions. Active front and rear steering approaches are very common in the publications that are focusing to enhance vehicle stability through steering control. Torque vectoring is also popular for enhancing the vehicle stability and this technique is gaining further recognition since the concept of in-wheel electric motors has been introduced to replace the heavy and complex mechanical differentials. In some papers yaw control has been suggested by using anti-lock braking system but torque vectoring using a differential or in-wheel electric motors has an added advantage of passenger comfort. The

electric vehicles have a promising future because of their environment friendliness and less dependency on heavy mechanical components. For this reason this thesis will use torque vectoring technique employing in-wheel motors to enhance the vehicle handling performance. For yaw stability LQR controller has been employed whereas keeping the tyre forces non-linearities in view sliding mode controller has been selected to keep the wheel slip within an optimal desired range.

Chapter 3

Vehicle, Tyre and Driver Modelling

Contents

3.1 Introduction

This chapter pertains to development of mathematical models for vehicle, tyre and driver, which will be used in chapters 4 and 5 for further investigation. The first section focuses on the mathematical representation of a vehicle. In this section first a simple two degrees of freedom bicycle model has been discussed and then more complex models have been introduced. The second section is about representation of tyre forces, corresponding moments and

techniques suitable for modelling these forces in computational analyses. It shows the steps that have been taken to develop a tyre model that can represent the tyre characteristics in terms of mathematical equations. This tyre model will be integrated with the vehicle model to simulate the behaviour of a complete vehicle in the later part of this thesis. The last section discuses a driver model, described in terms of a transfer function, that will be utilised to perform closed loop manoeuvres in chapter 5. This driver modelling technique is simple and explores the driver's ability to follow a desired path, by taking the lateral deviation at a look-ahead distance into account.

3.2 Vehicle Modelling

In this section various mathematical models have been discussed which are generally used to replace the physical vehicle in an analytical study. These models are used to analyse the vehicle handling behaviour and give insight to useful information while keeping the investigation costs low. The approach is to begin with the simplest vehicle model available in the literature and move towards the complex mathematical description and discuss their suitability with reference to this thesis. The vehicle modelling is a trade-off between the model's accuracy and its complexity. To keep the computational requirements minimal the vehicle mathematical models are simplified by sacrificing the information accuracy. For a low lateral acceleration handling regime a simple linear vehicle model suffice the purpose whereas for the extreme manoeuvres a more complex non-linear models are employed. Typically this lower range termed as the *primary handling regime* [Dixon 1988] and the lateral acceleration value is less than $0.3g$ for cars and $0.1g$ for trucks. For the higher lateral acceleration range non-linearities start to become more significant because of the lateral wheel load transfer and vehicle roll and therefore cannot be ignored. This handling range is generally termed as the *secondary handling regime* [Dixon 1988].

Therefore it's an analyst discretion to choose the level of complexity and the degree of freedom depending on the problem under investigation. For this thesis both linear and non-linear models have been developed; the linear one to generate the reference inputs for the control purpose and non-linear one to investigate the vehicle-controller interaction. This section begins with the introduction of the coordinate system, which has been used to describe the vehicle motion.

3.2.1 Coordinate system

For vehicle dynamics analysis usually two coordinate systems are of utmost importance. The inertial or earth-fixed coordinate system (X, Y, Z) and the body-fixed coordinate system (x, y, z). As the name suggests the inertial reference system is fixed to the earth at any convenient location and serves to define the orientation and location of the vehicle, whereas the second coordinate system is fixed to the vehicle's centre of gravity and moves along with it. The body-fixed coordinate system helps to define the motion of the vehicle and makes it easier to investigate the forces acting on it.

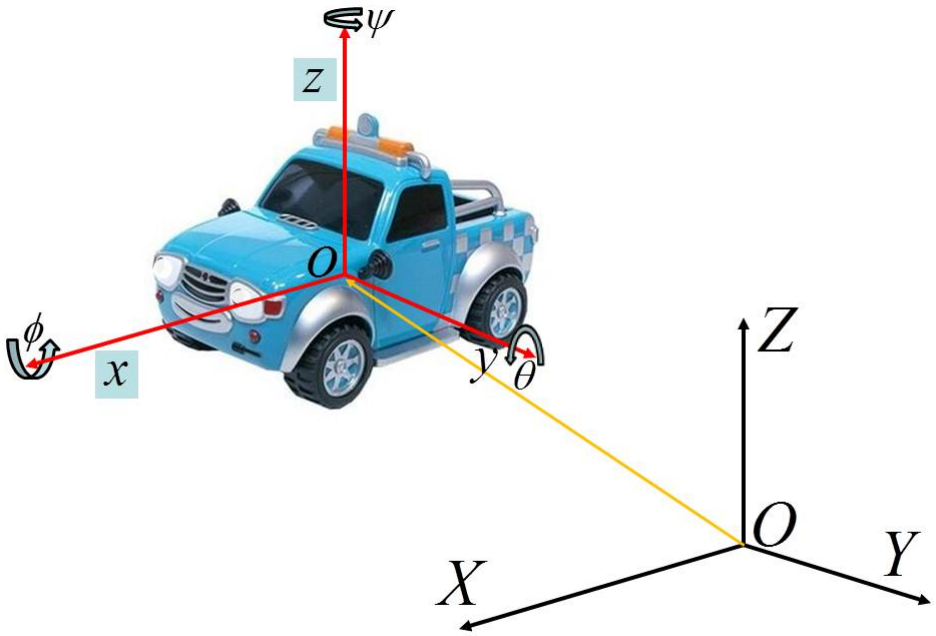

Figure 3.1: ISO coordinate system

For this thesis the ISO coordinate system has been selected to describe the direction of forces and moments for both axis systems. Figure. 3.1 shows the the positive sense of the forces and corresponding moments. The motions about x, y and z axes are termed as roll (ϕ), pitch (θ) and yaw (ψ) respectively.

3.2.2 Two degrees of freedom model (Bicycle model)

The dynamics of a vehicle in its simplest form can be represented by a two degrees of freedom model [Gillespie 1992, Wong 2001, Rajamani 2006], generally termed as bicycle model. The two degrees of freedom are vehicle's lateral

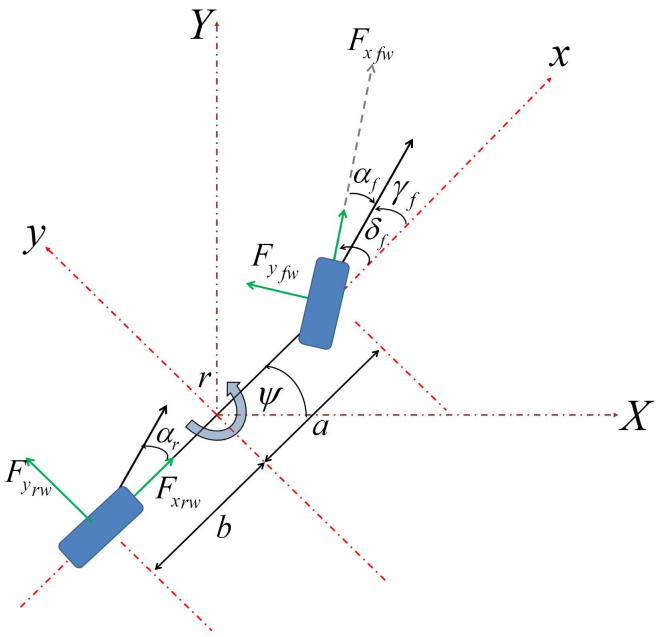

Figure 3.2: Two degrees of freedom *Bicycle* model

and yaw motion. The idea behind this model is based on the following assumptions, which are valid only when the vehicle is doing simple manoeuvres within the primary handling regime.

- the vehicle is moving with a constant longitudinal speed (u =constant) on a flat surface.
- the steering input to front tyres and the corresponding slip angles are small.
- the vehicle structure, including the suspension system, is rigid.
- the track width is small comparing to the radius of turn.
- there is no lateral weight transfer.
- aerodynamic forces are negligible.

With the above assumption the front and rear two tyres can be represented by a single wheel at the corresponding locations; as shown in the Fig. 3.2. To reduce the complexity of the model the heave motion (motion in the vertical direction), roll motion and pitch motion have been ignored. Although the vehicle is moving in the forwarding direction, the constant speed assumption eliminates this degree of freedom. The symbols used in Fig. 3.2 represent the

following parameters and states.

a = distance between the front axle and the vehicle's centre of mass.
b = distance between the rear axle and the vehicle's centre of mass.
ψ, r = yaw angle and yaw rate of the vehicle respectively.
δ_f = front steering angle.
γ_f = front tyre velocity angle.
$F_{x_{fw}}, F_{x_{rw}}$ = longitudinal tyre forces at front and rear respectively.
$F_{y_{fw}}, F_{y_{rw}}$ = lateral tyre forces at front and rear respectively.
α_f, α_r = Front and rear tyre slip angles respectively.

Now applying the Newton's second law of motion, the equations for lateral and yaw motions can be written as:

$$\begin{aligned} ma_y &= \sum F_y \\ I_z\dot{r} &= \sum M_z \end{aligned} \tag{3.1}$$

where

m = mass of the vehicle.
a_y = inertial acceleration of the vehicle in y-direction.
$\sum F_y$ = sum of forces acting on the vehicle in y-direction.
I_z = moment of inertia about z-axis.
$\sum M_z$ = sum of moments acting on the vehicle about z-axis.

It can be observed from Fig. 3.2 that the total force in y-direction and total moment about the z-axis can be written as follows:

$$\begin{aligned} \sum F_y &= F_{y_{fw}} cos\delta_f + F_{y_{rw}} \\ \sum M_z &= F_{y_{fw}} cos\delta_f \times a - F_{y_{rw}} \times b \end{aligned}$$

The inertial acceleration of the vehicle is the combination of two terms, one is the acceleration $\dot{v}$ due to the motion of the vehicle along y-axis and the other one is ur; hence $a_y = \dot{v} + ur$. Substituting these values in Eqn. 3.1, one can write the equation for vehicle's translational motion in lateral direction as

$$m(\dot{v} + ur) = F_{y_{fw}} cos\delta_f + F_{y_{rw}} \tag{3.2}$$

and the equation for rotational motion about z-axis as

$$I_z\dot{r} = F_{y_{fw}} cos\delta_f \times a - F_{y_{rw}} \times b \tag{3.3}$$

In the above equations the term $cos\delta_f$ can be taken as 1 because of the assumption that the steering angle is small. The small steering angle produces small tyre slip, which means that the tyre will be functioning in its linear range.

Within the linear range the tyre lateral force, as discussed later in section 3.3, can be defined as:

$$F_y = C_\alpha \alpha$$

Substitution of this definition of lateral force, in which C_α is the cornering stiffness of the tyre, in Eqn. 3.2 and 3.3 results in:

$$m(\dot{v} + ur) = 2C_{\alpha_f}\alpha_f + 2C_{\alpha_r}\alpha_r \tag{3.4}$$

and

$$I_z\dot{r} = 2C_{\alpha_f}\alpha_f \times a - 2C_{\alpha_r}\alpha_r \times b \tag{3.5}$$

In both of the above equations the term 2 is used to represent the force generated by two tyres in front and rear respectively. From Fig. 3.2 the front and rear tyres slip angles can be defined as follows:

$$\alpha_f = \delta_f - \gamma_f$$
$$\alpha_r = -\gamma_r$$

Using small angle approximations Rajamani [Rajamani 2006] has defined the terms γ_f and γ_r as follows:

$$\gamma_f = \frac{v + ar}{u}$$
$$\gamma_r = \frac{v - br}{u}$$

Substitution of the above values of γ_f and γ_r, in the corresponding equations, defines the tyre slip angles in terms of the vehicle states v, r and u. These tyre slip values can be replaced in Eqn. 3.4 and 3.5 and then these equations can be rearranged to define the system in a state space form as follows:

$$\dot{x} = Ax + Be \tag{3.6}$$
$$y = Cx + De \tag{3.7}$$

where x is a 2×1 state vector having v and r as the state variable, e is a scalar representing the input, which is δ_f in this case. The term y is again a scalar representing the system output. The matrices A (2×2), B (2×1) and C (1×2) define the relationship between the state, input and output variables. The matrices A and B for the bicycle model are given as:

$$A = \begin{bmatrix} \dfrac{-2(C_{\alpha_f} + C_{\alpha_r})}{mu} & \dfrac{2(C_{\alpha_r}b - C_{\alpha_f}a)}{mu} - u \\ \dfrac{2(C_{\alpha_r}b - C_{\alpha_f}a)}{I_z u} & \dfrac{-2(C_{\alpha_f}a^2 + C_{\alpha_r}b^2)}{I_z u} \end{bmatrix}, \quad B = \begin{bmatrix} \dfrac{2C_{\alpha_f}}{m} \\ \dfrac{C_{\alpha_f}a}{I_z} \end{bmatrix} \tag{3.8}$$

whereas the matrices C and D are dependant on the desired output.

3.2.3 Non-linear vehicle model with seven DOF

In the discussion above it has been assumed that the vehicle is moving with a constant speed and the steering angle is very small; however that may not be true for all the cases, therefore the equations of the bicycle model can be tailored to accommodate the effects. Moreover, while a vehicle is moving in the higher lateral acceleration range the lateral wheel load transfer cannot be neglected as it was done in the case of the bicycle model. Therefore, in this section all four wheel of the vehicle are considered, as shown in Fig. 3.3. In

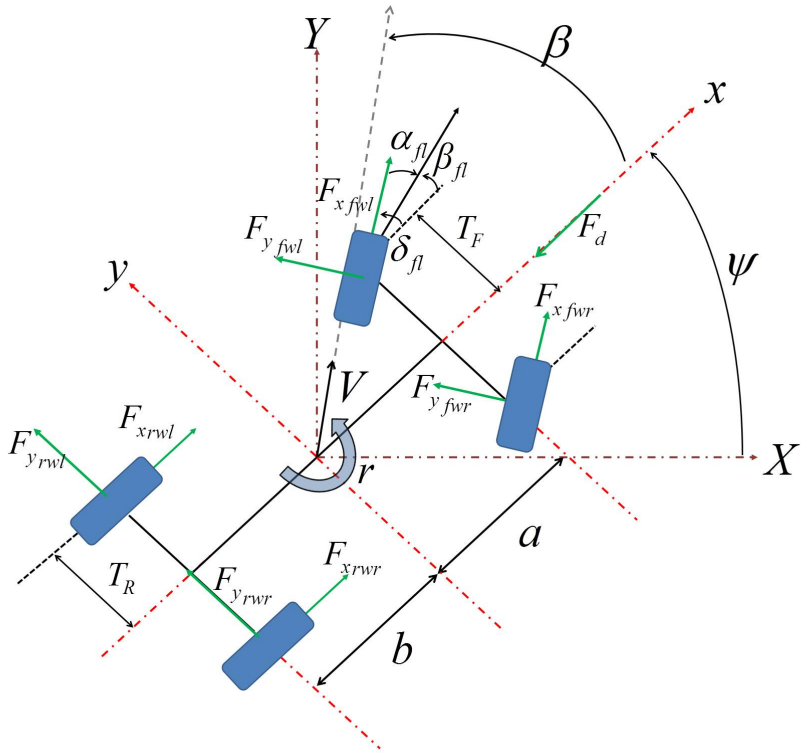

Figure 3.3: Vehicle model with seven degrees of freedom

the bicycle model the longitudinal force generated by tyres does not influence the total moment acting on the vehicle because the track width is neglected. However, in this model the track width is taken into account and therefore the contribution of the longitudinal force towards the total force and moment acting on the vehicle is taken into consideration. In this model the variation in longitudinal acceleration is also considered and hence, the freedom of rotation is introduced for each wheel. These equations of motion allow to introduce a driving or braking torque to the wheels so that the vehicle can be moved with a desired speed. These four degrees of freedom for wheels along with the

lateral, longitudinal and yaw motion of vehicle constituent toward the seven degrees of freedom. In addition, in this model the aerodynamic resistance F_d is also taken into account and has been introduced as a function of the vehicle speed.

The equation of motion for the longitudinal motion can be written as follows, by summing all the forces acting in the x-direction:

$$ma_x = m(\dot{u} - vr) = \sum_{i=1}^{n} F_x \tag{3.9}$$

The equation of motions for the lateral and yaw degrees of freedom have already been defined in Eqn. 3.1 as follows:

$$ma_y = \sum_{i=1}^{n} F_y$$
$$I_z\dot{r} = \sum_{i=1}^{n} M_z$$

Using Fig. 3.3 the sum of forces in longitudinal and lateral direction and the corresponding moments can be written as:

$$\begin{aligned}
\Sigma F_x =& F_{x_{fwl}}cos\delta_{fl} - F_{y_{fwl}}sin\delta_{fl} + F_{x_{fwr}}cos\delta_{fr} - F_{y_{fwr}}sin\delta_{fr} + F_{x_{rwl}} + F_{x_{rwr}} - F_d \\
\Sigma F_y =& F_{x_{fwl}}sin\delta_{fl} + F_{y_{fwl}}cos\delta_{fl} + F_{x_{fwr}}sin\delta_{fr} + F_{y_{fwr}}cos\delta_{fr} + F_{y_{rwl}} + F_{y_{rwr}} \\
\Sigma M_z =& (F_{x_{fwl}}sin\delta_{fl} + F_{y_{fwl}}cos\delta_{fl} + F_{x_{fwr}}sin\delta_{fr} + F_{y_{fwr}}cos\delta_{fr}) \times a \\
& -(F_{x_{fwl}}cos\delta_{fl} - F_{y_{fwl}}sin\delta_{fl} - F_{x_{fwr}}cos\delta_{fr} + F_{y_{fwr}}sin\delta_{fr}) \times T_F \\
& -(F_{y_{rwl}} + F_{y_{rwr}}) \times b - (F_{x_{rwl}} - F_{x_{rwr}}) \times T_R
\end{aligned} \tag{3.10}$$

The term F_d mentioned above is usually called drag force and is equal to $C_d u^2$, where C_d is the drag coefficient of air. Other force components in the above equations are tyre forces and are dependant on the tyre slip angle, discussed in detail in the section 3.3. As discussed for the bicycle model the slip angle for each tyre can be give as:

$$\begin{aligned}
\alpha_{fl} &= arctan(\frac{v + ar}{u - T_F r}) - \delta_{fl} \\
\alpha_{fr} &= arctan(\frac{v + ar}{u + T_F r}) - \delta_{fr} \\
\alpha_{rr} &= arctan(\frac{v - br}{u + T_R r}) \\
\alpha_{rl} &= arctan(\frac{v - br}{u - T_R r})
\end{aligned} \tag{3.11}$$

The above definitions of tyre slip angles are dependant on the corresponding velocities of each tyre and discussed in detail in various text books like Milliken and Milliken [Milliken 1996] and Genta [Genta 2006]. The terms T_F and T_R are the track widths at front and rear respectively, as shown in Fig. 3.3. The above equations contain the term *arctan* because the small angle approximation is no more valid for this model.

Figure 3.4 shows the longitudinal motion of the front left wheel. The wheel is moving in the forward direction with an angular velocity ω_{fl} because of the driving torque τ_{fl} acting on it. The term R_{fl} represents the effective radius of the wheel and $F_{x_{fwl}}$ is the longitudinal tyre force. The rotational equation

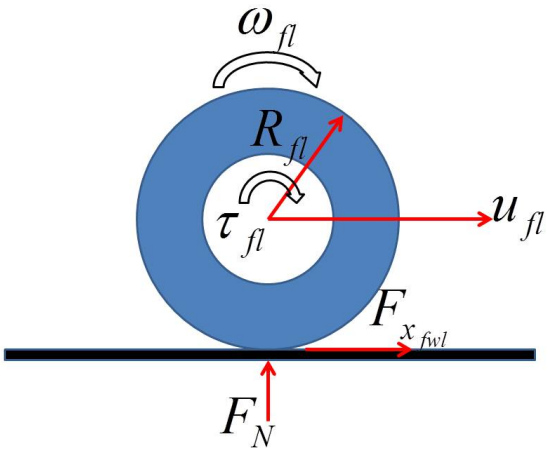

Figure 3.4: Longitudinal wheel model

of motion for this wheel can be written as:

$$\begin{aligned} I_{fwl}\dot{\omega}_{fl} &= \tau_{fl} - R_{fl}F_{x_{fwl}} \\ \dot{\omega}_{fl} &= \frac{1}{I_{fwl}}(\tau_{fl} - R_{fl}F_{x_{fwl}}) \end{aligned} \tag{3.12}$$

I_{fwl} and ω_{fl} in the above equation represent the wheel's moment of inertia and its angular velocity respectively. Following the same strategy equations of motion for other tyres can be given as:

$$\dot{\omega}_{fr} = \frac{1}{I_{fwr}}(\tau_{fr} - R_{fr}F_{x_{fwr}}) \tag{3.13}$$

$$\dot{\omega}_{rr} = \frac{1}{I_{rwr}}(\tau_{rr} - R_{rr}F_{x_{rwr}}) \tag{3.14}$$

$$\dot{\omega}_{rl} = \frac{1}{I_{rwl}}(\tau_{rl} - R_{rl}F_{x_{rwl}}) \tag{3.15}$$

3.2.4 Non-linear vehicle model with eight DOF

In the previous section it was assumed that the vehicle mass is a single entity and the forces acting on it does not create a rolling moment. However, to study the effect of rolling moment on the vehicle handling behaviour, a vehicle can be considered as having sprung and unsprung masses. The elastic nature of suspension system allows the sprung mass to lean sidewards during the extreme manoeuvres. The sprung mass has this roll movement about a fixed axis, which is termed as the roll-axis. During the high lateral acceleration manoeuvres the roll effect cannot be ignored because of its contribution towards the tyre forces in the form of wheels' load variation. As discussed earlier the increase in the wheel load beyond a certain point pushes its force producing capability into a non-linear region, therefore inclusion of a non-linear tyre model makes the vehicle representation more realistic.

Taking roll into account this model has the following eight degrees of freedom, as shown in Fig. 3.5:

- Longitudinal translation, u.
- Lateral translation, v.
- Yaw movement about the z-axis, ψ.
- Roll movement of the sprung mass about the roll axis, ϕ.
- Rotation of the each wheel, ω_i (where i represents each wheel of the vehicle).

Abe [Abe 2009] has used the Newtonian approach to solve for the equations of motion for this complex model. However, the Langrangian approach simplifies the solution for models of such complexity to a great extent [Gregory 2006]. Crolla [Crolla] has derived an eight degree of freedom vehicle model using the same approach and will be used in this thesis. The equations of motion for the model are given below whereas the detailed deriva-

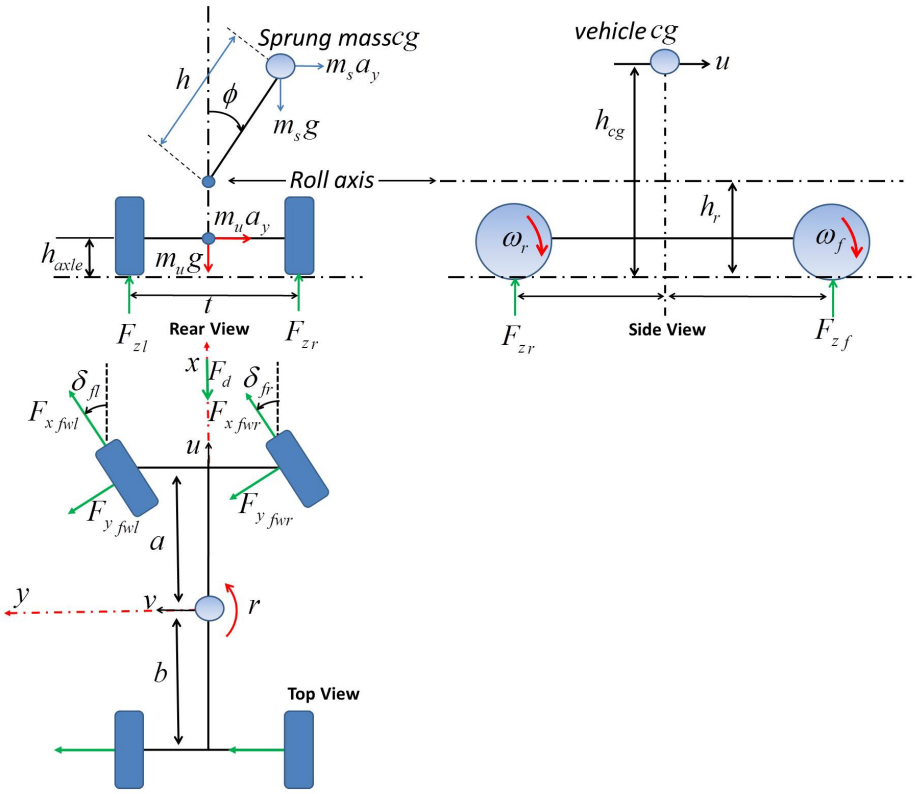

Figure 3.5: 8 DOF vehicle model

tion is given in Appendix B.

$$\dot{u} = \frac{1}{m}(mvr + \sum_{i=1}^{n} F_x + m_s h\dot{r}\phi - F_d) \tag{3.16}$$

$$\dot{v} = \frac{1}{m}(-mur + \sum_{i=1}^{n} F_y - m_s h\ddot{\phi}) \tag{3.17}$$

$$\dot{r} = \frac{1}{I_z}(\sum_{i=1}^{n} M_z + I_{xz}\ddot{\phi}) \tag{3.18}$$

$$\ddot{\phi} = \frac{1}{I_{xx}}[\sum_{i=1}^{n} M_x - m_s h(\dot{v} + ur) + I_{xz}\ddot{r}] \tag{3.19}$$

In the above equations $\sum_{i=1}^{n} F_x$, $\sum_{i=1}^{n} F_y$ and $\sum_{i=1}^{n} M_z$ have already been defined above in the Eq. 3.10, whereas the term $\sum_{i=1}^{n} M_x$ is equivalent to:

$$\sum_{i=1}^{n} M_x = [m_s gh - (K_{\phi f} + K_{\phi} r)]\phi - (C_{\phi f} + C_{\phi r})\dot{\phi}$$

Moreover, the term m_s denotes the sprung mass of the system, similarly the unsprung mass is represented by m_{us}. The total mass of the vehicle is combination of sprung and unsprung mass and is denoted by the term m in the above equations. $K_{\phi f}$ and $K_{\phi r}$ are the torsional stiffness coefficients for front and rear side respectively, whereas $C_{\phi f}$ and $C_{\phi r}$ denotes the constants known as torsional damping coefficients. The rotational equation of motion for each wheel is same as discussed in section 3.2.3.

3.2.5 In-wheel motor model

The seven and eight degrees of freedom models, both assume that the wheels rotation is because of torques acting on them. This torque is supplied to each wheel independently through an electric DC motor fitted within it. The equations of motion for a brushed DC motor [Ogata 2003] can be given as follows:

$$L_m \frac{dI}{dt} = E - R_m I - K_b \omega_m \tag{3.20}$$

$$J_m \frac{d\omega_m}{dt} = K_t I - B_m \omega_m - \tau \tag{3.21}$$

where E is the voltage applied to the motor, L_m is the inductance of the motor, I the current through the motor windings, R_m the motor winding resistance, K_b the motor's back electro magnetic force constant, ω_m the rotor's angular velocity, J_m the rotor's moment of inertia, K_t the motor's torque constant, B_m the motor's viscous friction constant, and τ_E the torque applied to the rotor by an external load.

The signal E, in Eqn. 3.20, is supplied to the DC motor by the yaw controller, discussed in Chapter 5. This voltage signal generates motor torque τ_m, which is equivalent to $K_t I$ given by Eqn. 3.21. The motor torque is transferred to the corresponding wheel through a reducer of ratio β_r and efficiency η_r, as discussed by Economou [Economou 1999]. Hence, the torque acting on the wheels can be calculated using the following equation, where i represents the position of each wheel. Figure 3.6 shows the motor model developed in Simulink.

$$\tau_i = \beta_{r_i} \eta_{r_i} \tau_{m_i} \tag{3.22}$$

3.2.6 Wheel load transfer

When the vehicle is in motion it is not mandatory that the loads acting on the wheels remain symmetrical. The wheel load difference becomes more

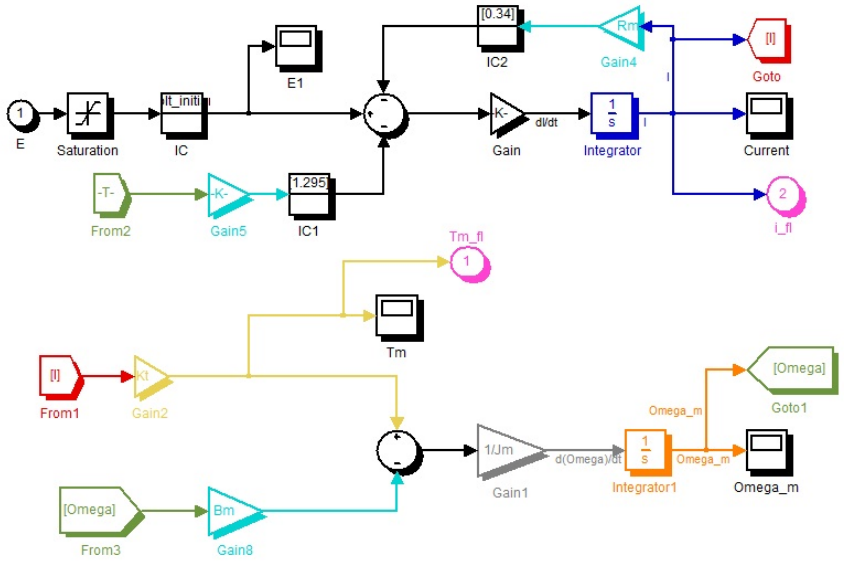

Figure 3.6: Simulink model of the DC in-wheel motor

prominent when the vehicle is accelerated/deaccelerated or when the vehicle enters into a cornering manoeuvre. During longitudinal acceleration mode the load transfers from the front axle to the rear axle, whereas while braking the load transition in the opposite direction takes place. Similarly during a cornering scenario the load shifts from the inner side to the outer one due the lateral force acting on the vehicle body. This effect is pronounced if the vehicle centre of gravity is located farther from its roll centre. The load shift from inner to outer side is same in magnitude therefore the wheel load on either side can be calculated by adding or subtracting the load shift value from the static load acting on the outer and inner wheels respectively.

During dynamics motion it is not convenient to determine the varying load on each wheel. However, with some assumptions the matter can be simplified and the forces can be approximated that cause the change. These assumptions along with the longitudinal and lateral load transfer calculation have been discussed in detail in many texts e.g. [Milliken 1996, Abe 2009]. In this thesis it has been assumed that the vehicle has attained steady state therefore the longitudinal acceleration is negligible and hence the longitudinal load transfer. Neglecting the longitudinal acceleration the lateral load transfer F_T is influenced by the following:

- Effect of body roll
- Effect of lateral acceleration
- Effect of unsprung mass

Suppose if the vehicle enters into a left turn then the left wheels of the vehicle experience less load as discussed above. Reference made to Fig. 3.5 the moment due to a small roll angle can be written as:

$$M_s = m_s a_y h cos(\phi) + m_s g h sin(\phi) \tag{3.23}$$

The force exerted on the roll centre due the lateral acceleration acting on the vehicle body is:

$$F_{ys} = m_s a_y \tag{3.24}$$

The load shift due the lateral acceleration action on the unsprung mass is equivalent to $m_u a_y$. Taking moment about the left wheel the lateral load transfer can be written as:

$$F_T = \frac{M_s + F_{ys} h_r + m_u a_y h_{axle}}{T_f} \tag{3.25}$$

The moment M_s is supported mainly supported by the vehicle suspension system therefore it can be related to the spring and damping coefficients in the following manner:

$$M_s = -K_\phi \phi - C_\phi \dot{\phi}$$

Similarly the lateral force F_{ys} can be distributed between the front and rear sides by multiplying with the corresponding terms. Taking what discussed above into account the vertical load on each wheel of a vehicle taking a left turn can be written as follow:

$$Fz_{fl} = \frac{mgb}{2l} - \frac{F_{ys} h_r b_s}{lt} - \frac{m_{uf} h_{uf} a_y}{t} - \left(\frac{-K_{\phi f}\phi - C_{\phi f}\dot{\phi}}{T_F}\right) \tag{3.26}$$

$$Fz_{fr} = \frac{mgb}{2l} + \frac{F_{ys} h_r b_s}{lt} + \frac{m_{uf} h_{uf} a_y}{t} + \left(\frac{-K_{\phi f}\phi - C_{\phi f}\dot{\phi}}{T_F}\right) \tag{3.27}$$

$$Fz_{rr} = \frac{mga}{2l} - \frac{F_{ys} h_r a_s}{lt} - \frac{m_{ur} h_{ur} a_y}{t} - \left(\frac{-K_{\phi r}\phi - C_{\phi r}\dot{\phi}}{T_R}\right) \tag{3.28}$$

$$Fz_{rl} = \frac{mga}{2l} + \frac{F_{ys} h_r a_s}{lt} + \frac{m_{ur} h_{ur} a_y}{t} + \left(\frac{-K_{\phi r}\phi - C_{\phi r}\dot{\phi}}{T_R}\right) \tag{3.29}$$

The above equations are based an assumption that roll centre height at front and rear is same i.e. h_r because the experimental vehicle used for this work had symmetry, which may not be case for other vehicles. Moreover, if the unsprung mass weighs very less then the vehicle centre of gravity and sprung mass centre of gravity can be considered to be located at the same position. In such case a_s and b_s, which are the distances of sprung mass COG from the front and rear axles respectively can be replaced by a and b in the above equations. These load equations have been used in the Simulink model to determine the individual wheel load in order to calculate the tyre forces.

3.3 Tyre Modelling

This section is aimed to develop basic understanding of the tyre forces; how they are generated and what factors influence them. This section also discusses various mathematical models that have gained popularity among researchers to simulate tyre behaviour in vehicle modelling. All this effort is directed towards selecting a suitable tyre model that can simulate realistic tyre behaviour with an appropriate computational requirement.

3.3.1 Composition and construction

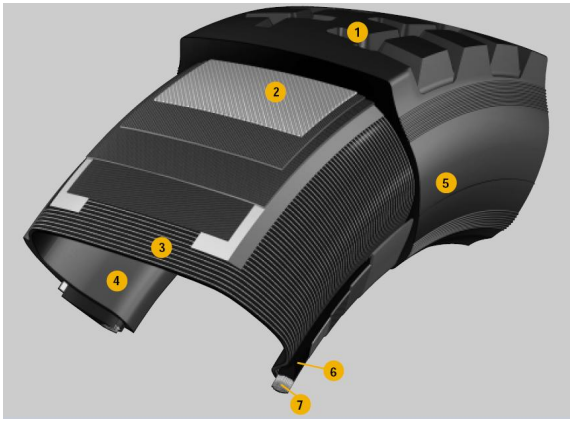

1	Tread
2	Steel belt
3	Fabric casing
4	Inner lining
5	Side wall
6	Bead reinforcement
7	Bead core

Figure 3.7: Construction of a radial tyre [web d]

A modern radial tyre for a wheeled vehicle is composed of rubber, as a major element, along with the fabric casing, nylon and steel-cords as shown in Fig. 3.7. The tyre's construction has a great influence on the vehicle ride, longitudinal performance and handling. The outer surface of a tyre that is called *tread* and is supported by a steel and textile plies forming the internal structure. The combination of visco-elastic response of rubber along with the stiffness and damping properties of the other structural elements makes the tyre dynamics quite complex.

3.3.2 Tyre coordinate system

Defining a coordinate system for tyre/road interaction facilitates the study of events happening in and around the contact patch. There are two popular coordinate or axis systems, named as SAE and ISO, which describe the forces and moments generated by a tyre. This work employs the ISO axis system to define tyre forces, to maintain consistency with the vehicle modelling approach. The coordinate system shown in Fig. 3.8 is known as the ISO tyre axis

system [sta 1992]. The intersection of the wheel plane and the ground plane is termed as x-axis and its positive sense is in the direction of the wheel heading. The y-axis lies at 90° to the x-axis in the ground plane and its positive sense is in the left hand direction of the wheel. The z-axis is perpendicular to the ground plane and its positive sense is in the upward direction. The ISO system is gaining popularity and Blundell [Blundell 2004] predicts it to be the coordinate system of the future.

3.3.3 Forces and moments

As mentioned earlier, the composition of a tyre constituents viscoelastic rubber in order to assist the suspension system in isolating the vehicle from the road disturbances. Due to such elastic structural arrangement when the tyre comes in contact with the ground, a portion of its structure deforms. The deformed portion in contact with the ground is generally referred as the ***contact patch*** in the relevant literature [Giles 1968] and serves as the origin of forces and moments that are required to steer, accelerate and decelerate a vehicle. Ramji et al [Ramji 2002] has stated these longitudinal and lateral forces to be mainly dependant upon the tyre elastic properties at small longitudinal and lateral slip values. As they increase the contribution of tyre elastic properties to these forces decreases and that of tyre/road friction increases. At large slip angles or longitudinal slip the tyre/road friction becomes the major factor in determining the tyre dynamic properties.

Figure 3.8 shows three forces originating from the contact patch. These

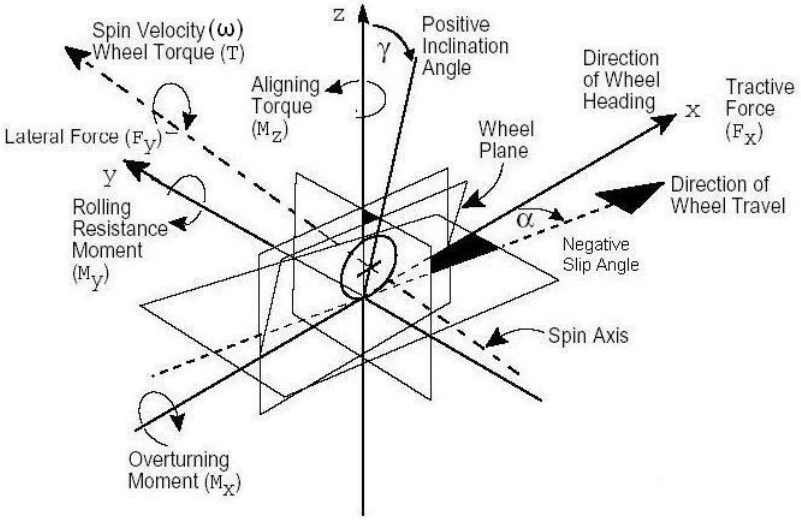

Figure 3.8: ISO tyre coordinate system [sta 1992]

forces are components of the resultant force acting on the tyre due to its interaction with the road surface. The force component acting along the x-axis is generally known as tractive or longitudinal force (F_x), whereas the component in the Y-direction is termed as lateral force (F_y). The force acting along the Z-axis is known as normal force (F_z). Similarly there are three moments acting on the wheel. Overturning moment (M_x) acts about the X-axis, rolling resistance moment (M_y) is the moment about the Y-axis whereas the aligning moment (M_z) acts on the tyre about the Z-axis. For the handling analysis the longitudinal (F_x) and lateral (F_y) forces and aligning moment (M_z) are of prime interest [Svendenius 2003]. These forces and moment will now be discussed in more detail.

3.3.3.1 Longitudinal tyre force

The wheel is said to be free rolling when its rolling velocity (V_r) is equal to the longitudinal velocity (V_x) of its centre. If a driving or braking torque is applied to a free rolling wheel, the friction between the tyre and the ground surface deforms the tyre tread thus producing a tractive or longitudinal force (F_x), see Fig. 3.9, which increases or decreases the rolling velocity of the wheel. Due to the highly deformable nature of the tyre components, the deformation and the force generation phenomenon is not very simple to understand [Tielking 1974].

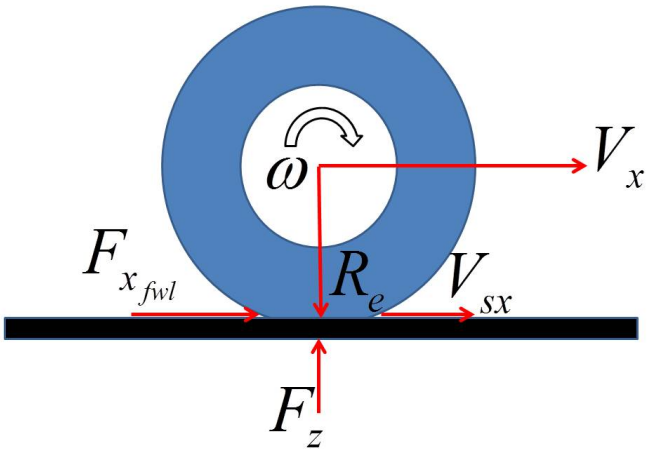

Figure 3.9: Side view of a wheel under traction (Adopted from Brach and Brach [Brach 2000])

According to the definition of a free rolling wheel:

$$V_x = V_r$$

Blundell [Blundell 2004] has defined the longitudinal velocity of the wheel as $V_x = \omega R_e$, where ω is the rotational speed of the wheel and R_e is its effective rolling radius. Using this relationship the rolling velocity of the wheel can be defined as:

$$V_r = \omega R_e \tag{3.30}$$

When braking torque is applied on a free rolling wheel, the contact patch moves in the backward direction. At the same time, due to the braking effect the angular velocity of the wheel decreases and these two factors in-conjunction with the adhesive force, present between the front tread elements and the ground, elongate the rubber material available within the contact area. This phenomenon continues till the the point is reached where the friction force is not sufficient enough to balance the elastic deformation force and sliding occurs. For these reasons the value of V_x and V_r do not remain the same as in the free rolling case. The difference between these is termed the ***longitudinal slip velocity*** (V_{sx}) and can be written as:

$$V_{sx} = V_x - V_r \tag{3.31}$$

Dividing V_{sx} by V_x gives a new quantity generally termed as the ***longitudinal slip parameter*** (S_x). It is a custom to describe tyre-forces as functions of the slip rather than the slip velocity [Svendenius 2003].

$$\begin{aligned} S_x &= \frac{V_{sx}}{V_x} \\ &= \frac{V_x - V_r}{V_x} \\ &= \frac{V_x - \omega R_e}{V_x} \end{aligned} \tag{3.32}$$

Figure 3.10 shows a graph between the longitudinal slip and longitudinal force. The curve falls down after touching the peak F_x value. Experiments have shown that the longitudinal force is maximum when the longitudinal slip is somewhere between $0.15 \sim 0.20$ [Wong 2001]. In order to keep F_x at the maximum, the value of V_x and V_r should decrease at the same rate. But due to the contact patch elongation and sliding phenomenon this does not happen and V_x decreases by lesser amount. For this reason the tyre longitudinal force is characterised by two different friction coefficients. $\mu_p F_z$ gives the peak value of the longitudinal force whereas $\mu_s F_z$ at $S_x = \pm 1$ shows the tractive force at pure sliding condition. Where F_z is the vertical force acting on the tyre and μ_p and μ_s are the peak and sliding values of the coefficient of road adhesion, respectively. Referring to Fig. 3.10, for the linear range the longitudinal force can be given as:

$$F_x = C_{S_x} S_x \tag{3.33}$$

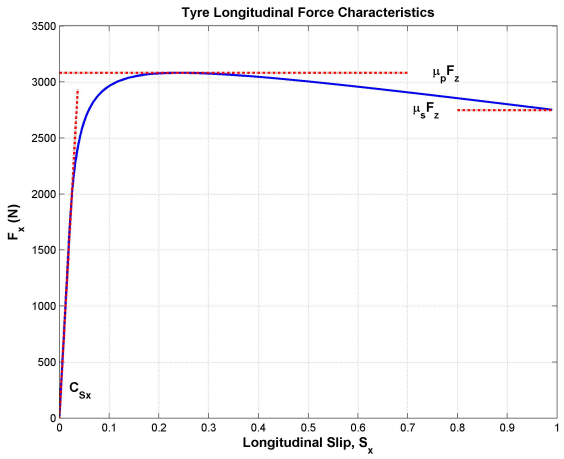

Figure 3.10: Effect of longitudinal slip on F_x

where

$$C_{S_x} = \frac{\partial F_x}{\partial S_x}|_{S_x=0}, \text{ longitudinal tyre stiffness parameter in N}$$

The value of V_{sx} becomes negative when V_x does not increase at the same amount as V_r increases. This situation is termed as sliding and generally occurs on a surface having low coefficient of friction. When the driving torque is applied the rotational velocity of the wheel increases but the vehicle does not move in the forward direction in the same manner. This difference in both velocities makes the value of V_{sx} negative.

For a locked wheel the angular speed ω reduces to zero and hence S_x becomes unity; whereas for a free rolling wheel the value of S_x is zero. Some texts like Pacejka [Pacejka 2006] use negative sign to define longitudinal slip for braking and positive slip for the driving torques. Following this convention the longitudinal slip can be written as:

$$S_x = \frac{\omega R_e - V_x}{V_x} \tag{3.34}$$

In this text the above definition for the slip parameter will be used.

3.3.3.2 Lateral tyre force

In the previous section longitudinal tyre force has been discussed, which helps to accelerate or brake the vehicle. However, in order to change the direction or steer the vehicle, the lateral force produced by a tyre is of utmost importance. Lateral tyre force is principally the function of tyre slip (α) and camber (γ) angles. Reference to Fig. 3.8, the tyre slip is the angle between the x-axis

and the direction of the horizontal velocity, whereas camber is the measure of angle between the xz-plane and the wheel plane. For a zero camber scenario the lateral tyre force is generally termed as ***cornering force*** whereas for the zero slip angle condition the lateral force due to camber is termed as ***camber thrust***. For the same angle, the slip produces more lateral force than the camber therefore it is counted as the major contributor towards the total lateral force generated by a tyre.

Experimental results have shown that the cornering force acts as a linear function of slip angle up to some extent and then enters into non-linear regime, as shown in Fig. 3.11. For a passenger car tyre this start of the deviation from linear lies somewhere between $4° \sim 5°$, whereas the maximum force point lies at about 18° [Wong 2001]. Like tractive force the cornering force is also a function of tyre deformation but this time the deformation is in the lateral direction.

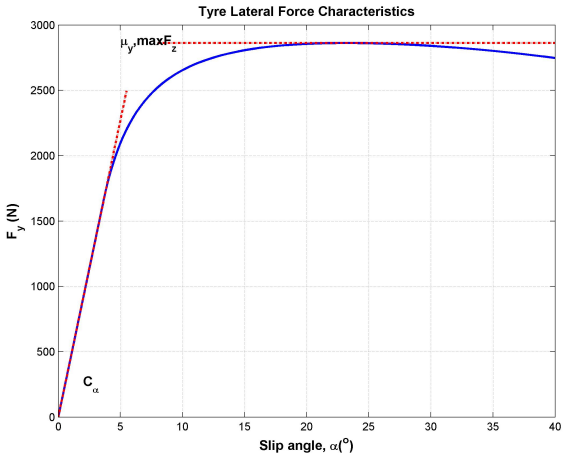

Figure 3.11: Lateral force versus tyre slip angle

Other factors that effect the tyre cornering behaviour include the normal force acting on it and its inflation pressure. Initially a small increment in the normal load generally increases the cornering force in a linear manner but later the relationship becomes non-linear. This sort of behaviour can effect the tyre performance during a turning manoeuvre due to load transfer. Moreover, variation in the normal force and inflation pressure varies the size of contact patch which directly effects the forces and moment generated.

In the linear region the lateral force [Wong 2001] produced by the tyre due these forces can be defined as follows.

$$F_y = C_\alpha \alpha + C_\gamma \gamma \tag{3.35}$$

where

$C_\alpha = \frac{\partial F_y}{\partial \alpha}|_{\alpha=0}$, lateral tyre stiffness parameter in N/deg
C_γ = Camber stiffness

3.3.3.3 Self aligning moment

The lateral deformation of tyre tread, due to the slip angle, is greater towards the rear as compare to the front of the contact patch. Therefore the lateral force generated is not balanced and the resultant force does not act at the centre of the contact patch, as shown in Fig. 3.12. Its line of action is somewhat

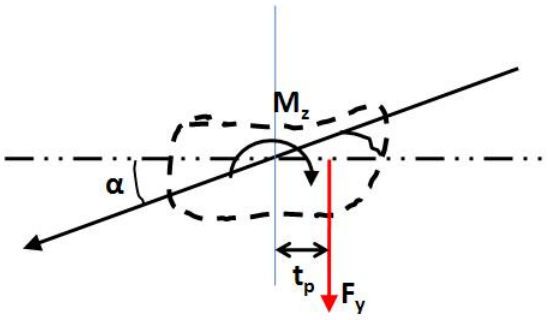

Figure 3.12: Contact patch deformation (Adopted from Giles [Giles 1968])

behind the centre point and therefore it produces a torque about the Z-axis, which is generally known as ***self aligning moment*** (M_z).

This moment provides feedback to the driver and generally helps to restore the steering to the zero slip angle position. The amount of this restoring moment is dependant on the distance, known as ***pneumatic trail*** (t_p), between the cornering force and the contact patch centre. It has been observed that as the slip angle increases the aligning moment also increases but after a certain point it starts decreasing [Giles 1968]. The reason behind this phenomenon is that the pneumatic trail starts becoming smaller and even shifts towards the negative side at large slip angles, shown in Fig. 3.13, because of sliding of the tread in the trailing part of the contact patch.
The equation for self aligning moment is given by Genta [Genta 2006] as follows:

$$M_z = (M_z)_\alpha \alpha + (M_z)_\gamma \gamma \tag{3.36}$$

where

$(M_z)_\alpha \alpha$ = Aligning stiffness coefficient due to α
$(M_z)_\gamma \gamma$ = Aligning stiffness coefficient due to γ

The term $(M_z)_\gamma \gamma$ in Eqn. 3.36 is small in value and it is usually neglected.

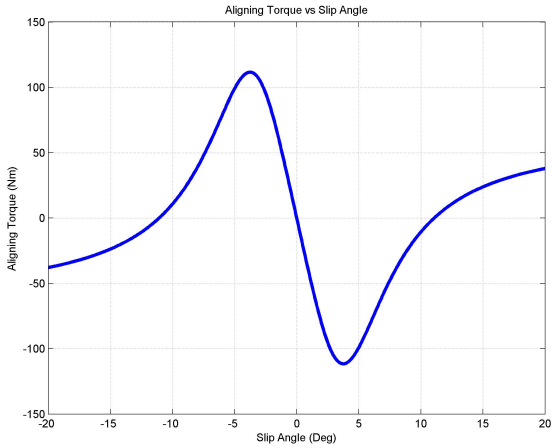

Figure 3.13: Aligning moment versus wheel slip angle

3.3.4 Combined slip

The discussion up to this point assumes the presence of longitudinal slip and tyre slip angle in isolation. However, the tyres on a moving vehicle face a multiple slip condition in which the longitudinal slip and the slip angle are both present together. This scenario is referred to as ***combined slip*** and an example of such condition is braking while cornering. As shown in Fig. 3.14 during cornering the lateral force is maximum whereas the longitudinal force is minimum; however, once the braking force is applied the longitudinal force starts building up thus decreasing the available force in lateral direction.

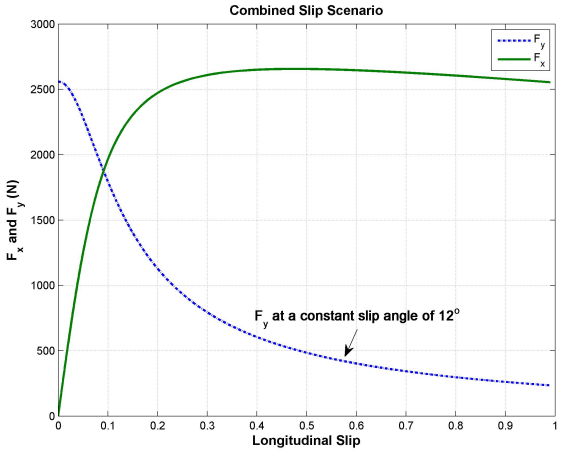

Figure 3.14: Effect F_x on F_y during the combined slip scenario

A common technique used for modelling this type of combined slip is based on the idea of the friction ellipse [Rajamani 2006]. This technique is based on the assumption that the longitudinal and lateral forces acting on the tyre cannot exceed their respective maximum values and the resultant force lies within the ellipse given by:

$$(\frac{F_y}{F_{y_{max}}})^2 + (\frac{F_x}{F_{x_{max}}})^2 = 1 \tag{3.37}$$

where $F_{y_{max}}$ and $F_{x_{max}}$ can be calculated analytically or experimentally for the pure slip conditions. Wong [Wong 2001] has described a simple procedure to predict the available cornering force in the presence of longitudinal force for a specific slip angle. This procedure has been developed on the basis of the above mentioned friction ellipse theory.

3.3.5 Dugoff tyre model

A simplified version of Dugoff's tyre model equations is given in [Guntur 1980], which provides tyre forces in pure slip as well as combined slip scenario. The longitudinal and lateral tyre forces are written as:

$$F_x = -\frac{C_{S_x} S_x}{(1 - S_x)} f(\lambda) \tag{3.38}$$

$$F_y = -\frac{C_\alpha tan\alpha}{(1 - S_x)} f(\lambda) \tag{3.39}$$

where λ is a non-dimensional parameter related to tyre/road friction coefficient μ and normal load F_z. The Dugoff's model assumes the normal load to be uniform and this has been represented by the definition of λ. It is given by:

$$\lambda = \frac{\mu F_z (1 - S_x)}{2\{(C_{S_x} S_x)^2 + (C_\alpha tan\alpha)^2\}^{1/2}} \tag{3.40}$$

where

$$\mu = \mu_o (1 - A_s V_s) \tag{3.41}$$

In the above equation V_s is the total sliding velocity, given by:

$$V_s = u_w [S_x^2 + (tan\alpha)^2]^{1/2} \tag{3.42}$$

The function $f(\lambda)$ is defined as:

$$f(\lambda) = \begin{cases} (2 - \lambda)\lambda & , \lambda < 1 \\ 1 & , \lambda \geq 1 \end{cases} \tag{3.43}$$

Equations 3.38 and 3.39 can be rewritten as:

$$F_x = F_{xd} f(\lambda) \tag{3.44}$$

$$F_y = F_{yd} f(\lambda) \tag{3.45}$$

where

$$F_{xd} = -\frac{C_{S_x} S_x}{(1 - S_x)} \tag{3.46}$$

$$F_{yd} = -\frac{C_\alpha tan\alpha}{(1 - S_x)} \tag{3.47}$$

In the above equations μ_o is the tyre/road friction coefficient when V_s is zero, A_s is the friction reduction factor and u_w is the velocity component in the wheel plane.

Figures 3.15 and 3.16 have been obtained by simulating the above mentioned Dugoff tyre model in Matlab/Simulink. The required parameters for this simulation have been taken from Dugoff et al. [Dugoff 1970]. In Fig. 3.15 it has been assumed that the wheel is in the free rolling state and the slip angle changes. The same run has been done for different values of normal load and the results suggest that an increment in the normal load raises the value of cornering force generated by a tyre, without effecting the value of cornering coefficient (C_α).

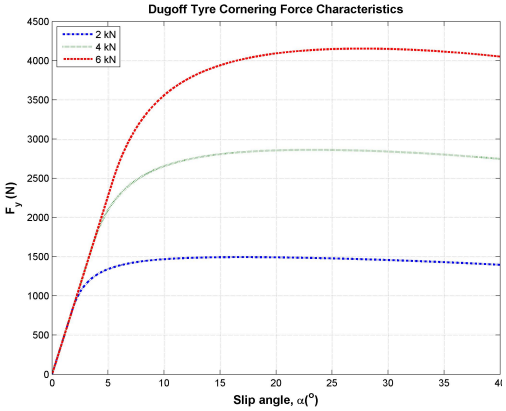

Figure 3.15: Tyre lateral force

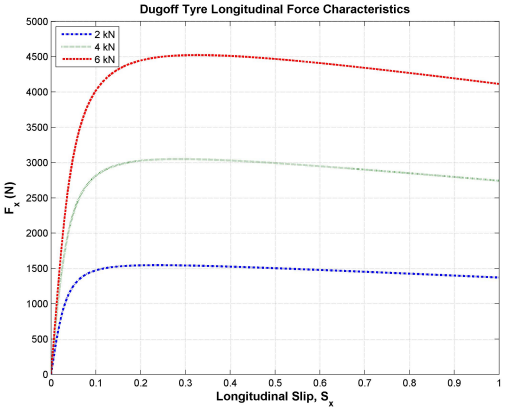

Figure 3.16: Tyre longitudinal force

Figure 3.16 shows the longitudinal force produced by the tyre at the zero slip angle condition. The result obtained by this simulation show the same sort of behaviour as we have observed in Fig. 3.10. These results also show that an increase in the normal load on the tyre causes an increase in the longitudinal

force. In contrary to the cornering coefficient (C_α) the longitudinal stiffness parameter (C_{S_x}) does not remain constant and it rises with an increase in the normal load. The physical reason behind this phenomenon is increase of the contact patch area due to the load increment while keeping the tyre inflation pressure constant. In these simulations constant inflation pressure has been assumed for all loads.

Figure 3.17 shows the tyre forces when combined slip exists. This figure depicts the effect of increase in longitudinal slip of the tyre on its lateral force at different slip angles. The circled portion in the figure highlights the non-elliptical, which is in the form of quarter ellipse and close to the friction ellipse theory. Moreover, it also highlights the fact that increase in slip angle decreases the maximum lateral force generated by the tyre.

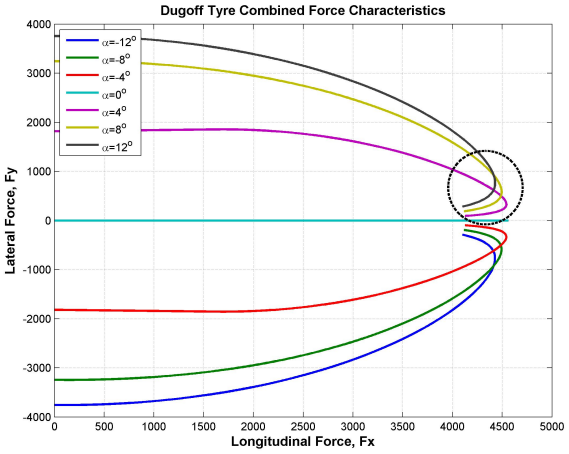

Figure 3.17: Combined slip simulation using Dugoff model

The above discussion suggests that the increase in the normal load on a wheel helps to generate higher tyre forces. According to the laws of dry friction, the frictional force between the two surfaces is dependant on the applied load and coefficient of friction between them i.e.

$$F_{friction} = \mu F_z \tag{3.48}$$

The tyres obey this law in a limited sense after which they show non-linear behaviour in this respect. This phenomenon can be better explained by plotting the peak values of coefficient of friction, in longitudinal and lateral direction, as a function of normal load on the tyre. This is shown in Fig. 3.18, which has been drawn by varying the value of the vertical load in the Dugoff model. The negative slopes for both directions show that with the increase in wheel load, the frictional coefficient decreases and therefore at higher load values the tyre

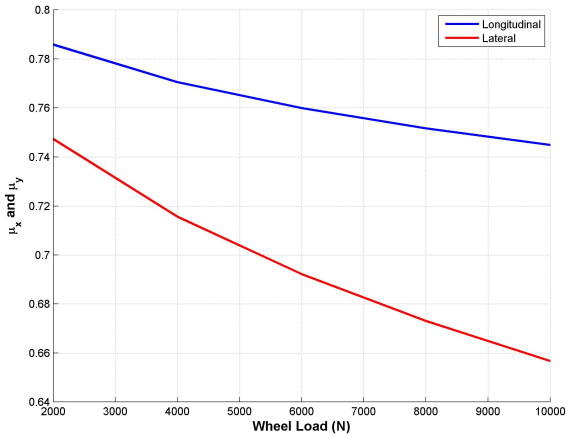

Figure 3.18: Effect of normal load on μ_x and μ_y

exhibits non-linear performance. The gradients of the slopes show that the lateral force to be more effected by the wheel load variation. The value of μ_y drops by 12.7% for raising the normal load from 2 kN to 10 kN, whereas for the same amount of load increment the value of μ_x decreases by 4.8 % of the original value.

3.4 Driver Model

Abe [Abe 2009] has described various techniques to model a driver behaviour in conjunction with a vehicle model. For a simple lane change manoeuvre he has treated the human driver as a linear continues feedback control and expressed the transfer function as follows

$$H(s) = \frac{h_{pg}}{1 + \tau_L s} \tag{3.49}$$

In the above equation h_{pg} is a gain value that defines the proportional action of a human driver, whereas τ_L defines the integral time that a human operator has to react in response to an action. This simple approach has been derived from the early work by Tustin [Tustin 1947] and McRuer & Krendel [McRuer 1959]. This model is based on an approach that a driver can sense the lateral deviation of the vehicle from the desired track by looking ahead of the vehicle. This look-ahead distance, L_H, in the forward direction is proportional to the forward speed of the vehicle and termed as the *preview distance*. The driver can correct the error in the vehicle's path and a future location by changing the steer angle, as shown in Fig. 3.19. As discussed earlier in the literature review, the driver's actions generally contain delay due

to information processing and dynamics due to the muscular system. The effect of such delay factor can be included by multiplying the transfer function, given in Eqn. 3.49, with $e^{-\tau_L s}$. However, this approach is not followed in this work because the steering system under investigation already includes the delay factor, which is greater in comparison to the response delay for an average driver. Abe [Abe 2009] has called this approach as the most fundamental understanding of the human driver's control model for dealing with the vehicle motion.

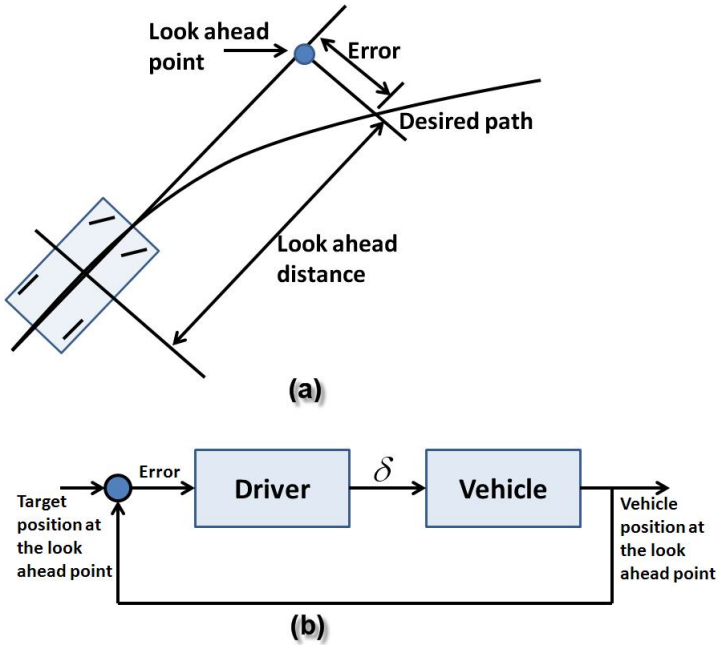

Figure 3.19: Driver steering a vehicle with look-ahead position feedback [Abe 2009]

This approach is suitable for a path that includes gentle curves and straight lines but does not provide an effective control for a path with rigorous manoeuvres. The reason for this failure is that this model is calculating the path error in the global coordinate system, which does not perform well or fails when the desired path has U-turns or zig-zag segments. For such cases Guo and Guan [Guo 1993] suggested an approach to transfer the future path information in the driver's local coordinate system. In this thesis Guo's approach has been combined with the above mentioned driver model. The advantage of combining the two approaches is that a very simple driver model, whose performance depends on a small set of parameters, becomes able to follow a complex track and hence provides an opportunity to do vehicle handling analysis with minimal possible resources.

In the simulations it is assumed that the global coordinates of the desired track are known and that information can be provided to the driver model, where they are transferred to the driver's local coordinate system by using the following relationship.

$$\begin{bmatrix} X \\ Y \end{bmatrix} = \begin{bmatrix} cos(\psi) & -sin(\psi) \\ cos(\psi) & sin(\psi) \end{bmatrix} \begin{bmatrix} x \\ y \end{bmatrix} \tag{3.50}$$

In the above equation ψ is the vehicle yaw angle, X, Y define the path location in global coordinate system and x, y is the path information in the driver's local coordinate system. In order to identify the vehicle current location the driver feedback block, shown in Fig. 3.20, calculates the distance covered by

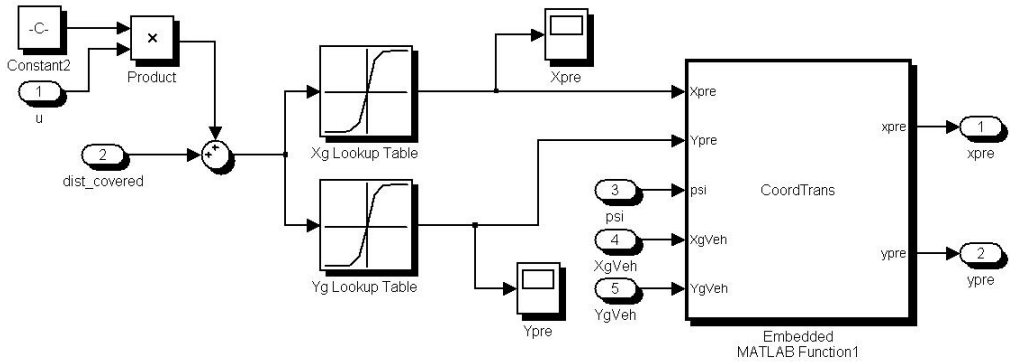

Figure 3.20: Simulink driver's feedback block to calculate the future path error

the vehicle and then find the desired future location by adding the look-ahead distance to the current value. This Simulink block uses two lookup tables to identify the desired location at the preview point. The desired future location and the current location of the vehicle is provided to an embedded matlab function, which calculates the lateral distance that the driver has to move the vehicle to keep it on the desired track. This lateral distance is the feedback for the driver model to calculate the steering angle for the purpose.

As discussed earlier the look-ahead distance in this model is calculated by multiplying the vehicle speed with a gain factor, which is taken as 0.9 in this thesis. Dividing the look-ahead distance with the vehicle velocity introduces another important parameter known as preview time of the driver. If the preview time is greater than the delay time, the system remains stable [Abe 2009]. The driver's characteristic values used in this work are given in Table 3.1.

In order to evaluate the driver model's ability to follow the desired track, a vehicle mounted with a GPS receiver was driven within the campus, as shown in Fig. 3.21. The track data was recorded on an accompanying laptop

Parameter	Value
h_{pg}	0.02
τ_L	0.2
L_H	0.9*u

Table 3.1: A driver's characteristics defined by a set of parameters

in terms of latitude, longitude and elevation coordinates. This data was later converted to global X and Y coordinate system using Matlab and provided to the driver model as the target track.

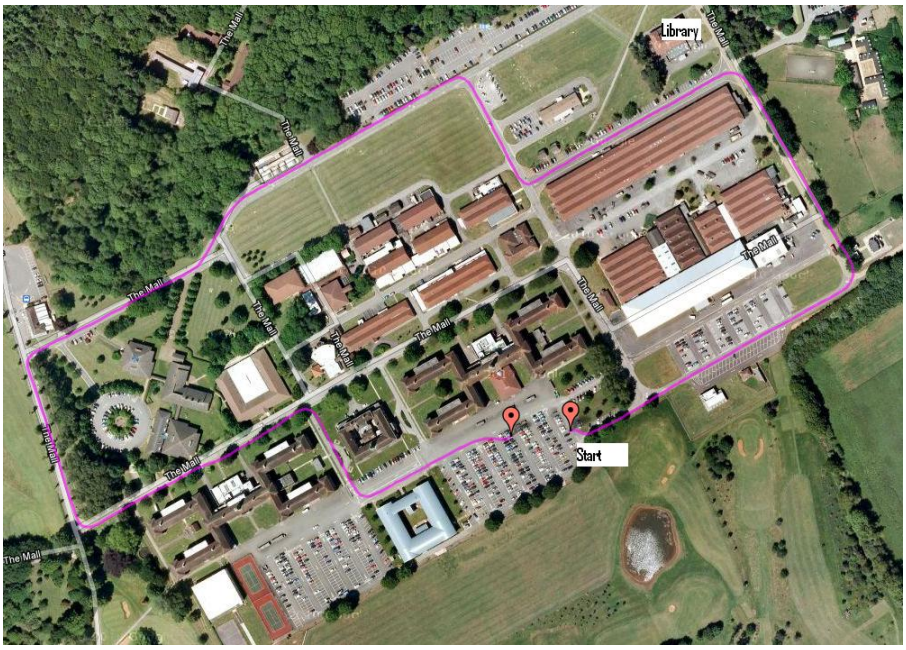

Figure 3.21: Google Maps showing the track recorded within the college

Figure 3.22 shows this transformation from GPS coordinate system to global coordinate system. The green curve is the trace of vehicle's position driven by the driver model discussed above. The error between the desired track and the vehicle's position trace is less than 2 mm at turning points, which is very minimal. The track has been divided into eleven segments and for each segment the expected value of the vehicle yaw angle has been mentioned. This identification facilitates to verify that whether the vehicle is following the track with a proper orientation or not. For this purpose the vehicle yaw angle was recorded during the simulation, which is shown in Fig. 3.23. This figure identifies the segments and the corresponding yaw angle of the model vehicle. The comparison of both figures suggests that the driver

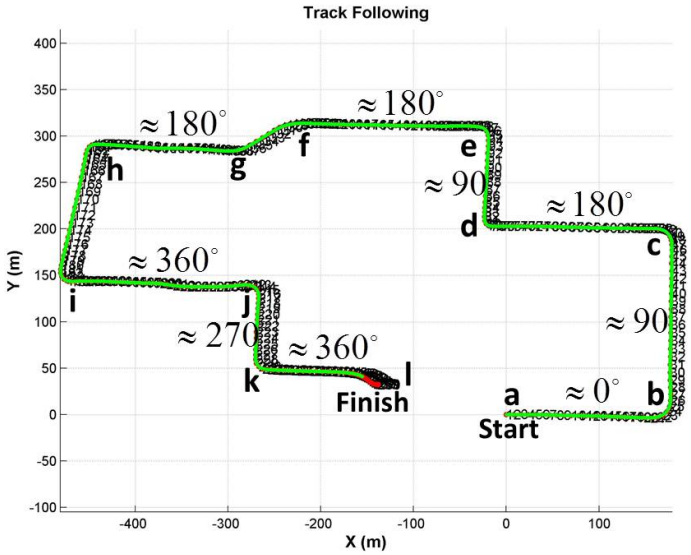

Figure 3.22: Driver following the desired track transferred in the global coordinate system

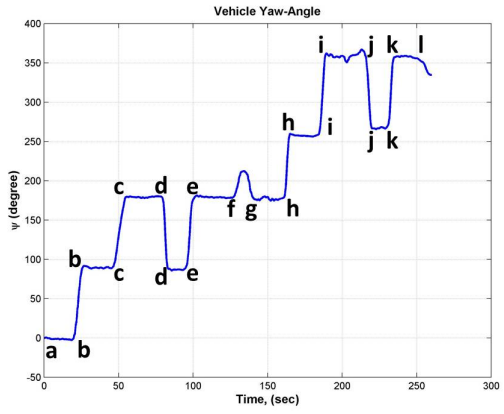

Figure 3.23: Yaw angle of the vehicle while following the track

model is able to manoeuvre the vehicle in a correct manner. The speed of the vehicle in this simulation is taken from the GPS data and shown in Fig. 3.24. As the figure suggests, the data recorded during the stationary phase at the stating point has not been taken into consideration. This was done to avoid the simulation failure due to the zero initial conditions error. The speed trace shown in the figure suggests that the driver model is able to follow the desired with a variable speed. This is because of the reason that the driver's preview distance is a function of the vehicle speed, as shown in Fig. 3.20.

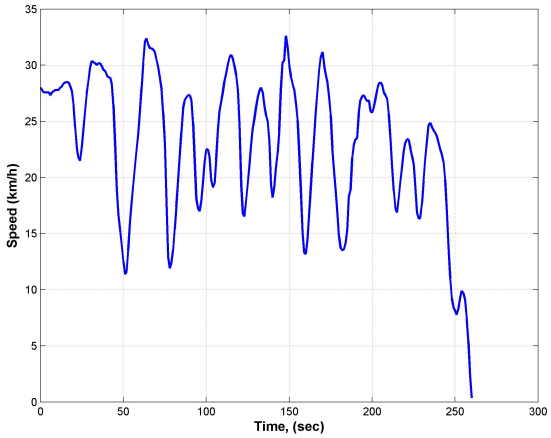

Figure 3.24: Trace of the vehicle speed while following the track

Thus it can be stated with confidence that the driver model discussed above is able to drive a vehicle on a desired track. Therefore this driver model will be used in conjunction with the non-linear vehicle model to assess the vehicle handling quality and integration of a control system for the response improvement.

Chapter 4

Testing and Model Validation

Contents

4.1 Introduction

This chapter primarily discusses the experimental work performed in support of the validation of the vehicle model. The chapter begins with the experiments performed to measure the lateral force characteristics of the test vehicle's tyres. The reason for placing this section before introducing the actual test vehicle is that these tyre characteristics are used in the subsequent sections. Then the subsystems and components are considered, following which

the steering actuator and system and then the whole vehicle testing is discussed. The vehicle testing covers both steady state (circular) and transient (lane change) testing. As the model of the steering is relatively simple is included in this chapter.

4.2 Tyre Test Rig Experiments

In chapter 3 various tyre models have been discussed that are capable to generate tyre forces required for vehicle handling analysis. This section discusses the experimental arrangement and the corresponding experiments carried out to measure the tyre lateral forces, which are required to validate the tyre modelling technique selected for this thesis. These experiments have been performed in a laboratory environment to investigate the tyre lateral force characteristics. The tyres used in these experiments belong to the test vehicle and are of radial type and bear the code 135/70R 13 of their side walls. This code indicates the nominal section width, the aspect ratio and the nominal diameter of the wheel rim. A tyre test rig, available in the Cranfield's Shrivenham campus, and shown in Fig. 4.1, has been used for the purpose.

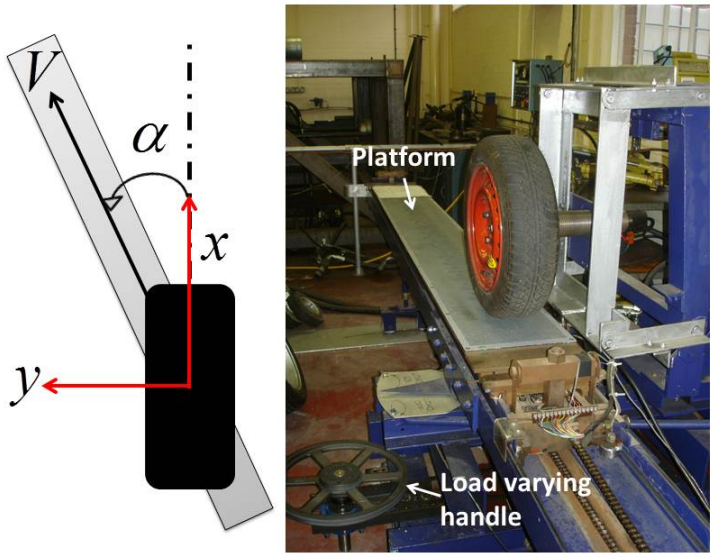

Figure 4.1: Tyre testing rig at Vehicle Dynamics Lab Shrivenham

In this arrangement the wheel remains fixed at its location and rotates when the platform slides underneath it. The rig has provision to vary the values of normal load, slip angle and camber angle. The platform can be rotated about

its vertical axis up to 10° in both directions from its mean position. This rotation of the platform while keeping the wheel fixed gives control over the slip angle, whereas its motion from right to left portrays the vehicle forward motion. The rig has arrangements to record the lateral force via strain gauges and the attached computer.

The experiments have been performed with two different tyre pressures to represent the front and rear tyre behaviour. The procedure was repeated five times for the front tyre and four times for the rear one. For each instance the normal load was varied, details of which are given in Table 4.1. During these tests the slip angle was varied from 0 to 9 degrees by rotating the platform, as described above.

Front (30 psi)	Rear (32 psi)
1.0	1.80
1.2	2.2
1.3	2.3
1.46	2.45
1.51	-

Table 4.1: Normal loads (in kN) used in the experiments

Figure 4.2 is an example of the data recorded during the experiments. Both the platform displacement and the lateral force generated by the tyre were

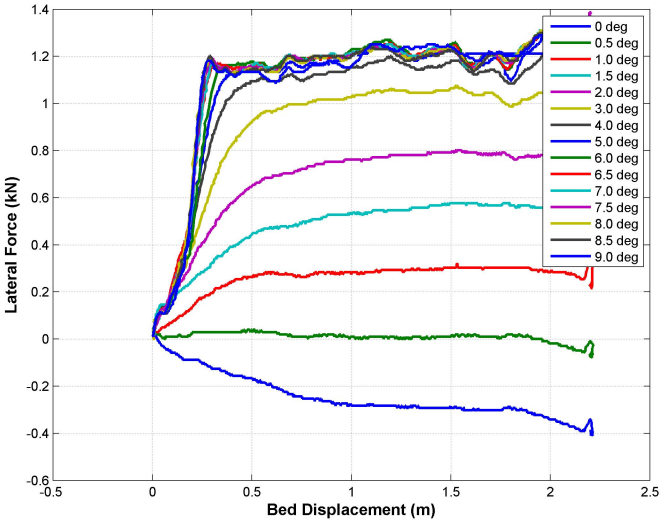

Figure 4.2: F_y with varying slip angle, $F_z = 1.2kN$, Pressure= $30psi$

provided by the corresponding sensors and recorded in the form of voltages.

This voltage data has been converted into displacement and force using the corresponding calibration chart. The curves show that during the transient stage the side force rises from a minimum value and attains a steady-state when the platform attained a constant velocity. This steady-state value for each slip angle is taken as the corresponding lateral force. The curve for zero-degree slip angle shows a negative lateral force, ideally which should be zero. The reason for this discrepancy can be any or combination of the following:

- the presence of a camber angle.
- the presence of conicity and/or ply steer.
- an experimental error.

Another point to observe is that after 4° of slip angle the lateral force values are quite close to each other. This represents the fact that the tyre force in the lateral direction started to saturate. Experimental data has been processed and represented in a more convenient form in Figures 4.3 and 4.4(enlarged view in Appendix D). The figures show that the existence of the lateral force at zero slip angle has been accommodated by adding the corresponding force for all the slip values. These results also support the discussion made in previous sections that the wheel load and tyre pressure influence the tyre characteristics.

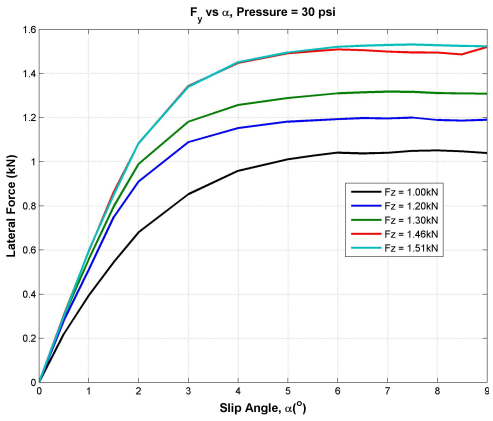

Figure 4.3: Front tyre characteristics

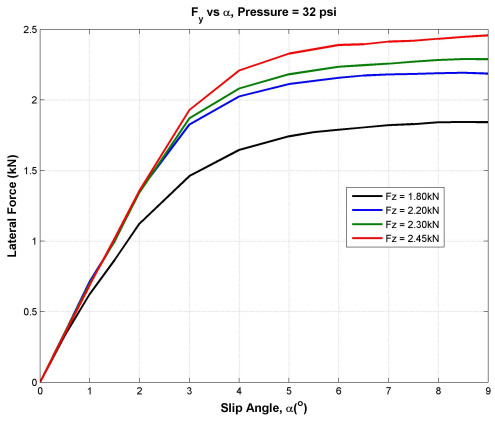

Figure 4.4: Rear tyre characteristics

The tyre cornering stiffness parameter, as described in section 3.3.3.2, is the slope of lateral tyre force curve plotted against the tyre slip angle. Generally the slope is calculated where the tyre slip angles are small because of linear relationship between F_y and α within this region. Using this definition the

Front (30 psi)		Rear (32 psi)	
$F_z(kN)$	$C_{\alpha_f}(kN/rad)$	$F_z(kN)$	$C_{\alpha_r}(kN/rad)$
1.0	22.67	1.80	35.86
1.2	29.32	2.2	41.02
1.3	31.99	2.3	41.02
1.46	34.04	2.45	41.02
1.51	34.25	-	-

Table 4.2: Front and rear tyre cornering stiffness values calculated by the experiments at various normal loads

values of C_α for the front and rear tyres are determined, using Fig. 4.3 and Fig. 4.4 respectively, and shown in Table 4.2.

4.2.1 Tyre model validation

The previous section describes the experiments performed to determine the lateral characteristics of tyres fitted on the test vehicle. However, the equipment available in the laboratory does not provide the longitudinal characteristics of the tyres. The Dugoff tyre model, discussed in section 3.3.5, requires lateral as well as longitudinal characteristics of a tyre to simulate its behaviour. Therefore, in this work the parameters related to the tyre's longitudinal characteristics are taken from Dugoff et al. [Dugoff 1970].

Figure 4.5 (enlarged view in Appendix E) shows the comparison between the lateral force characteristics recorded during the experiments and estimated by the Dugoff tyre model using Matlab/Simulink. Each graph in this figure represents a set of tyre data collected during the experiments and a curve from the Dugoff tyre model with the tuned parameters. Simulations have been performed for different normal loads and all the results correspond to what observed during the testing phase.
It can be observed from Fig. 4.6 that the percentage error between the estimated and experimental data is less than 5% for both cases, which is an acceptable range considering the complexity of tyre behaviour in view. Therefore one can state with a confidence that the Dugoff tyre model is a suitable choice to use in the later part of this thesis.

4.3 The Test Vehicle

This section introduces the test vehicle that has been used for experiments. The initial discussion is about the replacement of conventional steering system

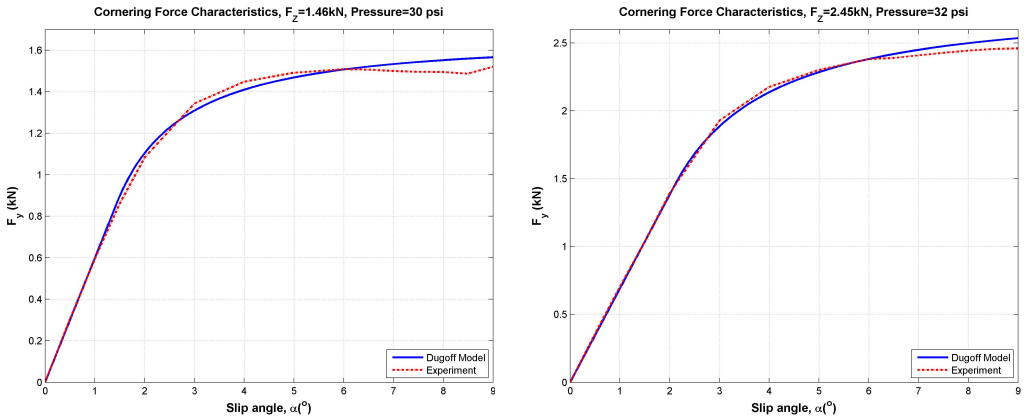

Figure 4.5: Experimental and Estimated lateral force characteristics

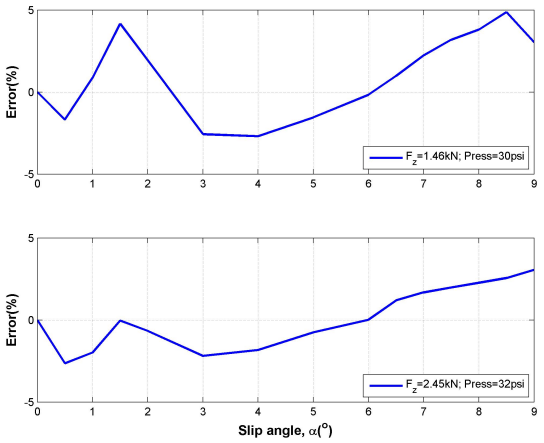

Figure 4.6: Error between the Experimental and Estimated F_y

with the steer-by-wire system, which follows sections pertaining to vehicle mounted sensors and experiments to measure the vehicle parameters.

Figure 4.7: The testing vehicle for experiments

The test vehicle, shown in Fig. 4.7, is a dune buggy converted to include a steer-by-wire system comprising two low cost linear actuators, a potentiometer to convert steering commands into the respective voltages, a data acquisition (DAQ) module and a laptop for data manipulation and gathering. The front and rear McPherson strut suspension has been altered to accommodate four of such actuators to make the vehicle four wheel steerable. However, for this thesis the rear wheels have been kept fixed and only front two wheels were allowed to steer during the investigation. The actuator's performance data sheet, provided by the supplier, suggests that the actuator can travel at a maximum speed of 45 mm/sec when a load of 2.3 kN is acting on it.

The steer-by-wire arrangement has been used successfully to replace the conventional steering arrangement, as shown in Fig. 4.8. Due to physical limitations it was not possible to fit the actuators in-line to each other on the vehicle chassis. The kinematic arrangement on the right side of the vehicle was slightly modified to accommodate the actuator's offset and therefore both of the actuators travel in different lengths to steer the two wheels in parallel. In the next step the actuators were fitted with two calibrated LVDTs, as visible in Fig. 4.8, to measure the actuators' displacement during the experiments.

The steering movement by the driver is converted in to corresponding voltage by the potentiometer. The output of the potentiometer is transferred to the data acquisition module, through a cable, from where it goes to the laptop. The laptop is loaded with the LabVIEW programme, shown in Appendix A,

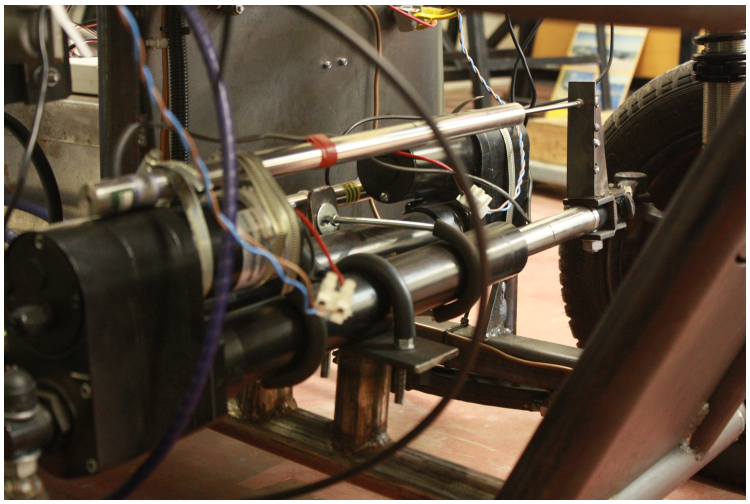

Figure 4.8: Front steering actuator and LVDT replacing the conventional steering at the left side of the test vehicle

that processes the input commands and generates the corresponding output for the actuators. This LabVIEW programme also records this information on the laptop's hard disk. The DAQ module acts as a medium for communication between the steering system and the laptop. The motion of each actuator is controlled by a dedicated servo controller, which is designed to generate a smooth actuator motion. The actuators require 24 V dc supply voltage to operate and therefore two 12 V batteries have been connected in series for the provision. The control voltage range of the servo controllers is $0 \sim 5\ V$, which is made available through the DAQ module.

4.3.1 Vehicle mounted sensors

The test vehicle is fitted with sensors, as shown in Fig. 4.9, to measure various variables that are required for the vehicle handling analysis. These variables are selected from the standards [sta 2004, sta 2003], which recommend variables that help to analyse the vehicle stability in steady and transient manoeuvres. Table 4.3 shows the variables to be measured and the corresponding transducers that were fitted on the vehicle to accomplish this and their detailed specifications are given in Appendix R. All the variables were collected at the rate of 100 Hz except the vehicle speed and position because the GPS device was only providing the output at 1 Hz. The raw data was recorded on the laptop hard drive using the DAQ module, which was later processed using MATLAB. The experimental data has been used to validate the vehicle models discussed in Chapter 3.

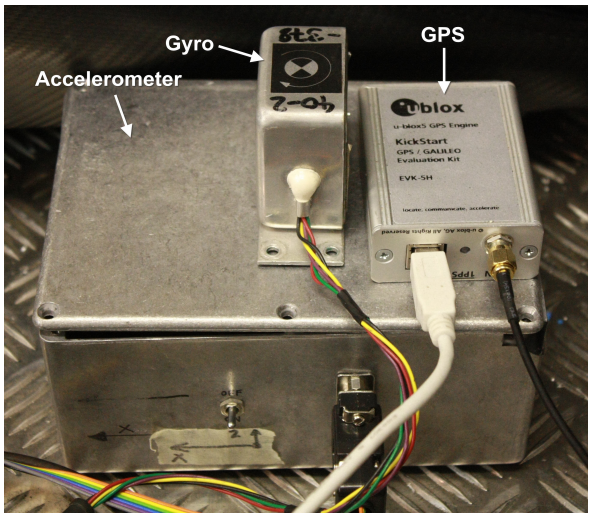

Figure 4.9: Vehicle mounted sensor pack used on the vehicle consisting of accelerometer, gyro and GPS

Measurement	Sensor	Model
Steering handle angle	Potentiometer	Bourns 3547
Front steer angle	LVDT	RDP LDC4000C
Lateral and longitudinal acceleration	Accelerometer	ADXL325
Yaw-rate	Gyro	ARS-C132-1A
Vehicle speed and location	GPS	u-blox 5

Table 4.3: Vehicle mounted sensors used in testing phase

As mentioned earlier each actuator is fitted with a calibrated LVDT to measure its displacement during the experiments. Each LVDT supplies 1 V for the displacement of 50 mm, so the corresponding voltage of each LVDT for the straight ahead position of wheels was measured. The deviation from this mean position gives the distance travelled by the actuator, which can be transformed into wheel steer angle as discussed in section 4.4.1.

4.3.2 Vehicle mass and centre of gravity calculations

In vehicle dynamics analysis the vehicle's mass and its centre of gravity (COG) play a pivotal role. The location of this point in the $XY-$plane can be obtained by weighing the vehicle and taking moment about the rear axle; however, the location in $XZ-$plane requires lifting the vehicle from one end and measure variation in its weight distribution in an inclined position [Mango 2004].

The experimental vehicle was weighed using four calibrated loads cells. The load on each wheel was noted once unmanned and then with a driver and a passenger. Figure 4.10 shows the load on each tyre and the location of the centre of gravity in the $XY-$plane. During the testing phase the vehicle was manned by a driver only; however presence of the auxiliary equipment during the experiments balances the passenger's weight. Hence the load and mass values related to the manned scenario in the Fig. 4.10 has been used as the vehicle parameters in this thesis.

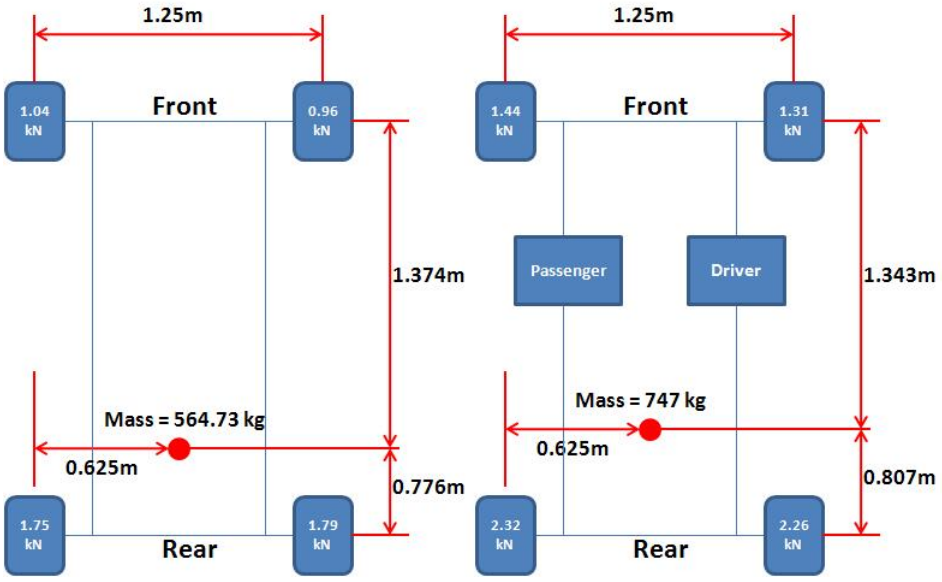

Figure 4.10: Load on each wheel and location of COG

Figure 4.11 shows the vehicle with the rear end being raised $440mm$ from the ground. Using the Pythagoras' theorem and other associated formulae the COG is estimated to be $490mm$ above the ground. The roll centre height is estimated from the geometry, wheel rates from the kinematics and the roll stiffness from the spring constants. The spring constants were calculated using the apparatus available within the Shrivenham's laboratory. These parameters are given in Appendix C.

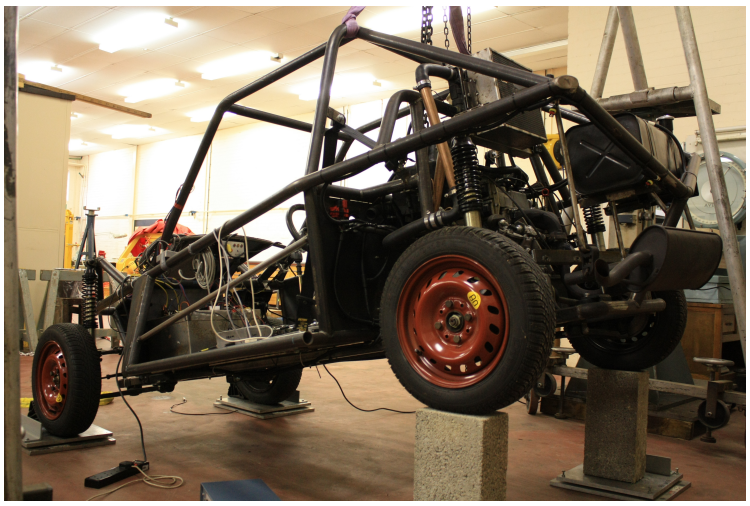

Figure 4.11: The test vehicle in the raised position to determine the height of the COG

The vehicle parameters mentioned in Fig. 4.10 can be used to determine an important term K_{us} referred as understeer coefficient or gradient in the text [Wong 2001, Rajamani 2006]. This term defines the vehicle behaviour during a straight line motion or a cornering manoeuvre in the form of steering input required by the driver to keep the vehicle on a required path. Substituting the required vehicle and tyre parameters in the following equation suggests that the experimental vehicle has a slight tendency to oversteer during cornering.

$$K_{us} = (\frac{W_{fl}}{C_{\alpha_{fl}}} + \frac{W_{fr}}{C_{\alpha_{fr}}}) - (\frac{W_{rl}}{C_{\alpha_{rl}}} + \frac{W_{rr}}{C_{\alpha_{rr}}}) \tag{4.1}$$

In the above equation the terms W_{fl}, W_{fr}, W_{rl} and W_{rr} represent the vertical forces acting on the front left, front right, rear right and rear left tyres respectively, whereas $C_{\alpha_{fl}}$, $C_{\alpha_{fr}}$, $C_{\alpha_{rl}}$ and $C_{\alpha_{rr}}$ are the cornering stiffnesses of the corresponding tyres, discussed in section 4.2. Taking these tyre properties into consideration, the value of K_{us} for the unloaded and manned vehicle can be calculated as $-0.60\ ^\circ/g$ and $-1.62\ ^\circ/g$ respectively. These values have

been obtained by substituting the tyre cornering stiffnesses and corresponding parameters for the test vehicle, shown in Fig. 4.10, into Eqn. 4.1.

4.4 Actuator's Response

In section 4.3 the test vehicle has been introduced. The discussion about the test vehicle mentions that the conventional steering system, consisting mechanical linkages, was replaced by a steer-by-wire system. This steer-by-wire system consists of two linear actuators along with other components and the purpose of these actuators is to steer the wheels left and right as per the driver's commands. Therefore, this section is focused on the tests carried out to assess the performance of these actuators because of their role to be critical. The section begins with the experiments carried out to calibrate the actuators and potentiometer and then the tests are discussed, which have been made to measure the actuator's response. As the steering commands can be represented by step, sinusoidal and combination of such inputs therefore in these tests similar sort of inputs with varying frequencies and amplitudes have been used. The later section uses the findings of these tests to describe the steer-by-wire system in terms of a mathematical model. This steering model integrated with the vehicle model, discussed in Chapter 3, will be used later in Chapter 5.

4.4.1 Actuators' calibration

The actuator's motion is linear and its purpose is to steer the wheel in left and right direction from its mean position. Therefore the first step was identify the relationship between the actuator's movement and the steer angle at the corresponding wheel. For this purpose the front side of the experimental vehicle was raised above the ground and both actuators' displacement was measured against a known voltage inputs. As mentioned earlier in section 4.3, the kinematic arrangement for both of the wheels is different in order to accommodate the actuators in the space available on the vehicle. Therefore both of the actuators travel in different lengths to steer the two wheels in parallel for the same steer angle.

Figure 4.12 shows the relationship between the supplied voltage and the distance travelled by the actuators. For the left wheel the input voltage range for the actuator is $4.1 \sim 1.84\,V$, which displaces the actuator to approximately $155\,mm$ from its closed or retracted position. Similarly the right side actuator moves approximately $231\,mm$ when the voltage is varied from $4.7 \sim 1.3\,V$. As identified in the Fig. 4.12 for a left turn the left wheel's actuator is retracted

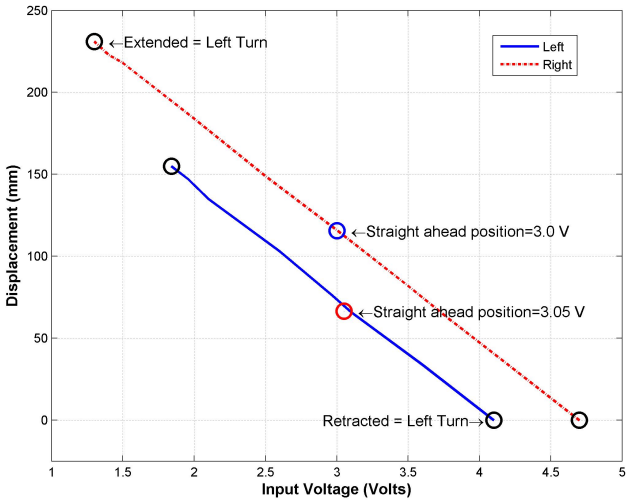

Figure 4.12: Steering actuator displacement versus input voltages

fully whereas the right actuator is extended to its allowable extreme position. For the straight ahead position of wheels the corresponding voltages of left and right actuators are 3.05 and 3.0 V respectively.

The displacement of each actuator allows the corresponding wheel to travel 70° from one extreme to the other. This information has been collected by physically measuring the steering angle for each wheel against the actuator motion. The relationship between the displacement and the wheels' steer angle is shown in Fig. 4.13. When the actuator's arm travels towards the right side of the driver from its mean position, the vehicle turns left and this angle is shown as positive in the figure. These figures suggest that each actuator requires independent signal to perform parallel steering.

4.4.2 Potentiometer calibration

The input commands coming from the driver are converted into corresponding voltages by the potentiometer attached to the steering-wheel. Therefore the output of the potentiometer was also calibrated with reference to the steering-wheel position. For the experimental run the wheel's rotation from its straight ahead position was fixed to be 30° on either side, which was taken from the experiments. The steering handle was constrained to rotate 180° on either side of its mean position. This arrangement was made to protect the potentiometer from any unwanted damage during the experiments; thus allowing a steering ratio of 6:1. Figure 4.14 shows the voltage data that was later used to synchronise the wheels behaviour to the driver's commands. As mentioned

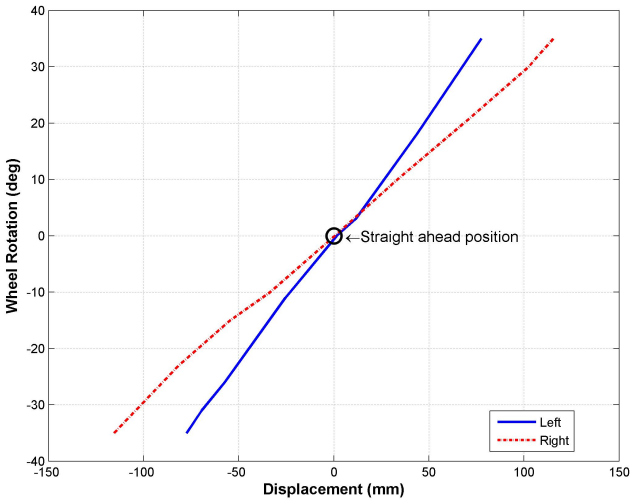

Figure 4.13: Steer wheel rotation versus actuator displacement

earlier the right wheel linkages were altered to accommodate the actuator; the alteration effect on the kinematics is obvious as the wheel rotation does not show symmetry about its mean point. This discrepancy has been catered by introducing a weight factor in the code written to control the wheels' motion.

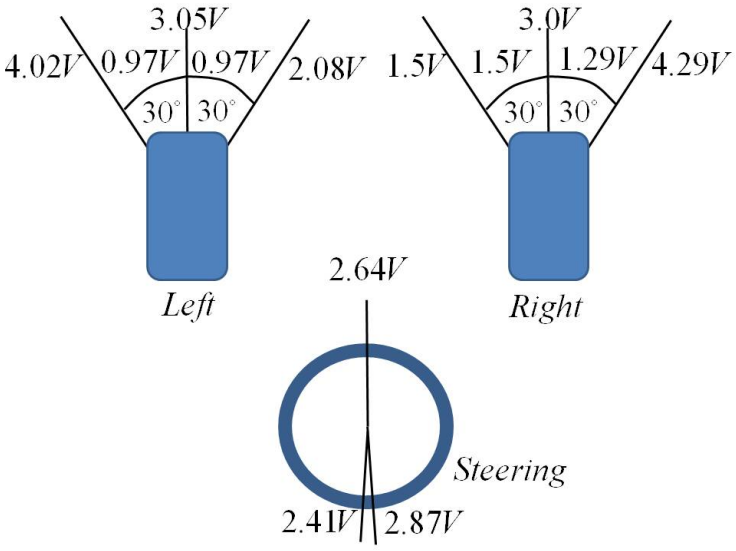

Figure 4.14: Voltage data for the potentiometer and both actuators

4.4.3 Square wave response

The layout diagram of the experimental set-up is shown in the Fig. 4.15. In

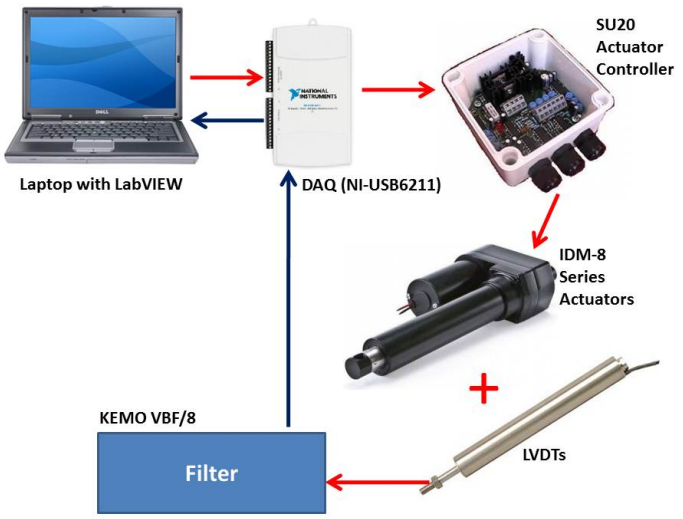

Figure 4.15: Experimental set-up layout

order to investigate the actuators' response they were fed with input in a form of square wave. The amplitude and frequency of the input signals were varied to establish the relationship between the input and output. Figures 4.16

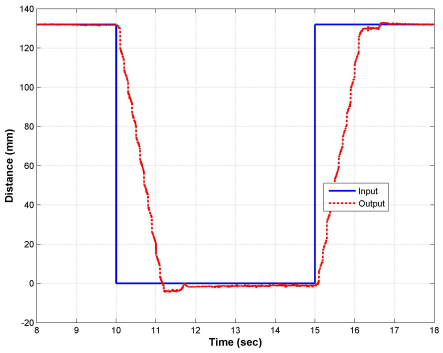

Figure 4.16: Response of the left actuator

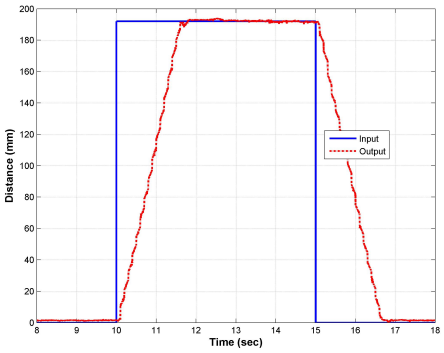

Figure 4.17: Response of the right actuator

and 4.17 (enlarged view in Appendix F) show the displacement versus time graph for the left and right actuator respectively. The data shown in both of these figures was collected when the actuators were commanded to move from

one end to other at the frequency of 0.1 Hz. This input rotated the wheels by 30° on each side of the straight ahead position. The input frequency of 0.1 Hz was chosen to allow the actuators to reach the end position fully and then move back. As mentioned earlier the left actuator displaces less than the right one and it is evident from the graphs. Both graphs are out of phase because to rotate the wheels parallel in the same direction, one actuator has to retract and the other has to extend. The input output data shown in the figures suggest that the actuators follow the input command signal with a lag. This lag results in a delayed actuators' response. The relationship between the input signal and the response can be approximated by calculating the slope of the output data. For the left side the value of slope is 103.1 mm/s and for the right wheel it can be approximated as 108.21 mm/s. These values remain valid for higher frequency inputs, as shown in Fig. 4.18 and Fig. 4.19 (enlarged view in Appendix G). These two graphs show the response of the left and right wheel actuators when the input signal's frequency was varied from 0.1 Hz to 0.2 Hz in steps. The graphs suggest that the actuators' output curves follow the same slope and therefore it can be deduced that the variation in frequency of the input signal does not effect the slope values in a significant manner.

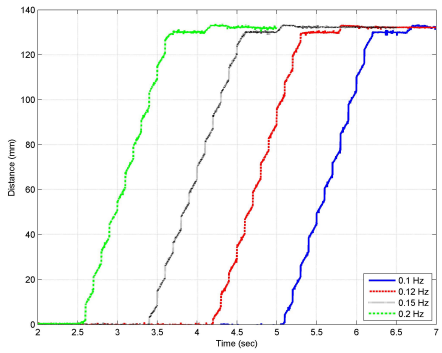

Figure 4.18: Actuator response for the left side to a square wave of varying frequencies

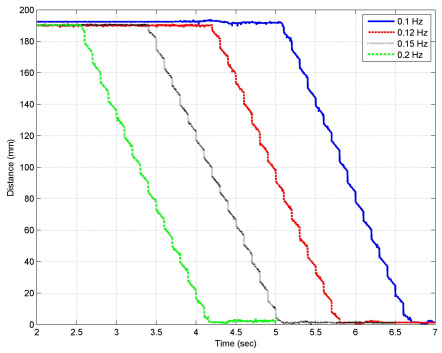

Figure 4.19: Actuator response for the right side to a square wave of varying frequencies

In order to find the influence of amplitude on the dynamic behaviour of the actuators, the experiments were repeated with varied input amplitudes. The results show that like frequency, amplitude variation also does not alter the response much. Figure 4.20 shows the curves for the right actuator's output for two inputs, one of 30° and the other of 15°, which steered the wheel on both sides from its mean position with the frequency of 0.1 Hz.

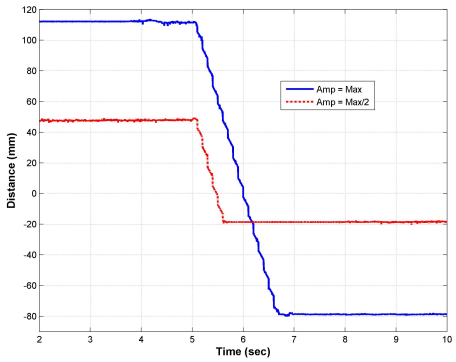

Figure 4.20: Actuator response with varied amplitudes

4.4.4 Steering system model

The response for the steering system and actuator show a relatively simple behaviour consisting of a scaling factor to compensate for the steering kinematics and a velocity saturation from the actuator. Using this analogy a MATLAB/Simulink model has been developed that imitate the delayed actuator response. Figure 4.21 shows a Simulink representation in which a rate limiter block has been used to model the delay. In order to compare the re-

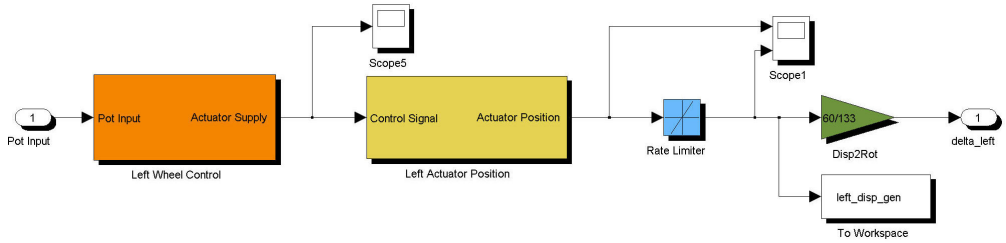

Figure 4.21: Simulink model representing the actuator dynamics

sponse of this steering system model with that of the actual actuators, it was excited with the inputs of same amplitudes and frequencies that were used during the testing in the laboratory. Figures 4.22 and 4.23 (enlarged view in Appendix H) show the actual and simulated responses for an input square wave, represented by a solid blue line, having frequency of 0.1 Hz and maximum amplitude. The figures show that the simulated response follows the actual response, collected through the LVDTs, in an acceptable manner. The root mean square error value between the actual and simulated response is 15 and 26 mm for the left and right actuator respectively. Although the output

voltages of the two LVDTs were passed through a dual channel variable filter (KEMO VBF/8) for noise cancellation. However, in experimental set-up it is not possible to cancel the noise from the voltage signals in an ideal manner. Keeping this limitation in view it can be stated that the actuator dynamics represented by the Simulink model agree quite closely to the real behaviour of the actuators and therefore can be used as a part of further investigation.

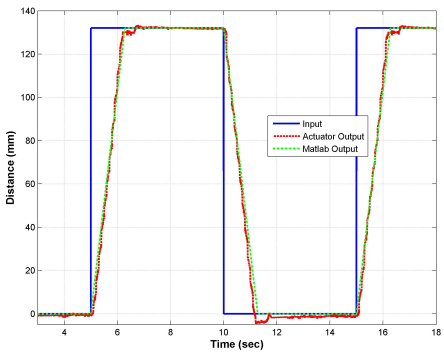

Figure 4.22: Left actuator response (Input amplitude = Maximum, Input frequency = 0.1 Hz)

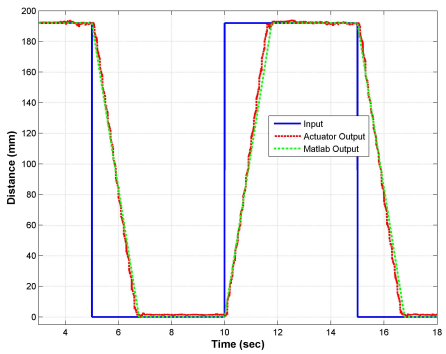

Figure 4.23: Right actuator response (Input amplitude = Maximum, Input frequency = 0.1 Hz)

4.4.5 Sine wave response

In this set of experiments the actuators were driven by sine wave inputs of varying frequencies and amplitudes to identify their behaviour in manoeuvres representing lane-change or obstacle avoidance. As in the case of square wave testing the same set-up was used for the experiments, as shown in Fig. 4.15. The input was generated using the LabVIEW code and the LVDTs were used to measure the actuators' displacement. The data was recorded on the computer using a separate analog input channel of the DAQ module for each LVDT. Later on the same input was generated using a MATLAB code and the output of the Simulink model was noted. The results shown in Fig. 4.24 suggests that the Simulink model for the left actuator performs well with this type of input and also confirms the performance of the model in representing the real system. Similar sort of results have been obtained for the right actuator as well. When the input frequency was raised above 0.2 Hz, a drop in actuators' displacement amplitude was observed. For these higher frequencies the phase lag between the input and the output was started to increase. This is shown by the frequency response plots in Figures 4.25 and 4.26 (enlarged view in Appendix I). These figures show the amplitude and phase response

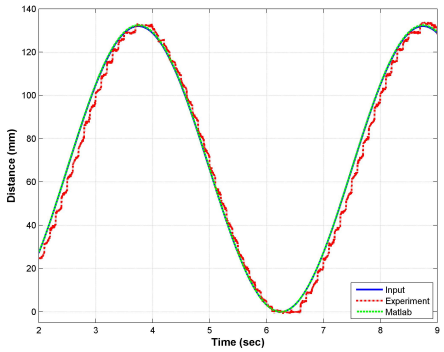

Figure 4.24: Left actuator's response for 0.2 Hz sine wave input with maximum amplitude

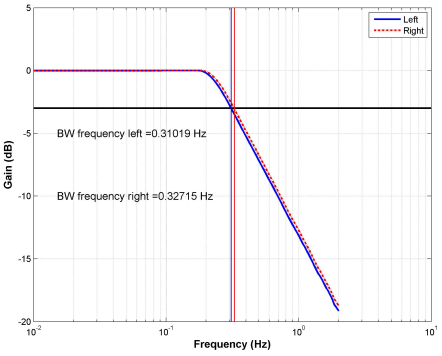

Figure 4.25: Amplitude response

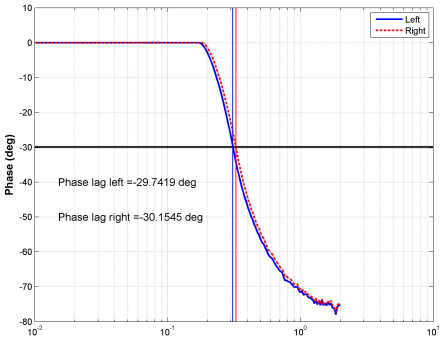

Figure 4.26: Phase response

for both actuators when subjected to a frequency range of 0.01 to 2 Hz. The amplitude response is nearly 0 dB up to 0.2 Hz and this is the case with the phase, below 0.2 Hz there is virtually zero degree lag. This implies that the actuators are following the input command with 0 dB gain and 0° phase up to 0.2 Hz. Figures 4.25 and 4.26 also show the bandwidth frequency (at -3 dB) for both of the actuators. It is 0.31 and 0.32 Hz for the left and right actuator respectively and at this the phase lag is approximately 30°. Generally the response (bandwidth) of a human operator is 2 to 3 Hz and a steering system, comprising the actuators of such bandwidth, could make it problematic for the driver to control the vehicle at high speeds. The same was found later to be true during the vehicle testing phase when the driver struggled to keep the vehicle on the desired path. The low bandwidth of the steering actuators was one of the main factors to avoid high speed manoeuvres during the vehicle testing phase, discussed in the next section.

4.5 Vehicle Testing

In this section the steady-state and transient testing of the experimental vehicle are discussed and their results are presented. The experimental data shown and discussed in this section was collected using the sensors, mentioned in section 4.3.1. The purpose of this exercise is to validate the vehicle models discussed in Chapter 3 using this experimental data. For simulation purpose the vehicle models have been modelled using Matlab/Simulink.

4.5.1 Steady-state circular testing

The steady-state handling characteristics have been investigated by driving the experimental vehicle on a 30 m radius path as shown in Fig. 4.27. The radii of 30 m was selected as that was the largest that could be accommodated safely on the college car park, which had been closed for the purpose of testing. The path shown in the figure is a traced using the GPS data collected during the manoeuvre and mapped out on Google Map to identify the obstacles in extending the path radii. The path was marked with cones to facilitate the driver in following the track.

Testing for sensors' calibration

The purpose of these tests was to calibrate the accelerometer and yaw-rate sensors' output. For this purpose the vehicle was driven with a very low constant speed in a circular path to attain a steady-state test. The idea behind these slow speed tests was based on the knowledge that when a vehicle is

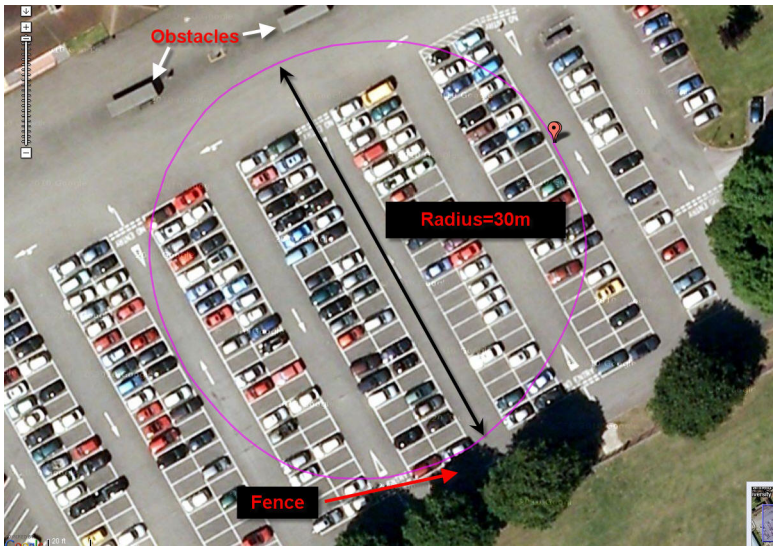

Figure 4.27: Steady state test track used for vehicle testing plotting on Google Map

moving with a very low speed on the test circle, which has a radius significantly larger than the track-width of the vehicle, the yaw-rate can be approximated by the following relationship [Rajamani 2006].

$$r = \frac{u}{R} \tag{4.2}$$

where r represents the yaw-rate, u is the speed in the longitudinal direction and R is the radius of the circular path.

This theoretical information can be used to evaluate the performance of the sensor measuring the yaw-rate, gyroscope in this case. In the first run, the path radius was fixed to be 30 meters and the vehicle speed was maintained at 10 km/h (2.78 m/s), which was the slowest possible speed to drive the vehicle. The data collected by the gyroscope has been represented in two phases in Fig. 4.28. The first phase which starts from 0 and finishes around 250 s is the acceleration phase in which the vehicle moves from the rest position to a constant velocity position. The second phase lies between 250 and 350 s in which the experimental has attained the steady-state. The mean value of the yaw-rate during this phase is approximately 4.9 deg/s, whereas the theoretical value calculated using Eqn. 4.2 is approximately 5.3 deg/s. The error of $7 \sim 8$ % between the measured and calculated values is in an acceptable range keeping in view several physical limitations. The difference can be of any reason like the driver not being able to keep the vehicle exactly on 30 m track or the speed information having the sensor bias or slight misalignment of

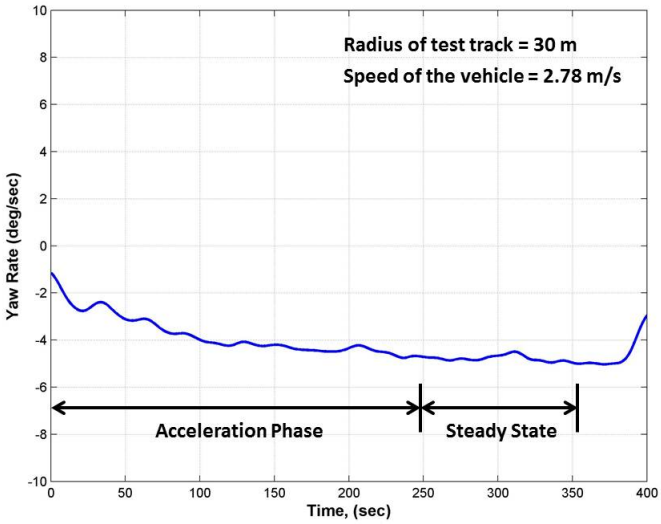

Figure 4.28: Vehicle yaw-rate while following the test track

the gyro sensor on the vehicle. Keeping these factors in view one can suggest that the gyroscope is providing acceptable information about the yaw-rate and this information may be used with care.

These slow speed tests were also aimed to verify the acceleration data; however, due to unknown technical error the accelerometer data was corrupted. Due to non-availability of the testing car park, the repetition was not possible and therefore yaw sensor data has been used for further validation.

Steady-state response

It is a recommended practice [sta 2004] to drive a vehicle on a constant radius path with variable speed to identify its steady-state circular driving behaviour. This can be managed in two ways, increasing the vehicle speed in a discrete manner for each test or steadily increasing the speed and recording the data in a continuous manner. In this case, the radius of the circular path was kept at 30 m and the vehicle was driven with different speeds. The standard [sta 2004] suggests to keep the vehicle in steady-state during this motion for 3 seconds at least and use that data to plot the steer angle against the lateral acceleration. However, due to loss of lateral acceleration data during the testing phase, the steer angle data at front wheels is plotted against the vehicle speed, as shown in Fig. 4.29. For low lateral acceleration range the vehicle lateral acceleration

can be estimated using the following relationship [Rajamani 2006].

$$a_y = \frac{u^2}{R} \tag{4.3}$$

But in order to keep the consistency with the experimental plot the simulated results are also plotted against the vehicle speeds instead of its lateral acceleration. The root mean square error between the experimental and simulated data, shown in Fig. 4.29, is approximately 0.3°, which is an acceptable range keeping in view the limitations of the driver to follow the track with precision

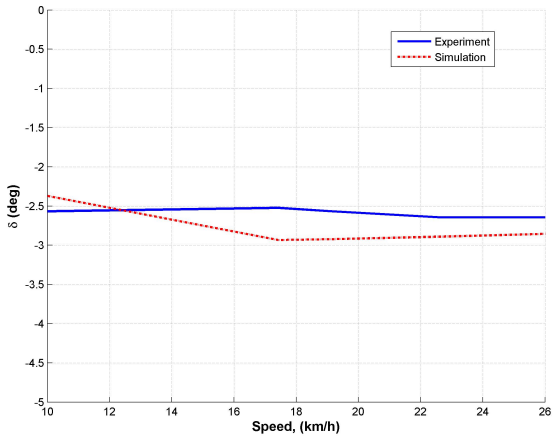

Figure 4.29: Constant radius testing for 30 m test track

and keeping the speed constant at all instants. As the figure suggests the maximum speed attained was approximately 26 km/h, beyond which it was difficult for the driver to avoid the obstacles while keeping the vehicle on the desired track.

Therefore the radius of the desired path was reduced to 20 m and a constant radius manoeuvre with increasing speed was performed to a point where it was not possible to control the vehicle safely. The reduction in the test track's radius allowed to run the test vehicle on a greater speed thus allowing to collect more sample data. This increase in the experimental data improved the quality of results, which is evident from Fig. 4.30. This figure presents the results gathered during this manoeuvre and compares with the simulated results collected using the Simulink models. In this case the vehicle models discussed in section 3.2.3 and 3.2.4, modelled in Matlab/Simulink, are simulated using the speed and steering commands that were recorded during the experiments. As mentioned earlier the purpose was to verify the validity of these Simulink models. The simulated curves for seven and eight degrees of

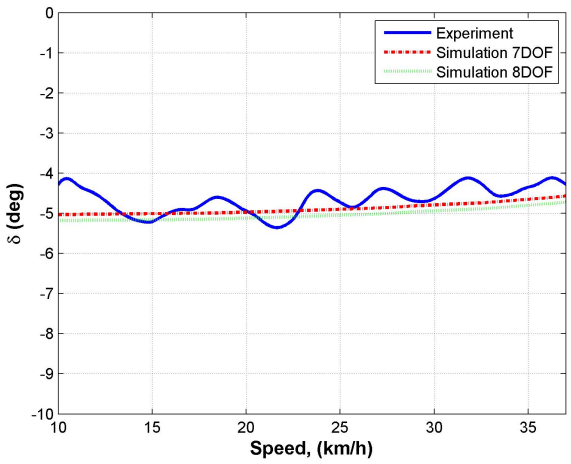

Figure 4.30: Constant radius testing for 20 m circular path

freedom models are following the experimental curve with an error of less than 14%, which is acceptable because of the reasons already discussed above.

It can be observed from Fig. 4.30 that the response of seven and eight degrees models is identical. This happens because of the fact that when a vehicle is subjected to low lateral acceleration range the roll degree of freedom does not have a visible effect. Using Eqn. 4.3 the maximum lateral acceleration, to which the test vehicle was subjected on the 30 m test track, can be estimated as 0.2 g and for the 20 m test track as 0.5 g. Thus for further validation purpose the seven degrees of freedom vehicle model, along with wheels load transfer, will be used and later on in Chapter 5 eight degrees of freedom model will also be used to assess the controller's performance.

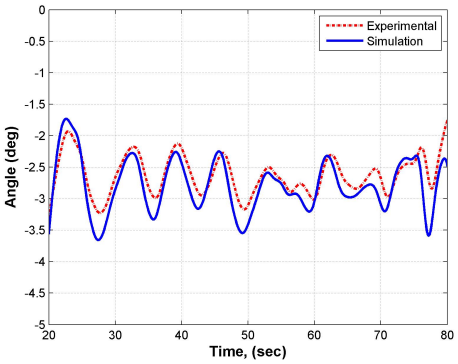

Figure 4.31: Right wheel angle $(7.24m/s)$

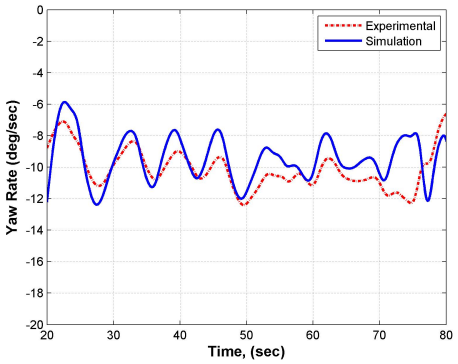

Figure 4.32: Vehicle yaw-rate $(7.24m/s)$

Figure 4.31 and 4.32 (enlarged view in Appendix J) show the correlation obtained between the few variables recorded during the testing and then simulated using the Simulink model. These figures represent the experimental and simulated data for a 30 m constant radius manoeuvre with the forward speed of approximately 26 km/h. Figure 4.31 shows the front right wheel movement and it shows that the simulated results follow the experimental curve with the root mean square error of 0.33° during the steady state. Similarly the yaw-rate curves shown in the Fig. 4.32 suggest that the simulated results follow the experimental data with an error having rms value of approximately 2 deg/s. The results obtained from constant radius testing suggest that the steady-state behaviour of the seven degrees of freedom model developed in MATLAB/Simulink has an agreement with that of the experimental vehicle.

4.5.2 Lateral transient response testing

Another aspect that is important in vehicle dynamics is the transient response. This also gives and additional set of data to help validate the vehicle model. It is of very much interest of the vehicle designer to investigate the vehicle performance once it is disturbed from its steady-state condition. The performance can evaluated by measuring driver input, vehicle yaw-rate and the lateral acceleration during these transient conditions. BS ISO 7401:2003 [sta 2003] explains the test methods to analyse the lateral transient response of a vehicle in detail. The general guidance has been taken from this document to measure the experimental vehicle response for a step input. These sort of tests provide useful information about the vehicle behaviour during critical manoeuvres like lane change or obstacle avoidance. Figure 4.33 shows the path that was followed during the the testing. The markers in the figure represent the cones, which were used to help the driver to perform the manoeuvre. To maintain safe operation of the vehicle its speed had to be kept low, the maximum speed achieved approximately 10 km/h.

Figures 4.35, 4.36, 4.37 and 4.38 (enlarged view in Appendix K and L) show the data recorded while following the path shown in Fig. 4.34. The first stretch of this path is the lane change manoeuvre as shown in the Fig. 4.33, whereas two 180° turns are also included for approaching the starting point. These figures also show the simulated results that were generated by using the driver commands and speed data, collected through the potentiometer and GPS module respectively, as inputs to the seven degrees of freedom model. To use the GPS data an interpolated look-up table was used because the speed data was not collected with the same frequency as that of the other data. It can be observed from these figures that simulated results the experimental responses with a little offset. Few of the factors, which can cause this

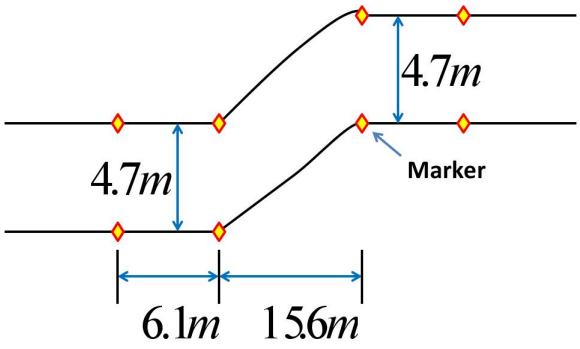

Figure 4.33: Lane change path

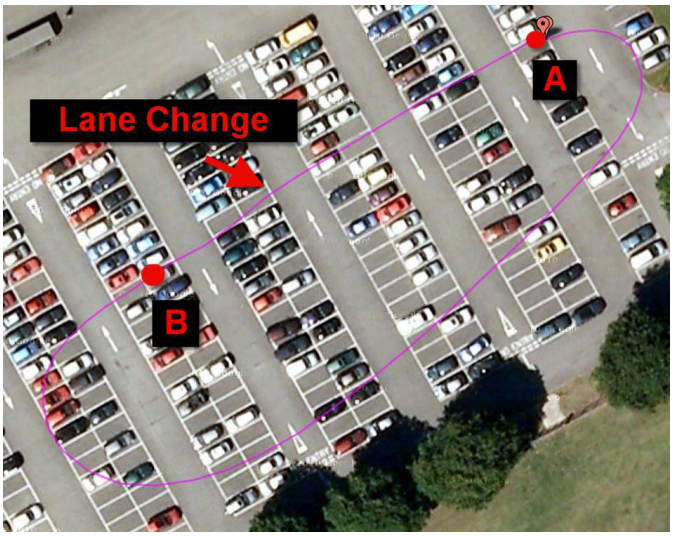

Figure 4.34: Lane change path followed by the test vehicle between A and B

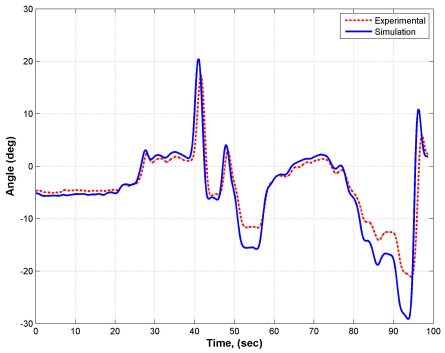

Figure 4.35: Right wheel angle ($2.21m/s$)

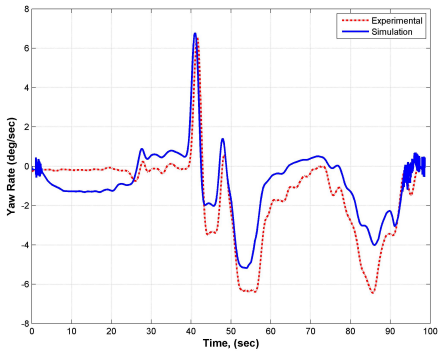

Figure 4.36: Vehicle yaw-rate ($2.21m/s$)

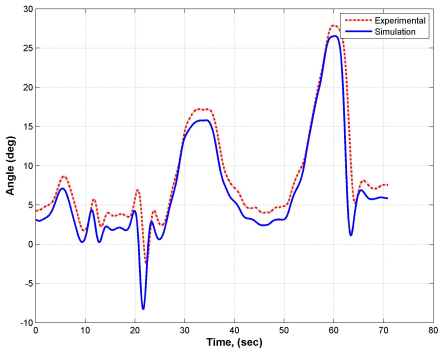

Figure 4.37: Right wheel angle ($2.73m/s$)

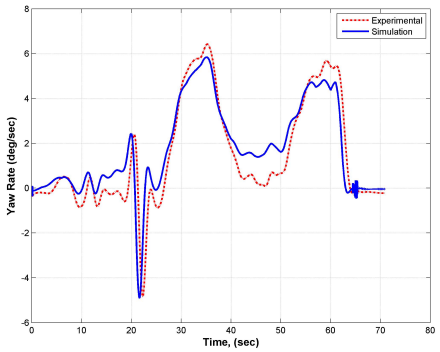

Figure 4.38: Vehicle yaw-rate ($2.73m/s$)

discrepancy, include the noise in the recorded signals especially from the potentiometer. Although an anti-alias filter was used to reduce the noise factor but still the output from the potentiometer contained stray signals. These unwanted inputs to the Simulink model made the simulated responses to distort. Another factor that may influenced the results was the time synchronisation among the recorded data. The experimental data was collected from different sensors having different output frequencies, therefore the time synchronisation was found to be an issue during the analysis phase. Keeping these constraints in view the broad agreement between the recorded and simulated data suggests that the Simulink model is able to generally represent the vehicle in dynamic conditions with an acceptable accuracy.

4.5.3 Driver model verification

During the experimental vehicle testing phase one phenomenon that was greatly observed was the effort that the driver was putting into keep the vehicle under control and follow the chosen path. The steer-by-wire system being different from a conventional steering system, in terms of feel and response time, was demanding more input in terms of steering wheel movement. The delay induced by the low-bandwidth steering actuators was not allowing the driver to steer it with ease. Same has been expressed by the test driver in the form of following comments after the experiments:

- *"Felt very unresponsive due to the delay, which was quite long."*
- *"Wound too much steering on because of the lag and ended up breaking the sensor at the end of the test due to this."*

Therefore it has been felt appropriate to include the driver model in the simulation environment to study the effect of the proposed control system on the human effort involved to keep such vehicle on the given track. For this purpose the driver model, discussed in section 3.4, has been integrated with the seven degrees of freedom vehicle model and used to follow the path shown in Fig. 4.34. In order to achieve this goal the latitude and longitude information collected with the help of GPS sensor has been used to define the points that the driver model has to to follow. Figure 4.39 shows the desired track transformed in the local coordinate system of the simulated vehicle. Figure 4.40 shows a green curve which is the trace of the path that the driver model followed during the simulation. Figure 4.41 shows the comparison of the simulated driver's commands to the experimental one recorded on the ground. Both of the curves show an acceptable correlation and therefore it can be concluded with confidence that the simulated driver model is able to mimic the driver behaviour and keep the vehicle on the chosen course.

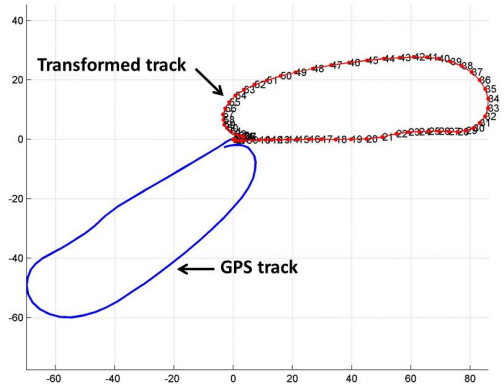

Figure 4.39: Track transformation

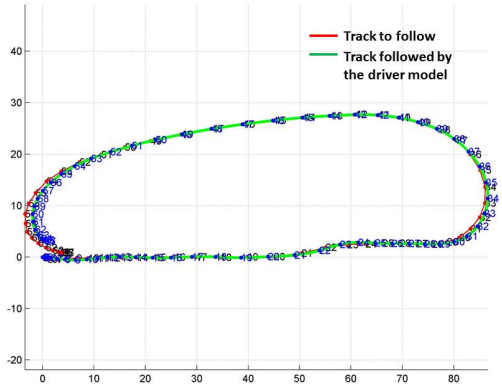

Figure 4.40: Track following

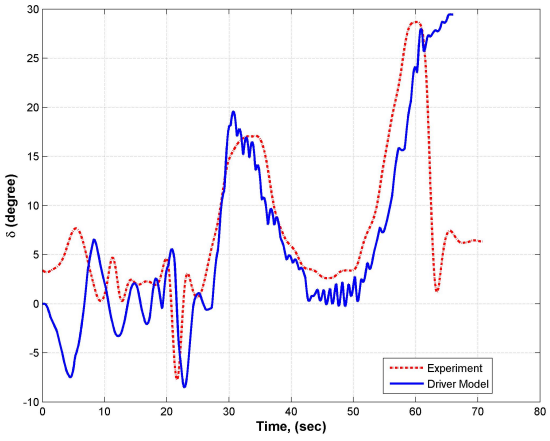

Figure 4.41: Driver commands comparison

Chapter 5

Control

Contents

5.1 Introduction

This chapter looks at the design of a controller to make the steer-by-wire vehicle, equipped with low performing actuators, behave like a conventional vehicle. Initially the open-loop behaviour of the vehicle is examined and shown to have poor performance, which makes it difficult for the driver to control. Then the driver model is brought into the loop and performance of whole system is also analysed, which shows that driver finds it difficult to control and keep the vehicle on the desired track. The next section discusses the cascade controller, consisting of two parts, designed to provide torque

vectoring for vehicle handling performance enhancement. The upper controller monitors the vehicle yaw-rate and generates a control signal based on the linear quadratic regulator theory. This control signal varies the torque value available on each wheel through the in-wheel motor. The lower controller is a robust sliding model controller, which keeps the wheel slip value within a desired range. The last section evaluates the controller performance by integrating it with the vehicle models discussed in Chapter 3. This section presents the simulated results of various manoeuvres and discusses the effect of the controller on the vehicle handling behaviour.

5.2 Background

In previous chapter it has been mentioned that the steady-state and transient handling response give insight about the vehicle's handling behaviour. For a conventional passive vehicle both of these responses vary with its speed and the vehicle handling can be categorised into linear and non-linear regimes. This classification is mainly due to the limitation of the tyres to generate lateral and longitudinal forces in a linear manner during a demanding manoeuvre. Such physical constraints directly effect the steady state and transient response of the vehicle in the non-linear handling regime thus influencing the ***steerability*** and ***stability*** of the vehicle.

As per Segel's definition, described in the literature review section, this thesis uses the handling term predominantly for the lateral dynamics of a vehicle. Therefore the focus of this chapter is to develop a vehicle controller that maintains the vehicle's lateral handling response within the desired boundaries thus making the vehicle steerable and stable during a demanding manoeuvre.

5.2.1 Fundamental vehicle responses

In chapter 4, the equation for understeer gradient (K_{us}) has been introduced. Figure 5.1 shows the effect of this term on the vehicle response during a steady state manoeuvre. This figure has been generated by simulating the bicycle model in Simulink and varying the location of the COG of the vehicle. A vehicle is termed as *understeer* when the value of K_{us} is positive, whereas a vehicle having a negative value for K_{us} is called *oversteer*. For a *neutralsteer* vehicle the understeer gradient is zero. In this figure vehicle of each type has been simulated to be following a circular track of 20 m radius and the curves show that for an understeer vehicle the requirement of steering input increases with increase in speed to keep it on the desired track. The speed at which the value of δ becomes twice the value of Ackerman angle is known as

characteristic speed. On the contrary the oversteer vehicle demands decrease in steering angle as the forward speed increases to counter the effect of rising yaw moment. The speed value above which the oversteer vehicle becomes unstable is termed as *critical speed*. For an ordinary driver it becomes difficult to keep the vehicle under control beyond this limit as the vehicle becomes unstable. For a neutral steer vehicle the forward speed does not have any influence and the vehicle is able to follow the circular track with a constant steer angle at all speeds.

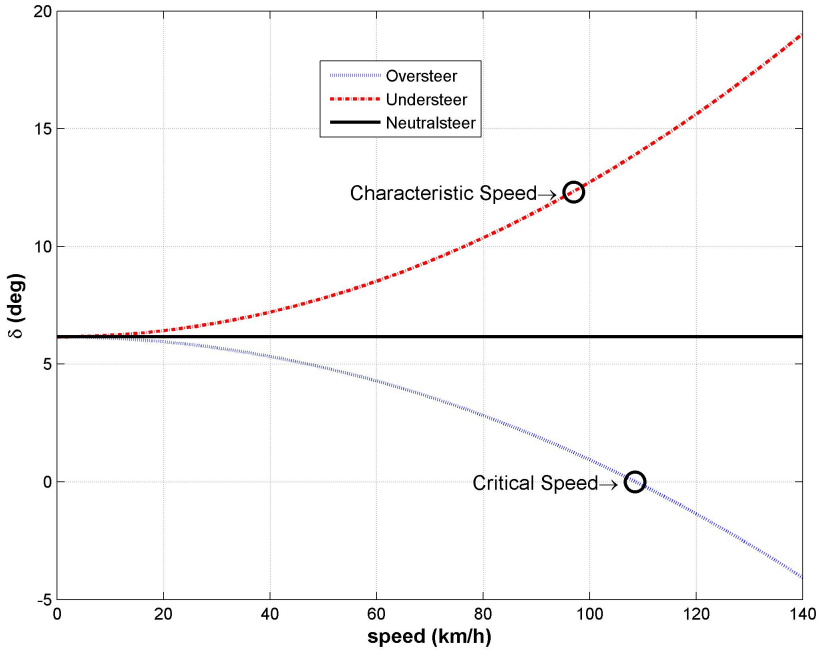

Figure 5.1: Steady state response with increasing speed

It is seen in Fig. 5.1 that for low speeds the understeer and oversteer vehicles behave like a neutral steer vehicle and the steer angle required to keep them on track does not vary in a significant manner. Similar sort of behaviour is also evident in Fig. 4.29 and Fig. 4.30, where the value of steer angle remains very much constant within the range of speed for which it was tested. The reason behind this sort of response is that the vehicle is moving within a region where its lateral acceleration is low. It has already been mentioned that the vehicle's lateral dynamics can be categorised into three sections depending on the lateral acceleration of the vehicle. Using the description given by Dixon [Dixon 1988] the three sections and the lateral acceleration ranges are as follows:

- Primary handling (0∼0.3g)
- Secondary handling (0.3g ∼0.6g)
- Final handling (0.6g ∼limit)

The primary handling region falls into the linear regime whereas the other two are considered as the non-linear handling domain for a vehicle.

In a similar manner the vehicle speed also influences its lateral transient response. This effect can be explained by plotting poles location of the system with reference to increasing speed. Figure 5.2 is a pole plot, generated using Simulink for illustration purposes, in which the vehicle bicycle model is acting as the dynamic system. The plot shows that as vehicle's speed increases the damping of the system decreases and therefore the poles move further away towards the imaginary axis. This reduced damping could make it challenging for an average driver to anticipate the response of an understeer vehicle at a high speed.

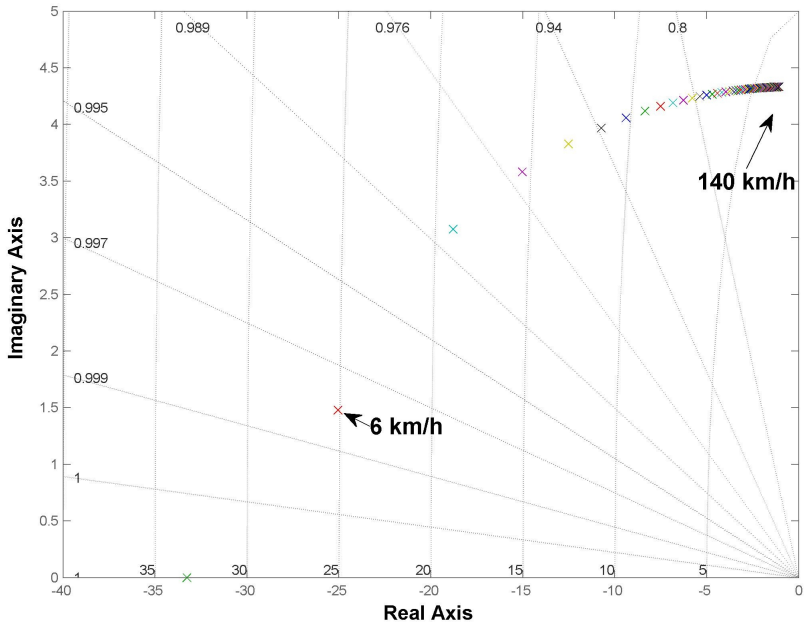

Figure 5.2: Pole location of vehicle bicycle model with varying speed for an understeer vehicle

5.2.2 Effect of steering dynamics on a vehicle's behaviour

The responses, mentioned above, which are generally considered to describe a vehicle's behaviour are greatly influenced by the characteristics of its steering system. Abe [Abe 2009] has described the same in the following manner:

"The vehicle actual US, OS steer characteristics not only depend on the tire characteristic and front and rear wheel positions, but also greatly depend on the steering system."

Thus the steering system dynamics can make a theoretically oversteer vehicle, based on the centre of mass location and tyre cornering stiffnesses, to behave like an understeer one and vice versa. This can be explained with the help of Fig. 5.3, which is a bode plot showing response of two vehicles models subjected to steering input of increasing frequency. One of the vehicles is modelled with an assumption that the steering dynamics is absent, whereas the other one includes the steering dynamics model discussed in section 4.4.4. The former model is termed as the conventional vehicle and later is called as the steer-by-wire vehicle in the following discussion.

These graphs contain two sorts of information; firstly, it is evident that the increase in steering frequency at higher longitudinal speeds affects the vehicle's response. Secondly, the inclusion of steering dynamics highlight its limiting effect on the overall response of the vehicle. These plots further show that the conventional vehicle remains responsive in a consistent manner to the steering input up to 1 Hz with a slight phase delay when moving with the speed of 50 km/h. However, a similar vehicle model including the corresponding dynamics of steer-by-wire system shows reduced performance when subjected to the same input conditions. The performance of the steer-by-wire vehicle drops excessively when the input frequency increases beyond 0.1 Hz and the vehicle yaw-rate gain drops down. The same is visible in a pronounced manner when the vehicles are moving at 100 km/h speed.

The yaw-rate gain plot also shows that the gain magnitude for both vehicles is a negative value when their speed is 50 km/h. This suggests that the amplitude of output is smaller than the amplitude of the input. The gain magnitude for the same vehicles, when moving with the speed of 100 km/h, is positive for the frequencies up to 0.1 Hz. This means that the vehicles are more sensitive to the steering inputs of lower frequencies at higher speeds. Furthermore, both yaw and lateral acceleration responses show that the steer-by-wire vehicle while travelling at the higher speed becomes unstable when the steering input of frequency higher than 1 Hz is supplied.

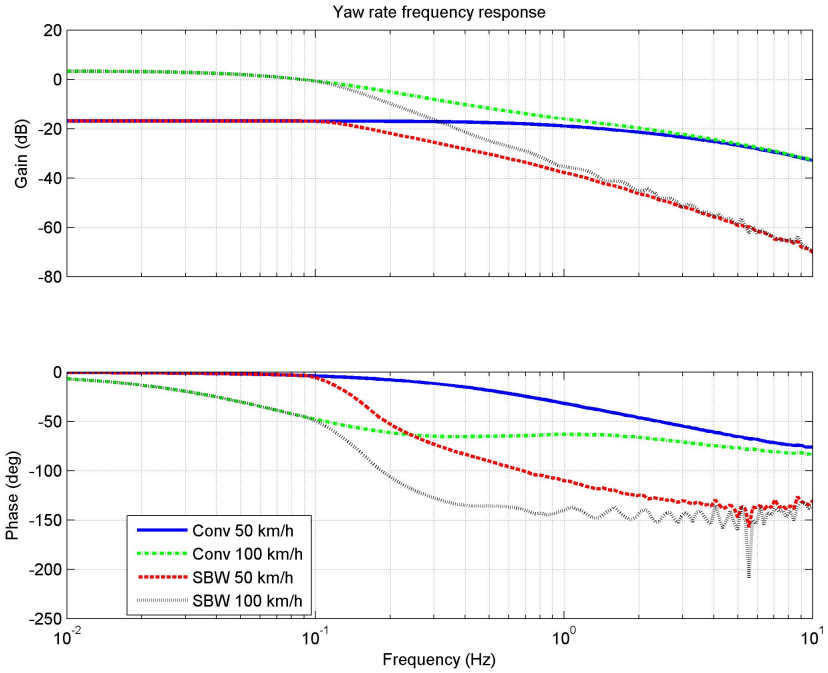

(a) Yaw-rate amplitude and phase plots

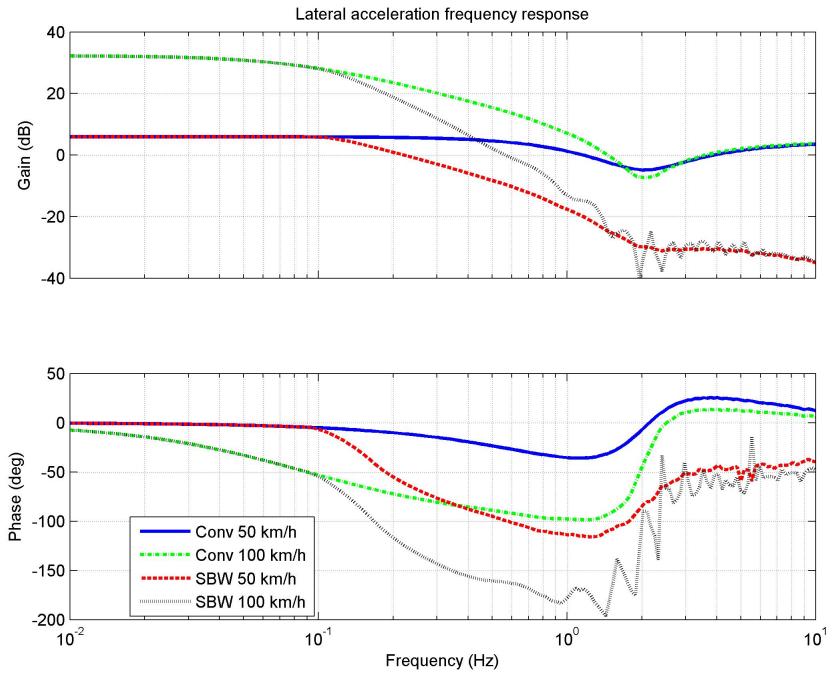

(b) Lateral acceleration amplitude and phase plots

Figure 5.3: Frequency response comparison of conventional and steer-by-wire vehicles

5.2.3 Driver's reaction with the steer-by-wire vehicle

The above discussion on the frequency response supports the observation made during the experimenting phase that the driver found it difficult to control the steer-by-wire vehicle with an increasing speed. This can be correlated to the actuators bandwidth, discussed in section 4.4.5. The bandwidth of a human driver is 2 to 3 Hz and it becomes really difficult for the driver to control the steer-by-wire vehicle in emergency manoeuvres like obstacle avoidance and high speed lane change. In order to investigate the increased driver's effort required to keep the steer-by-wire vehicle on the desired track, simulations were performed in which conventional and steer-by-wire vehicles, both integrated with the driver model presented in chapter 3, were driven on a straight path at a speed of 60 km/h and subjected to a sudden wind gust. This situation was simulated by introducing a lateral force in the form of an impulse. The terms conventional vehicle and steer-by-wire vehicle follow the same definition as described in section 5.2.1. For the vehicle modelling the seven degrees of freedom non-linear vehicle model has been used. Figure 5.4 shows that, for the same sort of situation, the steer-by-wire vehicle's driver had to put more effort into keep the vehicle on the desired track. The driver's effort for both cases can be compared on the basis of number of actions performed, the amplitude of input and the time taken by driver to bring the vehicle to a stable condition again.

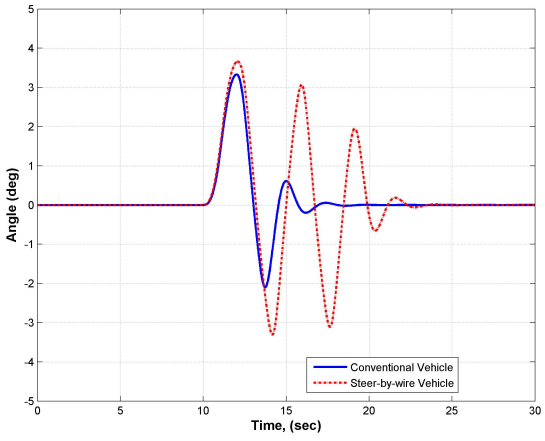

Figure 5.4: Driver's effort to keep the vehicle under control against a disturbance

With increase in speed it was observed that the front steering angle of the steer-by-wire vehicle was higher than that of the conventional vehicle, thus causing the tyres to operate in a saturated range. This limiting factor for

the steer-by-wire vehicle induces the non-linearities within the system earlier than it happens for a conventional steering arrangement. For higher speeds the results were further deteriorated as the steer by vehicle was unable to respond as per driver's requirements and therefore became unstable. Figure 5.5 shows the situation when the vehicle, moving at 80 km/h, was subjected to the side wind.

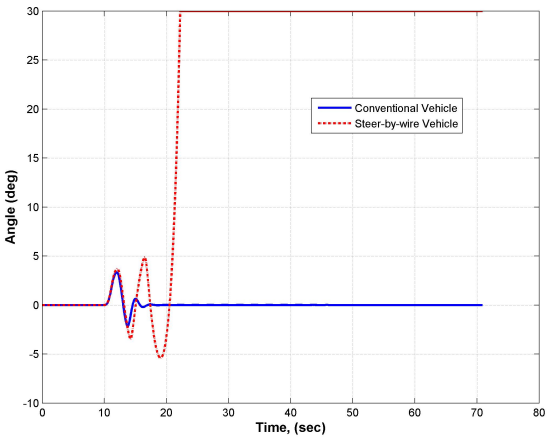

Figure 5.5: Steer-by-wire vehicle becomes unstable (u=80 km/h)

5.3 Control Objective and Strategy

In previous sections it has been established that inclusion of low performance actuator's dynamics in the steer-by-wire model reduces the steerability and stability of the system and significantly increased the work load of the driver. Therefore the objective of the proposed control technique is to enhance the steer-by-wire vehicle steerability and make it comparable to a conventional vehicle with mechanical steering system. Although steerability is a subjective phenomenon but generally it is termed as the ability of the vehicle to follow the driver's commands with ease. An average driver is able to steer a vehicle without difficulty while it is operating in a linear handling regime, whereas for well into the non-linear region the skill set of an expert driver is desired. It is evident from Fig. 5.3 that the steer-by-wire vehicle shows a poor behaviour even at lower speeds thus making it difficult to control. Therefore, the objective can be stated as to make the steer-by-wire vehicle respond to the driver input with little lag and in a damped manner thus making it to behave like a conventional steer vehicle.

As mentioned in the literature review a cascade type approach has been selected to achieve the desired goal. In this approach two separate control algorithms have been used in conjunction as shown in Fig. 5.6. The upper controller is based on the optimal control theory, where as the lower controller follows a more robust approach termed as sliding more control. The following sections discuss the general theory for both of these techniques, in brief, before discussing the control design and applying it to the steering by wire vehicle.

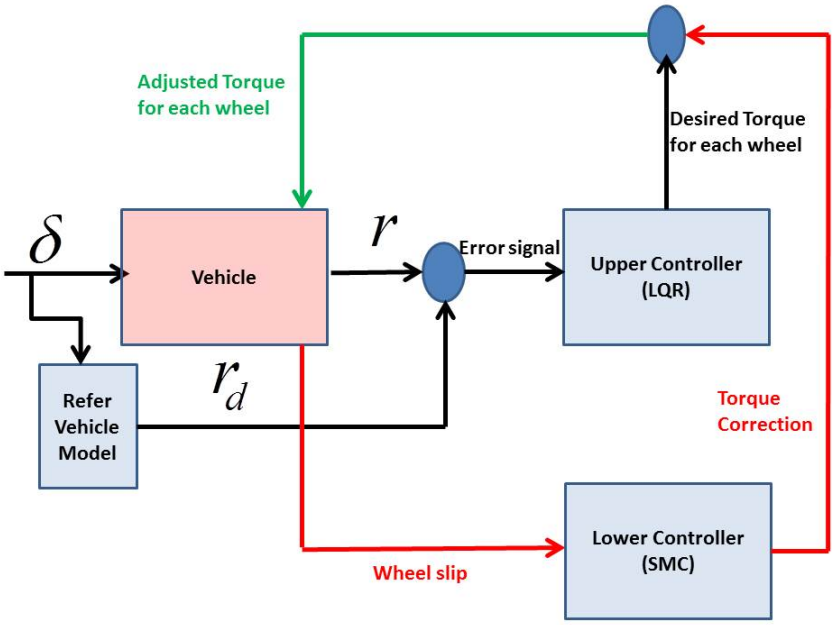

Figure 5.6: Proposed control system layout

5.3.1 Linear quadratic regulator (LQR)

This section discusses the design of an optimal control system that is described by a state space formulation. This approach seeks to control the plant so as to get the best possible performance from it. In order to achieve this aim, those aspects of the plant behaviour which it is desired to control are incorporated into a mathematical expression, and the controller design process synthesises a controller which will minimise that expression [Dutton 1998]. The theory behind this approach can be explained by supposing a linear system:

$$\dot{x} = Ax + Bu \tag{5.1}$$

$$y = Cx + Du \tag{5.2}$$

This system can be optimised by choosing a *performance index* or *cost function*, which once minimised causes the system to provide the desired operating

performance. Such sort of systems that are adjusted to provide a minimum performance index are often called an optimal control system. Assuming $u(t)$ be a control input that will minimise the cost function J i.e.

$$J = \frac{1}{2}\int_0^\infty (x^T Q x + u^T R u)\,\mathrm{d}t \tag{5.3}$$

where

Q is a +ve semi-definite
R is a +ve definite

These assumptions imply that the cost is non-negative, so its minimum value is zero. In order for the cost function to achieve its minimum value, both x and u must go zero, thus making it a regulator problem. When the state vector is to track non-zero values, J can be redefined to create an optimal servomechanism (tracking) problem.

Considering the system as a scalar, i.e. a first order system, a simple interpretation of the cost function can be taken as follows

$$J = \frac{1}{2}\int_0^\infty (qx^2 + ru^2)\,\mathrm{d}t \tag{5.4}$$

Now the J represents the weighted sum of energy of the state and control. Small q and r are used respectively when x and u are scalars. If r is very large relative to q, which implies the control energy is penalised heavily, the control effort will diminish at the expense of larger values of the state. This physically translates into smaller motors, actuators, and amplifier gains to implement the control law.

Likewise, if q is much larger than r, which means the state is penalised heavily, the control effort rises to reduce the state resulting in a damped system. In a general case Q and R represent respective weights on different states and control channels. By putting a larger weight on the first state, we are putting more emphasis on controlling this state and restricting the fluctuations in it.

To solve a LQR problem several procedures are available like Hamilton, Euler, Lagrange and Jacobi. One approach to finding a controller that minimises the LQR cost function is based on finding the positive definite solution of the steady-state Algebraic Riccati Equation (ARE), given below. The advantage of using steady-state equation instead of dynamic one is that the fixed coefficients make the problem simpler to solve.

$$A^T P + PA + Q - PBR^{-1}B^T P = 0 \tag{5.5}$$

It turns out that under the conditions stated below, the positive definite solution of the ARE results in an asymptotically stable closed loop system.

- The system is controllable, R is positive definite.
- Q can be factored as $Q = {C_q}^T C_q$ where C_q is any matrix such that (C_q, A) is observable.

These conditions are necessary and sufficient for the existence and uniqueness of the optimal controller that will asymptotically stabilise the system.

5.3.2 Sliding mode control (SMC)

In linear control design generally it is assumed that the parameters of the system model are reasonably known [Slotine 1991]; however, this does not stand true for the wheel slip control. This problem can be categorised as a non-linear phenomenon due to the fact that the wheel operates under highly uncertain conditions. The wheel performance is greatly influenced by a number of factors like tyre rubber properties, the vertical load acting on the wheel and the frictional coefficient between the tyre and ground. All these factors are dynamic in nature and their deviation from nominal values effects the tyre performance. Due to the problem's non-linear nature a robust controller is a suitable choice to achieve the desired results.

The concept of sliding mode control can be applied to a single-input system as well as a multi-input system. Slotine and Li [Slotine 1991] have presented the basics of a sliding mode control by considering a single-input dynamic system as follows:

$$x^{(n)} = f(\mathbf{x}) + b(\mathbf{x})u \tag{5.6}$$

where the scalar x is the output of interest, the scalar u is the control input, and $\mathbf{x} = [x\ \dot{x}\ ...\ x^{(n-1)}]^T$ is the state vector. In Eqn. 5.6 the function $f(\mathbf{x})$ (in general non-linear) is not exactly known, but the extent of the imprecision on $f(\mathbf{x})$ is upper bounded by a known continuous function of $\mathbf{x}$; similarly, the control gain $b(\mathbf{x})$ is not exactly known, but is of known sign and is bounded by known, continuous functions of $\mathbf{x}$. The control problem is to get the state $\mathbf{x}$ to track a specific time-varying state $\mathbf{x_d} = [x_d\ \dot{x_d}\ ...\ {x_d}^{(n-1)}]^T$ in the presence of model imprecision on $\mathbf{f}(\mathbf{x})$ and $\mathbf{b}(\mathbf{x})$. For the tracking task to be achievable using a finite control u, the initial desired state $\mathbf{x_d}(\mathbf{0})$ must be such that

$$\mathbf{x_d}(\mathbf{0}) = \mathbf{x}(\mathbf{0}) \tag{5.7}$$

Let $\tilde{x} = x - x_d$ be the tracking error in the variable x, and let

$$\tilde{\mathbf{x}} = \mathbf{x} - \mathbf{x_d} = [\tilde{x}\ \dot{\tilde{x}}\ ...\ \tilde{x}^{(n-1)}]^T$$

be the tracking error vector. Furthermore, a time-varying surface $S(t)$ can be defined in the state-space $\mathbf{R}^{(n)}$ by the scalar equation $s(\mathbf{x};t) = 0$, where

$$s(\mathbf{x};t) = (\frac{d}{dt} + \lambda)^{n-1}\tilde{x} \tag{5.8}$$

and λ is a positive constant. Given initial condition as in Eqn. 5.7, the problem of tracking $\mathbf{x} \equiv \mathbf{x}_(\mathbf{d})$ is equivalent to that of remaining on the surface $S(t)$ for all $t > 0$; indeed $s \equiv 0$ represents a linear differential equation whose unique solution is $\tilde{\mathbf{x}} \equiv \mathbf{0}$, given initial conditions in Eqn. 5.7. Thus, the problem of tracking the n-dimensional vector $\mathbf{x_d}$ can be reduced to that of keeping the scalar quantity s at zero. More precisely, the problem of tracking the n-dimensional vector $\mathbf{x_d}$ can in effect be replaced by a 1^{st}-order stabilisation problem in s. Furthermore, bounds on s can be directly translated into bounds on the tracking error vector $\tilde{\mathbf{x}}$, and therefore the scalar s represents a true measure of tracking performance. Specifically, assuming that $\tilde{\mathbf{x}}(0) = \mathbf{0}$, one gets

$$\forall t \geq 0, |s(t)| \leq \Phi \quad \Rightarrow \quad \forall t \geq 0, |\tilde{x}^{(i)}(t)| \leq (2\lambda)^i \varepsilon \text{ where } i = 0, ..., n-1 \tag{5.9}$$

In the above equation $\varepsilon = \Phi/\lambda^{n-1}$, where Φ and ε are the thickness and width of the boundary layer respectively as shown in Fig. 5.7.

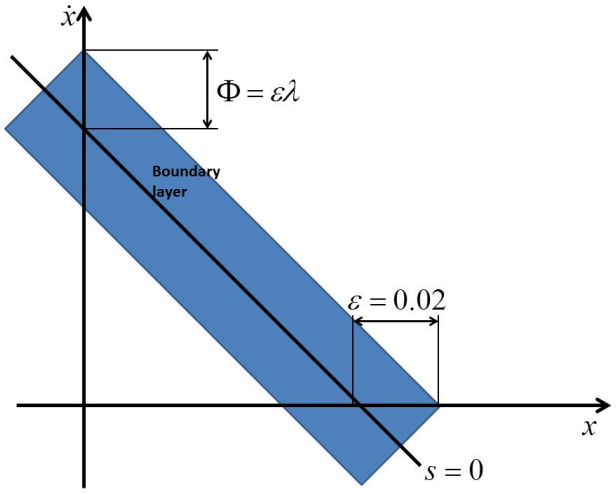

Figure 5.7: The boundary layer [Slotine 1991]

The control function u in Eqn. 5.6 can be obtained by introducing the Lyapunov function

$$V(x) = \frac{s^2(\mathbf{x};t)}{2} \tag{5.10}$$

where $s(\mathbf{x};t)$ is the sliding surface, defined in Eqn. 5.8. The stability criteria requires the condition $\dot{V}(x) \leq 0$ to be true. Substituting the Lyapunov function definition defined in Eqn. 5.10 in the stability condition reduces it to $s\dot{s} \leq 0$, which allows the control function to be defined such that s and $\dot{s}$ have opposite signs. Young et al [Young 1996] suggests the control function to be $-\eta sign(s)$, where η is a positive constant. This selection of the control law makes the system trajectories to slide towards the surface $S(t)$ and remains there. This condition is known as the *sliding condition* and is shown in Fig.5.8. Once the system trajectory reaches the sliding surface, the control system tries

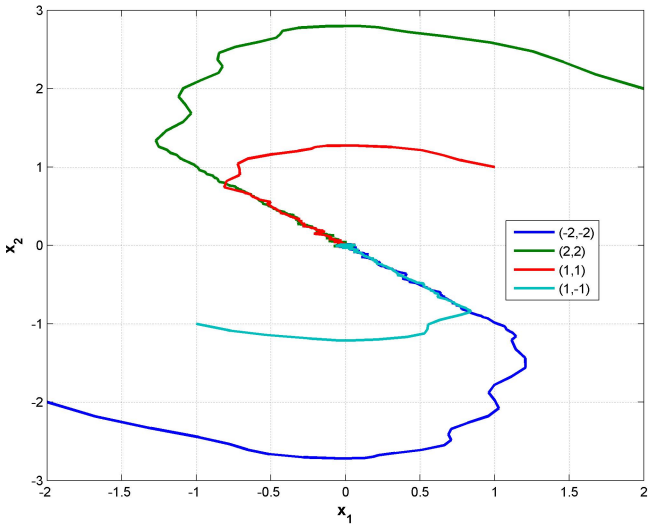

Figure 5.8: System trajectories bahviour with varied initial conditions

to keep it there by switching at infinite frequency. The practical limitation imposed by the discrete-time micro-controllers does not allow the ideal sliding mode to be implemented and discontinuities in the control result in oscillations at finite frequency referred to as *chattering* [Sabanovic 2004]. This chattering phenomenon, visible in Fig. 5.8, gives rise to high heat losses and high wear in electrical circuits and mechanical parts respectively and hence in majority of the cases is undesirable. Different approaches have been suggested by researchers to minimise this unwanted effect; Utkin in the first chapter of a book [Sabanovic 2004] suggested that the chattering caused by unmodelled dynamics may be eliminated in systems with Luenberger observers whereas Kuo-Kai Shyu et al [Shyu 1992] proposed a modified variable structure controller to alleviate this problem. In this thesis saturation function *sat* has been used to replace the discontinuous switching with smooth and continuous switching as suggested by Slotine and Li [Slotine 1991] and implemented by

Zheng et al [Zheng 2006] and many others. The new smooth switching function is defined below and replaces the term $-\eta sign(s)$ in the control output with $-\eta sat(\frac{s}{\Phi})$.

$$sat(\frac{s}{\Phi}) = \begin{cases} 1 & , \frac{s}{\Phi} > 1 \\ \frac{s}{\Phi} & , -1 \leq \frac{s}{\Phi} \leq 1 \\ -1 & , \frac{s}{\Phi} < -1 \end{cases} \tag{5.11}$$

Figure 5.9 shows the improvement achieved when the system approaches to the sliding surface. The chattering phenomenon which is visible in Fig. 5.8 has been replaced by a smooth line. Both of these figures have been generated in Simulink using random data to illustrate the concept.

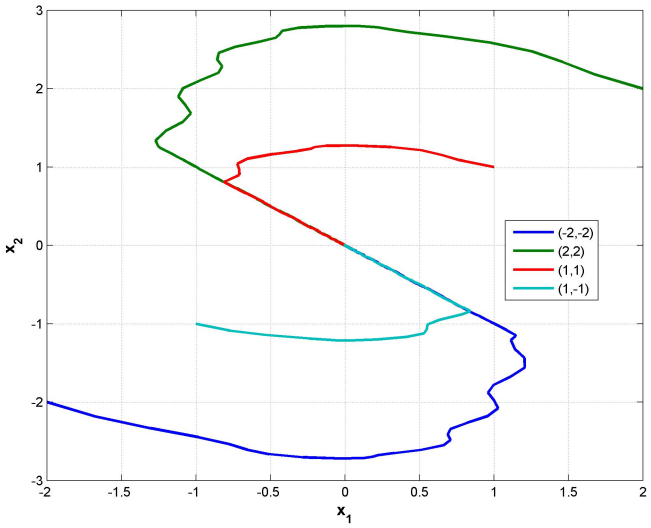

Figure 5.9: Elimination of chattering phenomenon by introducing $sat(\frac{s}{\Phi})$ function

5.3.3 Control strategy

The control system has been developed by bringing in-wheel motors into the vehicle model. The idea of electric vehicles is gaining popularity as awareness about the environment friendly transportation is spreading. An electric vehicle with in-wheel motors has some added advantages like torque at each wheel can be individually controlled, more space for occupants and luggage sans differential and auxiliaries. Moreover, this arrangement allows to gather important information about rotational speed of each wheel and the corresponding torque by monitoring the motor current.

It has already been observed that a steer-by-wire system with the low performance actuators effects the vehicle lateral handling characteristics. This limited handling behaviour can be improved by introducing a skid steering system in conjunction with the steer-by-wire system. The in-wheel motors can be utilised to develop an extra torque moment, which augments the yaw-rate response of the steer-by-wire vehicle. This technique is generally known as *torque vectoring*. The combination of in-wheel motors and steer-by-wire system not only enhances the vehicle performance but also improves the occupant safety and convenience.

Figure 5.10 shows the layout of the system in Simulink and it has been assumed that the vehicle is fitted with the necessary sensors to acquire the

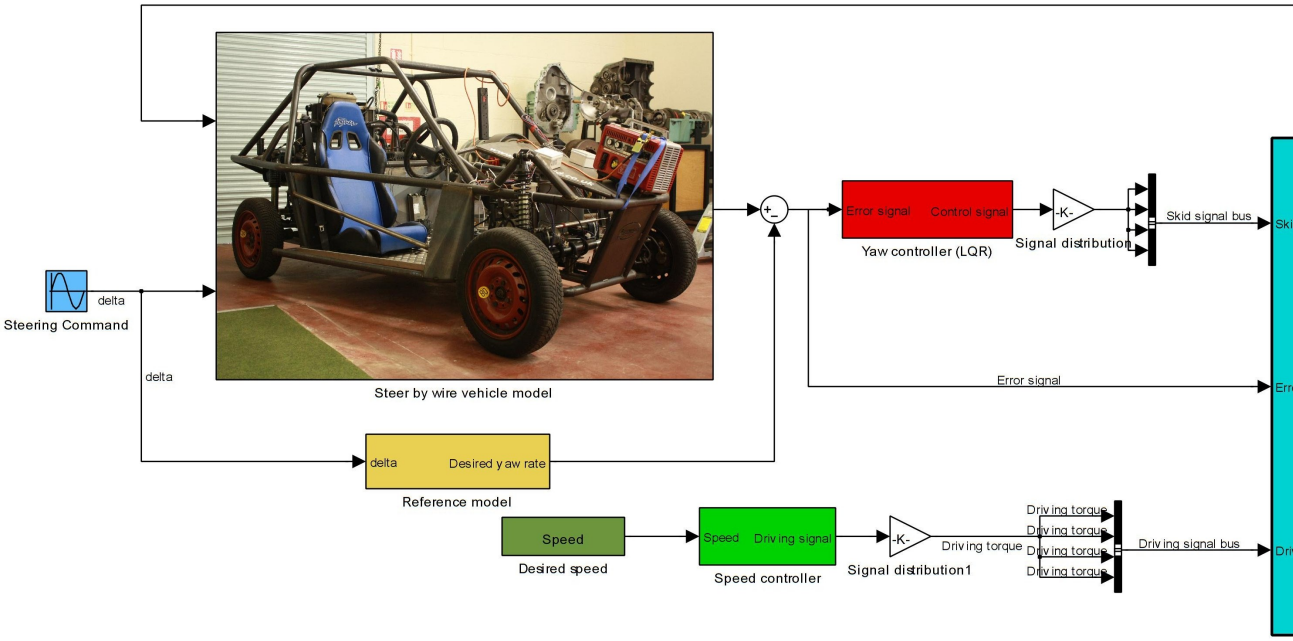

Figure 5.10: Layout of the control system in Simulink

vehicle states for the control system. The vehicle speed is maintained by a PI-controller, which generates the control signal for the in-wheel motors to keep the vehicle moving with the desired speed. When a steer command is introduced by the driver, the upper level yaw controller compares the vehicle yaw-rate, acquired using the yaw sensor, with that of the reference model. The error signal is used to calculate the torque adjustment at each wheel by using a logic block.

Table 5.1 shows the logic used to distribute torque on each wheel during left and right turning. Depending on the yaw-rate error between the desired and

the available yaw-rate, the logic block either add or subtract the demanded torque from the driving torque available on the wheels. The logic block also takes the steering angle into account to calculate the output. The addition and subtraction of torque make the left and right wheels rotate with different angular velocities thus generating skid steer effect. The resultant moment developed due to the skid effect helps the vehicle to achieve the desired yaw-rate. The output of the logic block, which is a voltage signal, goes to the in-

Left Turn		Right Turn	
Yaw error > 0	Yaw error < 0	Yaw error > 0	Yaw error < 0
Right wheels slow Left wheels fast	Right wheels fast Left wheels slow	Right wheels slow Left wheels fast	Right wheels fast Left wheels slow

Table 5.1: Logic for torque distribution on each wheel during left and right turns

wheel motors block where it is converted to the required torque and transferred to the wheel. The electric motor and wheel are connected by a reducer, as discussed in section 3.2.5, to bring the rotational speed and torque to the desired target. The efficiency of the reducer has been taken as 90% for this work.

Upper controller

For this work the LQR controller has been designed to bring the vehicle model yaw-rate equal to a desired level. For this purpose the controllability and observability of the system are evaluated first, which are important conditions for the control system design to exist. Kalman [Kalman 1959] stated that the general problem of optimal regulation is solvable if and only if the plant is completely controllable. Similarly, the concept of observability is useful in solving the problem of reconstructing unmeasurable state variables from the measurables ones in the minimum possible length of time [Kalman 1959].

The controllability of a system, described in the state space form $\dot{x} = Ax + Bu$, can be determined by finding the rank of matrix M [Dutton 1998], where M is

$$M = [B \vdots AB \vdots \cdots \vdots A^{n-1}B] \tag{5.12}$$

The system is said to be controllable if the rank of the above matrix is equivalent to the number of rows in matrix B. Equation **??** describes the vehicle bicycle model in state space form. The matrix B has 2 rows and the rank of matrix M can be determined as 2 by using the combination of *ctrb* and *rank* commands in Matlab. As both of the values are equal thus the system can be

termed as controllable. Dutton et al [Dutton 1998] has defined a system to be observable if it is possible to reconstruct the state-vector completely from measurements made by the system's output. This condition can be checked again by doing a rank test on a matrix N, given below.

$$N = [C^T \vdots A^T C^T \vdots (A^T)^2 C^T \vdots \cdots \vdots (A^T)^{n-1} C^T] \tag{5.13}$$

If the rank is equal to the number of columns in the matrix C, the system is termed as observable. For this work the system states are assumed to be observable, therefore $C = I$.

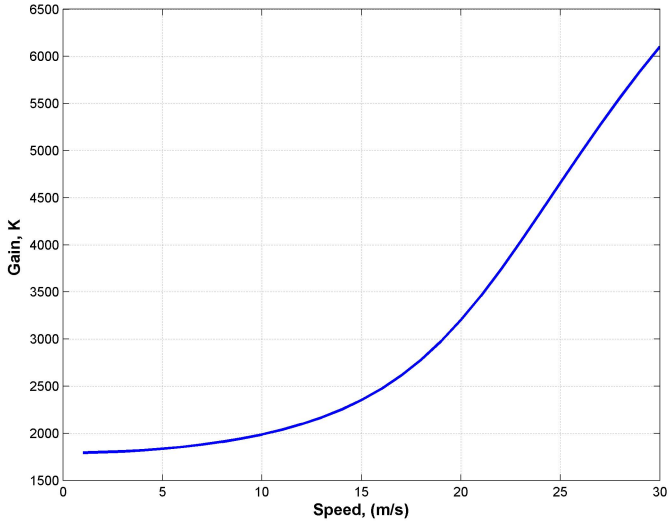

Figure 5.11: Optimal gain versus the longitudinal speed

The Matlab code written for this work checks the controllability and observability conditions and once they are met, calculates the control gain that is used by the Simulink model. As discussed in section 5.3.1 the weighting matrix Q has been selected as $C^T C$, whereas the value of R is chosen as 0.1. The control gain varies with change in the vehicle speed, therefore for simulation purposes the control gain is introduced in the form of a lookup table. Figure 5.11 shows the varying yaw rate feedback gain calculated to be included in the simulations.

Lower controller

The main function of lower controller is to keep the wheels' longitudinal slip within a desired limit so that the tyres can generate optimal traction. The upper controller's output varies the in-wheel motors' torque by varying their

rotational speed. In chapter 3 it has been discussed that rotational speed of a wheel effects the longitudinal tyre slip and their relationship has been described by Eqn. 3.34 as follows

$$S_x = \frac{\omega R_e - V_x}{V_x} \tag{5.14}$$

Selection of a optimal wheel slip value is a complicated decision especially when the tyre experiences a combined slip. This can be explained by considering the effect of wheel slip on tyre's potential to generate longitudinal and lateral forces. Figure 5.12 shows the force curves, for the tyre on the vehicle, plotted for constant tyre slip angles and increasing longitudinal slip values. As discussed earlier the tyre's ability to produce lateral force during cornering

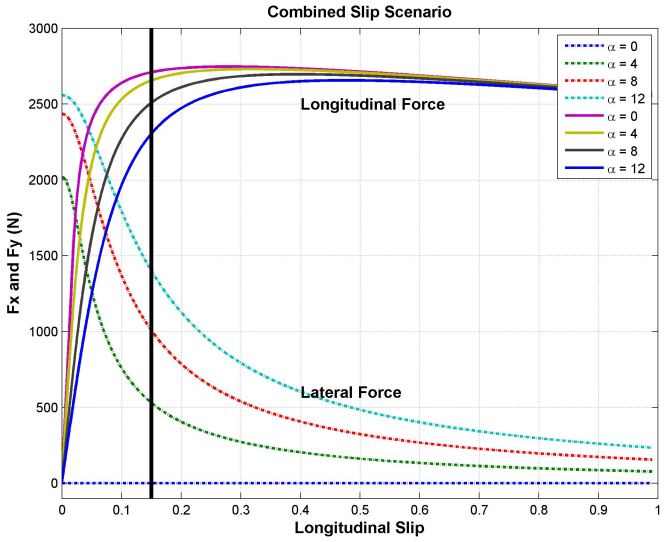

Figure 5.12: Tyre forces as a function of longitudinal and lateral slips

decreases as the longitudinal tyre slip increases. The longitudinal tyre force on the contrary increases and reaches to a maximum value when the value for S_x approaches 0.2; however, the available lateral force at that instant may not be sufficient for vehicle's lateral stability. Therefore it is important to limit the wheel slip to a value beyond which tyre's lateral force drops drastically. Such region has been marked by a black vertical line in Fig. 5.12. If the tyre is restricted to operate within this region, as discussed by Chun and Sunwoo [Chun 2005], it can generate optimal lateral and longitudinal forces that can help the vehicle to operate while being stable.

From the above discussion the control objective of the lower controller can be defined as to keep the wheel slip value within a desired range, shown

above in Fig. 5.12. This can be achieved by defining the sliding surface s as [Buckholtz 2002]

$$s = S_x - S_{x_d} \tag{5.15}$$

In order to keep the wheel slip value within the desired range the sliding surface must reaches to zero, when the slip value crosses the threshold. To determine a control law that brings the system to this state, Lyapunov function can be introduced as suggested in Eqn. 5.10. As discussed earlier the stability criteria requires the following condition to be true

$$s\dot{s} \leq 0 \tag{5.16}$$

To substitute the value of $\dot{s}$ in the above condition, derivative of Eqn. 5.15 with respect to time gives $\dot{s} = \dot{S_x} - \dot{S_{x_d}}$. The wheel slip defined by Eqn. 3.34 can be differentiated with respect to time to define $\dot{S_x}$ as follows

$$\begin{aligned}
\frac{d}{dt}(S_x) &= \frac{d}{dt}(\frac{\omega R_e - V_x}{V_x}) \\
\dot{S_x} &= \frac{V_x \frac{d}{dt}(\omega R_e - V_x) - (\omega R_e - V_x)\frac{d}{dt}(V_X)}{{V_x}^2} \\
&= \frac{\dot{\omega} R_e - \dot{V_x}}{V_x} - (\frac{\omega R_e - V_x}{V_x})\frac{\dot{V_x}}{V_x} \\
&= \frac{\dot{\omega} R_e - \dot{V_x}}{V_x} - \frac{S_x \dot{V_x}}{V_x}
\end{aligned} \tag{5.17}$$

In the above equation the tyre longitudinal force F_x can be introduced by replacing $\dot{\omega}$ with the following value, which has been obtained using the equation of motion for wheel rotation:

$$\dot{\omega} = \frac{1}{I_w}(T_b - R_e F_x)$$

The resultant equation after substitution and replacement can be given as follows:

$$\dot{S_x} = \frac{{R_e}^2 F_x}{I_w V_x} + \frac{\dot{V_x}(1 + S_x)}{V_x} + \frac{R_e T_b}{I_w V_x} \tag{5.18}$$

Substituting the value of $\dot{S_x}$ from Eqn. 5.18 in $\dot{s} = \dot{S_x} - \dot{S_{x_d}}$ gives

$$\dot{s} = \frac{{R_e}^2 F_x}{I_w V_x} + \frac{\dot{V_x}(1 + S_x)}{V_x} + \frac{R_e T_b}{I_w V_x} - \dot{S_{x_d}} \tag{5.19}$$

In the above equation the term T_b is the control output and can be approximated as follow to make $\dot{s} = 0$

$$\hat{T_b} = -\frac{I_w V_x}{R_e}(\frac{{R_e}^2 F_x}{I_w V_x} + \frac{\dot{V_x}(1 + S_x)}{V_x} - \dot{S_{x_d}}) \tag{5.20}$$

In order to satisfy the sliding condition regardless of the uncertainty of the model a smooth continuous switching function may be added in the control function $\hat{T}_b$ [Zheng 2006]. So the control output can written as

$$T_b = \hat{T}_b - \eta sat(\frac{s}{\Phi}) \tag{5.21}$$

where the smoothing function has the same definition as given in Eqn. 5.11. Figure 5.13 shows the lower controller implementation in Simulink. For this

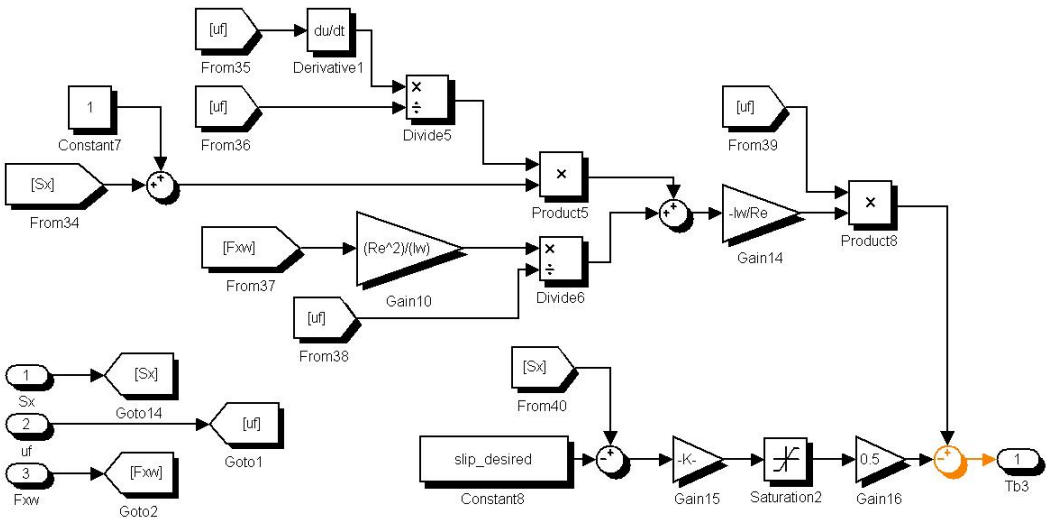

Figure 5.13: Simulink model of wheel slip controller

work the value of η and ε in wheel slip controller is taken as 0.5 and 0.02 respectively, whereas the desired optimal value for the tyre longitudinal slip has been selected as 0.15, as suggested in Fig. 5.12.

5.4 Simulation Results and Discussion

This section focuses on the simulations, and discussion about their results, carried out to validate the control design performance. In order to substantiate the effectiveness of the control system on vehicle's handling performance, the following open loop and closed loop test manoeuvres have been selected.

- J-Turn manoeuvre with a constant speed
- Sine steer manoeuvre
- Driver in-loop simulations

These testing manoeuvres provide an insight to a vehicle's response in the form of time based analysis. For the simulation purpose the seven and eight degrees of freedom non-linear vehicle models, discussed in chapter 3, have been used. Initially the seven degrees of freedom vehicle model has been used to establish the effectiveness of the proposed controller. Once established, then the controller will also be integrated with the eight degrees of freedom model to show that it is also capable of effecting the lateral response of the complex models.

5.4.1 J-Turn manoeuvre with a constant speed

The J-turn manoeuvre is a simple testing procedure which allows the evaluation of the vehicle's transient response as well as its steady-state behaviour. In this manoeuvre the vehicle first runs in a straight line and then enters into a turn when the steering wheel is quickly rotated from the straight ahead position to a new one and held constant. This step change in the steer angle results into a steady-state cornering after the settling time is over.

In this simulation the vehicle speed is desired to be kept constant and therefore a simple proportional-integral (PI) controller is added that maintains the speed against air-resistance and other resistive forces acting on the vehicle. The results discussed below are simulated while maintaining the vehicle's longitudinal velocity as 65 km/h and turning the steering wheel 18° towards the left. As the steering ratio for this model is 6:1; therefore the steer angle at each front wheel is 3°, as shown in Fig. 5.14 (enlarged view in Appendix N). Due to this sudden input the weight distribution on tyres is disturbed and the vehicle's load shifts from the left side towards the right. This can be observed in the second sub-figure of Fig. 5.14 where the vertical loading on the front and rear wheels is constant for the first 5 seconds. The load value for the front right and left wheels is 1.4 kN, whereas for the rear right and left wheels it is 2.25 kN for each wheel. After 5 seconds the vertical

loads on the right side wheels start rising and simultaneously start decreasing on the left side wheels.During this transfer period the total load on all the four tyres remain equivalent to the weight of the vehicle.

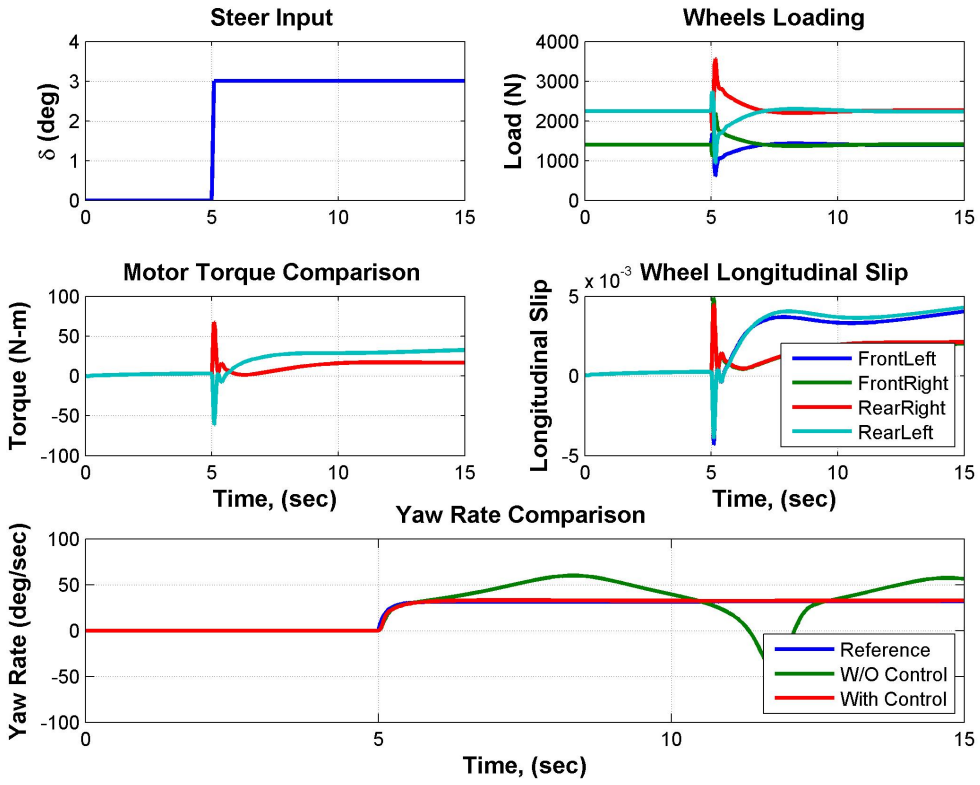

Figure 5.14: Output recorded for a J-Turn manoeuvre at 65 km/h speed

The third sub-figure shows the torque values generated by all the four in-wheel motors during the manoeuvre. The torque values for all the wheels remain the same, at 5 Nm for each wheel, during the straight running. When the vehicle enters into a turning manoeuvre the torque vectoring system, included in the Simulink model, contributes to transfer independent torque value on each wheel. As the vehicle is entering in a left turn manoeuvre the right wheels have to rotate at a higher velocity than that of the left wheels to generate yaw compensation as per the reference command. In order to achieve higher rotational velocity for the right wheels, driving torque is applied to these wheels. To slow down the left wheels at the same time a braking torque is applied to the front and rear left wheels, as shown in the corresponding figure. Once the vehicle attains a steady-state cornering the torque vectoring

block is still providing vectoring torque to keep the vehicle in a stable state. This time the left side wheels are moving with higher rotational velocity as compared to that of right side. This is because of the fact that the vehicle model has tendency to oversteer during cornering, as mentioned in chapter 4. This fact can be observed in the sub-figure corresponding to yaw-rate comparison, where the uncontrolled vehicle model becomes unstable because of this oversteer tendency.

The fourth sub-figure is showing the longitudinal wheel slips for all four wheels. Again these values are well within the desired region thus providing tyre forces in a balanced manner. On the contrary, the wheels of an uncontrolled vehicle, doing a similar manoeuvre, pass beyond the threshold value as shown in Fig. 5.15. This reduces the tyres ability to generate lateral and longitudinal forces required for the vehicle's stability.

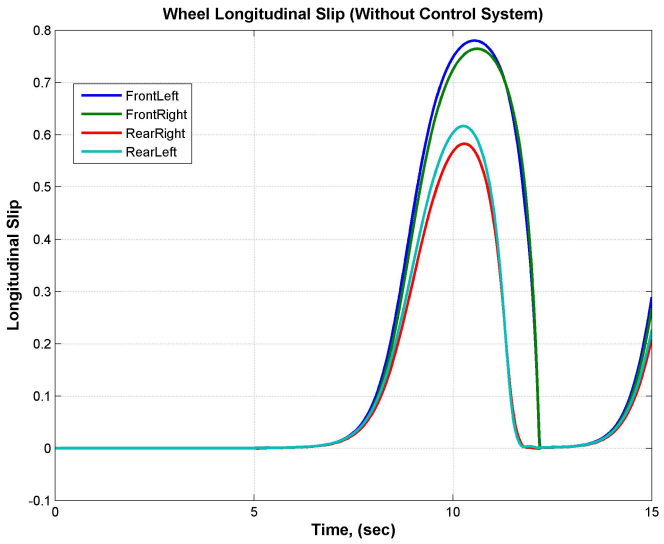

Figure 5.15: Longitudinal slip values for a vehicle without the control system

The fifth sub-figure of Fig. 5.14 shows the yaw-rate responses of the reference model, vehicle model with the designed control system and vehicle without a control system. This figure shows that the controlled vehicle follows the reference model whereas the uncontrolled steer-by-wire goes out of control.

The control system's effectiveness was further verified by performing this manoeuvre with varying steering inputs and longitudinal speeds. Figure 5.16 (enlarged view in Appendix O) is another set of figures which were generated by subjecting the moving vehicle at 55 km/h to a step steer input of 30°. The simulation has been stopped at 13 seconds because the vehicle model without

the control system failed beyond this point. Analysing the yaw-rate response curves, one can observe that the controlled vehicle is closely following the reference model. In this case the root mean square (RMS) error value is 2.82 deg/s, which is an acceptable value keeping the complexity of the non-linear model in view.

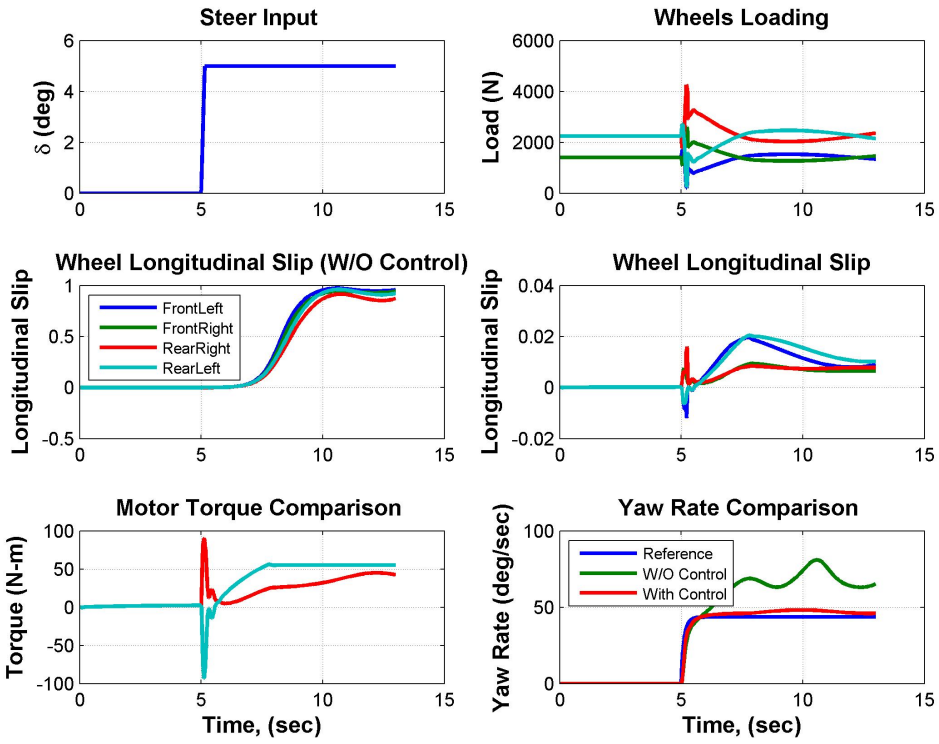

Figure 5.16: Output recorded for a J-Turn manoeuvre at 55 km/h speed

5.4.2 Sine steer manoeuvre

The sine steer manoeuvre is used to evaluate the vehicle's transient lateral handling response. In this test a single sine wave has been used as a steer input for the vehicle. The amplitude and frequency of the sine steer command has been varied to test the control system's effectiveness to keep the vehicle stable at different values of lateral acceleration. Figure 5.17 (enlarged view in Appendix P) shows information about various parameters and states recorded during a sine steer manoeuvre when a vehicle moving with a velocity of 70 km/h was subjected to a sine steer input of amplitude 3° and frequency 0.2

Hz. During this manoeuvre the lateral acceleration value of the uncontrolled vehicle shows that it enters into highly non-linear region where it is difficult for an ordinary driver to control. On the contrary the vehicle equipped with the designed control system follows the reference signal and remains stable. The root mean square error values for lateral acceleration and yaw-rate are 0.06 g and 1.8 deg/s respectively. The simulation results also show that wheel slip controller has kept the slip values in the desired region. The wheel slip values (not shown) for the uncontrolled vehicle were beyond the threshold value during this manoeuvre. Again the same manoeuvre with different speeds and

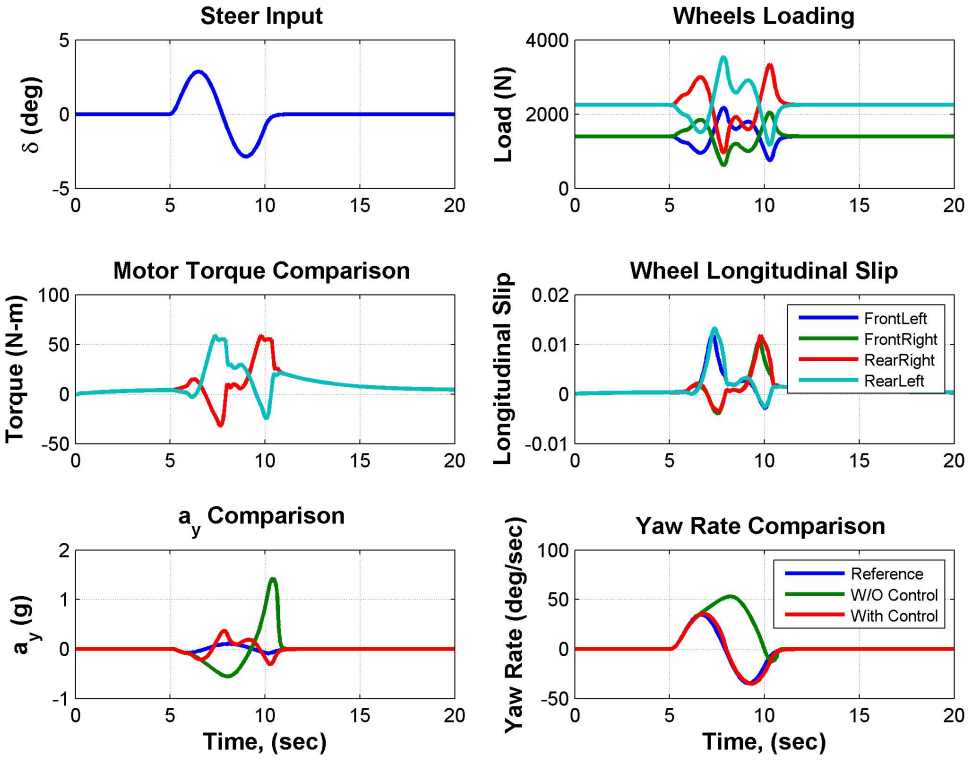

Figure 5.17: Output recorded for a sine steer manoeuvre at 70 km/h speed

steer inputs of various amplitudes and frequencies were performed. Figure 5.18 (enlarged view in Appendix Q) shows output of a simulation which duplicates obstacle avoidance manoeuvre at high speed. This is a critical manoeuvre for vehicles travelling on high speed highways/motorways. The results suggest that the uncontrolled vehicle again becomes unstable whereas the torque vectoring block keeps the controlled vehicle stable by transferring different torque

value to each wheel. The RMS error values between the reference and controlled lateral acceleration and yaw-rate are 0.09 g and 2.13 deg/s respectively. The design goal of the control system, as mentioned earlier, is to compensate

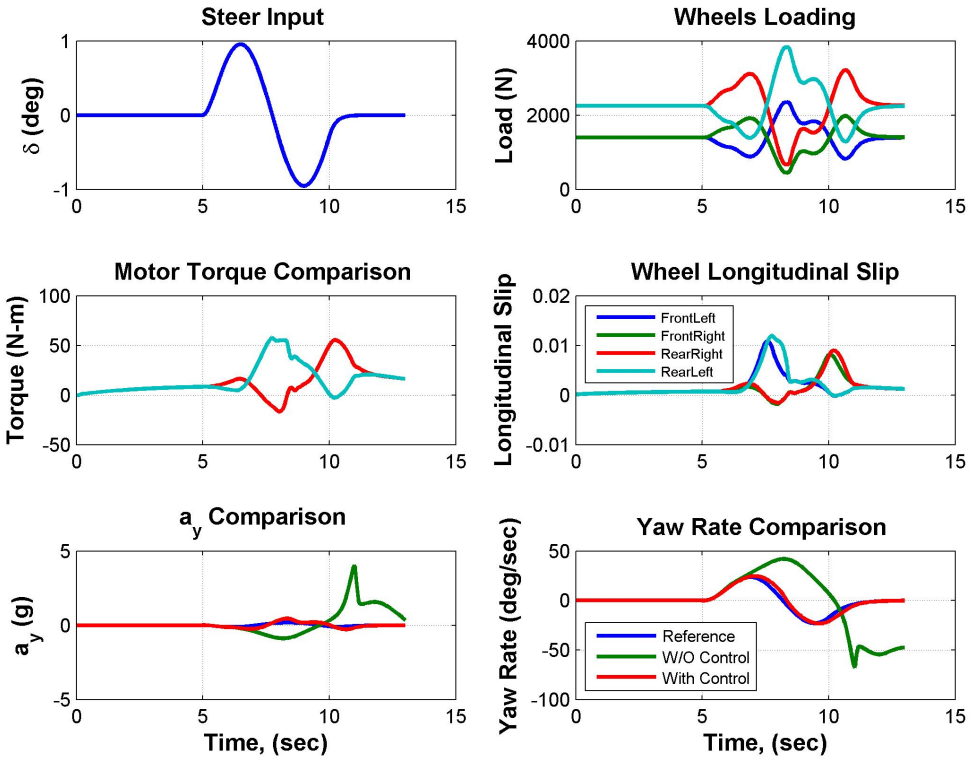

Figure 5.18: Output recorded for a sine steer manoeuvre at 100 km/h speed

the steer by wheel vehicle's response with torque vectoring in order to make it closer to a conventional vehicle. For this purpose simulations were performed in which a non-linear vehicle model fitted with a conventional steering system and a non-linear vehicle model fitted with the steer-by-wire system along with the designed control system were run in parallel. The initial conditions and input steer commands for both models were kept the same. Figure 5.19 shows the comparison of their yaw-rate output. In this simulation both of the vehicles were moving with a constant speed of 60 km/h and then subjected to a sine steer input having amplitude of 4°. The result suggest that the steer by vehicle with the control system is following the conventional vehicle closely. The RMS error value for these curves is 0.47 deg/s.

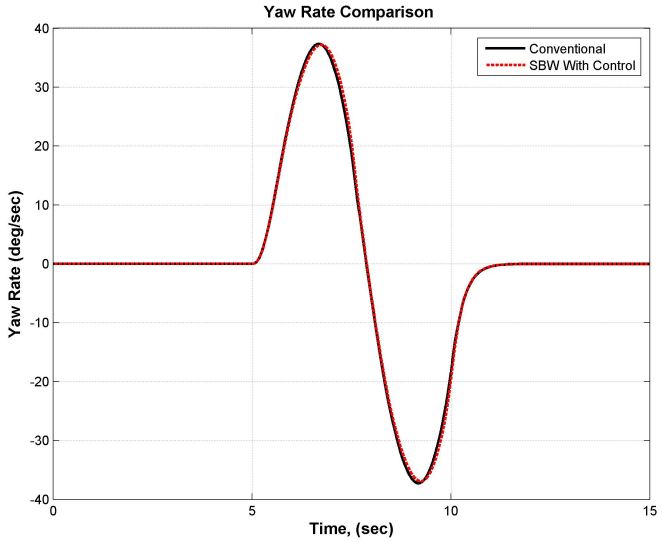

Figure 5.19: Yaw-rate comparison of the conventional and SBW controlled vehicles

5.4.3 Driver in-loop simulations

As discussed earlier in the section 4.5.3 that the driver was controlling the vehicle with difficulty during the experimenting phase because of the delay introduced due to the steer-by-wire system. Therefore, simulations have been performed to evaluate the effect of control system on the driver's performance. For this purpose two non-linear vehicle models, with driver model in loop, have been used for these simulations; one equipped with the designed control system and other without it. The experimental phase of the test vehicle involved lane change manoeuvre and it was noted that the driver struggled to bring the vehicle from transient to steady state. Hence, a desired track, similar to one shown in Fig. 4.33, was generated in Matlab. A very similar approach has been used by Ishio et al. [Ishio 2008] to evaluate vehicle handling quality while driver in loop scenario. The simulations have been performed with the various speeds and lane change widths; but this section includes results collected at the speed of 70 and 85 km/h for a lane change width of 3 m. The uncontrolled vehicle was not able to complete the manoeuvre beyond the speed of 70 km/h, hence the simulation done at the speed of 85 km/h only includes the result from the controlled vehicle.
Figure 5.20 shows three subplots; the top one shows the vehicles' lateral movement in meters, the middle subplot is the driver's input in terms of steering wheel angle and the last one is vehicles' yaw-rate recorded during the manoeuvre. It is evident from the lateral movement plot that the vehicle, without

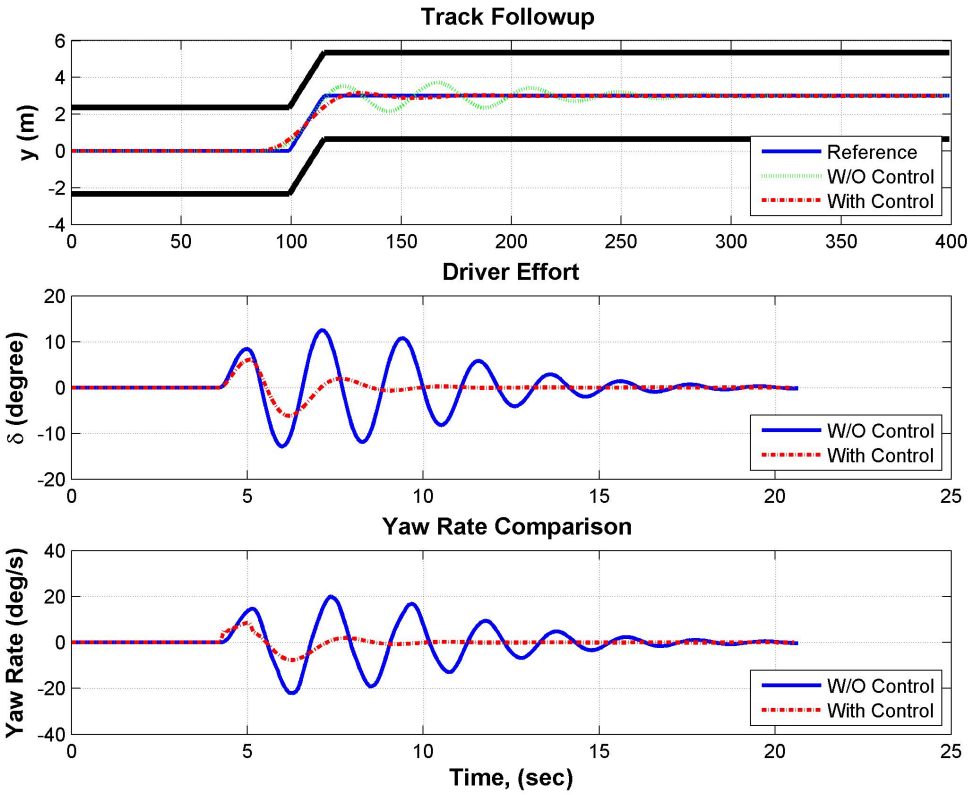

Figure 5.20: Driver controlling the controlled and uncontrolled vehicles at the speed of 70 km/h

the control system, settles after covering more distance than the vehicle with the control system. The controlled signal has a slower rise time and therefore has less overshoot value in comparison to the uncontrolled output. The peak overshoot value for the controlled response is 0.16 m, whereas for the uncontrolled one the value is 0.53 m. The middle one shows the driver's effort to bring the vehicle to a desired state, which is the reference path shown in lateral movement subplot. The frequency with which the driver commands are generated suggests that the driver is in panic condition and working hard to keep the vehicle under his control. On the contrary the driver's action on the steering wheel of the vehicle with the control system suggests that the driver is performing the manoeuvre with ease. The number of oscillation for this curve is lower as compared to that of the driver of the uncontrolled vehicle. The third subplot is showing the yaw-rate for both of the vehicles during this scenario. The uncontrolled vehicle is touching a higher value of 20 deg/s whereas the controlled vehicle is touching 7 deg/s as the maximum value.

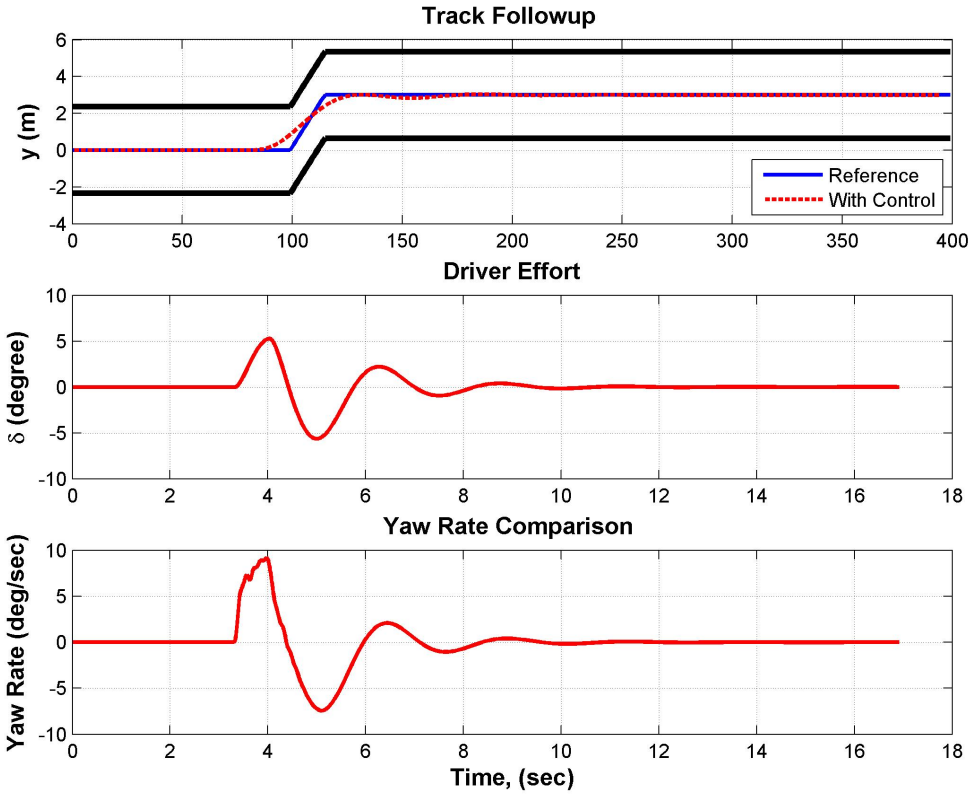

Figure 5.21: Driver controlling the vehicle with the control system at the speed of 85 km/h

The simulation for the uncontrolled vehicle started failing beyond the speed of 70 km/h; however the controlled vehicle was able to perform the manoeuvre even at a higher speed. Figure 5.21 shows the output for the same manoeuvre at the speed of 85 km/h for a vehicle with the control system. again the overshoot of in the first subplot is negligible. The driver's input to the steering wheel is of 0.5 Hz, which is more than the upper range of actuators as discussed earlier, but the controller keeps the vehicle stable and the manoeuvre is completed without any failure. This higher frequency input to the vehicle without the control system makes it unstable and it does not follow the desired path correctly; hence the simulation fails.

5.4.4 Integration of the proposed controller with the eight DOF model

In the previous sections the seven degrees of freedom vehicle model has been used. As discussed in Chapter 3, the roll degree of freedom plays an important roll in the lateral response of a vehicle and therefore it is necessary to find the influence of control algorithm on the vehicle roll. In this section the simulation results are presented in which the eight degrees of freedom vehicle model is integrated with the driver model and the proposed controller. All the four wheels have in-wheel motors as in the case of previous simulations. In this simulation the driver model has to perform a lane change manoeuvre and follow a reference path shown with the blue solid curve in Fig. 5.22.

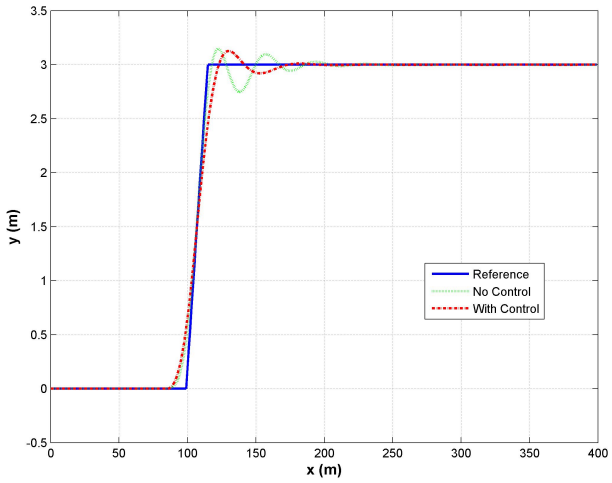

Figure 5.22: Track comparison for the uncontrolled and controlled vehicle models

The look-ahead distance for the driver model was set as 1.2 times the speed of the vehicle, which was 13.8 m/s in this simulation. Figure 5.22 shows that both uncontrolled and controlled vehicles are able to complete the manoeuvre, but the controlled vehicle's deviation from the desired path is 40% less than the deviation of the uncontrolled vehicle. Although the rise time of the controlled response is slower than that of the uncontrolled one, but the uncontrolled vehicle took more time to settle. Figure 5.23 shows the driver

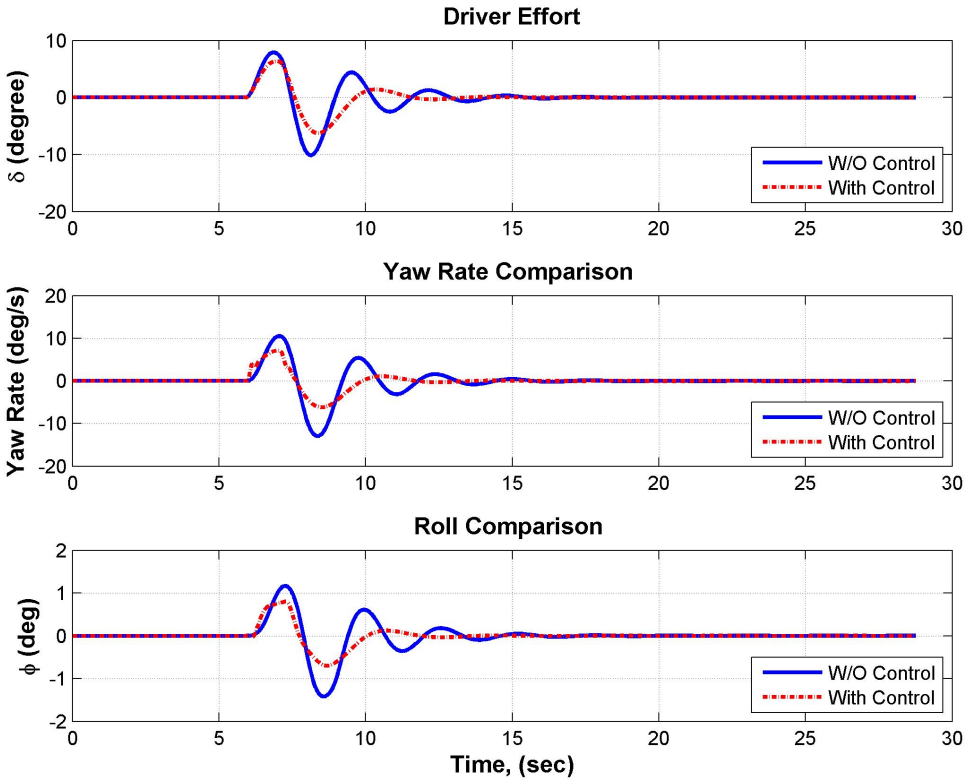

Figure 5.23: Comparison of 8 DOF vehicle with and without the controller at the speed of 50 km/h

effort, vehicle yaw rate and vehicle roll angle measured during the simulation. The first subplot of the figure shows the driver's effort to keep the vehicle on the reference track. Like previous results the amplitude and number of actions performed by the driver model for uncontrolled vehicle are more than that of the controlled vehicle. Thus it shows that the proposed controlled helped the driver to complete the manoeuvre with ease. The second and third subplots from the top represent the vehicle yaw rate and vehicle roll respec-

tively. The yaw rate graph shows that the uncontrolled vehicle's yaw rate is approximately 50% higher than the yaw rate value of the controlled vehicle, when both enter into the lane change manoeuvre. Similar effect on the roll response of the vehicle can be observed while analysing the last subplot of Fig. 5.23. The controlled vehicle is showing a damped response in comparison to the uncontrolled vehicle. When the vehicle enters into the manoeuvre, the roll angle of the uncontrolled vehicle is measured to be 45% higher than the roll angle of the controlled vehicle. These results suggest that the proposed controller not only assists driver to control the steer-by-wire vehicle but also improves the lateral response of the vehicle thus making it to behave like a conventional vehicle.

Chapter 6

Conclusions

6.1 Overview

The vision for the future vehicles is to make them efficient, safe and smart. Steer-by-wire technology fits well with the idea and currently is under investigation in concept vehicles. Despite having a number of advantages, the technology has not yet made its way to the commercial vehicles because of a number of limitations. One of these is the cost factor because the majority of the concept vehicles are using high end solutions to implement the idea. In order to make this concept commercially feasible, low cost solutions need to be determined. Generally lowering the cost jeopardises the performance of the system and critical systems like steering mechanism in vehicles cannot be compromised in terms of performance. Therefore, the aim of this work was to enhance the low performing steering system using torque vectoring. Keeping future vehicles in view, an electric vehicle driven by four in-wheel motors has been modelled in MATLAB/Simulink and the low performance steer-by-wire system's model was incorporated in it.

6.2 Conclusions

The thesis has shown that the handling response of the low performing steer-by-wire vehicle can be improved using torque vectoring. The results included in the thesis also show that the designed controller makes the steer-by-wire vehicle with control to perform lane change manoeuvre with 20% higher speed than that of the steer-by-wire without control. It has also been shown the steer-by-wire vehicle with control subjected to a J-turn manoeuvre perform like the conventional vehicle, whereas the steer-by-wire vehicle without control was unable to complete the test at the speed of 18 m/s. These results suggest that the aim set for this thesis has successfully been achieved.

The objectives set to achieve this aim have also been met, but with some limitations. The review of the available literature suggests that there is very limited literature available that includes steering dynamics, validated by experimentation, into account. Moreover, no article was found in which the

steering by wire system comprising of low performance actuators has been discussed.

In this thesis, a vehicle model having eight degrees of freedom has been developed and validated partially with the experimental results. The uniqueness of this vehicle model is that it contains low performance steer-by-wire steering system, which is also validated experimentally. This vehicle model is ready to be used for future investigation related to this domain.

This work also involved the investigation and development of a cascade controller for torque vectoring. The upper controller is based on LQR theory, whereas the lower one is a robust sliding mode controller. The results show that the low performance steer-by-wire vehicle integrated with the proposed controller is able to perform like a conventional vehicle. Although the proposed controller has provided satisfactory results by only monitoring the vehicle yaw-rate, but the performance might have further improved by taking other vehicle states into account.

6.3 Further Work

The results presented in this thesis are limited to the test vehicle, which is a modified dune buggy. However, the validated vehicle model with seven and eight degrees of freedom are available from this work and can be used with the parameters of other vehicles to verify the effectiveness of the proposed torque vectoring controller. This investigation can be further extended by including the vehicles showing oversteer and understeer behaviour.

As mentioned earlier the actuators used in this work have the bandwidth of 0.3 Hz, which is significantly less than the bandwidth of a human driver. In future work the actuators of comparatively better bandwidth can be included in the vehicle model and can be investigated in terms of torque requirements. Moreover, this work assumes that the in-wheel motors are functioning without lag. The future work can investigate the effect of in-wheel motor lag on the low performance steer-by-wire vehicle's handling response.

6.4 Publications

- Hybrid steering of wheeled vehicles, with David Purdy, Amer Hameed. *Accepted for the FISITA 2012 World Automotive Congress, Beijing, China.* Paper Number: F2012-G06-005

- Vehicle handling parameters estimation in a virtual environment, with Amer Hameed. *Proceedings of the ASME 2010 International Mechanical*

Engineering Congress & Exposition, Vancouver, Canada. Paper Number: IMECE2010-40944

- Implementation of Low Cost Inertial Measurement Unit (IMU) Integrated with a Global Positioning System (GPS) Receiver- A Study, with Saurav Talukdar and Amer Hameed. *SAE World Congress & Exhibition, April 2011, Detroit, MI, USA.* Paper Number: 2011-01-1040.

Appendix A

LabVIEW model

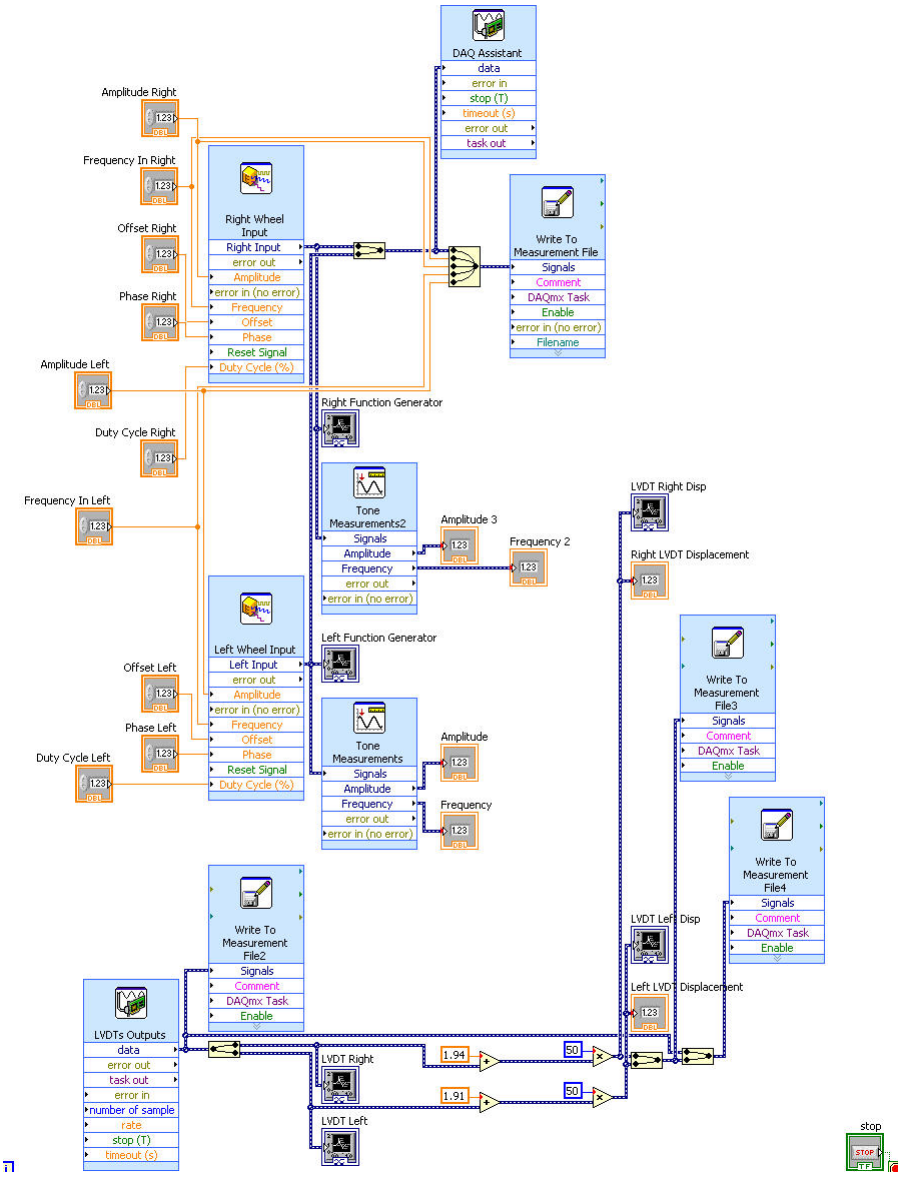

Figure A.1: LabVIEW code to control and record the actuators' displacement

Appendix B

Non-linear vehicle model with eight DOF

For calrity following equations have been taken from Crolla [Crolla]. These equations are also available in other texts like [Abe 2009] and [Giles 1968]. Crolla has explained the eight degrees of freedom using the Langrangian approach. Junjie [He 2005] followed the same approach to express the total kinetic and potential energies in terms of the primary variables describing the system. These are then converted into a set of partial differential equations called Langrange's equations.The partial derivatives are then evaluated to give the equation of motion. The general Langrange's equations may be written as:

$$\frac{d}{dt}\left(\frac{\partial T}{\partial \dot{q}_i}\right) - \frac{\partial T}{\partial q_i} + \frac{\partial V}{\partial q_i} + \frac{\partial D}{\partial \dot{q}_i} = Q_i, \quad i = 1 \text{ to } n \tag{B.1}$$

where

n	the number of degrees of freedom of the system.
q_i	the generalised coordinates describing the system.
Q_i	the generalised force applied to the system.
T	the total kinetic energy.
V	the total potential energy.
D	the total dessipated energy.

This form of Lagrange's equation may be applied directly to systems where integration of the real velocities $\dot{q}_i$ with respect to time yields corresponding coordinates q_i. In the case of the vehicle dynamics model developed in this thesis, proper coordinates are longitudinal and lateral displacements of the vehicle COG, X and Y, the yaw angle ψ of the moving vehicle x axis with respect to the inertial X axis, and the body roll angle ϕ about the roll axis. However, as u, v and r which are of interest are velocities in the moving vehicle axes system, the modified Lagrangian equations in which the above three velocities and the remaining real coordinate ϕ are used as the generalised motion variables will be employed to generate the equations of motion. With reference to Fig. 3.5, the two sets of velocities in the two coordinate systems, i. e. the vehicle fixed and earth fixed, have the following

relationships:

$$\begin{bmatrix} u \\ v \\ r \\ p \end{bmatrix} = \begin{bmatrix} cos\psi & sin\psi & 0 & 0 \\ -sin\psi & cos\psi & 00 & \\ 0 & 0 & 1 & 0 \\ 0 & 0 & 0 & 1 \end{bmatrix} \begin{bmatrix} \dot{X} \\ \dot{Y} \\ \dot{\psi} \\ \dot{\phi} \end{bmatrix} \tag{B.2}$$

where $p = \dot{\phi}$ is the roll velocity of the sprung mass.

The modified Langrangian equations for $u,\ v,\ r$ and ϕ take on the special forms:

$$\frac{d}{dt}\left(\frac{\partial T}{\partial u}\right) - r\frac{\partial T}{\partial v} = Q_1, \quad q_1 = u \tag{B.3}$$

$$\frac{d}{dt}\left(\frac{\partial T}{\partial v}\right) - r\frac{\partial T}{\partial u} = Q_2, \quad q_2 = v \tag{B.4}$$

$$\frac{d}{dt}\left(\frac{\partial T}{\partial r}\right) - v\frac{\partial T}{\partial u} + u\frac{\partial T}{\partial v} = Q_3, \quad q_3 = r \tag{B.5}$$

$$\frac{d}{dt}\left(\frac{\partial T}{\partial \dot{\phi}}\right) - \frac{\partial T}{\partial \phi} + \frac{\partial V}{\partial \phi} + \frac{\partial D}{\partial \dot{\phi}} = Q_4, \quad q_4 = \phi \tag{B.6}$$

Kinetic energy

Both transitional and angular velocities contribute to the kinetic energy. The total kinetic energy of the vehicle T can be expressed in terms of the four velocities $u,\ v,\ r$ and p and split into three terms: $T_s,\ T_f$ and T_r, corresponding to the sprung mass and the front and rear axles, respectively. With the assumption of small roll angles, the three terms can be expressed as:

$$T_s = \frac{1}{2}m_s[(u - hr\phi)^2 + (v + h\dot{\phi})^2] + \frac{1}{2}(I_{xxs}\dot{\phi}^2 - 2I_{xz}r\dot{\phi} + I_{zzs}r^2) \tag{B.7}$$

$$T_f = \frac{1}{2}m_{uf}({u_f}^2 + v_f^2) + \frac{1}{2}I_{zzf}r^2 \tag{B.8}$$

$$T_r = \frac{1}{2}m_{ur}({u_r}^2 + v_r^2) + \frac{1}{2}I_{zzr}r^2 \tag{B.9}$$

where

$$u_f = u_r = u$$
$$v_f = v + ar,\ v_r = v - br$$

Potential and dissipative energy

The total potential energy V is built up in the suspension and through the reduction in height of the sprung mass COG as it rolls. Here, the suspension is

assumed to be linear and thereby can be approximated by a constant torsional stiffness coefficient $K_{\phi f} + K_{\phi r}$ and a constant torsional damping coefficient $C_{\phi f} + C_{\phi r}$. The corresponding potential and dissipative energies are given as:

$$V_\phi = \frac{1}{2}(K_{\phi f} + K_{\phi r})\phi^2 \tag{B.10}$$

$$V_g = -m_s g h(1 - cos\phi) \tag{B.11}$$

$$D = \frac{1}{2}(C_{\phi f} + C_{\phi r})\dot{\phi}^2 \tag{B.12}$$

If the suspension forces are nonlinear, the potential and dissipated energy terms in Equations B.10 and B.12 must be included in the generalised forces acting on the body. In fact, with reference to Eqn. B.1, any potential and dissipated energy may be differentiated with respect to q_i and $\dot{q}_i$, respectively, and the resulting terms may be included with Q_i on the right hand side of the Lagrange equation. Thus, the terms V and D in Eqn. B.1 may be moved from the left hand side of the Lagrange equation and included instead with Q_i, as $-\partial V/\partial\phi$ and $-\partial D/\partial\dot{\phi}$, respectively. Equation B.6 may therefore be rearranged as:

$$\frac{d}{dt}\left(\frac{\partial T}{\partial \dot{\phi}}\right) - \frac{\partial T}{\partial \phi} = Q_4 \tag{B.13}$$

where

$$Q_4 = m_s g h sin\phi - (K_{\phi f} + K_{\phi r})\phi - (C_{\phi f} + C_{\phi r})\dot{\phi}$$

Generalised forces

Refering to Equations refeqn:LE3a, B.4, B.5, B.6 and B.1310), there are four generalised forces, corresponding to the generalised coordinates u, v, r and ϕ. The generalised forces Q_i are derived from the virtual work:

$$\delta W = \sum_{i=1}^{4} Q_i \delta q_i \tag{B.14}$$

where δq_i is a small displacement in the generalised coordinate q_i, with $\delta q_j = 0$ when $i \neq j$. Here, q_i refers to the quasi coordinates x and y (X and Y cannot be found by directly integrating u and v), and the real coordinates ψ and ϕ. For the vehicle model considered here the virtual work can be described as a function of $\delta x, \delta y, \delta\psi$ and $\delta\phi$:

$$\delta W = Q_1\delta x + Q_2\delta y + Q_3\delta\psi + Q_4\delta\phi \tag{B.15}$$

where

$$Q_1 = \sum F_x$$
$$Q_2 = \sum F_y$$
$$Q_3 = \sum M_z$$
$$Q_4 = \sum M_x$$

Substituting the corresponding values and with small angle assumption for roll angle ϕ, the equations of motion for the vehicle with respect to four motion variables $u,\ v,\ r$ and ϕ are expressed as:

$$\begin{aligned} m(\dot{u} - vr) + (m_{ur}b - m_{uf}a)r^2 - 2m_s hr\dot{\phi} - m_s h\dot{r}\phi &= \sum F_x \\ m(\dot{v} + ur) + (m_{uf}a - m_{ur}b)\dot{r} + m_s h\ddot{\phi} - m_s hr^2\phi &= \sum F_y \\ I_{zz}\dot{r} + (m_{uf}a - m_{ur}b)ur + (m_{uf}a - m_{ur}b)\dot{v} - I_{xz}\ddot{\phi} &= \sum M_z \\ I_{xx}\ddot{\phi} - m_s h^2 r^2\phi + m_s h(\dot{v} + ur) - I_{xz}\dot{r} &= \sum M_x \end{aligned} \tag{B.16}$$

where

$$m = m_s + m_{uf} + m_{ur}$$
$$I_{xx} = I_{xxs} + m_s h^2$$
$$I_{zz} = I_{zzs} + m_s {l_{cg}}^2 + I_{zzf} + m_{uf} {l_f}^2 + I_{zzr} + m_{ur} {l_r}^2$$
$$I_{zzf} = m_{uf}(\tfrac{T_f}{2})^2$$
$$I_{zzr} = m_{ur}(\tfrac{T_r}{2})^2$$

Equation B.16 may be arranged as:

$$\begin{aligned} \dot{u} &= \frac{\sum F_x + (m_{uf}a - m_{ur}b)r^2 + 2m_s hr\dot{\phi} + m_s h\dot{r}\phi}{m} + vr \\ \dot{v} &= \frac{\sum F_y - (m_{uf}a - m_{ur}b)\dot{r} - m_s h\ddot{\phi} + m_s hr^2\phi}{m} + ur \\ \dot{r} &= \frac{\sum M_z - (m_{uf}a - m_{ur}b)(\dot{v} + ur) + I_{xz}\ddot{\phi}}{I_{zz}} \\ \ddot{\phi} &= \frac{\sum M_x - m_s h(\dot{v} + ur) + m_s h^2 r^2\phi + I_{xz}\dot{r}}{I_{xx}} \end{aligned} \tag{B.17}$$

Since the yaw and roll rates are known to be small compared to the vehicle speed and $(m_{uf}a - m_{ur}b)$ is also a small value, the product of these terms in Eqn. B.17 may be left out for simplicity. Therefore, the above

equations of motion can be simplified as:

$$\begin{aligned}
\dot{u} &= \frac{\sum F_x + m_s h \dot{r} \phi}{m} + vr \\
\dot{v} &= \frac{\sum F_y - m_s h \ddot{\phi}}{m} + ur \\
\dot{r} &= \frac{\sum M_z + I_{xz} \ddot{\phi}}{I_{zz}} \\
\ddot{\phi} &= \frac{\sum M_x - m_s h(\dot{v} + ur) + I_{xz} \dot{r}}{I_{xx}}
\end{aligned} \tag{B.18}$$

Appendix C

Vehicle Parameters

Vehicle Parameters:
$a = 1.3434\ m$
$b = 0.8066\ m$
$l = 2.15\ m$
I_z= 1775 kgm^2
m= 747 kg
C_d= 0.30
R_e= 0.25 m
I_{fw}= 2.1 kgm^2
I_{rw}= 2.1 kgm^2
$T_F = T_R = 1.28\ m$
$h_{cg} = 0.490\ m$
$h_r = 0.155\ m$
K_{phi_f}= 12204 Nm/rad
K_{phi_r}= 20110 Nm/rad
C_{phi_f}=1023 N/s
C_{phi_r}=1000 N/s
I_{wy}=2.1 kgm^2
I_{zz}=1775 kgm^2
I_{xx}=447.1 kgm^2
I_{xz}=21.09 kgm^2
m_{u_f}=51.58*2 kg
m_{u_r}=32.62*2 kg

Appendix D

Enlarged Figures 4.3 and 4.4

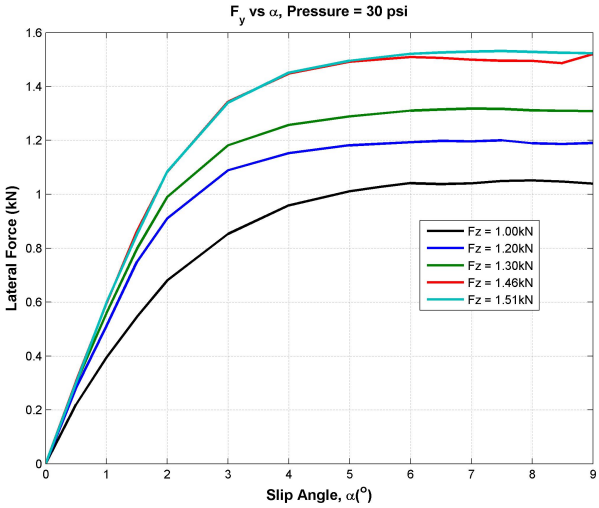

Figure D.1: Front tyre characteristics

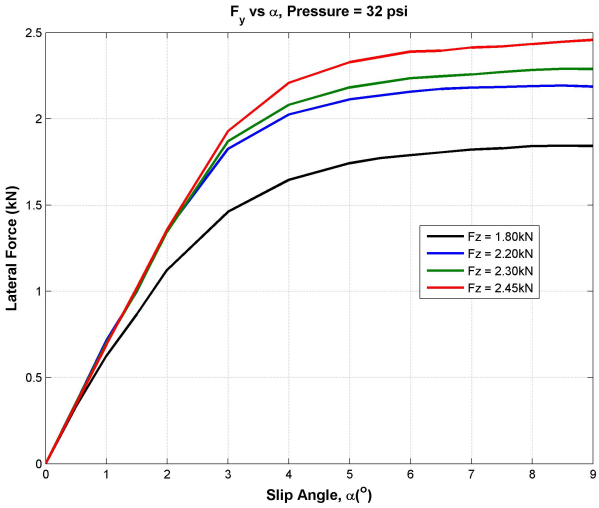

Figure D.2: Rear tyre characteristics

Appendix E
Enlarged Figure 4.5

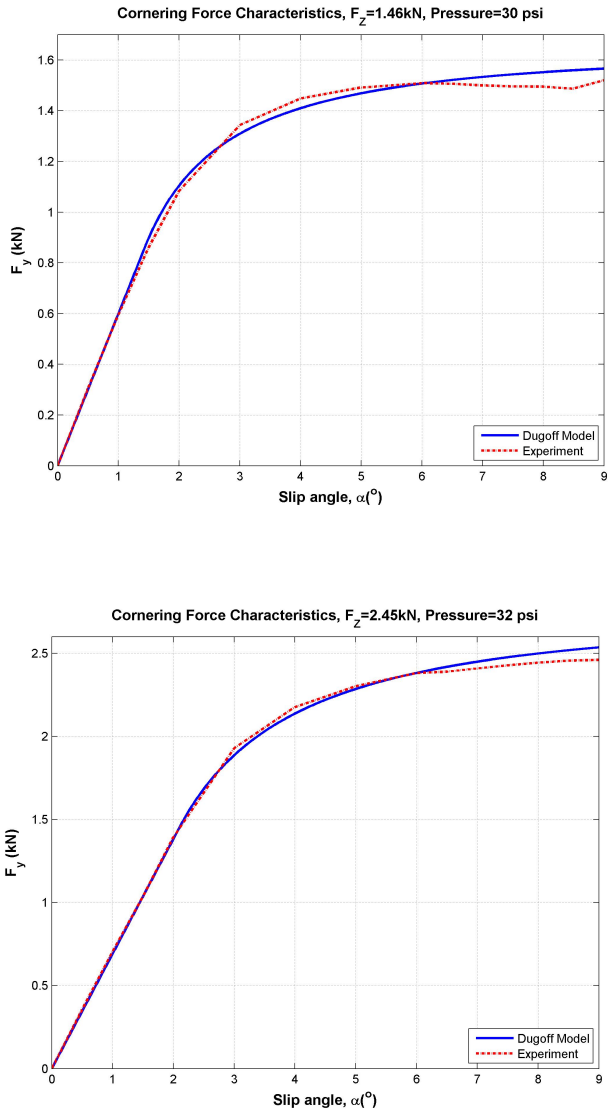

Figure E.1: Experimental and Estimated lateral force characteristics

Appendix F

Enlarged Figures 4.16 and 4.17

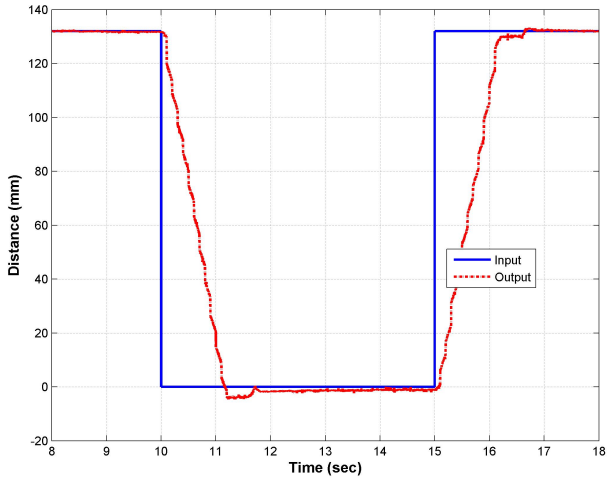

Figure F.1: Response of the left actuator

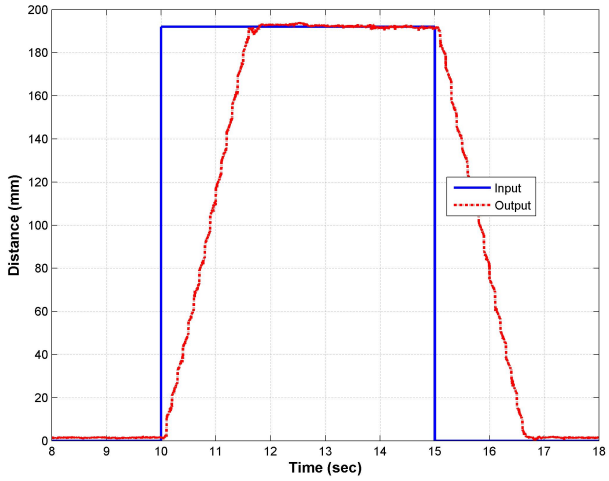

Figure F.2: Response of the right actuator

Appendix G

Enlarged Figures 4.18 and 4.19

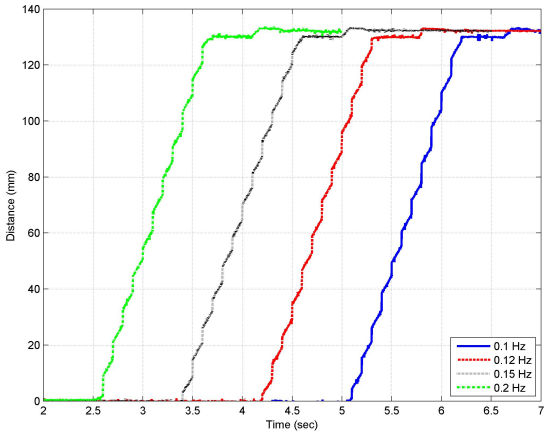

Figure G.1: Actuator response for the left side to a square wave of varying frequencies

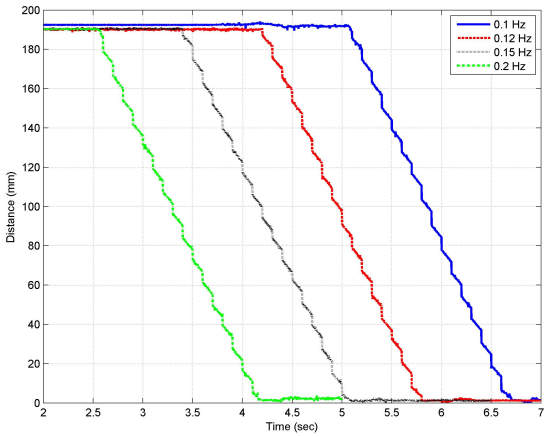

Figure G.2: Actuator response for the right side to a square wave of varying frequencies

Appendix H

Enlarged Figures 4.22 and 4.23

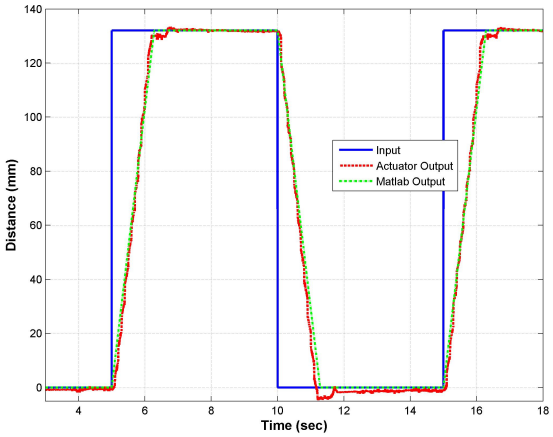

Figure H.1: Left actuator response (Input amplitude = Maximum, Input frequency = 0.1 Hz)

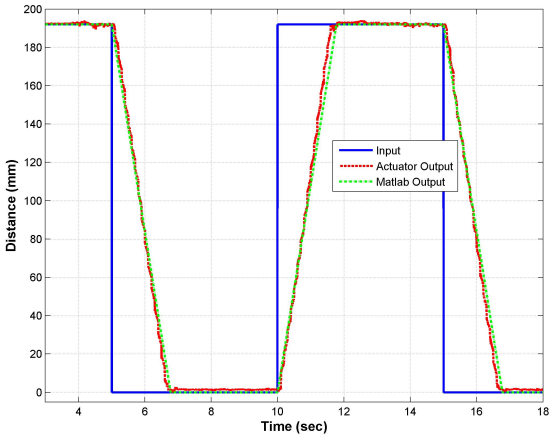

Figure H.2: Right actuator response (Input amplitude = Maximum, Input frequency = 0.1 Hz)

Appendix I

Enlarged Figures 4.25 and 4.26

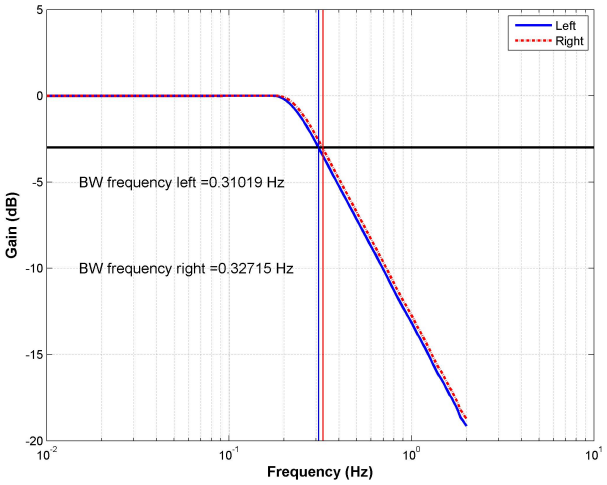

Figure I.1: Amplitude response

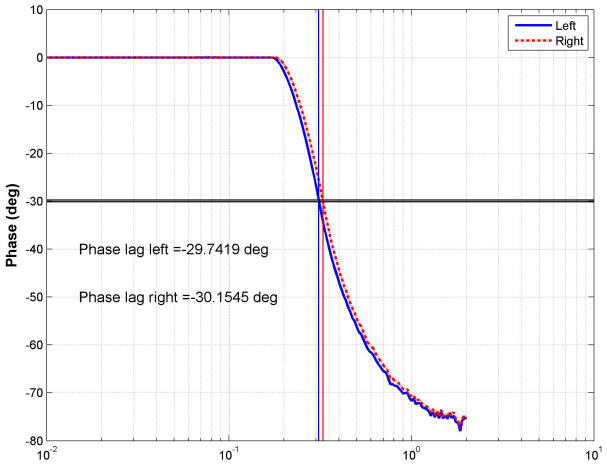

Figure I.2: Phase response

Appendix J

Enlarged Figures 4.31 and 4.32

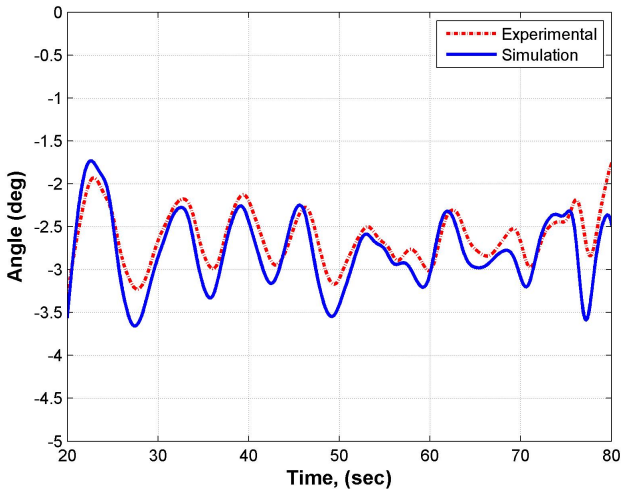

Figure J.1: Right wheel angle ($7.24m/s$)

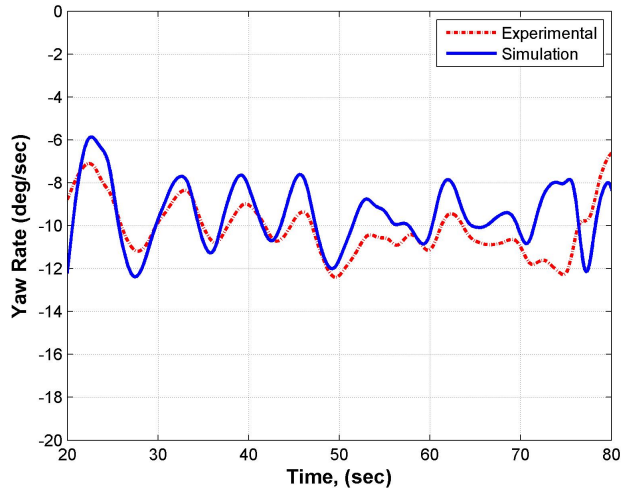

Figure J.2: Vehicle yaw-rate ($7.24m/s$)

Appendix K

Enlarged Figures 4.35 and 4.36

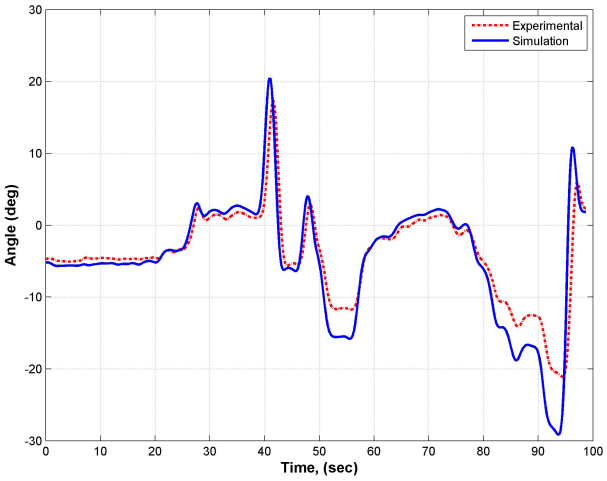

Figure K.1: Right wheel angle ($2.21 m/s$)

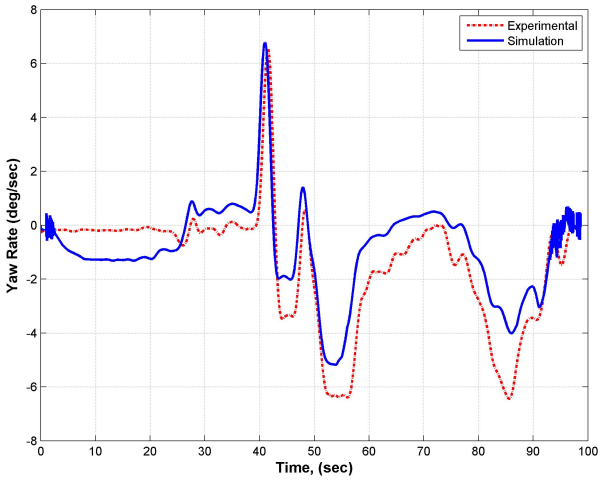

Figure K.2: Vehicle yaw-rate ($2.21 m/s$)

Appendix L

Enlarged Figures 4.37 and 4.38

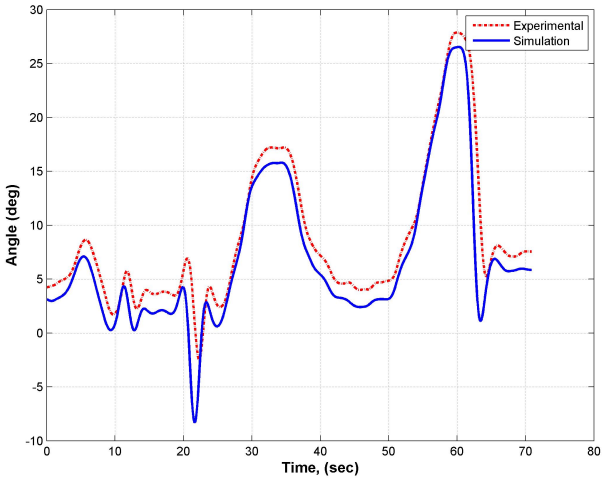

Figure L.1: Right wheel angle ($2.73m/s$)

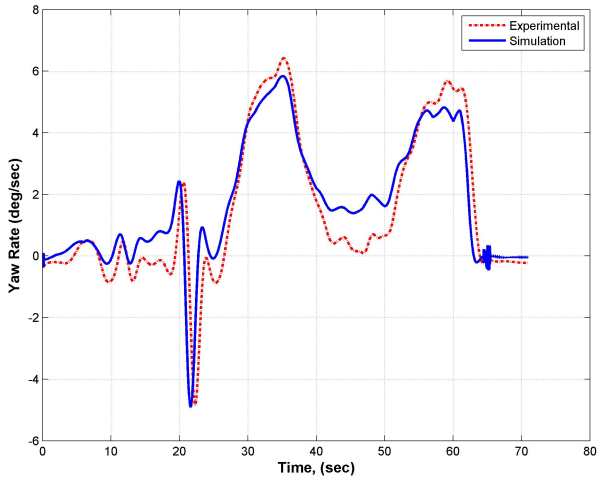

Figure L.2: Vehicle yaw-rate ($2.73m/s$)

Appendix M

Enlarged Figure 4.40

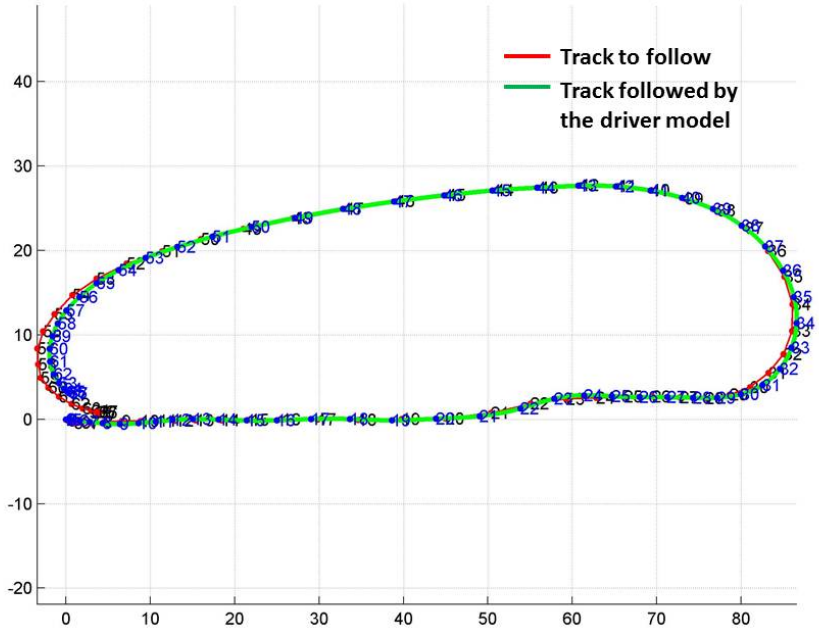

Figure M.1: Track following

Appendix N

Enlarged Figure 5.14

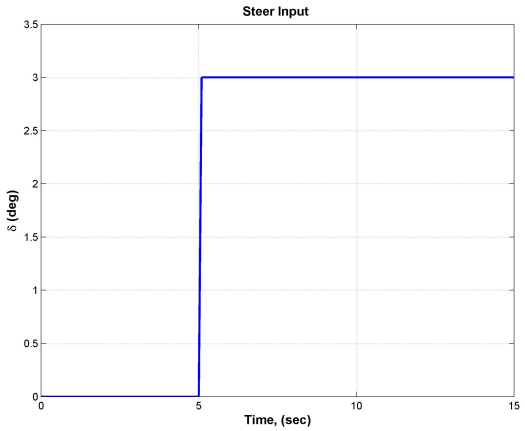

Figure N.1: Steer input for the J-Turn manoeuvre at 55 km/h speed

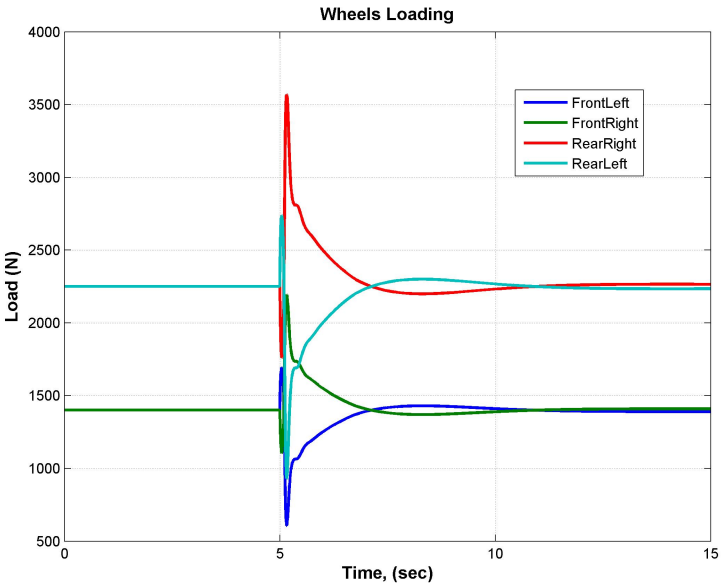

Figure N.2: Variation in the wheel loading

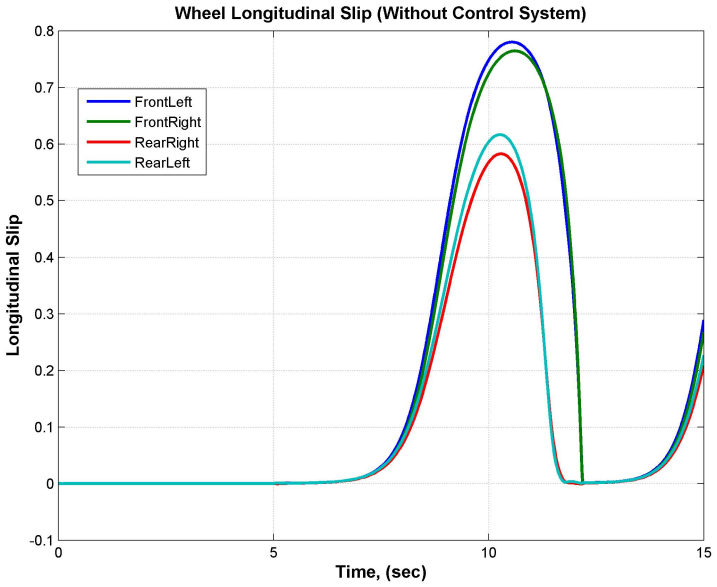

Figure N.3: Wheel longitudinal slip without the control system

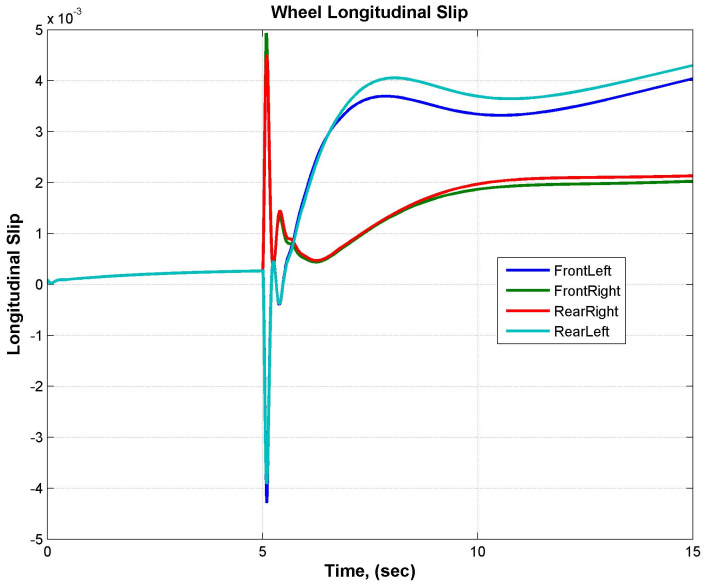

Figure N.4: Wheel longitudinal slip with the control system

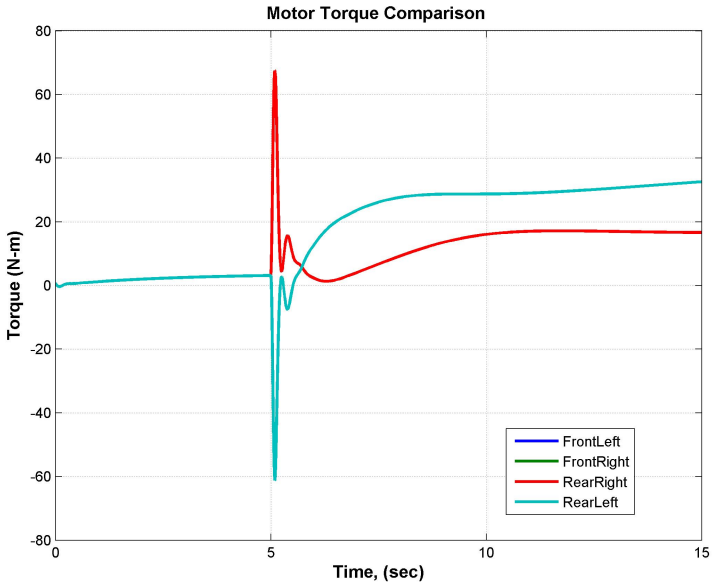

Figure N.5: Wheel motors torque

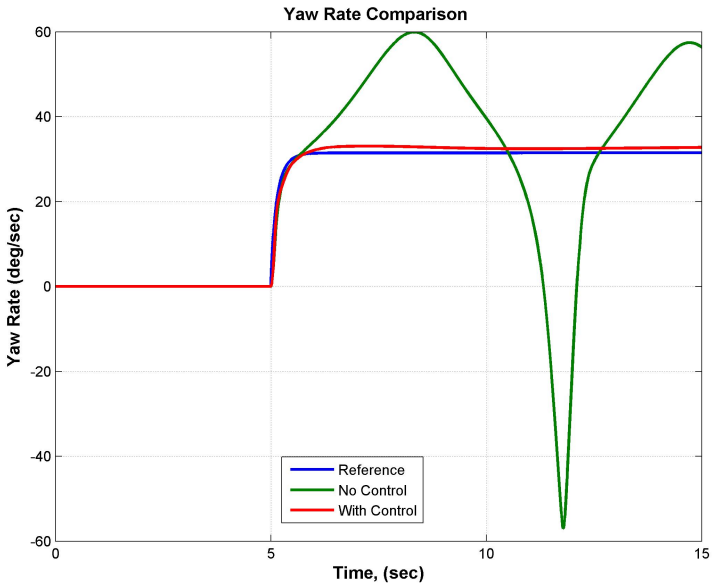

Figure N.6: Yaw comparison

Appendix O

Enlarged Figure 5.16

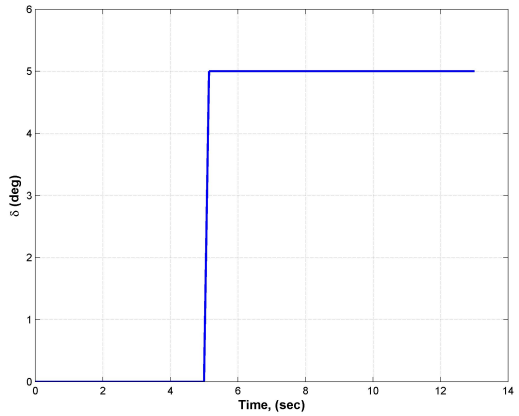

Figure O.1: Steer input for the J-Turn manoeuvre at 55 km/h speed

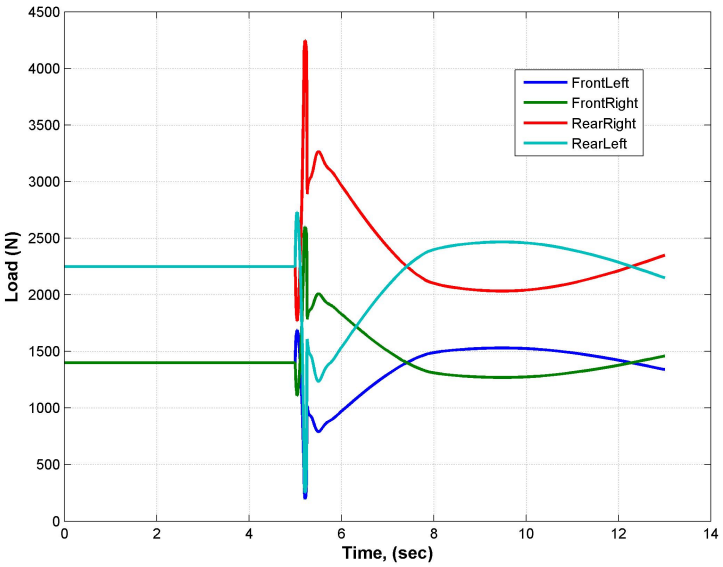

Figure O.2: Variation in the wheel loading

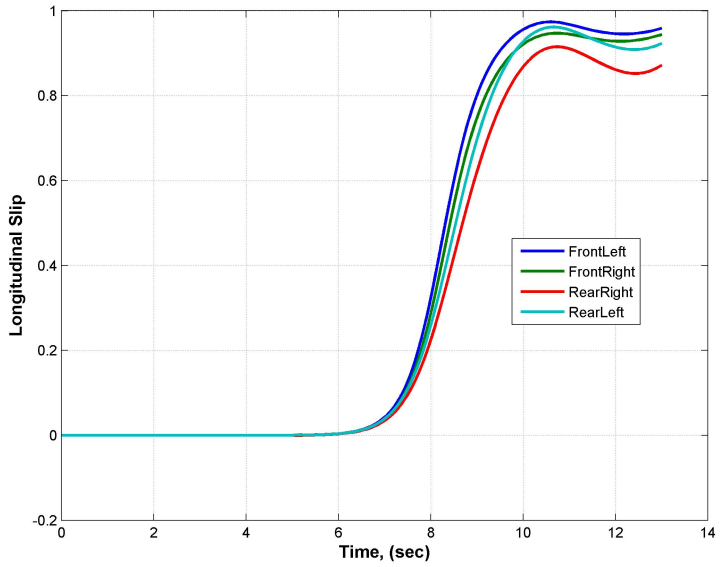

Figure O.3: Wheel longitudinal slip without the control system

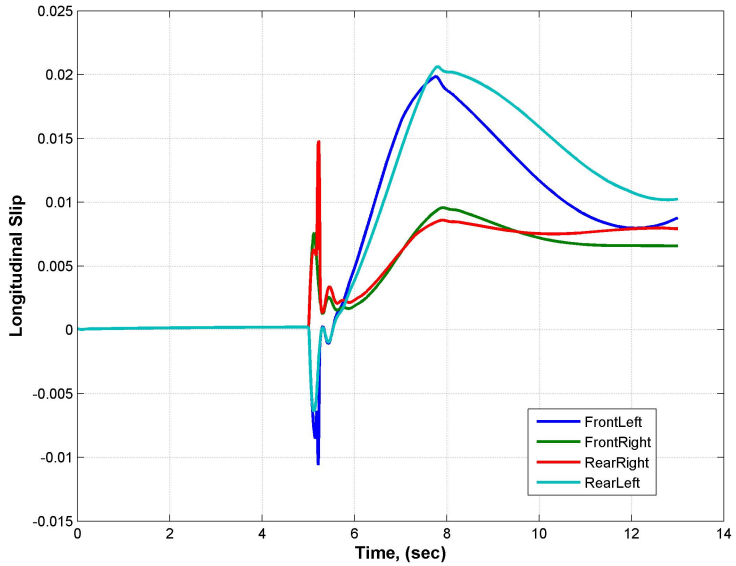

Figure O.4: Wheel longitudinal slip with the control system

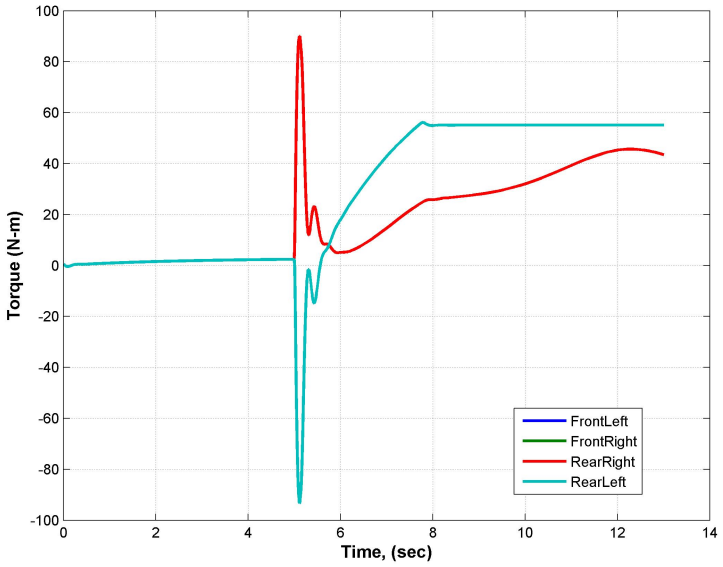

Figure O.5: Wheel motors torque

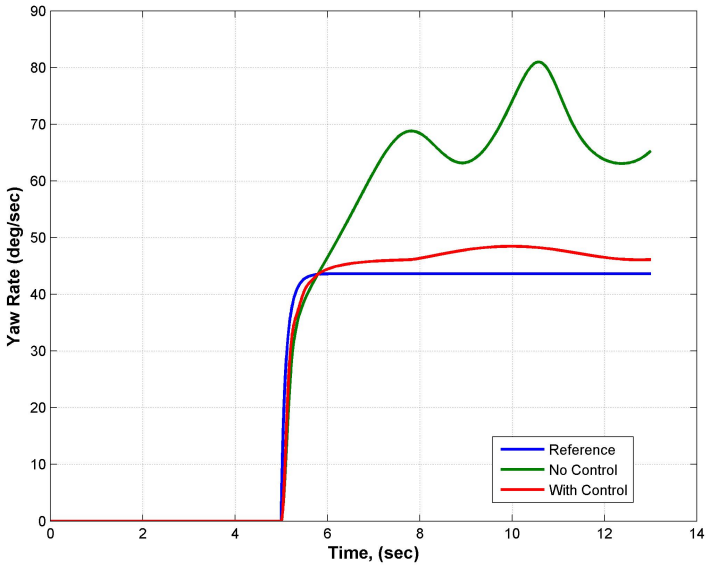

Figure O.6: Yaw comparison

Appendix P

Enlarged Figure 5.17

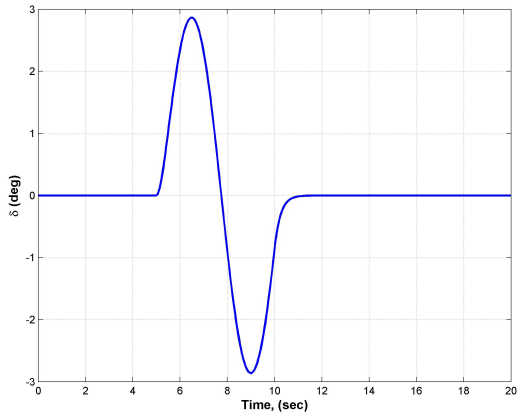

Figure P.1: Steer input for the Sine-steer manoeuvre at 70 km/h speed

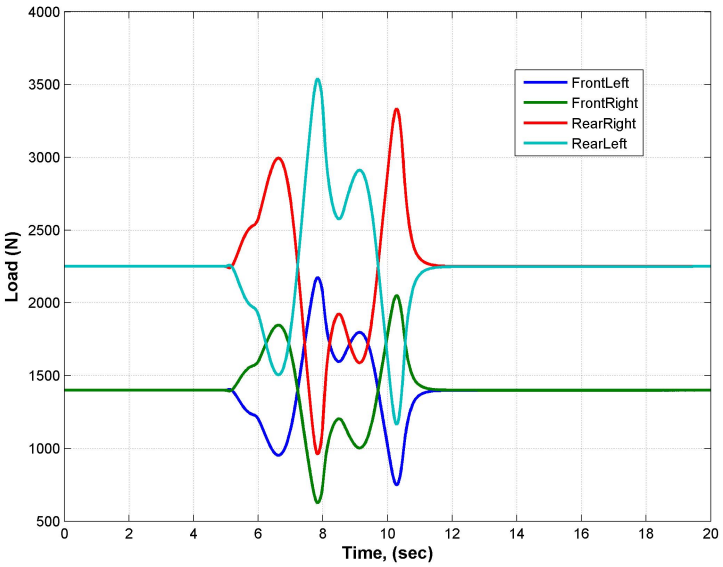

Figure P.2: Variation in the wheel loading

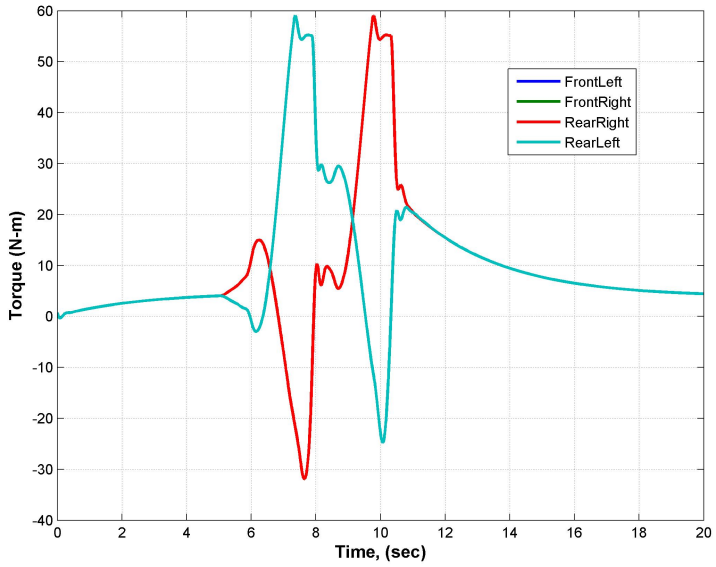

Figure P.3: Wheel motors torque

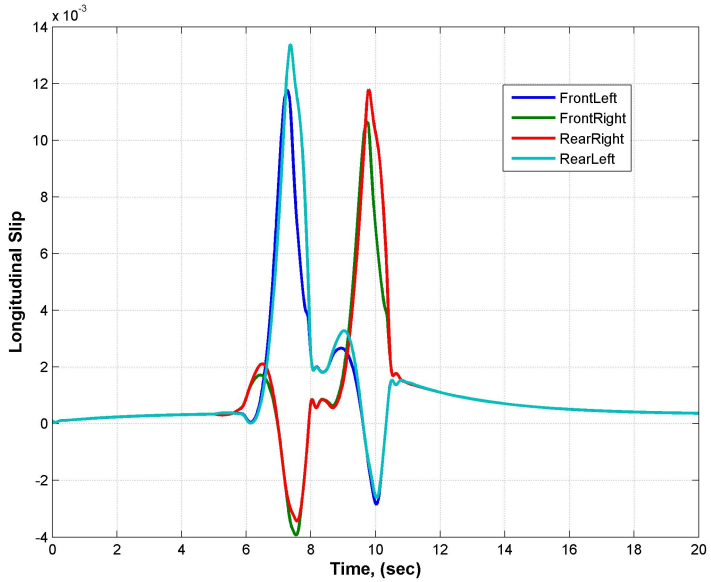

Figure P.4: Wheel longitudinal slip with the control system

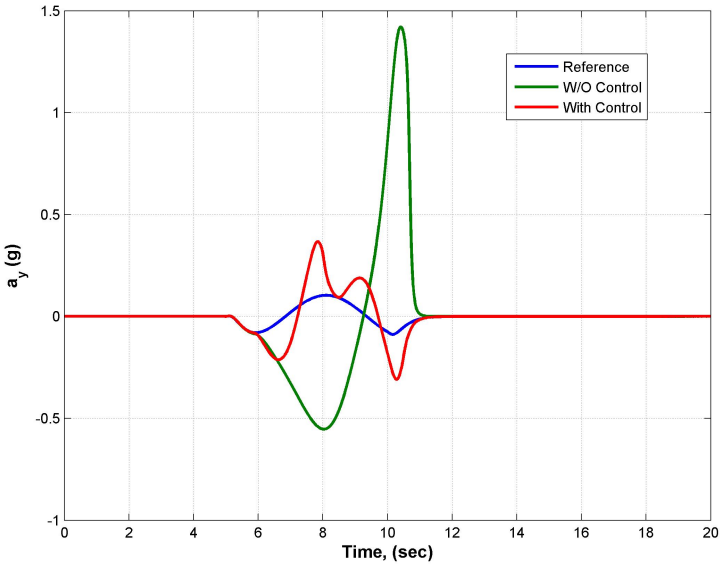

Figure P.5: Lateral acceleration comparison

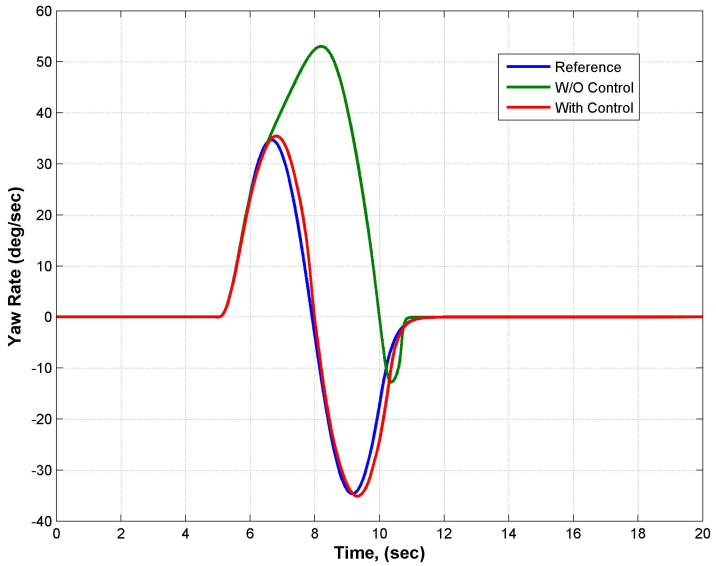

Figure P.6: Yaw comparison

Appendix Q

Enlarged Figure 5.18

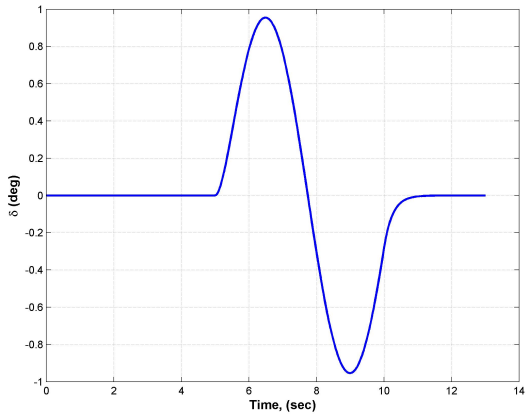

Figure Q.1: Steer input for the Sine-steer manoeuvre at 70 km/h speed

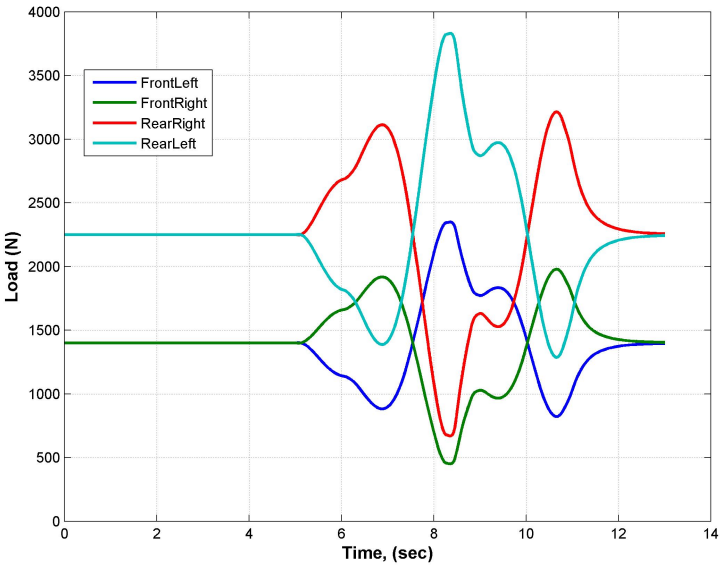

Figure Q.2: Variation in the wheel loading

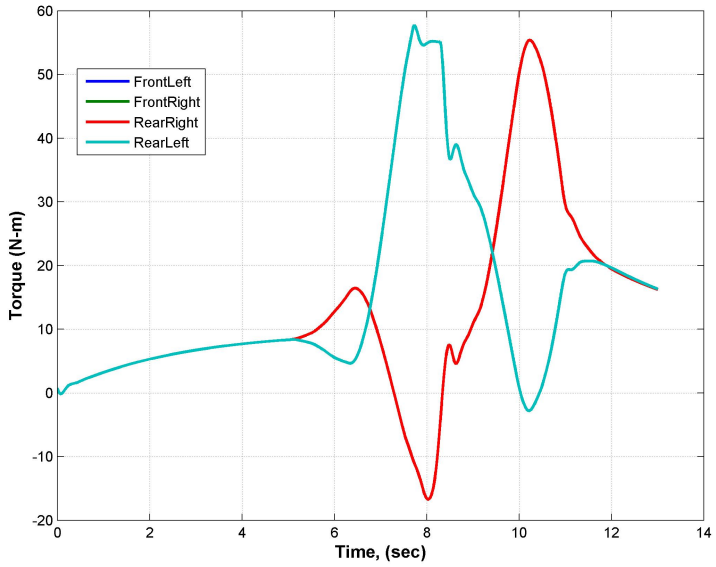

Figure Q.3: Wheel motors torque

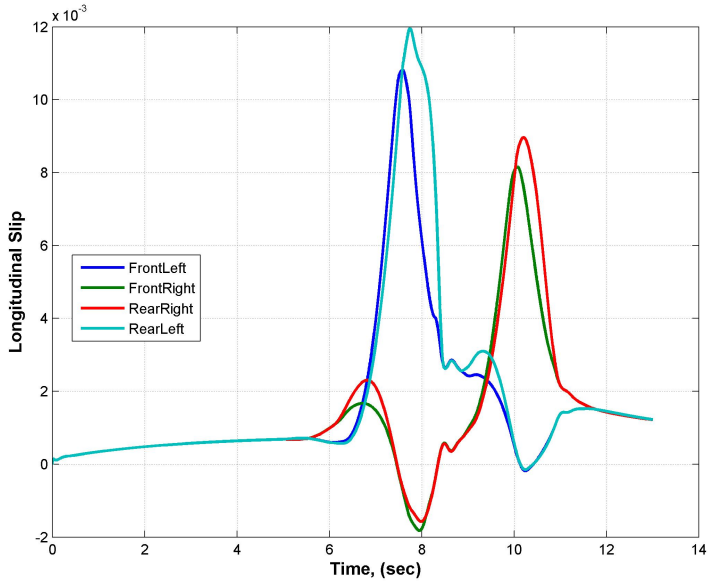

Figure Q.4: Wheel longitudinal slip with the control system

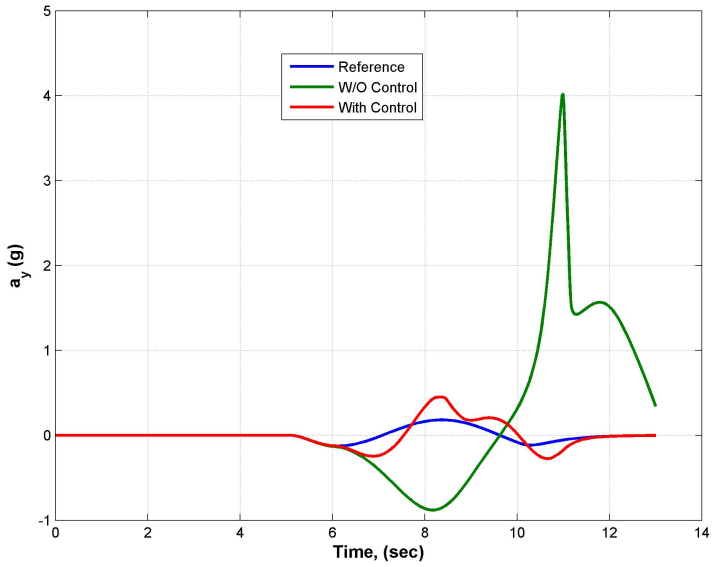

Figure Q.5: Lateral acceleration comparison

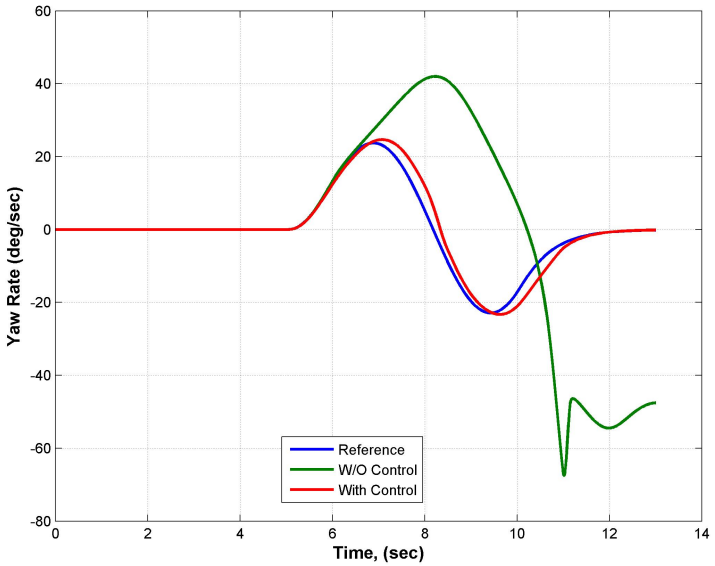

Figure Q.6: Yaw comparison

Appendix R
Sensor specifications

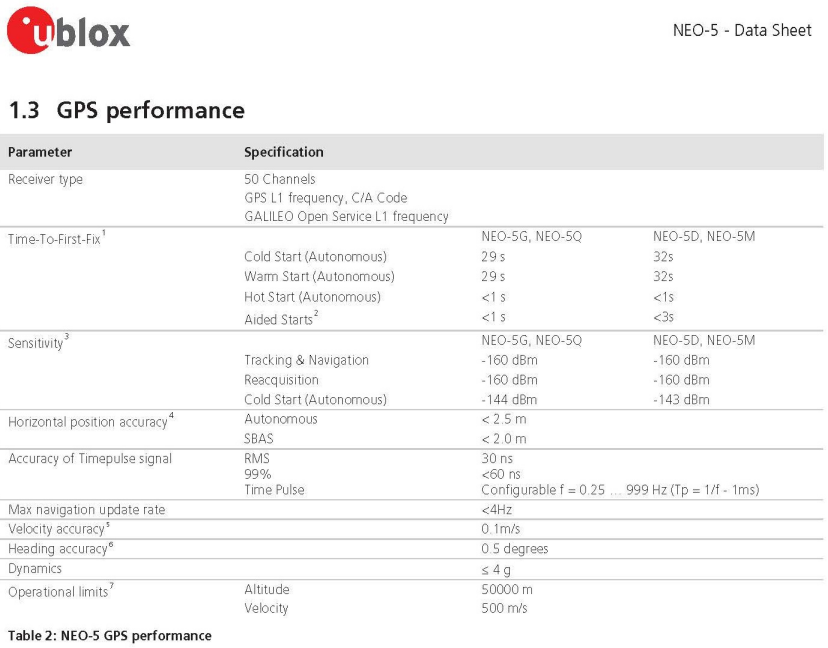

NEO-5 - Data Sheet

1.3 GPS performance

Parameter	Specification		
Receiver type	50 Channels GPS L1 frequency, C/A Code GALILEO Open Service L1 frequency		
Time-To-First-Fix[1]		NEO-5G, NEO-5Q	NEO-5D, NEO-5M
	Cold Start (Autonomous)	29 s	32s
	Warm Start (Autonomous)	29 s	32s
	Hot Start (Autonomous)	<1 s	<1s
	Aided Starts[2]	<1 s	<3s
Sensitivity[3]		NEO-5G, NEO-5Q	NEO-5D, NEO-5M
	Tracking & Navigation	-160 dBm	-160 dBm
	Reacquisition	-160 dBm	-160 dBm
	Cold Start (Autonomous)	-144 dBm	-143 dBm
Horizontal position accuracy[4]	Autonomous	< 2.5 m	
	SBAS	< 2.0 m	
Accuracy of Timepulse signal	RMS 99% Time Pulse	30 ns <60 ns Configurable f = 0.25 ... 999 Hz (Tp = 1/f - 1ms)	
Max navigation update rate		<4Hz	
Velocity accuracy[5]		0.1m/s	
Heading accuracy[6]		0.5 degrees	
Dynamics		≤ 4 g	
Operational limits[7]	Altitude	50000 m	
	Velocity	500 m/s	

Table 2: NEO-5 GPS performance

Figure R.1: Data sheet for the GPS sensor

Model 3547

Electrical Characteristics[1]	Wirewound Element	Hybritron® Element
Standard Resistance Range	1K to 50K ohms	1K to 10K ohms
Total Resistance Tolerance	±3 %	±10 %
Independent Linearity	±0.25 %	±0.25 %
Independent Linearity (Maximum Practical)	±0.20 %	±0.20 %
Effective Electrical Angle	1080 ° +10 °, -0 °	1080 ° +10 °, -0 °
Absolute Minimum Resistance/End Voltage	1 ohm or 0.1 % maximum (whichever is greater)	0.7 % maximum
Noise/Output Smoothness	100 ohms maximum	0.15 % maximum
Max. Wiper Current @ 5K ohms	20 mA	10 mA
Dielectric Withstanding Voltage (MIL-STD-202, Method 301)		
Sea Level	1,000 VAC minimum	1,000 VAC minimum
Insulation Resistance (500 VDC)	1,000 megohms minimum	1,000 megohms minimum
Resolution	See How to Order chart	Essentially infinite
Power Rating (Voltage Limited By Power Dissipation)		
+70 °C	1 watts	1 watts
+125 °C	0 watt	0 watt

Environmental Characteristics[1]		
Operating Temperature Range		
Dynamic	-40 °C to +125 °C	-40 °C to +125 °C
Static	-55 °C to +125 °C	-55 °C to +125 °C
Temperature Coefficient (Over Static Temperature Range)	±50 ppm/°C	±100 ppm/°C
Temperature Cycling (5 Cycles Over Static Temperature Range)	±2 % TR shift max.	±4 % TR shift max.
Vibration (15 Gs, 10 Hz to 2 kHz)		
Wiper Bounce	0.1 ms max.	0.1 ms max.
Shock (100 Gs, 6 ms sawtooth)		
Wiper Bounce	0.1 ms max.	0.1 ms max.
Load Life (1,000 hours @ 70 °C)	±2 % TR shift max.	±5 % TR shift max.
Rotational Life		
No Load	750,000 shaft revolutions	1,500,000 shaft revolutions
Powered (MIL-PRF-12934)	600,000 shaft revolutions	1,200,000 shaft revolutions
Moisture Resistance (Mil-Std-202, Method 103)	±2 % TR shift max.	±5 % TR shift max.
IP Rating	IP 50	IP 50

Mechanical Characteristics[1]	
Mechanical Angle	1080 ° +10 °, -0 °
Backlash	1.0 ° max.
Stop Strength	53 N-cm (75 oz-in.) min.
Torque	
Starting	0.5 N-cm (0.7 oz.-in.) max.
Running	0.5 N-cm (0.7 oz.-in.) max.
Mounting	170-200 N-cm (15-18 in.-lb.) max.
Shaft Runout T.I.R.	0.08 mm (0.003 in.)
Lateral Runout T.I.R.	0.13 mm (0.005 in.)
Shaft End Play T.I.R.	0.15 mm (0.006 in.)
Shaft Radial Play T.I.R.	0.08 mm (0.003 in.)
Pilot Diameter Runout T.I.R.	0.08 mm (0.003 in.)
Weight	
Single	18 gm (0.63 oz.) typ.
Dual	34 gm (1.2 oz.) typ.
Shaft Side Load (Max. Allowable)	
Nickel Plated Brass Shaft w/Brass Bushing	50 gmf (1.7 ozf)
Stainless Steel Shaft w/Bronze Bushing	250 gmf (8.8 ozf)
Terminals	Gold-plated solder lugs
Solder Process - Manual	
Solder Type	96.5 Sn/3.0 Ag/0.5 Cu solid wire or no-clean rosin cored wire
Temperature Profile	370 °C (700 °F) for 3 seconds maximum
Wash Process	Not recommended
Mounting Hardware	One lockwasher and one mounting nut is shipped with each potentiometer
Recommended Panel Thickness (Bushing Mount)	2.46-3.81 mm (0.097-0.150 in.)
Marking	Manufacturer's symbol, model number, product code and date code
Standard Packaging	Plastic trays (5 pcs./tray)

[1]*At room ambient: +25 °C nominal and 50 % relative humidity nominal, except as noted. For other options, please consult factory.*

Figure R.2: Data sheet for the potentiometer

ANALOG DEVICES

Small, Low Power, 3-Axis ±5 *g* Accelerometer

ADXL325

FEATURES

3-axis sensing
Small, low profile package
4 mm × 4 mm × 1.45 mm LFCSP
Low power: 350 µA typical
Single-supply operation: 1.8 V to 3.6 V
10,000 *g* shock survival
Excellent temperature stability
Bandwidth adjustment with a single capacitor per axis
RoHS/WEEE lead-free compliant

APPLICATIONS

Cost-sensitive, low power, motion- and tilt-sensing applications
Mobile devices
Gaming systems
Disk drive protection
Image stabilization
Sports and health devices

GENERAL DESCRIPTION

The ADXL325 is a small, low power, complete 3-axis accelerometer with signal conditioned voltage outputs. The product measures acceleration with a minimum full-scale range of ±5 *g*. It can measure the static acceleration of gravity in tilt-sensing applications, as well as dynamic acceleration, resulting from motion, shock, or vibration.

The user selects the bandwidth of the accelerometer using the C_X, C_Y, and C_Z capacitors at the X_{OUT}, Y_{OUT}, and Z_{OUT} pins. Bandwidths can be selected to suit the application with a range of 0.5 Hz to 1600 Hz for X and Y axes and a range of 0.5 Hz to 550 Hz for the Z axis.

The ADXL325 is available in a small, low profile, 4 mm × 4 mm × 1.45 mm, 16-lead, plastic lead frame chip scale package (LFCSP_LQ).

FUNCTIONAL BLOCK DIAGRAM

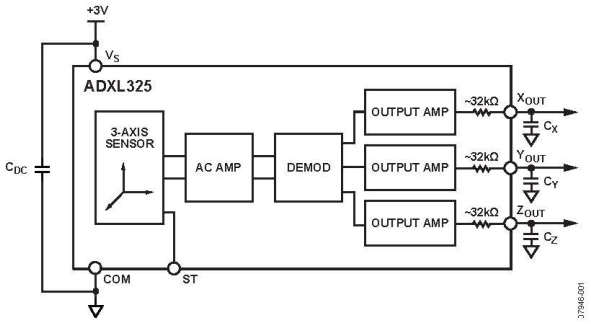

Figure 1.

One Technology Way, P.O. Box 9106, Norwood, MA 02062-9106, U.S.A.
Tel: 781.329.4700 www.analog.com
Fax: 781.461.3113

Figure R.3: Data sheet for the accelerometer

Specifications

Angular Rate		
Range:	±100°/sec	Up to ±500°/sec available
Scale Factor:	10°/sec/V	
Scale Factor Accuracy:	1%	Constant temperature
Scale Factor Temperature Coefficient:	3%	
Bias: Zero Bias	< 1.5°/sec	
Bias: Over Temperature Range	±10°/sec	
Warm-up Drift	< 2%	Full scale range
Non-Linearity	< 0.05%	Full scale range
Bandwidth	50 Hz	
Noise:	< 0.1% rms	Full scale range
Environmental		
Temperature: Operating	-20°C to +50°C	
Temperature: Storage	-55°C to +85°C	
Vibration: Operating	2.5g rms	20 Hz to 2 kHz
Vibration: Survival	10g rms	20 Hz to 2 kHz
Shock: Survival	500g	10ms ½ sine wave
Electrical		
Input Power: Positive	12 to 16VDC	0.2W
Input Power: Negative	-12 to -16VDC	0.2W
Input Current:	10mA @ ±15VDC	
Analog Output	±10VDC	
Output Impedance:	1000 Ohm	
Physical		
Size: Including Mounting Flanges	1.13"W x 3.00"L x 2.07"H	2.9 x 7.6 x 5.3 (cm)
Weight:	2oz (0.1lb)	60g (0.1kg)
Connection:	Wire Bundle	
Life:	> 50,000 Hours MTBF	

- Specifications are subject to change without notice.
- This product may be subject to export restrictions. Please consult the factory.

Connections/Dimensions

Wire Color	Function
Green	**-15 VDC Power**
Black	**Ground**
Red	**+15 VDC Power**
Violet	**Angular Rate Output**
Yellow	**Bias Input**

Please note that all wires are 24 AWG and approx. 12 inches in length.

Power:

Ground (Black), +15 VDC (Red), and -15 VDC (Green). Each input voltage should be within ±5%. Higher or reverse voltages may cause component damage, a lower voltage may cause faulty operation.
The power inputs should be well filtered; power line noise may cause noise to appear on the outputs. Current draw is approximately 10 mA from each supply.

Output:

The signal output (Violet) is protected by 1K series resistor and will not be damaged by intermittent short circuits. These resistors protect the circuit from ringing caused by capacitive loading of long wires.
The output is 0.0 VDC at zero angular rate. Approximately 20% over-range is available.

Bias Input:

The bias input (Yellow) may be used to provide a DC bias for the output signal. The circuit will allow the output to be biased over a range of approximately ±13 VDC before saturation occurs. The bias input has a 10K input impedance. If this input is not used, the connection can be either left open or grounded with no effect on the rate output. Grounding the bias input is preferred if a low noise ground is available.

Figure R.4: Data sheet for the gyro

References

[Abe 1999] M Abe. *Vehicle dynamics and control for improving handling and active safety: From four-wheel steering to direct yaw moment control.* Proceedings of the Institution of Mechanical Engineers, Part K: Journal of Multi-body Dynamics, vol. 213, no. 2, pages 87–101, 1999. 26, 39

[Abe 2009] M. Abe. Vehicle handling dynamics: Theory and application. Elsevier Ltd., Oxford, UK, 2009. vii, 26, 37, 56, 59, 72, 73, 74, 113, 147

[Ackermann 1990] J. Ackermann. *Robust car steering by yaw rate control.* In Decision and Control, 1990., Proceedings of the 29th IEEE Conference on, pages 2033 –2034 vol.4, dec 1990. 8, 26, 38

[Ackermann 1997] J. Ackermann and T. Bünte. *Yaw disturbance attenuation by robust decoupling of car steering.* Control Engineering Practice, vol. 5, no. 8, pages 1131 – 1136, 1997. 10

[Ackermann 1999] J. Ackermann, T. Bünte and D. Odenthal. *Advantages Of Active Steering For Vehicle Dynamics Control.* In In Proc. 32nd International Symposium on Automotive Technology and Automation, pages 263–270, 1999. 8, 10, 40

[Ahn 2012] Changsun Ahn, Huei Peng and H. Eric Tseng. *Robust estimation of road friction coefficient using lateral and longitudinal vehicle dynamics.* Vehicle System Dynamics, pages 1–25, 2012. 9

[Allen 1997] R. Wade Allen and Theodore J. Rosenthal. *A Vehicle Dynamics Tire Model for Both Pavement and Off-Road Conditions.* In Society of Automotive Engineers, numéro SAE 970559, 1997. 34

[Bajçinca 2005] N. Bajçinca, R. Cortesão and M. Hauschild. *Robust Control for Steer-by-Wire Vehicles.* Auton. Robots, vol. 19, pages 193–214, September 2005. 26

[Bakker 1987] E. Bakker, L. Nyborg and H. B. Pacejka. *Tyre Modelling for Use in Vehicle Dynamics Studies.* In Society of Automotive Engineers, numéro SAE 870421, 1987. 32, 33

[Bakker 1989] E. Bakker, L. Lidner and H. B. Pacejka. *A New Tire Model with an Application in Vehicle Dynamics Studies.* In Society of Automotive Engineers, numéro SAE 890087, 1989. 32, 33

[Bang 2001] M. S. Bang, S. H. Lee, C. S. Han, D. B. Maciuca and J. K. Hedrick. *Performance enhancement of a sliding mode wheel slip controller by the yaw moment control.* Proceedings of the Institution of Mechanical Engineers, Part D: Journal of Automobile Engineering, vol. 215, no. 4, pages 455–468, 2001. 44

[Barter 1969] N. F. Barter. *Measurement of Vehicle Handling by Tethered Testing.* Proceedings of the Institution of Mechanical Engineers: Automobile Division, vol. 184, no. 1, pages 219–231, 1969. 24

[Becker 1931] G. Becker and H. Fromm und H. Maruhn. Schwingungen in automobillenkungen "shimmy". M. Krayn, Berlin, 1931. 22, 28

[Bernanrd 1977] J. E. Bernanrd, L. Segel and R. E. Wild. *Tire Shear Force Generation During Combined Steering and Braking Maneuvers.* In Society of Automotive Engineers, numéro SAE 770852, 1977. 31

[Blundell 1999a] M V Blundell. *The modelling and simulation of vehicle handling Part 1: Analysis methods.* Proceedings of the Institution of Mechanical Engineers, Part K: Journal of Multi-body Dynamics, vol. 213, no. 2, pages 103–118, 1999. 25

[Blundell 1999b] M V Blundell. *The modelling and simulation of vehicle handling Part 2: Vehicle modelling.* Proceedings of the Institution of Mechanical Engineers, Part K: Journal of Multi-body Dynamics, vol. 213, no. 2, pages 119–134, 1999. 25

[Blundell 2000a] M V Blundell. *The modelling and simulation of vehicle handling Part 3: Tyre modelling.* Proceedings of the Institution of Mechanical Engineers, Part K: Journal of Multi-body Dynamics, vol. 214, no. 1, pages 1–32, 2000. 25

[Blundell 2000b] M V Blundell. *The modelling and simulation of vehicle handling Part 4: Handling simulation.* Proceedings of the Institution of Mechanical Engineers, Part K: Journal of Multi-body Dynamics, vol. 214, no. 2, pages 71–94, 2000. 25

[Blundell 2004] M. Blundell and D. Harty. The multibody systems approach to vehicle dynamics. Elsevier Ltd., Oxford, UK, 2004. 29, 62, 64

[Blundell 2007] M. V. Blundell and D. Harty. *Intermediate tyre model for vehicle handling simulation.* Journal of Multi-body Dynamics, vol. 221, pages 41–62, 2007. 30, 32

[Boada 2005] B. L. Boada, M. J.L. Boada and V. DÃaz. *Fuzzy-logic applied to yaw moment control for vehicle stability.* Vehicle System Dynamics, vol. 43, no. 10, pages 753–770, 2005. 44

[Brach 2000] R. Matthew Brach and Raymond M. Brach. *Modelling Combined Braking and Steering Tire Forces.* In Society of Automotive Engineers, numéro SAE 2000-01-0357, 2000. vii, 63

[Brach 2009] Raymond M. Brach and R. Matthew Brach. *Tire Models for Vehicle Dynamic Simulation and Accident Reconstruction.* In Society of Automotive Engineers, numéro SAE 2009-01-0102, 2009. 34

[Bradley 1930] J. Bradley and R. F. Allen. *Factors affecting the behaviour of rubber-tyred wheels on road surfaces.* In Proceedings of the Institution of Mechanical Engineers, Automobile Division, volume 25, pages 63–92. Sage Publications, 1930. 22, 28

[Broulheit 1925] G. Broulheit. *La Suspension de la Direction de la Voiture Automobile: Shimmy et Danadinementmill.* Societe des Ingenieurs Civils de France, vol. Bulletin 78, 1925. 22, 28

[Buckholtz 2002] Kenneth R. Buckholtz. *Reference Input Wheel Slip Tracking Using Sliding Mode Control.* Numeéro 2002-01-0301 de SAE TECHNICAL PAPER SERIES, 400 Commonwealth Drive, Warrendale, PA 15096-0001 U.S.A, March 2002. SAE International, SAE 2002 World Congress. 34, 44, 127

[Burgio 2010] Gilberto Burgio, Alberto Girelli, Jacopo Palandri and Diego Alessandri. *Active Rear Steering System and Controller Design to Improve Vehicle Driving and Handling Behavior.* In FISITA 2010, World Automotive Congress, numéro F2010B020, 2010. 18

[Casanova 2000] Daniele Casanova. *On minimum time vehicle manoeuvering: The theoretical optimal lap.* PhD thesis, Cranfield University, UK, 2000. 34

[Chatzikomis 2009] C. Chatzikomis and K. Spentzas. *A path-following driver model with longitudinal and lateral control of vehicle's motion.* Forschung im Ingenieurwesen, vol. 73, pages 257–266, 2009. 10.1007/s10010-009-0112-5. 36

[Chen 2001] Bo-Chiuan Chen and Huei Peng. *Differential-Braking-Based Rollover Prevention for Sport Utility Vehicles with Human-in-the-loop Evaluations*. Vehicle System Dynamics, vol. 36, no. 4-5, pages 359–389, 2001. 26

[Chu 2010] Liang Chu, Mingfa Xu, Yongsheng Zhang, Yang Ou and Yanru Shi. *Vehicle Dynamics Control based on optimal sliding mode control theory*. In Computer, Mechatronics, Control and Electronic Engineering (CMCE), 2010 International Conference on, volume 3, pages 486 –491, aug. 2010. 44

[Chun 2005] Kyunghan Chun and Myoungho Sunwoo. *Wheel slip tracking using moving sliding surface*. Proceedings of the Institution of Mechanical Engineers, Part D: Journal of Automobile Engineering, vol. 219, no. 1, pages 31–41, 2005. 126

[Crolla] David Crolla. *Vehicle Dynamics, Control and Suspension*. Lecture Notes, Cranfield University. 56, 147

[Dick 2005] Robert Dick. Mercedes and auto racing in the belle epoque 1895 - 1915. McFarland and Company, Inc., Publishers, 2005. 8

[Ding 2010a] N. Ding and S. Taheri. *A Modified Dugoff Tire Model for Combined-slip Forces*. Tire Science and Technology, vol. 38, no. 3, pages 228–244, 2010. 30, 34

[Ding 2010b] Nenggen Ding and Saied Taheri. *An adaptive integrated algorithm for active front steering and direct yaw moment control based on direct Lyapunov method*. Vehicle System Dynamics, vol. 48, no. 10, pages 1193–1213, 2010. 27, 44

[Dixon 1988] J. C. Dixon. *Linear and non-linear steady state vehicle handling*. In Proceedings of the Institution of Mechanical Engineers, Automobile Division, volume 202, pages 173–186. Sage Publications, 1988. 26, 48, 111

[Dixon 1996] John C Dixon. Tires, suspension and handling. Numeéro ISBN: 978-1-56091-831-8. Society of Automotive Engineers, 1996. 26

[Doniselli 1994] C. Doniselli, G. Mastinu and R. Cal. *Traction Control for Front-Wheel-Driver Vehicles*. Supplement to Vehicle System Dynamics, vol. 23, no. ISSN: 0042-3114, pages 87–104, 1994. 40, 41

[Drakunov 2000] S.V. Drakunov, B. Ashrafi and A. Rosiglioni. *Yaw control algorithm via sliding mode control.* In American Control Conference, 2000. Proceedings of the 2000, volume 1, pages 580 –583 vol.1, sep 2000. 26

[Du 2006] Y Du, A Lion and P Maißer. *Modelling and Control of An Electromechanical Steering System in Full Vehicle Models.* Proceedings of the Institution of Mechanical Engineers, Part I: Journal of Systems and Control Engineering, vol. 220, no. 3, pages 239–249, 2006. 14, 20

[Dugoff 1969] H. Dugoff, P. S. Fancher and L. Segel. *Tire Performance Characteristics Affecting Vehicle Response to Steering and Braking Control Inputs.* Rapport technique CST - 460, University of Michigan, USA, 1969. 31

[Dugoff 1970] H. Dugoff, P. S. Fancher and L. Segel. *An Analysis of Tire Traction Properties and Their Influence on Vehicle Dynamic Performance.* In Society of Automotive Engineers, numéro SAE 700377, 1970. 31, 32, 70, 83

[Dutton 1998] Ken Dutton, Steve Thompson and Bill Barraclough. The art of control engineering. Addison-Wesley, 1998. 117, 124, 125

[Eckert 2010] Alfred Eckert, Bernd Hartmann and Dr.-Ing. Peter E. Rieth. *Emergency Steer Assist - Advanced Driver Assistance System for Emergency Lane Change Maneuvers.* In FISITA 2010, World Automotive Congress, numéro F2010E017, 2010. 16

[Economou 1999] John Theodoros Economou. *Modelling and control of multi wheel skid steer vehicles.* PhD thesis, Royal Military College of Science, Shrivenham, 1999. 58

[Ellis 1994] J. R. Ellis. Vehicle hanling dynamics. Mechanical Engineering Publications Limited, London, UK, 1994. 26

[Esmailzadeh 2001] E. Esmailzadeh, G.R. Vossoughi and A. Goodarzi. *Dynamic Modeling and Analysis of a Four Motorized Wheels Electric Vehicle.* Vehicle System Dynamics, vol. 35, no. 3, pages 163–194, 2001. 42, 44

[Esmailzadeh 2002] E Esmailzadeh, A Goodarzi and G R Vossoughi. *Directional stability and control of four-wheel independent drive electric vehicles.* Proceedings of the Institution of Mechanical Engineers, Part K: Journal of Multi-body Dynamics, vol. 216, no. 4, pages 303–313, 2002. 44

[Fiala 1954] E. Fiala. *Sietenkrafte am rollenden Luftreifen (Lateral forces on the rolling pneumatic tyres).* VDI-Zeitschrift, vol. 96, pages 973–979, 1954. 28

[Frömmig 2010] Lars Frömmig, Torben Pawellek, Ferit Küçükay, Durukan Bedük and Orhan Atabay. *Evaluation (of the steering behaviour) of Electro-mechanical Steering Systems.* In FISITA 2010, World Automotive Congress, numéro F2010C065, 2010. 16

[Furukawa 1997] Yoshimi Furukawa and Masato Abe. *Advanced Chassis Control Systems for Vehicle Handling and Active Safety.* Vehicle System Dynamics: International Journal of Vehicle Mechanics and Mobility, vol. 28, pages 59–86, 1997. 39, 41

[Garrott 1981] W. Riley Garrott, Douglas L. Wilson and Richard A. Scott. *Digital Simulation for Automobile Maneuvers.* SIMULATION, vol. 37, no. 3, pages 83–91, 1981. 24

[Genta 2006] G. Genta. Motor vehicle dynamics : Modeling and simulation. World Scientific Publishing Co., Singapore, 2006. 32, 55, 67

[Ghike 2009] C Ghike, T Shim and J Asgari. *Integrated control of wheel drive-brake torque for vehicle-handling enhancement.* Proceedings of the Institution of Mechanical Engineers, Part D: Journal of Automobile Engineering, vol. 223, no. 4, pages 439–457, 2009. 44

[Giles 1968] J. G. Giles. Steering, suspension and tyres. Iliffe Books Ltd, London, 1968. vii, 62, 67, 147

[Gillespie 1992] Thomas D. Gillespie. Fundamentals of vehicle dynamics. SAE International, USA, 1992. 22, 26, 49

[Goodarzi 2007] A Goodarzi and E Esmailzadeh. *Design of a VDC System for All-Wheel Independent Drive Vehicles.* IEEE ASME Transactions on Mechatronics, vol. 12, no. 6, pages 632–639, 2007. 44

[Goodarzi 2008] A Goodarzi, A Sabooteh and E Esmailzadeh. *Automatic path control based on integrated steering and external yaw-moment control.* Proceedings of the Institution of Mechanical Engineers, Part K: Journal of Multi-body Dynamics, vol. 222, no. 2, pages 189–200, 2008. 26, 44

[Gregory 2006] R . Douglas Gregory. Classical mechanics. Cambridge University Press, The Edinburgh Building, Cambridge CB2 2RU, UK, 2006. 56

[Guntur 1980] R. Guntur and S. Sankar. *A friction circle concept for Dugoff's tyre friction model.* International Journal of Vehicle Design, vol. 1, no. 4, pages 373–377, 1980. 32, 34, 69

[Guo 1983] Konghui Guo and Paul S. Fancher. *Preview-Follower Method for Modeling Closed-Loop Vehicle Directional Control.* In Ninteenth Annual Conference on Manual Control, MIT Cambridge, Massachusetts, numéro 19890068145, 1983. 35

[Guo 1993] K. Guo and H. Guan. *Modelling of Driver/Vehicle Directional Control System.* Vehicle System Dynamics, vol. 22, no. 3-4, pages 141–184, 1993. 36, 37, 73

[Hales 1969] F. D. Hales. *Vehicle Handling Qualities.* Proceedings of the Institution of Mechanical Engineers: Automobile Division, vol. 184, no. 1, pages 233–248, 1969. 24

[Harada 1995] Hiroshi Harada. *Control strategy of active rear wheel steering in consideration of system delay and dead times.* JSAE Review, vol. 16, no. 2, pages 171 – 177, 1995. 26, 38

[Hayama 2000] R. Hayama, K. Nishizaki, S. Nakano and K. Katou. *The vehicle stability control responsibility improvement using steer-by-wire.* In Intelligent Vehicles Symposium, 2000. IV 2000. Proceedings of the IEEE, pages 596 –601, 2000. 10, 11

[He 2005] Junjie He. *Integrated Vehicle Dynamics Control Using Active Steering, Driveline and Braking.* PhD thesis, The University of Leeds, UK, 2005. 147

[Horiuchi 1999] S. Horiuchi, K. Okada and S. Nohtomi. *Improvement of vehicle handling by nonlinear integrated control of four wheel steering and four wheel torque.* JSAE Review, vol. 20(4), pages 459–464, 1999. 40

[Horiuchi 2000] Shinichiro Horiuchi and Naohiro Yuhara. *An Analytical Approach to the Prediction of Handling Qualities of Vehicles With Advanced Steering Control System Using Multi-Input Driver Model.* Journal of Dynamic Systems, Measurement, and Control, vol. 122, no. 3, pages 490–497, 2000. 36

[Hsu 2009] Yung-Hsiang Judy Hsu. *Estimation and control of lateral tire forces using steering torque.* PhD thesis, Stanford University, USA, 2009. 34

[ichiro Sakai 1999] Shin ichiro Sakai, Hideo Sado and Yoichi Hori. *Motion Control in an Electric Vehicle with Four Independently Driven In-Wheel Motors*. IEEE ASME Transactions on Mechatronics, vol. 4, no. 1, pages 9–16, 1999. 41

[ichiro Sakai 2001] Shin ichiro Sakai and Yoichi Hori. *Advanced motion control of electric vehicle with fast minor feedback loops: basic experiments using the 4-wheel motored EV "UOT Electric March II"*. JSAE Review, vol. 22, no. 4, pages 527 – 536, 2001. 41

[Isermann 2001] Rolf Isermann. *Diagnosis Methods for Electronic Controlled Vehicles*. Vehicle System Dynamics, vol. 36, no. 2-3, pages 77–117, 2001. 15

[Isermann 2002] R. Isermann, R. Schwarz and S. Stolzl. *Fault-tolerant drive-by-wire systems*. Control Systems, IEEE, vol. 22, no. 5, pages 64 – 81, oct 2002. 20

[Ishio 2008] Jun Ishio, Hiroki Ichikawa, Yoshio Kano and Masato Abe. *Vehicle-handling quality evaluation through model-based driver steering behaviour*. Vehicle System Dynamics, vol. 46, no. sup1, pages 549–560, 2008. 37, 135

[Ito 1986] K. Ito, T. Fujishiro, T. Kawabe, K. Kanai and Y. Ochi. *A New Way of Controlling a Four Wheel Steering Vehicle (in Japanese)*. Transactions of the SICE, vol. 23, pages 828–834, 1986. 11

[Jürgensohn 2007] Thomas Jürgensohn. *Control Theory Models of the Driver*. In P. Carlo Cacciabue, editeur, Modelling Driver Behaviour in Automotive Environments, pages 277–292. Springer London, 2007. 35

[Kaiser 2011] G. Kaiser, F. Holzmann, B. Chretien, M. Korte and H. Werner. *Torque Vectoring with a feedback and feed forward controller - applied to a through the road hybrid electric vehicle*. In Intelligent Vehicles Symposium (IV), 2011 IEEE, pages 448 –453, june 2011. 43

[Kalman 1959] R. Kalman. *On the general theory of control systems*. Automatic Control, IRE Transactions on, vol. 4, no. 3, page 110, dec 1959. 124

[Kang 2005] Sangmin Kang, Maru Yoon and Myoungho Sunwoo. *Traction control using a throttle valve based on sliding mode control and load torque estimation*. Proceedings of the Institution of Mechanical Engineers, Part D: Journal of Automobile Engineering, vol. 219, no. 5, pages 645–653, 2005. 44

[Kasselmann 1969] J. T. Kasselmann and T. W. Keranen. *Adaptive Steering.* Bendix Technical Journal, vol. 2, pages 26–35, 1969. 8

[Kim 2008] Donghyun Kim, Sungho Hwang and Hyunsoo Kim. *Vehicle Stability Enhancement of Four-Wheel-Drive Hybrid Electric Vehicle Using Rear Motor Control.* Vehicular Technology, IEEE Transactions on, vol. 57, no. 2, pages 727 –735, march 2008. 44

[Kleine 1998] Sven Kleine and Johannes L Van Niekerk. *Modelling and Control of a Steer-By-Wire Vehicle.* Vehicle System Dynamics, vol. Supplement 28, pages 114–142, 1998. 9, 34

[Krauter 1975] Allan I. Krauter. *Determination of Tire Characteristics from Vehicle Brhaviour.* In Society of Automotive Engineers, numéro 750211 de SAE TECHNICAL PAPER SERIES. SAE International, 1975. 31, 32

[Krempl 1967] G. Krempl. *Untersuchungen an Kraftfahrzeugreifen.* Automobil-technische Zeitschrift, vol. 69, January & August 1967. 32

[Kreutz 2009] Marlene Kreutz, Martin Horn and Josef Zehetner. *Improving vehicle dynamics by active rear wheel steering systems.* Vehicle System Dynamics, vol. 47, no. 12, pages 1551–1564, 2009. 26

[Lanchester 1936] F. W. Lanchester. *Motor car suspension and independent springing.* In Proceedings of the Institution of Mechanical Engineers, Automobile Division, volume 30, pages 668–762. Sage Publications, 1936. 22

[Leung 2010] King Tin Leung. *Road vehicle state estimation using low-cost GPS/INS.* PhD thesis, Cranfield University, UK, 2010. 34

[Macadam 2003] Charles C. Macadam. *Understanding and Modeling the Human Driver.* Vehicle System Dynamics, vol. 40, no. 1-3, pages 101–134, 2003. 35

[Mango 2004] Nicholas Mango. *Measurement & Calculation of Vehicle Center of Gravity Using Portable Wheel Scales.* In Society of Automotive Engineers, numéro 2004-01-1076, 2004. 88

[Mashadi 2010] B Mashadi, M Majidi and H Pourabdollah Dizaji. *Optimal vehicle dynamics controller design using a four-degrees-of-freedom model.* Proceedings of the Institution of Mechanical Engineers, Part D: Journal of Automobile Engineering, vol. 224, no. 5, pages 645–659, 2010. 27

[Mashadi 2011] B Mashadi, S Mostaani and M Majidi. *Vehicle stability enhancement by using an active differential.* Proceedings of the Institution of Mechanical Engineers, Part I: Journal of Systems and Control Engineering, vol. 225, no. 8, pages 1098–1114, 2011. 44

[McRuer 1959] Duane T. McRuer and Ezra S. Krendel. *The human operator as a servo system element.* Journal of the Franklin Institute, vol. 267, no. 5, pages 381 – 403, 1959. 72

[Milliken 1956] William F. Milliken and David W. Whitcomb. *General introduction to a programme of dynamic research.* Proceedings of the Institution of Mechanical Engineers, Automobile Division, vol. 1956, no. 1956, pages 287–309, 1956. 22, 23

[Milliken 1996] William F. Milliken and Douglas L. Milliken. Race car vehicle dynamics. Society of Automotive Engineers Inc., Great Britain, 1996. 55, 59

[Mirzaei 2008] M Mirzaei, G Alizadeh, M Eslamian and S Azadi. *An optimal approach to non-linear control of vehicle yaw dynamics.* Proc. IMechE Part I: Journal of Systems and Control Engineering, vol. 222, pages 217–229, 2008. 34

[Mokhiamar 2002] O. Mokhiamar and M. Abe. *Active wheel steering and yaw moment control combination to maximize stability as well as vehicle responsiveness during quick lane change for active vehicle handling safety.* Proceedings of the Institution of Mechanical Engineers, Part D: Journal of Automobile Engineering, vol. 216, no. 2, pages 115–124, 2002. 36

[Mokhiamar 2003] O Mokhiamar and M Abe. *Examination of different models following types of yaw moment control strategy for improving handling safety of a car-caravan combination.* Proceedings of the Institution of Mechanical Engineers, Part D: Journal of Automobile Engineering, vol. 217, no. 7, pages 561–571, 2003. 44

[Mokhiamar 2006] Ossama Mokhiamar and Masato Abe. *How the four wheels should share forces in an optimum cooperative chassis control.* Control Engineering Practice, vol. 14, no. 3, pages 295 – 304, 2006. 44

[Niederkofler 2011] Haymo Niederkofler, Andrés Eduardo Rojas Rojas and Josef Dürnberger. *Development of a single wheel steer-by-wire system: Implementation aspects and failure handling.* In S. Iwnicki, Roger Goodall and T.X. Mei, editeurs, The dynamics of vehicles on roads and

on tracks : Proceedings of 22nd IAVSD Symposium held in Manchester, UK, August 14-19, 2011, numéro ISBN: 9781905476596. Manchester Metropolitan University, 2011. 17, 18

[Odhams 2009] A M C Odhams and D J Cole. *Application of linear preview control to modelling human steering control.* Proceedings of the Institution of Mechanical Engineers, Part D: Journal of Automobile Engineering, vol. 223, no. 7, pages 835–853, 2009. 37

[Oertel 1999] Ch. Oertel and A. Fandre. *Ride Comfort Simulations and Steps Towards Life Time Calculations: RMOD-K and ADAMS.* In International ADAMS Users' Conference - Berlin, 17-19 November 1999. 30

[Ogata 2003] Katsuhiko Ogata. System dynamics. Prentice Hall, 2003. 58

[Okada 1973] T. Okada, T. Takiguchi, M. Nishioka and G. Utsunomiya. *Evaluation of Vehicle Handling and Stability of Computer Simulation at the First Stage of Vehicle Planning.* In Society of Automotive Engineers, numéro SAE 730525, 1973. 24

[Olley 1938] Maurice Olley. *National influences on american passenger car design.* In Proceedings of the Institution of Mechanical Engineers, Automobile Division, volume 32, pages 509–541. Sage Publications, 1938. 22, 23

[Olley 1946] Maurice Olley. *Road manners of the modern car.* In Proceedings of the Institution of Mechanical Engineers, Automobile Division, volume 41, pages 147–182. Sage Publications, 1946. 22

[Orend 2005] Ralf Orend. *Modelling and Control of a Vehicle with Single-Wheel Chassis Actuators.* In Proceedings of the 16th IFAC World Congress, volume 16, 2005. 17

[Osborn 2006] Russell P. Osborn and Taehyun Shim. *Independent control of all-wheel-drive torque distribution.* Vehicle System Dynamics, vol. 44, no. 7, pages 529–546, 2006. 26, 44

[Pacejka 1991] H.B. Pacejka and R.S. Sharp. *Shear Force Development by Pneumatic Tyres in Steady State Conditions: A Review of Modelling Aspects.* Vehicle System Dynamics, vol. 20, no. 3-4, pages 121–175, 1991. 32

[Pacejka 1992] H. B. Pacejka and E. Bakker. *The Magic Formula Tyre Model.* Vehicle System Dynamics, vol. 21, no. Supplement, pages 1–18, 1992. 32, 33

[Pacejka 2006] H. B. Pacejka. Tyre and vehicle dynamics. Elsevier Ltd., Oxford, UK, 2006. 30, 33, 65

[Park 2001] Kihong Park, Seung-Jin Heo and Inho Baek. *Controller design for improving lateral vehicle dynamic stability.* JSAE Review, vol. 22, no. 4, pages 481 – 486, 2001. 44

[Peng 1994] C. Peng, P. A. Cowell, C. J. Chisholm and J. A. Lines. *Lateral Tyre Dynamic Characteristics.* Journal of Terramechanics, vol. 31, no. 6, pages 395–414, 1994. vii, 28, 29, 30, 33

[Pimentel 2004] Juan R. Pimentel. *An Architecture for a Safety-Critical Steer-by-Wire System.* In Society of Automotive Engineers, numéro 2004-01-0714, 2004. 15

[Platt 1968] M. Platt. *Lanchester and the motor vehicle.* In Proceedings of the Institution of Mechanical Engineers, Automobile Division, volume 183, pages 137–153. Sage Publications, 1968. 22

[Plöchl 2007] Manfred Plöchl and Johannes Edelmann. *Driver models in automobile dynamics application.* Vehicle System Dynamics, vol. 45, no. 7-8, pages 699–741, 2007. 35

[Rajamani 2006] R. Rajamani. Vehicle dynamics and control. Springer, USA, 2006. 49, 52, 69, 89, 99, 101

[Ramji 2002] K. Ramji, V. K. Goel and V. H. Saran. *Stiffness properties of small-sized pneumatic tyres.* Journal of Automobile Engineering, vol. 216, no. 2, pages 107 – 114, 2002. 62

[Rieveley 2007] Robert J. Rieveley and Bruce P. Minaker. *Variable Torque Distribution Yaw Moment Control For Hybrid Powertrains.* In Society of Automotive Engineers, numéro SAE 2007-01-0278, 2007. 44

[Ro 1996] P I Ro and H Kim. *Four Wheel Steering System for Vehicle Handling Improvement: A Robust Model Reference Control Using the Sliding Mode.* Proceedings of the Institution of Mechanical Engineers, Part D: Journal of Automobile Engineering, vol. 210, no. 4, pages 335–346, 1996. 26, 39

[Rossetter 2003] Eric J. Rossetter. *A potential field framwwork for active vehicle lanekeeping assistance*. PhD thesis, Stanford University, USA, 2003. 34

[Ryu 2002] Jihan Ryu, Eric J. Rossetter and J. Christian Gerdes. *Vehicle Sideslip and Roll Parameter Estimation using GPS*. In Proceedings of the International Symposium on Advanced Vehicle Control (AVEC), Tokyo, 2002. Japan Society of Automotive Engineers. 12

[Ryu 2004] Jihan Ryu and J. Christian Gerdes. *Integrating Inertial Sensors With Global Positioning System (GPS) for Vehicle Dynamics Control*. Journal of Dynamic Systems, Measurement, and Control, vol. 126, no. 2, pages 243–254, 2004. 26

[Sabanovic 2004] A. Sabanovic, L. M. Fridman and S. Spurgeon, editeurs. Variable structure systems: from principles to implementation. Institution of Engineering and Technology, Philadephia, PA, 2004. 121

[Salaani 1999] M. Kamel Salaani, Dennis A. Guenther and Gary J. Heydinger. *Vehicle Dynamics Modeling for the National Advanced Driving Simulator of a 1997 Jeep Cherokee*. In SAE Technical Paper, numéro 1999-01-0121, March 1999. 26

[Sawase 2006] Kaoru Sawase, Yuichi Ushiroda and Takami Miura. *Left-Right Torque Vectoring Technology as the Core of Super All Wheel Control (S-AWC)*. Mitsubushi Motors Technical Review, pages 16–23, 2006. 43

[Sayers 1996] Michael W. Sayers and Dongsuk Han. *A Generic Multibody Vehicle Model for Simulating Handling and Braking*. Vehicle System Dynamics, vol. 25, no. sup1, pages 599–613, 1996. 24

[Segawa 2001] Masaya Segawa, Shiro Nakano, Osamu Nishihara and Hiromitsu Kumamoto. *Vehicle stability control strategy for steer by wire system*. JSAE Review, vol. 22, no. 4, pages 383 – 388, 2001. 11

[Segel 1956] Leonard Segel. *Theoretical prediction and experimental substantiation of the response of the automobile to steering control*. In Proceedings of the Institution of Mechanical Engineers, Automobile Division, volume 1956, pages 310–330. Sage Publications, 1956. 23, 24, 31

[Segel 1957] Leonard Segel. *Research in the Fundamentals of Automobile Control and Stability*. In Society of Automotive Engineers, numéro SAE 570044, 1957. 23, 31

[Sharp 1991] Robin S. Sharp. *Computer codes for road vehicle dynamic models.* In In Proceedings of Autotech '91, Birmingham, numéro 427/16/064. Mechanical Engineering Publications, London, November 1991. 25

[Sharp 2000] R.S. Sharp, D. Casanova and P. Symonds. *A Mathematical Model for Driver Steering Control, with Design, Tuning and Performance Results.* Vehicle System Dynamics, vol. 33, no. 5, pages 289–326, 2000. 36, 37

[Sharp 2002] Robin S. Sharp. *Fundamentals of the Lateral Dynamics of Road Vehicles.* In Hassan Aref and James W. Phillips, editeurs, Mechanics for a New Mellennium, pages 127–146. Springer Netherlands, 2002. 25

[Sharp 2003] R. S. Sharp and M. Bettella. *Tyre Shear Forces and Moment Descriptions by Normalisation of Parameters and the "Magic Formula".* Vehicle System Dynamics, vol. 39, no. 1, pages 27–56, 2003. 34

[Sheridan 1966] T.B. Sheridan. *Three Models of Preview Control.* Human Factors in Electronics, IEEE Transactions on, vol. HFE-7, no. 2, pages 91 – 102, june 1966. 35

[Shino 2001] Motoki Shino and Masao Nagai. *Yaw-moment control of electric vehicle for improving handling and stability.* JSAE Review, vol. 22, no. 4, pages 473 – 480, 2001. 44

[Shladover 1995] Stevem E. Shladover. *Review of the State of Development of Advanced Vehicle Control Systems (AVCS).* Vehicle System Dynamics, vol. 24, no. 6-7, pages 551–595, 1995. 37

[Shoop 2001] Sally A. Shoop. *Finite Element Modeling of Tire-Terrain Interaction.* Rapport technique ERDC/CRREL TR-01-16, US Army Corps of Engineers - Enigineer Research and Development Center, Hanover, USA, November 2001. 30

[Shyu 1992] Kuo-Kai Shyu, Yao-Wen Tsai and Chee-Fai Yung. *A modified variable structure controller.* Automatica, vol. 28, no. 6, pages 1209 – 1213, 1992. 121

[Siegler 2002] Blake Siegler. *Lap time simulation for racing car design.* PhD thesis, The University of Leeds, UK, 2002. 34

[Slotine 1991] Jean-Jacques E. Slotine and Weiping Li. Applied nonlinear control. Prentice Hall, Upper Saddle River, NJ, 1991. ix, 119, 120, 121

[sta 1992] *Glossary of Terms for road vehicle dynamics and road holding ability.* The British Standards Institution, 1992. vii, 62

[sta 2003] *Road vehicles - Lateral transient response test methods- Open-loop test methods*, 2003. 86, 103

[sta 2004] *Passenger cars - Steady-state circular driving behaviour - Open-loop test methods*, 2004. 86, 100

[sta 2010] *Functional Safety of Electrical Electronic Programmable Electronic Safety-related Systems*, 2010. 13

[Svendenius 2003] J. Svendenius. Tire models for use in braking applications. Licentiate thesis, Lund University, Department of Automatic Control, November 2003. 63, 64

[Szostak 1988] H. T. Szostak. *Analytical Modeling of Driver Response in Crash Avoidance Maneuvering. Volume II: An Interactive Tire Model for Driver/Vehicle Simulation.* Rapport technique DOT-HS-807-271, National Highway Traffic Safety Administration, 1988. 34

[Tekin 2010] Gökhan Tekin and Y. Samim Ünlüsoy. *Design and simulation of an integrated active yaw control system for road vehicles.* International Journal of Vehicle Design, vol. 52, no. 1/2/3/4, pages 5–19, 2010. 44

[Tielking 1974] J. T. Tielking and N. K. Mital. *A comparitive evaluation of five tire traction models.* Rapport technique Project 329180, University of Michigan, USA, 1974. 63

[Tomizuka 1995] Masayoshi Tomizuka and J. Karl Hedrick. *Advanced Control Methods for Automotive Applications.* Vehicle System Dynamics, vol. 24, no. 6-7, pages 449–468, 1995. 38, 39

[Tuncay 2011] R.N. Tuncay, O. Ustun, M. Yilmaz, C. Gokce and U. Karakaya. *Design and implementation of an electric drive system for in-wheel motor electric vehicle applications.* In Vehicle Power and Propulsion Conference (VPPC), 2011 IEEE, pages 1 –6, sept. 2011. 43

[Tustin 1947] A. Tustin. *The nature of the operator's response in manual control, and its implications for controller design.* Electrical Engineers - Part IIA: Automatic Regulators and Servo Mechanisms, Journal of the Institution of, vol. 94, no. 2, pages 190 –206, may 1947. 72

[Wang 2011a] J. Wang, Q. Wang, L. Jin and C. Song. *Independent wheel torque control of 4WD electric vehicle for differential drive assisted steering.* Mechatronics, vol. 21, no. 1, pages 63 – 76, 2011. 43

[Wang 2011b] Rongrong Wang and Junmin Wang. *Fault-Tolerant Control With Active Fault Diagnosis for Four-Wheel Independently Driven Electric Ground Vehicles.* Vehicular Technology, IEEE Transactions on, vol. 60, no. 9, pages 4276 –4287, nov. 2011. 19, 20

[web a] *http://bit.ly/f5tuOO.* Internet. vii, 29

[web b] *http://edition.cnn.com/2011/12/12/tech/innovation/in-wheel-motor/index.html.* Internet. 42

[web c] *http://goo.gl/AHdYR.* Internet. 21

[web d] *http://www.shining-wit.net/rick/buggy/design/wheels/index.html.* Internet. vii, 61

[web e] *Uniform Provisions Concerning the Approval of Vehicles with Regard to Steering Equipment (http://goo.gl/sd6CW).* Internet. 21

[Weiskircher 2011] Thomas Weiskircher, Joseph Ezeti Diang and Steffen Müller. *Control Performance and Energy Consumption of an Electric Vehicle with Single-Wheel Drives and Steer-by-Wire.* In S. Iwnicki, Roger Goodall and T.X. Mei, editeurs, The dynamics of vehicles on roads and on tracks : Proceedings of 22nd IAVSD Symposium held in Manchester, UK, August 14-19, 2011, numéro ISBN: 9781905476596. Manchester Metropolitan University, 2011. 18, 21

[Whitcomb 1956] David W. Whitcomb and William F. Milliken. *Design Implications of a General Theory of Automobile Stability and Control.* Proceedings of the Institution of Mechanical Engineers: Automobile Division, vol. 10, no. 1, pages 367–425, 1956. 23

[Wilwert 2003] C. Wilwert, YeQiong Song, F. Simonot-Lion, Loria-Trio and T. Clement. *Evaluating quality of service and behavioral reliability of steer-by-wire systems.* In Emerging Technologies and Factory Automation, 2003. Proceedings. ETFA '03. IEEE Conference, volume 1, pages 193 – 200 vol.1, sept. 2003. 21

[Wilwert 2005] Cédric Wilwert, Nicolas Navet, Ye-Qiong Song and Françoise Simonot-Lion. *Design of automotive X-by-Wire systems.* In Richard Zurawski, editeur, The Industrial Communication Technology Handbook. CRC Press, 2005. http://www.taylorandfrancis.com/. 12

[Wong 2001] J. Y. Wong. Theory of ground vehicles. Wiley, New York, USA, 2001. 30, 32, 33, 49, 64, 66, 69, 89

[Xiong 2009] Lu Xiong and Zhuoping Yu. *Control allocation of vehicle dynamics control for a 4 in-wheel-motored EV*. In Power Electronics and Intelligent Transportation System (PEITS), 2009 2nd International Conference on, volume 2, pages 307 –311, dec. 2009. 44

[Xu 2011] Kun Xu, Guoqing Xu, Weimin Li, Linni Jian and Zhibin Song. *Anti-skid for Electric Vehicles based on sliding mode control with novel structure*. In Information and Automation (ICIA), 2011 IEEE International Conference on, pages 650 –655, june 2011. 44

[Yao 2006] Yixin Yao. *Vehicle Steer-by-Wire System Control*. In Society of Automotive Engineers, numéro 2006-01-1175. Visteon Corporation, 2006. 13

[Yih 2005] P. Yih and J.C. Gerdes. *Modification of vehicle handling characteristics via steer-by-wire*. Control Systems Technology, IEEE Transactions on, vol. 13, no. 6, pages 965 – 976, nov. 2005. 11, 26

[Yoshioka 1999] Tohru Yoshioka, Tomohiko Adachi, Tetsuro Butsuen, Haruki Okazaki and Hirotaka Mochizuki. *Application of sliding-mode theory to direct yaw-moment control*. JSAE Review, vol. 20, no. 4, pages 523 – 529, 1999. 44

[Young 1996] K.D. Young, V.I. Utkin and U. Ozguner. *A control engineer's guide to sliding mode control*. In Variable Structure Systems, 1996. VSS '96. Proceedings., 1996 IEEE International Workshop on, pages 1 –14, dec 1996. 121

[Yu 1994] Ssu-Hsin Yu and John J. Moskwa. *A Global Approach to Vehicle Control: Coordination of Four Wheel Steering and Wheel Torques*. Journal of Dynamic Systems, Measurement, and Control, vol. 116, no. 4, pages 659–667, 1994. 8, 21, 38

[Zheng 2006] Shuibo Zheng, Houjun Tang, Zhengzhi Han and Yong Zhang. *Controller design for vehicle stability enhancement*. Control Engineering Practice, vol. 14, no. 12, pages 1413 – 1421, 2006. 26, 44, 122, 128

[Zhou 2010] Hongliang Zhou and Zhiyuan Liu. *Vehicle Yaw Stability-Control System Design Based on Sliding Mode and Backstepping Control Approach*. Vehicular Technology, IEEE Transactions on, vol. 59, no. 7, pages 3674–3678, 2010. 44

List of Symbols

α_f, α_r Front and rear tyre slip angles respectively, page 47

β_r Ratio of the reducer connecting the DC motor to the wheel, page 54

δ_f Front steering angle of the vehicle, page 47

η_r Ratio of the reducer, page 54

γ_f Front tyre velocity angle, page 47

γ_r Rear tyre velocity angle, page 48

ω_m Angular velocity of the DC motor, page 54

ω_{fl}, ω_{fr}, ω_{rr}, ω_{rl} Angular velocities of the front left, front right, rear right and rear left wheels respectively, page 51

ϕ Roll of the vehicle, page 45

ψ Yaw angle of the vehicle, page 45

$\sum F_y$ Sum of forces acting on the vehicle in y-direction, page 47

$\sum M_z$ Sum of moments acting on the vehicle in z-direction, page 47

τ_E Torque applied to the rotor by an external load, page 54

τ_{fl}, τ_{fr}, τ_{rr}, τ_{rl} Torque acting on the front left, front right, rear right and rear left wheels respectively, page 51

θ Pitch of the vehicle, page 45

a Distance between the front axle and the vehicle's centre of mass, page 47

a_s, b_s Distance of sprung mass COG from the front and rear axles respectively, page 56

a_y Inertial acceleration of the vehicle in y-direction, page 47

b Distance between the rear axle and the vehicle's centre of mass, page 47

B_m Motor's viscous friction constant, page 54

C_d Drag coefficient of air, page 50

$C_{\alpha_f}, C_{\alpha_r}$ Cornering stiffness of the front and rear tyre respectively, page 48

$C_{\phi f}$ Front torsional damping coefficient, page 53

$C_{\phi r}$ Rear torsional damping coefficient, page 53

E Voltage applied to the DC motor, page 54

F_d Air drag force, page 50

F_x Tractive or longitudinal tyre force, page 58

F_y Lateral tyre force, page 58

F_z Normal load on tyre, page 58

$F_{x_{fw}}, F_{x_{rw}}$ Longitudinal tyre forces at front and rear respectively, page 47

$F_{y_{fw}}, F_{y_{rw}}$ Lateral tyre forces at front and rear respectively, page 47

h_r Roll centre height at front and rear, page 56

h_{axle} Height of axle from the ground, page 55

I Current through the motor, page 54

I_z Moment of inertia about z-axis, page 47

I_{fwl}, I_{fwr}, I_{rwr}, I_{rwl} Moment of inertia of the front left, front right, rear right and rear left wheels respectively, page 51

J_m Rotor's moment of inertia, page 54

K_b Motor's back emf constant, page 54

K_t Motor's torque constant, page 54

$K_{\phi f}$ Front torsional stiffness coefficient, page 53

$K_{\phi r}$ Rear torsional stiffness coefficient, page 53

l Wheel base of the vehicle, page 56

L_m Inductance of the DC motor, page 54

m Mass of the vehicle, page 47

m_s Sprung mass of the vehicle, page 53

M_z Aligning moment of tyre, page 58

m_u Unsprung mass of the vehicle, page 53

r Yaw rate of the vehicle, page 47

R_e Effective rolling radius of the wheel, page 59

R_m Motor winding resistance, page 54

R_{fl}, R_{fr}, R_{rr}, R_{rl} Effective radius of the front left, front right, rear right and rear left wheels respectively, page 51

T_F, T_R Track width at front and rear respectively, page 50

u Longitudinal velocity of the vehicle, page 46

v Lateral velocity of the vehicle, page 47

V_r Rolling velocity of the wheel, page 59

V_x Longitudinal velocity of the wheel, page 59

X, Y, Z Earth-fixed coordinates, page 45

x, y, z Body-fixed coordinates, page 45